

Model Transformations and Periodic Trajectory Calculations

for Stability Assessments of Modular Multilevel Converter-Based Systems

Philippe De Rua

Supervisor:
Prof. dr. ir. Jef Beerten

Dissertation presented in partial
fulfillment of the requirements for the
degree of Doctor of Engineering
Science (PhD): Electrical Engineering

November 2023

Model Transformations and Periodic Trajectory Calculations

for Stability Assessments of Modular Multilevel Converter-Based Systems

Philippe DE RUA

Dissertation presented in partial fulfillment of the requirements for the degree of Doctor of Engineering Science (PhD): Electrical Engineering

Examination committee:

Em. prof. dr. ir. Jean-Pierre Celis, chair

Prof. dr. ir. Jef Beerten, supervisor

Prof. dr. ir. Ruth Vazquez Sabariego

Prof. dr. ir. Johan Suykens

Prof. dr. ir. Agusti Egea Alvarez

(University of Strathclyde, Glasgow, United Kingdom)

Prof. dr. ir. Gilbert Bergna Diaz

(Norwegian University of Science and Technology, Trondheim, Norway)

Dr. ir. Adedotun Agbemuko

(Elia, Belgium)

November 2023

© 2023 KU Leuven – Faculty of Engineering Science
Uitgegeven in eigen beheer, Philippe De Rua, Kasteelpark Arenberg 10 box 2445, B-3001 Leuven (Belgium)

Alle rechten voorbehouden. Niets uit deze uitgave mag worden vermenigvuldigd en/of openbaar gemaakt worden door middel van druk, fotokopie, microfilm, elektronisch of op welke andere wijze ook zonder voorafgaande schriftelijke toestemming van de uitgever.

All rights reserved. No part of the publication may be reproduced in any form by print, photoprint, microfilm, electronic or any other means without written permission from the publisher.

Preface

There were numerous reasons for me to write this doctoral thesis, one of them was the desire to bring answers to the questions I had when I set out on this academic journey. *How do we linearise if we do not have an equilibrium? Can we just sweep harmonics under the rug? Do these harmonics have any impact on stability?* While some questions remain without definitive answers, I am confident that the reasonings and methods laid out in this text will be a helpful guide for anyone diving into the same or similar questions, wishing to gather insights based on overviews and comparisons of multiple methods, and to find new ideas to push their limits in the direction of either more simplicity or accuracy.

The exploration into modelling, control and stability assessments of electrical power systems relying on power-electronic converters has been a fascinating adventure and a rewarding endeavour, shaped by the support of mentors, colleagues, friends and family to whom I would like to express my gratitude.

First and foremost, I express my sincere appreciation to my supervisor Prof. Jef Beerten for the opportunity he gave me to pursue a PhD in his team at KU Leuven, for his guidance, patience and moral support throughout this journey. Thank you Jef for your continued trust and for having always brought the essential pinch of doubt whenever I was stuck in dangerous certainties, and vice versa.

I would like to express my gratitude to the FOD Economy, Belgium, for having funded my first PhD year through the Neptune projet, and to Fonds voor Wetenschappelijk Onderzoek (FWO) for believing in my capacity to continue on that path and funding the following four years of research.

I would like to thank the members of the supervisory committee and of the evaluation committee for their valuable time and advice. Thank you Prof. Ruth Vazquez Sabariego, Prof. Agusti Egea Alvarez and Prof. Johan Suykens for evaluating my progress over the past five years and for the discussions which

helped me take new perspectives on my work. Thank you Prof. Gilbert Bergna Diaz for having welcomed me at NTNU as part of a mind-opening PhD exchange and for having taken the time to explain Lyapunov's theory *in human*, thank you Dr. Adedotun Agbemuko for also joining the evaluation committee and for the engaging discussions on harmonic linearisation and co., thank you Em. Prof. Jean-Pierre Celis for chairing the evaluation committee.

I would like to extend my recognition to the researchers and colleagues who helped me find my way through the PhD. Thank you Prof. Wim Michiels for your patience and help with delayed systems, Katrien De Cock for your advice and verification of the mathematical proof of the stability criterion, Kamran Sharifabadi for your repeated encouragements and your essential guidance within CIGRE WG B4.81, Gianmarco Ducci for your valuable help with the implementation of numerical shooting methods, Valerio Salis and Sjur Føyen for our insightful discussions about the harmonic state space.

I would like to thank the staff and my colleagues at KU Leuven/EnergyVille as well as at NTNU for the discussions, the laughs, and the coffee breaks. More special thanks to Özgür for our very friendly yet progress-driving competition between harmonic state space and dynamic phasors, Eros for having been such a fervent user of the evolving Matlab toolbox, Fran for having shared the workload when I needed it the most, Thomas for your endless support and the numerous pandemic-proof and cross-border coffee breaks, Tanguy for your timely and indispensable feedback on the thesis. Dear colleagues, I cannot emphasise enough how crucial your help has been in keeping this project alive through the last years, thank you once more.

Lastly, my most profound recognition goes to my family and friends, who are my foundations and my roof wherever I find myself to be.

Philippe De Rua

Abstract

The ongoing transition from conventional fossil fuel-based power plants to renewable energy sources, coupled with the continued electrification of the industry, transportation, residential, and commercial sectors, is enabled by substantial transformations within the electrical power system. New means of generating electricity, such as wind farms, are frequently located at considerable distances from population centres, whereas rooftop photovoltaic panels are often integrated into urban landscapes, bringing them closer to end-users. These advancements are significant, marking not only a departure from the conventional centralised power generation paradigm of the past century, but also from the reliance on the large synchronous generators of traditional power plants, as renewable sources are typically connected to the grid through power-electronic converters. Moreover, to mitigate the intermittent and uncertain nature of renewable energy production, there is a growing need for enhanced cross-border and long-distance grid interconnections. In this context, high-voltage direct current (HVDC) transmission technology plays an increasingly pivotal role and is expected to become the backbone of the electrical power system. Naturally, HVDC systems need to interface with existing alternating current (AC) systems, a task primarily accomplished through large-scale power-electronic converters.

What merits particular attention is the distinct dynamic behaviour of power-electronic converters in contrast to that of synchronous generators. Relying on switched semiconductor devices with little to no intrinsic energy storage, power-electronic converters are also capable of reacting to disturbances within very small time frames and over broad frequency ranges. Consequently, in today's technology mix, new forms of adverse interactions between converters and their nearby electrical environment have started to emerge, some of which may have severe consequences. A comprehensive investigation and a better understanding of the mechanisms underlying these interactions are crucial in taking proactive measures to prevent undesirable dynamic phenomena from deteriorating the proper and stable operation of modern and future power systems.

Among the various types of converters, the modular multilevel converter (MMC) stands out due to its enhanced efficiency and scalability, which come at the cost of an elaborate topology and a complex control structure. While multiple methodologies exist for studying potential adverse interactions involving power-electronic converters, methods that were suitable for the previous generations of the power system start to lack accuracy when addressing the particular features of the MMC, such as the multi-harmonic time-periodic nature of its variables in steady state as well as non-negligible control delays.

In this thesis, mathematical frameworks are studied and developed to enable more accurate small-signal stability assessments specifically addressing unsolved challenges of MMC-based HVDC systems. An overview of periodic trajectory calculation techniques motivates the development of a Fourier-based collocation method to efficiently calculate the steady-state harmonic content of the MMC while accounting for nonlinearity in its dynamic equations. In combination with linearisation, an in-depth review of approximation and transformation methods from time-periodic to time-invariant models demonstrates the advantages of frequency-lifting approaches, such as the harmonic state space, in terms of flexibility and accuracy. Lastly, a generalisation of the harmonic state space is established to enable modal analysis of systems involving the MMC and accounting for both its time-periodic and time-delayed characteristics while discarding common delay approximations.

Beknopte samenvatting

De voortdurende overgang van conventionele op fossiele brandstoffen gebaseerde energiecentrales naar hernieuwbare energiebronnen, gekoppeld aan de voortdurende elektrificatie van de industrie, transport, residentiële en commerciële sectoren, wordt mogelijk gemaakt door ingrijpende veranderingen binnen het elektrische energiesysteem. Nieuwe methoden voor het opwekken van elektriciteit, zoals windmolenvelden, bevinden zich vaak op aanzienlijke afstanden van bevolkingscentra, terwijl fotovoltaïsche panelen op daken vaak zijn geïntegreerd in stedelijke landschappen, waardoor ze dichter bij eindgebruikers komen. Deze vooruitgang is significant en markeert niet alleen een breuk met het conventionele gecentraliseerde opwekkingsparadigma van de afgelopen eeuw, maar ook met de afhankelijkheid van de grote synchrone generatoren van traditionele energiecentrales, aangezien hernieuwbare bronnen doorgaans zijn verbonden met het net via vermogen elektronische omvormers. Bovendien is er, om de onderbroken en onzekere aard van de productie van hernieuwbare energie te verminderen, een groeiende behoefte aan verbeterde internationale en langeafstandsverbindingen. In deze context speelt de technologie voor hoogspanningsgelijkstroomtransmissie (HVDC) een steeds belangrijkere rol en wordt verwacht dat het de ruggengraat wordt van het elektrische energiesysteem. Natuurlijk moeten HVDC-systeem interageren met bestaande wisselstroomsystemen, een taak die voornamelijk wordt volbracht door grootschalige omvormers.

Wat bijzondere aandacht verdient, is het onderscheidende dynamische gedrag van omvormers in tegenstelling tot dat van synchrone generatoren. Vertrouwend op geschakelde halfgeleiderapparaten met weinig tot geen intrinsieke energieopslag, zijn omvormers ook in staat om te reageren op storingen binnen zeer korte tijdsbestekken en over brede frequentiegebieden. Als gevolg hiervan beginnen er vandaag de dag in de technologiemix nieuwe vormen van ongewenste interacties tussen omvormers en hun nabije elektrische omgeving te ontstaan, waarvan sommige ernstige gevolgen kunnen hebben. Een grondig onderzoek en een beter begrip van de mechanismen die aan deze interacties ten grondslag

liggen, zijn cruciaal om proactieve maatregelen te nemen en te voorkomen dat ongewenste dynamische fenomenen de stabiele werking van moderne en toekomstige energiesystemen in gevaar brengen.

Onder de verschillende soorten omvormers springt de modulaire multilevel omvormer (MMC) eruit vanwege zijn verbeterde efficiëntie en schaalbaarheid, die gepaard gaan met een uitgebreide topologie en een complexe regelstructuur. Hoewel er meerdere methoden zijn om mogelijke ongewenste interacties met omvormers te bestuderen, beginnen methoden die geschikt waren voor de vorige generaties van het energiesysteem, nauwkeurigheid te missen bij het aanpakken van de bijzondere kenmerken van de MMC, zoals de harmonische tijdsperiodieke aard van zijn variabelen in stationaire toestand en niet te verwaarlozen rekentijdvertragingen.

In deze scriptie worden wiskundige denkkaders bestudeerd en ontwikkeld om meer nauwkeurige stabiliteitsbeoordelingen van kleine signalen mogelijk te maken, waarbij specifiek wordt ingegaan op onopgeloste uitdagingen van op MMC gebaseerde HVDC-systeem. Een overzicht van technieken voor de berekening van periodieke banen motiveert de ontwikkeling van een op Fourier gebaseerde collocatiemethode om de stationaire harmonische inhoud van de MMC efficiënt te berekenen, rekening houdend met de niet-lineariteit in zijn dynamische vergelijkingen. In combinatie met linearisatie toont een diepgaand overzicht van benaderings- en transformatiemethoden van tijdsperiodieke naar tijdinvariante modellen de voordelen van frequentieverhogende methoden, zoals de harmonische toestandsruimte, aan in termen van flexibiliteit en nauwkeurigheid. Ten slotte wordt een algemene formulering van de harmonische toestandsruimte vastgesteld om modale analyse van systemen met de MMC mogelijk te maken en rekening te houden met zowel zijn tijdsperiodieke als tijdsvertragde kenmerken, waarbij gangbare vertragingbenaderingen worden weggelaten.

Contents

| | |
|---|------------|
| Abstract | iii |
| Beknopte samenvatting | v |
| Contents | vii |
| List of Abbreviations | xii |
| List of Symbols | xiv |
| Introduction | 1 |
| Rationale | 1 |
| Examples of problematic real-life events | 7 |
| Research questions and objectives | 10 |
| Outline and contributions of the thesis | 13 |
| 1 Converter modelling and fundamentals of stability analysis | 19 |
| 1.1 Introduction | 19 |
| 1.2 Modular multilevel converter modelling and control | 20 |
| 1.2.1 Circuit differential equations | 23 |
| 1.2.2 Overview of MMC control | 25 |
| 1.2.3 Control differential equations | 28 |
| 1.2.4 Closed-loop operation and steady-state waveforms . . . | 32 |
| 1.2.5 Simplified single-phase MMC model | 35 |
| 1.3 Fundamentals of stability analysis | 37 |
| 1.3.1 Nonlinear systems and linearisation | 37 |
| 1.3.2 Linear time-invariant systems | 45 |
| 1.3.3 Linear time-periodic systems | 50 |
| 1.4 Chapter conclusion | 58 |

| | |
|---|-----------|
| 2 Non-lifting transformation methods | 61 |
| 2.1 Introduction | 61 |
| 2.2 Floquet-Lyapunov theory | 62 |
| 2.2.1 The monodromy matrix | 62 |
| 2.2.2 Floquet transformation | 64 |
| 2.2.3 Conclusion | 67 |
| 2.3 Averaging technique | 68 |
| 2.3.1 Problem statement and existing result | 69 |
| 2.3.2 Preliminary considerations | 70 |
| 2.3.3 Establishing a sufficient stability criterion | 72 |
| 2.3.4 Criterion analysis and choice of parameters | 75 |
| 2.3.5 Numerical applications | 77 |
| 2.3.6 Discussion | 80 |
| 2.4 Frame rotations | 80 |
| 2.4.1 Transformation of linear time-invariant systems | 81 |
| 2.4.2 Transformation of nonlinear time-invariant systems | 86 |
| 2.4.3 Application to the MMC | 88 |
| 2.4.4 Discussion and conclusion | 92 |
| 2.5 Chapter conclusion | 94 |
| 3 Frequency-lifting transformation methods | 95 |
| 3.1 Introduction | 95 |
| 3.2 Frequency-lifting and the harmonic state space | 97 |
| 3.2.1 Mathematical operations in a frequency-lifted framework | 97 |
| 3.2.2 Derivation of the harmonic state-space representation | 103 |
| 3.2.3 Numerical application: HSS-based modal analysis | 108 |
| 3.2.4 Comparisons with other transformation methods | 115 |
| 3.2.5 Conclusion | 120 |
| 3.3 Harmonic linearisation | 120 |
| 3.3.1 Numerical approach: frequency scans | 121 |
| 3.3.2 Analytical approach | 123 |
| 3.3.3 Conclusion | 129 |
| 3.4 The harmonic transfer function | 130 |
| 3.4.1 The HTF from the HSS formulation | 130 |
| 3.4.2 The HTF from the impulse response | 132 |
| 3.4.3 The HTF as a generalisation of harmonic linearisation | 137 |
| 3.4.4 Numerical applications | 143 |
| 3.4.5 Discussion and conclusion | 148 |
| 3.5 Chapter conclusion | 149 |

| | |
|--|------------|
| 4 Modal analysis of frequency-lifted delayed systems | 153 |
| 4.1 Introduction | 153 |
| 4.2 Delay modelling for modal analysis | 154 |
| 4.3 Fundamentals of delayed systems | 159 |
| 4.3.1 Characteristic roots of LTI-DDEs | 159 |
| 4.3.2 States and state space of delay differential equations | 161 |
| 4.3.3 Infinitesimal generator | 162 |
| 4.3.4 Matrix approximation of the infinitesimal generator | 163 |
| 4.3.5 Scaling and shifting the eigenvalue problem | 166 |
| 4.3.6 Eigenvectors calculation and eigenvalue convergence test | 167 |
| 4.4 Generalised HSS framework for delayed systems | 168 |
| 4.4.1 Linearisation of NTP-DDE into LTP-DDE formulation | 169 |
| 4.4.2 Time delay of a signal in the frequency-lifted framework | 169 |
| 4.4.3 Transformation of LTP-DDE into DHSS formulation | 170 |
| 4.4.4 Unforced DHSS for modal analysis | 171 |
| 4.4.5 Transformation of DHSS into HTF formulation | 172 |
| 4.5 Numerical application to an MMC-based system | 173 |
| 4.5.1 Modal stability analysis | 174 |
| 4.5.2 Transfer-function-based stability analysis | 176 |
| 4.5.3 Validation against numerical integration | 179 |
| 4.6 Discussion and chapter conclusion | 181 |
| 5 Calculation of periodic trajectories | 183 |
| 5.1 Introduction | 183 |
| 5.2 Overview of calculation methods | 185 |
| 5.3 Frequency-domain and hybrid-domain methods | 190 |
| 5.3.1 Mathematical operations with harmonic vectors | 190 |
| 5.3.2 Frequency-domain methods for linear and quadratic systems | 194 |
| 5.3.3 Mathematical operations with sampled-time vectors | 195 |
| 5.3.4 Hybrid-domain method for nonlinear systems | 200 |
| 5.4 Fourier-based collocation method | 201 |
| 5.5 Validation and numerical applications | 208 |
| 5.5.1 Application to a simple RLC circuit | 208 |
| 5.5.2 Application to the MMC | 211 |
| 5.5.3 The Floquet exponents from the collocation method | 214 |
| 5.5.4 Illustrative harmonic propagation study | 217 |
| 5.6 Chapter conclusion | 221 |
| Conclusion and future work | 223 |
| Summary and conclusions | 223 |
| Overview of contributions | 226 |
| Future work | 228 |

| | |
|---|------------|
| A Supporting content on transformations | 233 |
| A.1 Sequence and harmonic components: intuitive description | 233 |
| A.2 Basic frame transformations | 238 |
| A.2.1 Clarke transformation | 238 |
| A.2.2 Frame rotations | 238 |
| A.2.3 Park transformation | 239 |
| A.2.4 Fortescue transformation | 239 |
| B Supporting content on modelling | 240 |
| B.1 Additional MMC control loops | 240 |
| B.1.1 Direct voltage control | 240 |
| B.1.2 Alternating voltage control | 241 |
| B.1.3 Circulating current control in uncompensated modulation | 242 |
| B.2 MMC control tuning | 244 |
| B.2.1 Phase-locked loop | 244 |
| B.2.2 Power control loops | 245 |
| B.2.3 Direct voltage control loop | 247 |
| B.2.4 Alternating voltage control loop | 248 |
| B.2.5 Alternating current control loop | 249 |
| B.2.6 Circulating current control loop | 250 |
| B.2.7 Summary of parameters | 251 |
| B.3 TLC modelling and control | 252 |
| B.3.1 Stationary-frame TLC model | 252 |
| B.3.2 Simplified rotating-frame TLC model | 256 |
| B.4 MMC-based test systems | 257 |
| B.4.1 System layout | 257 |
| B.4.2 Cable models | 259 |
| B.5 Simplified MMC: Analytical expressions of partial derivatives . | 262 |
| C Supporting content on implementation | 265 |
| C.1 Matlab toolbox | 265 |
| C.2 Numerical integration of differential equations | 269 |
| C.2.1 Integrating ordinary differential equations | 270 |
| C.2.2 Integrating delay differential equations | 270 |
| Bibliography | 275 |
| List of Figures | 287 |
| List of Tables | 289 |
| List of Publications | 290 |
| Curriculum Vitae | 293 |

List of Abbreviations

| | |
|-------------|------------------------------------|
| AC | alternating current |
| AV | alternating voltage |
| CC | circulating current |
| CM | common mode |
| DC | direct current |
| DDE | delay differential equation |
| DFT | discrete Fourier transform |
| DHSS | delayed harmonic state space |
| DM | differential mode |
| DV | direct voltage |
| EMP | exponentially-modulated periodic |
| GNC | generalised Nyquist criterion |
| HL | harmonic linearisation |
| HSS | harmonic state space |
| HTF | harmonic transfer function |
| HVDC | high-voltage direct current |
| IDFT | inverse discrete Fourier transform |
| LC | inductance-capacitance |

| | |
|------------------------|---|
| LTI | linear time-invariant |
| LTI_c | linear time-invariant system operating at a constant point |
| LTI_p | linear time-invariant system following a periodic trajectory |
| LTP | linear time-periodic |
| MIMO | multi-input multi-output |
| MMC | modular multilevel converter |
| NTI | nonlinear time-invariant |
| NTI_c | nonlinear time-invariant system operating at a constant point |
| NTI_p | nonlinear time-invariant system following a periodic trajectory |
| NTP | nonlinear time-periodic |
| NTP_p | nonlinear time-periodic system following a periodic trajectory |
| ODE | ordinary differential equation |
| OWF | offshore wind farm |
| PCC | point of common coupling |
| PI | proportional integral |
| PLL | phase-locked loop |
| PNSE | positive and negative sequence extraction |
| PQ | active and reactive power |
| PR | proportional resonant |
| RFA | root finding algorithm |
| RLC | resistance-inductance-capacitance |
| SIMO | single-input multi-output |
| SISO | single-input single-output |
| SOGI | second-order generalised integrator |
| TF | transfer function |
| TLC | two-level converter |
| VSC | voltage-source converter |

List of Symbols

Main notation guideline

| | | |
|-----------------------------|------------------|-------------------------|
| Lightface letters: | x, X | scalars |
| Boldface lowercase letters: | \boldsymbol{x} | vectors |
| Boldface uppercase letters: | \boldsymbol{X} | matrices |
| Upper-bar notation: | \bar{x} | steady-state quantities |
| Upper-tilde notation: | \tilde{x} | deviation quantities |
| Star superscript notation: | x^* | reference quantities |

| | |
|------------------|--|
| j | Imaginary unit of complex numbers |
| f_1 | Fundamental frequency [Hz] |
| ω_1 | Fundamental angular frequency [rad/s] |
| T_1 | Fundamental period [s] |
| \mathbb{N} | Set of natural numbers |
| \mathbb{Z} | Set of integer numbers |
| \mathbb{R} | Set of real numbers |
| \mathbb{C} | Set of complex numbers |
| $\Phi(t_2, t_1)$ | State transition matrix from time t_1 to time t_2 |
| $\Psi(t)$ | Fundamental matrix at time t |
| Ψ | Monodromy matrix at time t_0 (no explicit arguments) |
| $\mathbf{A}(t)$ | State matrix in a linear state-space representation |
| $\mathbf{B}(t)$ | Input matrix in a linear state-space representation |
| $\mathbf{C}(t)$ | Output matrix in a linear state-space representation |

| | |
|-------------------|--|
| $D(t)$ | Feedthrough matrix in a linear state-space representation |
| n | Number of state variables |
| m | Number of input variables |
| p | Number of outputs variables |
| d | Number of delayed variables |
| $\mathcal{D}\{\}$ | Domain definition |
| $\mathcal{F}\{\}$ | Discrete Fourier Transform |
| $\mathcal{K}\{\}$ | Frequency-lifting |
| $\mathcal{L}\{\}$ | Laplace Transform |
| $\mathcal{R}\{\}$ | Frequency-lifting with constant Fourier coefficients |
| $\mathcal{S}\{\}$ | Sampling |
| $\mathcal{T}\{\}$ | (block-)Toeplitz matrix form |
| n_u, n_l | Upper- and lower-arm insertion indices [-] |
| i_u, i_l | Upper- and lower-arm currents [A] |
| v_u, v_l | Upper- and lower-arm inserted voltages [V] |
| v_s | Differential-mode inserted voltage [V] |
| v_c | Common-mode inserted voltage [V] |
| v_{Cu}, v_{Cl} | Upper- and lower-arm sum capacitor voltages [V] |
| v_C^Σ | Differential-mode sum capacitor voltage [V] |
| v_C^Δ | Common-mode sum capacitor voltage [V] |
| i_s | Differential-mode arm current, or simply alternating current [A] |
| i_c | Common-mode arm current, or simply circulating current [A] |
| i_d | Common-mode direct current, or simply direct current [A] |
| v_d | Common-mode direct voltage, or simply direct voltage [V] |
| ϕ | Phase identifier in a three-phase abc frame |
| φ | Phase identifier in an orthogonal $\alpha\beta$ frame |

Introduction

Rationale

Over the last two centuries, electricity has evolved from an untapped physical phenomenon into an everyday need in the industry, transportation, residential and commercial sectors. The use of electricity has become a keystone for the operation of our society and is now omnipresent in our lives. In the future, reliance on electricity will increase even further as the world population continues to grow and as the electrification of appliances continues to spread [1].

Despite its apparent simplicity, the nearly effortless act of plugging a device into a wall socket hides the elaborate process of electricity production and distribution, which involves several steps that occur behind the scenes. First, electricity must be generated from energy sources, after what it is transported and distributed through lines and cables before reaching the end consumer. The whole chain is referred to as the *electrical power system*. An important characteristic of electricity supply via such system is that the total generation should precisely meet the total consumption at all times. Other constraints supporting the proper operation of an electrical power system are described by the notion of *power quality*, which defines the availability of electrical voltages and currents at compliant amplitudes and frequencies, and the preservation of their waveforms in steady state [2]. Additionally, a stable operation must be ensured such that flows of electrical power are guaranteed to persist despite the spectrum of disturbances to which they are constantly subjected, and despite the variety of transients occurring as a consequence of these disturbances. Failing to fulfil these requirements may result in severe consequences, such as the unintentional interruption of power supply to consumers or irreversible damage to electrical equipment.

In recent years, the energy sources from which electricity is produced have been changing fast and significantly, and so have the devices that enable and control

the generation, transmission and distribution of electrical power. Driven by the energy transition as well as by numerous technological advances, these changes bring solutions to existing problems but also come with their sets of challenges, which must be addressed in order to ensure the continued and reliable operation of the electrical power system. For instance, replacing coal and gas power plants with renewable energy sources such as wind and solar plants, while being a decisive step forward to tackle climate change, leads to higher variability and uncertainty of power generation [3].

There are nowadays two main categories of electrical systems, commonly referred to as alternating current (AC) systems and direct current (DC) systems, with as principal difference the way in which they transmit electricity. On the one hand, AC systems rely on alternating voltages and currents whose direction varies periodically at a frequency called the *fundamental frequency*, generally 50 or 60 Hz. On the other hand, DC systems rely on direct voltages and currents, whose direction remains constant. While most transmission and distribution networks are AC systems, DC transmission presents clear advantages with respect to AC transmission when it comes to the interconnection of asynchronous AC systems and to the cost-effective transmission of electricity at high voltage and over long distances [4]. For these reasons, high-voltage direct current (HVDC) technology has been used increasingly to bring electrical energy from remote areas to load centres, but also to connect islands, offshore wind farms and offshore oil platforms to shore, and is foreseen to become the backbone of the electrical transmission system in the future [5].

To enable power exchange between AC and DC systems, their interconnection requires the conversion of currents and voltages from one type to the other. Today, power-electronic converters typically serve this purpose. For instance, the DC power output of photovoltaic panels is transformed into AC power by means of a power-electronic converter. In type-4 wind turbines, power is extracted from the wind by a variable-speed turbine. In this case, the corresponding variable-frequency AC power is transformed into DC power by a first power-electronic converter, while a second power-electronic converter completes the transformation into AC power at the fundamental grid frequency [6]. As far as HVDC systems are concerned, their connection to AC systems relies nowadays on large-scale power-electronic converters with ratings reaching thousands of megawatts. However, the dramatic increase in the use of such power-electronic devices over the last decades has resulted in new, sometimes undesirable behaviours that may degrade both power quality and stability properties of the electrical system, and which should naturally be prevented [7, 8].

The dynamic characteristics of power-electronic devices are quite different from those of large synchronous generators used in traditional hydro and thermal power plants [7]:

- On the one hand, synchronous generators consist of heavy rotating masses capable of holding substantial amounts of kinetic energy, which can be rapidly supplied to (or drawn from) the network to accommodate for variations of the total electrical generation and consumption in the system. On the other hand, power-electronic converters rely instead on semiconductor valves switched at high frequency and have little to no intrinsic energy storage.
- Like synchronous generators, the voltages and currents of power-electronic converters are regulated by a controller. However, as a consequence of the high-frequency switching that characterises power-electronic converters, their controllers are designed to react within much smaller time scales than those traditionally considered for synchronous generators. For this reason, the frequency range in which adverse dynamic interactions between electrical devices can be observed is also wider.
- Unlike large synchronous generators in hydro and thermal plants, which are normally designed to generate alternating currents and voltages at the fundamental frequency only, semiconductor switching in power-electronic converters generally also produce parasitic oscillatory components, i.e. currents and voltages at other frequencies than the fundamental frequency, hence they contribute to a degradation of power quality. These parasitic oscillatory components are referred to as *switching harmonics*. Their name suggests that they appear at multiples of the fundamental frequency, even though switching may also lead to generating inter-harmonics. In practice, switching harmonic generation is influenced by converter topology, converter control and power-electronics hardware [9].

Overall, the distinctive behaviour of power-electronic converters compared to the generators they are meant to replace or among which they are supposed to operate, has led to an expanded range and an increased risk of undesirable dynamic behaviours involving power-electronic converters [10]. In this context, it is crucial to recognise the significant advancements that have taken place in terms of converter technology over the last decades. In particular, since the inception of HVDC transmission links, the underlying converter technology has undergone a remarkable evolution. Starting with line-commutated converters, innovation has first replaced the original mercury-arc valves by thyristor valves before the dawn of forced-commutated voltage-source converters (VSCs) relying on insulated-gate bipolar transistors. Topologies have evolved too, with a trend towards increased numbers of *discrete internal voltage levels*: intuitively, the more discrete voltage levels, the smoother the voltage waveforms generated by a converter. For high-voltage and medium-voltage applications, the simplest converters with two or three levels are now giving way to recent inventions

such as the modular multilevel converter (MMC) [11], each arm of which may contain several hundreds of discrete voltage levels. Since its introduction at the beginning of the 21st century, the MMC has attracted considerable attention from the research and industry communities for its numerous advantages such as increased scalability, reduced emissions of switching harmonics and higher conversion efficiency [12], and has now become the prevalent VSC topology for HVDC applications.

Despite being one of the latest improvements in the field of conversion technology, the MMC is, just as any power-electronic converter, not exempt from the risk of contributing to undesired oscillations and unstable behaviours. Problematic events involving the MMC have been reported from real-life projects in recent years [13–15], where unwanted oscillations have been observed at frequencies ranging from a few tens of hertz up to the kilohertz range (a selection of real-life interaction events is presented in the following section). For this reason, specific studies must be conducted in order to identify the risk of undesired phenomena, to analyse and understand their potential causes, and to prevent them from (re)occurring.

Amongst conducted studies, numerical simulations and analyses of mathematical models are common approaches. Models generally consist of a set of differential equations which are established from fundamental principles of physics to describe the dynamic behaviour of the considered system. Next, the models are submitted to various tests, typically consisting of observing their response to perturbations of their operating conditions. Disturbances are usually classified into large and small disturbances, and the corresponding studies are referred to as *large-signal* and *small-signal analyses*, respectively. While the study of large disturbances normally relies on models capable of accounting for a broad variety of nonlinear behaviours, the impact of small disturbances can be analysed based on local linear approximations of the nonlinear equations. Although more restrictive, the small-signal assumption is extensively used as it supports the application of well-known traditional methods of linear systems theory, such as modal¹ and transfer-function-based analyses, which provide essential insights into systems dynamics. In particular, such traditional methods help assessing the stability of a given operating point, i.e. determining whether the system will tend to return to that same operating point after a disturbance or whether it will tend to diverge away from it.

A precondition to the application of the aforementioned traditional methods is the existence of an equilibrium of the system, i.e. an operating point at which its variables are constant in the absence of external perturbations, and around

¹ In this thesis, *modal analysis* refers to a study based on eigenvalues or characteristic roots calculations, together with their corresponding eigenvectors and participation factors.

which a local linear approximation can be determined. For power-electronic converters, such equilibria may not exist due to the fact that not all variables are constant, even in steady-state: alternating quantities and quantities subject to switching harmonics naturally vary in time. In this case, the system does not operate at a constant operating point in steady state but follows a time-periodic trajectory. To address the issue of having to deal with such periodic trajectories instead of equilibria, switching harmonics are customarily considered small enough to be seen as small perturbations of otherwise ideal operating trajectories and are then neglected—a simplification generally valid for the study of phenomena with characteristic frequencies below half of the switching frequency [16]. As a consequence of this simplification, the remaining oscillatory components that make the followed trajectory periodic are the alternating quantities characteristic of AC systems. These can be addressed by means of widespread methods such as frame rotations, which allow transforming the oscillatory components at fundamental frequency into constant values in steady state. This enables substituting the initial time-periodic trajectory with an equilibrium on which the traditional methods of linear systems theory can eventually be applied.

In comparison with simpler converters such as the two-level VSC, analysing the MMC's time-periodic trajectories presents a magnified complexity that results from the unique topology of this converter. First, each arm of the MMC consists of a string of submodules, which are foundational to its characteristically large number of discrete internal voltage levels [12]. Each submodule contains a capacitor, the set of which makes the arms capable of storing a certain amount of energy. This causes internal energy flows between the arms as the voltages across the strings of submodules vary. Not only do these flows require more-elaborate control structures, they also give rise to multiple oscillatory components within internal currents and voltages. These oscillations appear at harmonics of the fundamental grid frequency and are observed also under normal operating conditions. Normally unnoticed from the AC or DC connections of the converter, these internal harmonic components are rather unique to the MMC: they are not the consequence of semiconductor switching, but the consequence of the way in which the MMC modulates alternating quantities into direct quantities, and vice versa [17].

The difficulty of generalising transformation methods such as frame rotations to systems with variables comprising oscillatory components at more frequencies than the fundamental grid frequency hinders the application of traditional stability analysis methods to the time-periodic trajectories of the MMC. To circumvent this issue, the force of habit and the lack of immediate knowledge of a better approach initially led to assuming that the MMC's internal oscillatory components could be neglected, just as is customarily done with switching

harmonics. This assumption enabled using the traditional methods of stability analysis for MMCs and MMC-based applications, even though the reduced modelling accuracy resulting from neglecting potentially relevant frequency components (and any related control loops) could lead to incorrect stability assessments. Recently, with the steadily increasing share of converter-based transmission and generation, the need for more accurate models and methods delivering reliable conclusions on the risks of adverse dynamic behaviours has pushed towards reconsidering the initial simplification. The development of appropriate techniques that enable accounting for oscillatory components at multiple frequencies when studying the stability of periodic trajectories is an important step towards ensuring the continued and reliable operation of MMCs and of the networks within which they are operated.

Methods have thus been introduced to address in more rigorous ways the multi-frequency characteristics of the MMC's steady-state trajectories. For instance, the harmonic state-space representation [18], a method that relies on Fourier theory and that is capable of addressing periodicity of state-space models in a highly flexible way, has gained attention over the last decade. However, the *at-first-sight* complexity of the harmonic state-space method and of its underlying mathematical theory has hindered the identification of the types of systems and analyses for which it is useful, and those for which it is in fact necessary. Consequently, it is imperative to develop a deeper understanding of the fundamental principles of this method and to compare its capabilities with other state-of-the-art techniques.

Aside from the time-periodic characteristics of trajectories followed by the MMC, the switched nature of power-electronic converters and their control via digital signal processors also play a role in the overall dynamic behaviour of converter-based systems. Specifically, switching times, in combination with sampling, analog-to-digital conversion, communication and calculation times, introduce delays between the moment of measurement and the moment at which the converter generates the electrical quantities resulting from calculations based on that particular measurement [19]. This is true in normal operation but also when the converter must react to disturbances, which can lead to potentially inadequate reactions and even unstable behaviours. While delays of about 150 μs are typically mentioned for two-level VSCs with sampling frequencies of the order of 10 kHz [20, 21], references such as [13] have implied that time-delays of MMCs could be much longer, sometimes lying in the range of 400-600 μs , a difference explained by the increased complexity of controlling the numerous MMC submodules.

Time delays such as those encountered in MMCs are largely responsible for a specific characteristic at high frequencies, called *non-passivity* [22]. As non-passivity can lead to instabilities and undesired oscillations, delays must be

included in converter models to perform accurate stability assessments [19, 23]. However, not unlike the internal oscillatory quantities of the MMC, time delays have often been either disregarded or simplified, thereby leading to reduced modelling accuracies. Given the recent occurrence of delay-induced instabilities in MMC-based systems [13] (see also the presentation of real-life interaction events in the following section), there is a growing need for enhanced modelling of time delays and more precise analyses of their impact on stability. This thesis addresses the combined challenge of accounting for the potentially large delays of the MMC when studying the small-signal stability of its time-periodic trajectories.

Examples of problematic real-life events

Many problematic real-life events involving power-electronic converters have been reported from the industry over the last decades. Such events have been caused by various triggers or disturbances such as faults, variations of power generation or consumption, the energisation of transformers or the switching of transmission lines. Through specific mechanisms detailed in [8], such triggers have led to voltage, current and frequency deviations outside their acceptable range of values, but also to undesired and sometimes growing oscillations at frequencies both below and above the fundamental frequency. At times, these phenomena have caused interruptions of operation of power-electronic converters, power plants, and even large synchronous areas.

In particular, technical report [24] covers an event which occurred in the United Kingdom in 2019, where a lightning strike on a transmission line triggered an "unexpected wind farm control system response" at the Hornsea offshore wind farm (OWF). It was later shown that this adverse response was due to an "insufficiently-damped electrical resonance" in the subsynchronous frequency range. The oscillations caused the OWF to trip when the over-current limit was reached, and 737 MW of wind power generation were lost. Simultaneously, the lightning strike had impacted traditional onshore power plants which tripped as well. The total generation loss of nearly 1.7 GW eventually resulted in a blackout, which impacted an estimated 1.1 million people.

Interactions involving VSC-HVDC-connected offshore wind farms

Whereas the Hornsea OWF from the previous example is connected to shore via AC transmission, OWFs are increasingly installed worldwide with VSC-HVDC connections to shore, which also face unexpected control responses and adverse

interactions. For instance, [25] refers to a case of unstable oscillations at a German HVDC link connecting OWFs in the North Sea. While a first OWF was in normal operation, AC cables were switched on to connect a second OWF to the same HVDC station. This switching operation immediately lead to growing 451 Hz oscillations. The mechanisms behind such unstable supersynchronous behaviour were studied in [26] and [27] concerning the BorWin1 and DolWin1 HVDC links, respectively. These studies identify possible control interactions between the HVDC converter and the wind turbines as a major challenge in the connection of OWFs to shore. The authors of [27] emphasise the importance of tuning the controllers of both HVDC and wind turbine converters in a way that oscillations be damped, or at least not amplified, would the converters start interfering with them.

The events described in [28] and [29] are also concerned with VSC-HVDC links connecting OWFs. In the first reference, the authors describe a situation in which the offshore VSC entered a blocking state, causing a temporary islanding (i.e. isolated operation) of the OWF. The islanded OWF being left without frequency control and with only negligible local load, the voltage started to rise with peaks up to 1.3 pu. Simultaneously, a natural resonance involving the saturated transformer inductances and cable capacitances was triggered, which led to current oscillations near 830 Hz. The controllers of both the HVDC converter and wind turbine converters appeared to be involved in this interaction.

Interactions involving onshore VSC-HVDC systems

Aside from the previous events, which were concerned with the VSC-HVDC connection of OWFs, other cases of interactions involving onshore VSC-HVDC systems were reported in the past years. In the event described in [29], an instability occurred after a busbar was decoupled at the onshore HVDC station of an offshore link in Germany, which modified the impedance of the AC grid as seen from the VSC. This resulted in sustained 1.5 kHz current oscillations. A similar configuration was the scene of subsynchronous oscillations during the testing phase of the Nanhui MMC-based HVDC link in China [15].

In [14], the authors describe a 1.7 kHz oscillation which led to tripping of the Inelfe MMC-based VSC-HVDC link between France and Spain. The phenomenon was described as an "interaction between the HVDC link and the surrounding AC network". Post-event analysis relying on control replicas showed that the control instability depended on both the AC line parameters and the AC grid configuration.

Similarly, references [13, 30] refer to 1.27 kHz oscillations observed at the Luxi asynchronous back-to-back HVDC link which interconnects the provinces of Yunnan and Guangxi in China. The back-to-back system is composed of one MMC-based VSC-HVDC link in parallel with two line-commutated HVDC links. The high-frequency oscillations occurred when the line-commutated converters were shut down. Their passive AC filters were disconnected and only one out of three AC lines was in service at the Guangxi side. The instability seemed to have been caused by non-passivity of the MMC due to its control delay and the instantaneous voltage feedforward of its AC current controller. The resulting harmonics led to an increased operation of the AC transformer tap changer, which then had to be taken out-of-service for maintenance.

Furthermore, [15] mentions a case of high-frequency oscillations (above 1 kHz) at the Zhoushan multiterminal VSC-HVDC grid in China. The oscillations occurred when one of the five terminals was switched from grid-connected to islanded control mode.

While the events described so far were concerned with interactions at the AC-side of power-electronic converters, cases of DC-side interactions have also started to appear. For instance, references [31, 32] report cases of 23.6 Hz, 25.2 Hz and 550 Hz oscillations at the DC side of the Xiamen MMC-based bipolar HVDC project in China. In [33], an analysis of the latter event reveals that the cause of the 550 Hz oscillations was an interaction between control loops of the MMCs and natural resonances related to the 10 km-long DC cables and their smoothing reactors.

Discussion

Although not exhaustive², the selection of described interaction events provides evidence for the reality of adverse interactions involving HVDC converters in general, and the MMC in particular, leading to sustained or growing oscillations from subsynchronous frequencies up to the kilohertz range. Such phenomena, which depend on both converter control tuning, grid characteristics and operating modes, require detailed analyses to identify and mitigate the risk of control interactions. This thesis addresses the challenge of developing new methods suitable for the accurate analysis of MMC-based HVDC systems.

² The interested reader is referred to published article [8] and references therein. The work presented in [8] was carried out as part of this doctoral research and provides a comprehensive overview of real-life problematic events involving power-electronic converters, as well as a classification of underlying mechanisms. See also the List of Publications.

Research questions and objectives

In general terms and in light of the context described in the rationale, this thesis is primarily concerned with developing mathematical frameworks capable of carrying out accurate studies of electrical power systems involving the MMC in HVDC applications such as the connection of OWFs to shore. Specifically, there is a need to continue extending the application of small-signal stability assessments to the trajectories of nonlinear systems whose variables contain multiple frequency components in steady state, while bearing in mind the importance of accounting for control dynamics and time delays which largely impact the stability properties of converter-based systems.

In this section, research questions are formulated precisely and naturally provide a clear pathway towards defining the research objectives of this thesis. Key foundational ideas are briefly introduced to provide an overview of the thought process, however a more comprehensive presentation of the most relevant concepts will be provided in the subsequent chapters.

Addressing time periodicity

As mentioned in the rationale, the working principle of the MMC implies that several internal voltages and currents present multiple harmonic components in steady state. These oscillatory components can be seen as the consequence of the periodic excitation of this converter's nonlinear dynamics, where the periodic excitation is essentially related to the connection to an AC system. The calculation of the resulting harmonic components is particularly important as it is a prerequisite to efficiency estimation and component sizing, but also to performing accurate stability assessments. On the one hand, identifying constant operating points of dynamic systems is a well known calculation which, for state-space representations, is immediately equivalent to solving a set of algebraic equations. When it comes to identifying periodic trajectories, the time-dependency of variables implies that their time derivatives are non-zero and remain part of the set of equations to be solved, hence the relative simplicity of the original problem is lost. This leads to the following research question:

Research Question 1. *How can we calculate periodic trajectories of nonlinear systems subject to periodic inputs?*

In the literature, various approaches have been introduced for the calculation of periodic trajectories. As far as electrical power systems are concerned, many methods take their roots in the context of harmonic studies. In such studies, converters and other nonlinear devices have traditionally been represented by

sources of harmonic currents and, lacking more appropriate and sufficiently efficient calculation methods, couplings across frequencies have often been disregarded, with as direct consequence the impossibility of properly reflecting the impact of nonlinearity onto the calculated waveforms. In this context, two objectives are proposed:

Objective 1a. *To review existing methods dedicated to the calculation of periodic trajectories of nonlinear systems such as the MMC, to describe their strengths and identify their limitations.*

Objective 1b. *To propose an improved method for the calculation of periodic trajectories of the MMC, overcoming the limitations of current methods.*

Once the steady-state harmonic spectrum of internal MMC quantities is known, analysing the small-signal stability of the corresponding periodic trajectory is enabled by linearising the differential equations around that trajectory. First, it is noted that linearisation around a constant operating point results in a local linear time-invariant (LTI) approximation, on which the application of traditional methods from LTI systems theory informs about stability of the original equilibrium. On the other hand, linearisation around a periodic trajectory results instead in a local linear time-periodic (LTP) approximation. The fact that the aforementioned traditional methods are not directly applicable to the study of LTP systems prevents a direct stability assessment of the original periodic trajectory and leads to the following research question:

Research Question 2. *How can we analyse the small-signal stability of periodic trajectories of the MMC?*

As far as small-signal stability analyses are concerned, three transformation and approximation approaches allow addressing the periodic aspect of the considered trajectories. The first approach consists in transforming the LTP approximation—which results from linearising around the periodic trajectory—into an equivalent LTI approximation. The second approach consists in transforming the periodic trajectory *itself* into a constant operating point, thereby avoiding linearisation around a periodic trajectory in the first place [34]. In both cases, the concept of transformation is instrumental to the small-signal stability analysis of periodic trajectories by means of traditional methods. Yet, it is at times unclear which transformation methods can be used for which types of systems and under which assumptions. For this reason, the following objective is proposed:

Objective 2. *To review existing methods dedicated to the transformation of nonlinear systems operating along periodic trajectories into linear time-invariant systems, for the eventual purpose of carrying out small-signal stability assessments.*

A third possible option is the one that was originally considered for the MMC, which consisted in simply neglecting harmonic components within its variables, or similarly, neglecting the harmonic components in the coefficients of the resulting LTP approximation. This leads to the following research question:

Research Question 3. *Can we draw reliable conclusions from small-signal stability analyses when harmonic components in the coefficients of linearised time-periodic approximations are simply neglected?*

Intuitively, sufficiently small harmonic components could technically be seen as small perturbations of an otherwise harmonic-free trajectory, and could thus be safely neglected without impacting the outcome of the stability assessment. The difficulty is naturally to determine when an oscillatory component is indeed sufficiently small to be neglected. The following objective is proposed to address this challenge:

Objective 3. *To establish a mathematical criterion capable of determining whether the oscillatory components of the coefficients of LTP systems are sufficiently small to be neglected in the context of a small-signal stability assessment.*

Addressing time delays

As also mentioned in the rationale, the controlled MMC does not only follow a time-periodic trajectory in steady state, but also displays a time-delayed behaviour, which is susceptible to lead to instabilities and undesired high-frequency oscillations. To carry out accurate stability assessments, it is therefore necessary to account for the time-delayed behaviour of the system. While it is rather straightforward to account for delays in frequency-domain models, frequency-domain analyses may lack the insights of time-domain modal analyses. In the time domain, however, the presence of exact delay representations hinders traditional eigenvalue calculations, in particular because there is not only one but multiple matrices that describe the relationship between the state variables, their time derivatives and their past values. To still make the calculation of eigenvalues possible, common approximations of the exact delays are often used. For instance, the Padé approximation allows transforming delay differential equations into ordinary differential equations (i.e. differential equations without delays), which solves the problem. However, Padé approximations are inaccurate at high frequencies, precisely where delays typically cause non-passivity and where exact delay representations are of interest for precise stability assessments. This leads to the following research question:

Research Question 4. *How can we account for the time-delayed behaviour of the MMC in the eigenvalue-based small-signal stability assessment of its periodic trajectories, without relying on Padé approximations?*

In the case of the MMC, the challenge is to perform a modal analysis of a delayed system while also accounting for the periodic characteristics of its linear approximations. Two main types of methods are identified: those dedicated to delayed LTP systems and those dedicated to delayed LTI systems. Naturally, the second category of methods is only applicable to the MMC after having transformed its local LTP approximations into LTI approximations. Yet, such preliminary transformation into an LTI representation is advantageous as it also enables the application of transfer-function-based stability assessments. For this reason, the second category of methods is explored in this thesis.

Amongst existing methods for the transformation of LTP systems into LTI systems, Objective 2 will help identifying the harmonic state space as a particularly suitable framework for the MMC. However, the current formulation of the harmonic state space does not account for delays. Consequently, the following objective is introduced:

Objective 4. *To generalise the original harmonic state-space method for the transformation of LTP delay-differential equations into LTI delay-differential equations.*

The aim of this thesis is to fulfil Objectives 1a to 4, thereby bringing answers to their corresponding Research Questions.

Outline and contributions of the thesis

The remainder of this thesis is composed of five chapters and a conclusion, which are organised as follows:

- **Chapter 1,** entitled **Converter modelling and fundamentals of stability analysis**, introduces the differential equations used to model the MMC and its controller. After identifying the main characteristics of the model and observing its typical steady-state waveforms, the concepts of linearisation, LTI and LTP systems are presented along with the fundamentals of small-signal stability analysis based on eigenvalues and transfer functions. It is explained why the latter techniques from LTI systems theory are not directly applicable to LTP systems, which motivates the presentation of calculation and transformation methods enabling the small-signal stability assessment of periodic trajectories.

- **Chapter 2**, entitled **Non-lifting transformation methods**, begins with a review of the Floquet-Lyapunov theory for LTP systems, with particular attention dedicated to the concept of monodromy matrix and to the Floquet transformation, both of which offer fundamental insights into the stability properties of LTP systems.

Next, an averaging technique is considered to obtain LTI approximations of LTP systems by simply neglecting the oscillatory part of their periodic coefficients. In this context, a mathematical criterion is developed to determine whether and when these oscillatory components are indeed sufficiently small to be neglected in a stability assessment. Developing this criterion is an original contribution of this thesis. Its application to models of the two-level VSC and of the MMC further motivate the need for transformation methods that do account for oscillatory components in the coefficients of LTP systems.

Lastly, the technique of frame rotations is presented and the assumptions under which they are able to transform periodic trajectories into equilibria are identified. The conclusions motivate the introduction of even more general methods applicable to a wider set of operating conditions.

- **Chapter 3**, entitled **Frequency-lifting transformation methods**, presents the technique of frequency-lifting as well as the underlying harmonic balance principle, which are described in detail through different forms such as the harmonic state-space representation, the harmonic linearisation technique as well as the harmonic transfer function representation. In particular, the presentation of the harmonic transfer function as a generalised formulation of the harmonic linearisation technique is an original contribution of this thesis.

The relationships between different lifting and non-lifting methods are also highlighted. It is emphasised that, unlike the harmonic transfer function, which is capable of accounting for exact delays in the frequency domain, the original harmonic state-space method is only applicable to systems without exact delay representations. This motivates extending the application of the harmonic state-space approach to delayed systems in the following chapter.

- **Chapter 4**, entitled **Modal analysis of frequency-lifted delayed systems**, reviews the fundamentals of delayed systems and introduces a generalisation of the harmonic state-space formulation capable of accounting for both time-periodic and time-delayed behaviours of linearised MMC models. The generalised delayed harmonic state space (DHSS) is an original contribution of this thesis. It enables the application of both modal and transfer-function-based analyses in a unique framework without

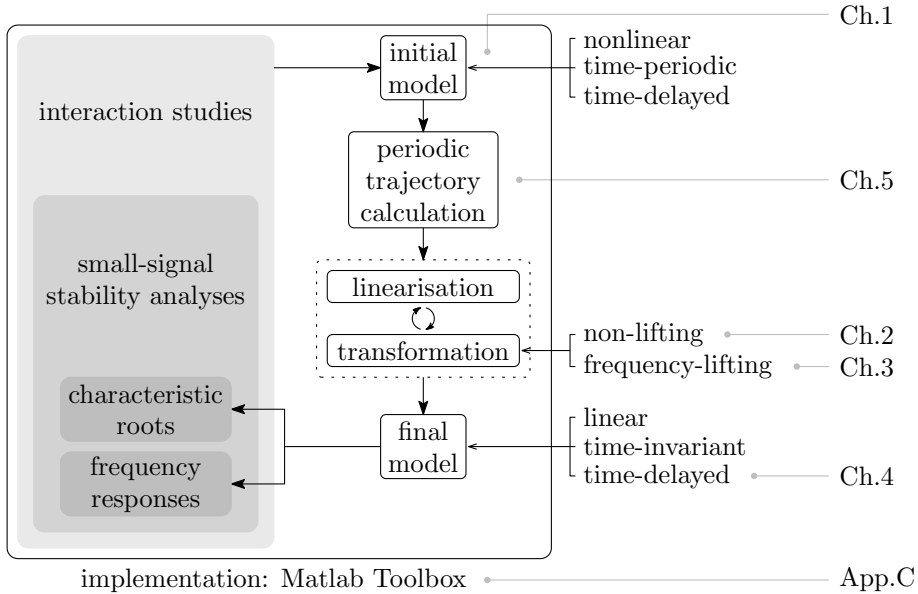


Figure 1: Thesis structure

requiring the approximation of delayed dynamics by means of ordinary differential equations.

- **Chapter 5**, entitled **Calculation of periodic trajectories**, addresses a fundamental prerequisite of Chapters 2 to 4 and reviews existing methods dedicated to the calculation of periodic trajectories of nonlinear delayed systems. The fundamentals of traditional frequency-domain and hybrid-domain methods are provided. Next, a Fourier-based collocation method is developed to address challenges touching upon the MMC specifically, which is an original contribution of this thesis. The results are validated against an independent integration-based approach and the calculation times are compared with a state-of-the-art shooting method. The advantages and limitations of the Fourier-based collocation method are highlighted.
- **The conclusion** summarises the main contributions and outcomes of the thesis, and provides recommendations for future work.

The structure of the thesis is shown in Fig. 1. In the context of interaction studies and small-signal stability analyses, Chapter 1 starts with a description of a stationary-frame model of the MMC. The following chapters establish the necessary building blocks towards transforming this initial nonlinear time-

periodic model into a linearised time-invariant model which supports the calculation of eigenvalues/characteristics roots and frequency responses. After determining steady-state trajectories of the dynamic system (Chapter 5), linearisation and transformations are used to respectively address nonlinearity and time-periodicity. It is emphasised that linearisation may be applied before or after a transformation, depending on the nature of the latter. Both non-lifting transformations (Chapter 2) and frequency-lifting transformations (Chapter 3) are covered. The remaining time-delayed property is addressed in Chapter 4.

It is noted that, although the calculation of periodic trajectories is a prerequisite to the linearisation and transformation steps, its topic is covered last, in Chapter 5. The main motivation for this choice is that the Fourier-based collocation method is described more straightforwardly after having covered the principles of frequency-lifting in Chapters 3 and 4. Consequently, when covering the topic of transformation methods, it will be assumed that the relevant periodic trajectories are known *a priori* and, unless otherwise stated, all periodic trajectories involved in numerical applications throughout Chapters 2 to 4 are obtained by means of the Fourier-based collocation method described in Chapter 5.

The content provided in Chapters 1 to 5 is supported by the following appendices.

Appendix A: Supporting content on transformations

- **Appendix A.1** gives a short didactic presentation of the concepts of sequences in three-phase systems as well as harmonic components, both notions appearing repeatedly throughout the thesis. The presentation relies on an analogy, which is an original contribution of this thesis.
- **Appendix A.2** describes the Clarke transformation, frame rotations and Park transformation used when modelling the MMC in Chapter 1 as well as in the discussion of frame rotations in Chapter 2. The Fortescue transformation used to calculate the sequence content of three-phase variables is also presented.

Appendix B: Supporting content on modelling

- **Appendix B.1** completes the description of the MMC controller, initiated in Section 1.2.3, with remaining loops for the direct voltage, alternating voltage and circulating current controllers.
- **Appendix B.2** describes the tuning of the MMC control loops presented in Section 1.2.3 and Appendix B.1.

- **Appendix B.3** describes models of a two-level VSC and its controller, which are used in the thesis as illustrative examples.
- **Appendix B.4** describes the model of a point-to-point MMC-based HVDC link connecting an offshore grid composed of three aggregated offshore wind farms. This test system and its sub-circuits are used throughout the thesis as illustrative examples.
- **Appendix B.5** provides the analytical expressions of the partial derivatives of a simplified single-phase MMC model given in Section 1.2.5.

Appendix C: Supporting content on implementation

- **Appendix C.1** briefly presents the Matlab toolbox developed as part of this thesis, which implements a selection the theoretical concepts covered in the main chapters. The toolbox supports the identification and small-signal stability analysis of periodic trajectories, relying on the Fourier-based collocation method for steady-state trajectory calculations and on frequency-lifting as main transformation method. Beyond automating the aforementioned calculations, this original contribution aims to lay the foundations of future software tools supporting steady-state harmonic as well as dynamic studies of modern power systems, benefiting both academic research and industry stakeholders. The toolbox also fosters replicability of the results presented in this thesis.
- **Appendix C.2** provides a high-level presentation of the selected approaches to the numerical integration of differential equations in Matlab. The presentation covers both cases of ordinary and delay differential equations.

Chapter 1

Converter modelling and fundamentals of stability analysis

1.1 Introduction

Although models transformations and periodic trajectories calculations find applications in many fields of science and engineering, the MMC is the main driver for their presentation in this thesis. Hence, this first chapter is dedicated to presenting a model of the MMC and of its controller.

Section 1.2 presents the operating principle of the MMC and provides the so-called *arm-averaged* differential equations describing the dynamic behaviour of its electrical circuit, also referred to as its *power stage*. A representative control structure is described and its differential equations are given before identifying the main characteristics of the complete system. Lastly, a simplified single-phase MMC model is introduced as one of the illustrative examples used throughout the thesis. Section 1.3 sets the MMC model in a more general context by distinguishing linear from nonlinear systems, time-invariant from time-varying systems as well as constant operating points from periodic trajectories. Next, the fundamentals of stability analysis of both LTI and LTP systems are introduced. In particular, it is shown that traditional stability techniques dedicated to LTI systems cannot be directly applied to LTP systems, which highlights the need to address the periodic nature of the MMC's dynamic behaviour.

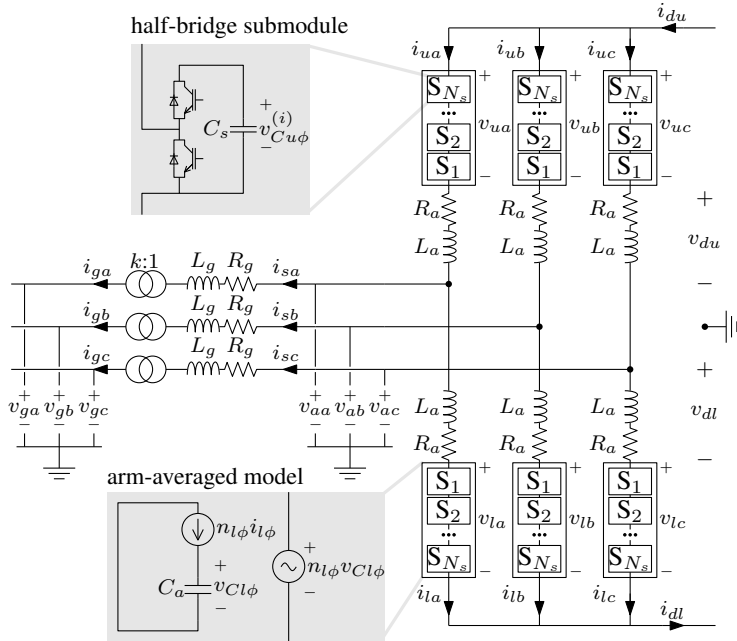


Figure 1.1: MMC circuit diagram

1.2 Modular multilevel converter modelling and control

The three-phase MMC is composed of three legs identified as $\phi \in \{a, b, c\}$, as shown in Fig. 1.1. Each leg comprises an upper arm (u) and a lower arm (l), and each arm comprises a string of N_s submodules (S_1, \dots, S_{N_s}) consisting of a capacitor and semiconductor switches. The case of half-bridge submodules is considered, which contain two semiconductor switches and one capacitor. During normal operation, the switches are controlled to either insert the capacitor within the arm or to bypass it. When a submodule capacitor is inserted, its voltage contributes to the overall voltage across the arm. The upper- and lower-arm inserted voltages $v_{u\phi}, v_{l\phi}$ are expressed as

$$v_{u\phi} = \sum_{i=1}^{N_s} n_{u\phi}^{(i)} v_{Cu\phi}^{(i)} \quad v_{l\phi} = \sum_{i=1}^{N_s} n_{l\phi}^{(i)} v_{Cl\phi}^{(i)}, \quad (1.1)$$

where $n_{u\phi}^{(i)}, n_{l\phi}^{(i)}$ are the i th submodules insertion indices, equal to 1 in inserted mode and to 0 in bypass mode, and where $v_{Cu\phi}^{(i)}, v_{Cl\phi}^{(i)}$ are the corresponding

i th submodules capacitor voltages within the upper and lower arms of phase ϕ , respectively.

Naturally, the inserted capacitors are charged or discharged depending on the direction of the arm currents $i_{u\phi}$ and $i_{l\phi}$. In practice, the string of submodules is placed in series with an arm reactor of inductance L_a to limit the switching transients. Moreover, in mathematical models, an equivalent arm resistance R_a is included to represent the semiconductor losses. The top and bottom ends of the legs meet at the positive and negative DC poles respectively, which have voltages v_{du} and $-v_{dl}$ with respect to the ground. Finally, the mid-point of each leg is connected to the three-phase AC grid via a transformer represented by its series components, i.e. the leakage inductance L_g and winding resistance R_g . The AC grid voltage and legs mid-point voltage are noted $v_{g\phi}$ and $v_{a\phi}$ with respect to the ground.

Assumptions and simplifications

Several typical assumptions are introduced to facilitate the modelling of the MMC and of its connection to the AC grid.

Assumption 1. *The three-phase transformer winding configuration is a star-star ($Y-Y$) connection.*

Under Assumption 1, the transformer does not introduce phase-shifting of currents and voltages between its sides. Consequently, it can be represented by three single-phase transformers with a transformation ratio noted k .

Assumption 2. *The neutral point of the star (Y) connection is not grounded at the converter side.*

Under Assumption 2, no zero-sequence currents¹ flow between the converter and the AC grid.

Assumption 3. *The submodules switching dynamics are negligible and an ideal sorting algorithm² determines the status of each submodule (inserted or*

¹ A didactic presentation of sequence components in a three-phase system is given in Appendix A.1.

² During the process of modulating the inserted arm voltage, a selection of submodules are inserted in the arm. Their voltages increase or decrease depending on the direction of the arm current, while the voltage of bypassed capacitors remains roughly constant. To maintain the voltage of all submodule capacitors close to nominal value, the capacitors with lowest voltage should be inserted in priority for charging arm currents, while those with the largest voltage should be inserted in priority for discharging arm currents. This explains the need for a dedicated sorting algorithm [12, Ch.5].

bypassed). The submodules voltages $v_{Cu\phi}^{(i)}$, $v_{Cl\phi}^{(i)}$ are perfectly balanced within their respective strings.

Under Assumption 3, the upper- and lower-arm sum-capacitor voltages can be defined³ and then approximated as:

$$v_{Cu\phi} \triangleq \sum_{i=1}^{N_s} v_{Cu\phi}^{(i)} \approx N_s v_{Cu\phi}^{(i)}, \quad v_{Cl\phi} \triangleq \sum_{i=1}^{N_s} v_{Cl\phi}^{(i)} \approx N_s v_{Cl\phi}^{(i)}. \quad (1.2)$$

To describe the proportion of sum-capacitor voltages inserted within the arms, upper- and lower-arm insertion indices are defined as:

$$n_{u\phi} \triangleq \frac{1}{N_s} \sum_{i=1}^{N_s} n_{u\phi}^{(i)}, \quad n_{l\phi} \triangleq \frac{1}{N_s} \sum_{i=1}^{N_s} n_{l\phi}^{(i)}. \quad (1.3)$$

Consequently, the arm-inserted voltages in (1.1) can be rewritten as:

$$v_{u\phi} = \sum_{i=1}^{N_s} \frac{n_{u\phi}^{(i)}}{N_s} N_s v_{Cu\phi}^{(i)} = n_{u\phi} v_{Cu\phi} \quad (1.4a)$$

$$v_{l\phi} = \sum_{i=1}^{N_s} \frac{n_{l\phi}^{(i)}}{N_s} N_s v_{Cl\phi}^{(i)} = n_{l\phi} v_{Cl\phi}. \quad (1.4b)$$

Assumption 4. The number of submodules in each arm is sufficiently large for the step between two discrete voltage levels to be negligible.

Under Assumption 4, the insertion indices $n_{u\phi}, n_{l\phi}$ take continuous values between 0 and 1. In summary, the string of submodules is approximated by a single perfectly-modulated submodule without switching harmonics and with equivalent capacitance C_a , obtained as:

$$C_a = \frac{C_s}{N_s} \quad (1.5)$$

with C_s the individual submodules capacitance. The simplified model of the chains of submodules that results from Assumptions 3 and 4 is referred to as the *arm-averaged* model.

³ While the sum-capacitor voltages are commonly written $v_{Cu\phi}^{\Sigma}$ and $v_{Cl\phi}^{\Sigma}$, the Σ notation is discarded in this thesis to keep the notation simple.

1.2.1 Circuit differential equations

The application of Kirchhoff's laws to the circuit in Fig. 1.1 results in the differential equations that describe the dynamics of arm currents $i_{u\phi}$, $i_{l\phi}$, transformer current $i_{s\phi}$ and sum-capacitor voltages $v_{Cu\phi}$, $v_{Cl\phi}$ for each phase $\phi \in \{a, b, c\}$ [12]:

$$\left. \begin{aligned} L_a \frac{di_{u\phi}}{dt} &= -R_a i_{u\phi} - v_{u\phi} + v_{du} - v_{a\phi} \\ L_a \frac{di_{l\phi}}{dt} &= -R_a i_{l\phi} - v_{l\phi} + v_{dl} + v_{a\phi} \end{aligned} \right\} \quad (1.6a)$$

$$L_g \frac{di_{s\phi}}{dt} = -R_g i_{s\phi} + v_{a\phi} - \frac{1}{k} v_{g\phi} \quad (1.6c)$$

$$C_a \frac{dv_{Cu\phi}}{dt} = n_{u\phi} i_{u\phi} \quad (1.6d)$$

$$C_a \frac{dv_{Cl\phi}}{dt} = n_{l\phi} i_{l\phi}. \quad (1.6e)$$

The above system can be simplified by taking the sum and difference of (1.6a) and (1.6b), and by using (1.6c) to eliminate the legs mid-point voltages. Additionally, upper- and lower-arm quantities are generally expressed in terms of their common mode (CM) and differential mode (DM) values: for each leg, the CM inserted voltage $v_{c\phi}$, DM inserted voltage $v_{s\phi}$, CM arm current $i_{c\phi}$, and DM arm current $i_{s\phi}$ are defined as [12]:

$$v_{c\phi} \triangleq \frac{v_{l\phi} + v_{u\phi}}{2} \quad v_{s\phi} \triangleq \frac{v_{l\phi} - v_{u\phi}}{2} \quad (1.7a)$$

$$i_{c\phi} \triangleq \frac{i_{u\phi} + i_{l\phi}}{2} \quad i_{s\phi} \triangleq i_{u\phi} - i_{l\phi}. \quad (1.7b)$$

Similar considerations are applied to the quantities at the DC side: the CM direct voltage v_d , DM direct voltage v_d^Δ , CM direct current i_d , and DM direct current i_d^Δ are defined as:

$$v_d \triangleq v_{du} + v_{dl} \quad v_d^\Delta \triangleq v_{du} - v_{dl} \quad (1.8a)$$

$$i_d \triangleq \frac{i_{du} + i_{dl}}{2} \quad i_d^\Delta \triangleq i_{du} - i_{dl}, \quad (1.8b)$$

where i_d and i_d^Δ are related to the AC-side CM and DM arm currents by:

$$i_d = \sum_{\phi=a,b,c} i_{c\phi} \quad i_d^\Delta = \sum_{\phi=a,b,c} i_{s\phi} = 3i_{sz}. \quad (1.9)$$

In this thesis, the DM arm current $i_{s\phi}$, which corresponds to the transformer current, is referred to as the *alternating current*, while the CM arm current $i_{c\phi}$ is referred to as the *circulating current*. Moreover, the CM direct voltage v_d and CM direct current i_d are simply referred to as the *direct voltage* and *direct current*, respectively. Lastly, in (1.9), i_{sz} corresponds to the zero-sequence component of the alternating currents.

Relying on the above, system (1.6) becomes:

$$\left\{ \begin{array}{l} L_e \frac{di_{s\phi}}{dt} = -R_e i_{s\phi} + v_{s\phi} - v_{g\phi} + \frac{v_d^\Delta}{2} \end{array} \right. \quad (1.10a)$$

$$\left\{ \begin{array}{l} L_a \frac{di_{c\phi}}{dt} = -R_a i_{c\phi} - v_{c\phi} + \frac{v_d}{2} \end{array} \right. \quad (1.10b)$$

$$\left\{ \begin{array}{l} C_a \frac{dv_{Cu\phi}}{dt} = n_{u\phi} \left(i_{c\phi} + \frac{i_{s\phi}}{2} \right) \end{array} \right. \quad (1.10c)$$

$$\left\{ \begin{array}{l} C_a \frac{dv_{Cl\phi}}{dt} = n_{l\phi} \left(i_{c\phi} - \frac{i_{s\phi}}{2} \right), \end{array} \right. \quad (1.10d)$$

where $L_e = L_g + L_a/2$ and $R_e = R_g + R_a/2$ are referred to as the equivalent AC-side inductance and resistance. It is emphasised that the DM and CM inserted voltages are functions of states and control variables:

$$v_{s\phi} = \frac{1}{2}(n_{l\phi}v_{Cl\phi} - n_{u\phi}v_{Cu\phi}), \quad v_{s\phi} = \frac{1}{2}(n_{l\phi}v_{Cl\phi} + n_{u\phi}v_{Cu\phi}). \quad (1.11)$$

Clarke transformation, described in Appendix A.2, is applied to (1.10a) to separate the zero-sequence dynamics from the positive and negative sequences:

$$\left\{ \begin{array}{l} L_e \frac{di_{s\varphi}}{dt} = -R_e i_{s\varphi} + v_{s\varphi} - v_{g\varphi} \end{array} \right. \quad (1.12a)$$

$$\left\{ \begin{array}{l} L_e \frac{di_{sz}}{dt} = -R_e i_{sz} + v_{sz} - v_{gz} + \frac{v_d^\Delta}{2}, \end{array} \right. \quad (1.12b)$$

with $\varphi \in \{\alpha, \beta\}$ referring to the coordinates in an orthogonal $\alpha\beta$ frame of reference, and z referring to the zero-sequence component. As a consequence of Assumption 2, the zero-sequence current i_{sz} in (1.12b) is equal to zero, and so is its time derivative. Eq. (1.12b) becomes an algebraic relationship between the voltages: $v_{gz} = v_{sz} + v_d^\Delta/2$.

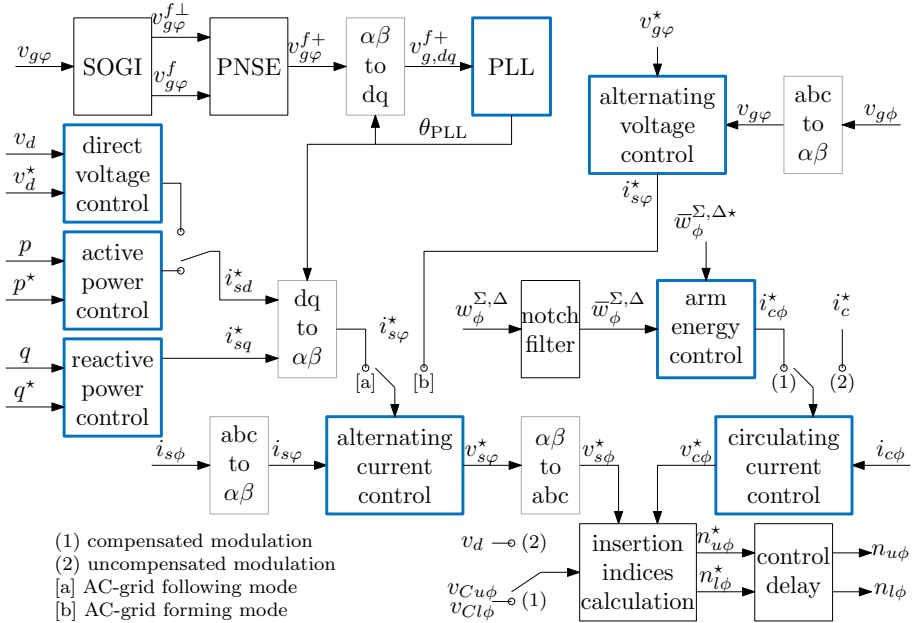


Figure 1.2: Overview of MMC control structure, with control blocks in blue, changes of variables and frame rotations in grey, filters and other calculations in black.

1.2.2 Overview of MMC control

To operate within a power system and to satisfy a number of conditions related to objectives, performance and stability (which are detailed in this section), the power stage of the MMC is controlled according to a set of control laws. Although there are countless approaches to the control of the MMC, a typical scheme relying on cascaded feedback loops is presented in this section.

The inputs of the controller are the measured currents, measured voltages, and the control references. The outputs of the controller are the insertions indices $n_{u\phi}$, $n_{l\phi}$. Among classical cascaded controllers of the MMC, two main approaches exist for the calculation of the insertion indices: the uncompensated and the compensated modulations, which are described in [12, Ch.3] under the names of Direct Voltage Control and Closed-Loop Voltage Control, respectively. These modulation strategies are taken into account in Fig. 1.2 and are summarised here.

In the uncompensated modulation, the reference insertion indices are calculated as:

$$n_{u\phi}^* = \frac{v_{c\phi}^* - v_{s\phi}^*}{v_d} \quad n_{l\phi}^* = \frac{v_{c\phi}^* + v_{s\phi}^*}{v_d}, \quad (1.13)$$

where the star notation refers to a reference quantity, and where $v_{c\phi}^*$ and $v_{s\phi}^*$ are the CM and DM inserted voltage references. Their sum and difference are normalised by the direct voltage v_d . This approach does not require a dedicated arm-energy controller, however it leads to second-harmonic oscillations in the circulating currents, which are customarily removed with a dedicated second-harmonic suppression control loop.

In the compensated modulation, the reference insertion indices are calculated as:

$$n_{u\phi}^* = \frac{v_{c\phi}^* - v_{s\phi}^*}{v_{Cu\phi}} \quad n_{l\phi}^* = \frac{v_{c\phi}^* + v_{s\phi}^*}{v_{Cl\phi}}, \quad (1.14)$$

where the sum-capacitor voltages $v_{Cu\phi}$ and $v_{Cl\phi}$ are used for normalisation. Unlike the uncompensated modulation, this scheme requires additional control loops to regulate the energy within the arms. This task is typically achieved by means of arm energy controllers.

Both the compensated and uncompensated modulation approaches involve CM and DM inserted voltage references. These references are the result of cascaded control loops, which are below outlined for several modes of operation.

- Through their ability to separately vary the phase angle and the magnitude of the legs mid-point voltages (which are approximately equal to the DM inserted voltage v_s), VSCs are capable of independently regulating the active and reactive powers flowing through their AC connection. Acting on these powers can contribute to directly or indirectly regulate other quantities within the electrical environment of the converter, for instance the magnitude and phase angles of the alternating voltage $v_{g\phi}$, the magnitude of the direct voltage v_d and, when relevant, even influence the fundamental AC grid frequency. For the illustrative systems considered in this thesis, only three specific cases are encountered, with the objective of controlling:
 1. the active power and the reactive power;
 2. the direct voltage magnitude and the reactive power;
 3. the magnitude and phase angle of the alternating voltage.

The first two cases, in which the converter does not actively control the alternating voltage, are referred to as *AC-grid-following modes*. This is unlike the third case, which is referred to as an *AC-grid-forming mode*. This mode is considered for instance when the MMC acts as a voltage source for an otherwise isolated grid. In this thesis, the frequency of the alternating voltage is kept constant.

- According to Fig. 1.2, in the AC-grid-following modes, the active power, reactive power and direct voltage controllers generate alternating current references in an orthogonal frame rotating at the fundamental grid frequency⁴. The resulting direct and quadrature (dq) current components are transformed into $\alpha\beta$ components based on the phase angle of the positive-sequence alternating voltage at fundamental frequency, which is determined by a phase-locked loop (PLL). In the AC-grid-forming mode, the alternating voltage controller generates directly the $\alpha\beta$ components of the alternating current references.
- The fundamental-frequency positive-sequence alternating voltage, whose phase angle is measured by the PLL, is obtained via two successive steps. First, the measured alternating voltage is processed with a second-order generalised integrator (SOGI), which acts both as a band-pass filter and as an *in-quadrature* voltage generator, i.e. it also provides a duplicate alternating voltage that lags the original by 90° . Next, the filtered and in-quadrature voltages are used to separate the positive sequence from the negative sequence of the voltage in a dedicated positive and negative sequence extraction (PNSE).
- The alternating current controller regulates the error between the actual alternating currents and their references, and generates the DM inserted voltage references in the $\alpha\beta$ frame. The resulting $\alpha\beta$ components are transformed into abc components by means of an inverse Clarke transformation.
- In parallel with the above-described steps, circulating current references are defined according to whether a compensated or an uncompensated modulation is chosen. The circulating current controller regulates the error between the actual circulating currents and their references, and generates the CM inserted voltage references directly in the abc frame.

⁴ See Appendix A.2 for a brief introduction to rotating frames.

1.2.3 Control differential equations

The following paragraphs are dedicated to presenting the control equations more specifically. To enhance clarity, both transfer functions and state-space representations are given. In the state-space representations, control state variables are indicated by the letter η as well as appropriate subscripts.

To keep this section reasonably short, the equations of the direct voltage, alternating voltage and circulating current controllers are provided in Appendix B.1. The tuning of the control loops and all circuit and control parameters are provided in Appendix B.2.

Alternating voltage filter

Feedback loops within the controller rely on comparing measured quantities with their references. To involve only the relevant components of the measured quantities in the comparison, noise and other parasitic components are filtered out. Although all measured quantities are normally filtered before use, only the alternating voltage filter is explicitly included here.

The alternating voltage $v_{g\varphi}$ is filtered in the $\alpha\beta$ frame by means of a band-pass filter centred at the fundamental angular frequency ω_1 . In a stationary frame, the advantage of a band-pass filter over a low-pass filter is that there is no phase-shift of the filtered quantity at the resonant frequency; low-pass filters are more suitable when filtering variables that are normally constant in steady state. The transfer function of the band-pass filter is:

$$v_{g\varphi}^f = \frac{\omega_1 s}{s^2 + \omega_1 s + \omega_1^2} v_{g\varphi}, \quad (1.15)$$

with $v_{g\varphi}^f$ the filtered alternating voltage. An equivalent state-space representation is given by:

$$\begin{cases} \frac{d\eta_{g\varphi}}{dt} = -\omega_1 v_{g\varphi}^f \\ \frac{dv_{g\varphi}^f}{dt} = \omega_1(\eta_{g\varphi} + v_{g\varphi} - v_{g\varphi}^f). \end{cases} \quad (1.16)$$

SOGI-PNSE

In general, it can be expected that the converter has to operate within some degree of alternating voltage unbalance. In that case, the fundamental-frequency positive- and negative-sequence voltage components can be separated, which

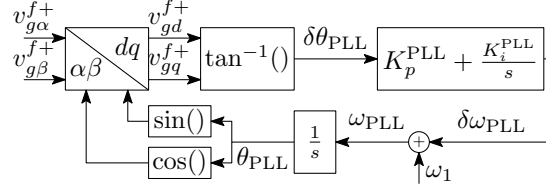


Figure 1.3: Block-diagram of the phase-locked loop

allows synchronising the control loops to the positive sequence only and prevents the negative sequence from disturbing the controller via the PLL. The zero-sequence voltage is naturally discarded by means of Clarke transformation. In addition to the second-order band-pass filter in the SOGI, the quadrature components of both $\alpha\beta$ components are obtained as [12]:

$$v_{g\varphi}^{f\perp} = \frac{\omega_1^2}{s^2 + \omega_1 s + \omega_1^2} v_{g\varphi}, \quad (1.17)$$

with $v_{g\varphi}^{f\perp}$ the filtered *in-quadrature* alternating voltage. An equivalent state-space representation is given by:

$$\begin{cases} \frac{d\eta_{g\varphi}^\perp}{dt} = \omega_1(v_{g\varphi} - v_{g\varphi}^{f\perp}) \\ \frac{dv_{g\varphi}^\perp}{dt} = \omega_1(\eta_{g\varphi}^\perp - v_{g\varphi}^{f\perp}). \end{cases} \quad (1.18)$$

The positive and negative sequences are eventually obtained as:

$$v_{g\alpha}^{f+} = \frac{1}{2}(v_{g\alpha}^f - v_{g\beta}^{f\perp}) \quad v_{g\beta}^{f+} = \frac{1}{2}(v_{g\alpha}^{f\perp} + v_{g\beta}^f) \quad (1.19a)$$

$$v_{g\alpha}^{f-} = \frac{1}{2}(v_{g\alpha}^f + v_{g\beta}^{f\perp}) \quad v_{g\beta}^{f-} = \frac{1}{2}(-v_{g\alpha}^{f\perp} + v_{g\beta}^f). \quad (1.19b)$$

Phase-locked loop

The objective of the PLL displayed in Fig. 1.3 is to observe the phase angle of the filtered positive-sequence alternating voltage, which is achieved by tracking its d -axis component. More precisely, the space vector of the filtered positive-sequence alternating voltage ($\vec{v}_g^{f+} = v_{\alpha}^{f+} + jv_{\beta}^{f+}$, with j the imaginary unit) is projected onto the dq axes of a rotating frame, and the angle of the rotation is calculated in such a way that the q -axis component of the projection vanishes in steady state. This ensures that the d axis is then aligned with the rotating space vector \vec{v}_g^{f+} . The difference between the calculated angle of rotation and

the true phase angle of the space vector is called *deviation angle* and is obtained as:

$$\delta\theta_{\text{PLL}} = \tan^{-1}(v_{gq}^{f+}, v_{gd}^{f+}). \quad (1.20)$$

A proportional integral (PI) controller with proportional and integral coefficients K_p^{PLL} and K_i^{PLL} regulates the deviation angle to zero by accelerating or decelerating the frame rotation via a frequency deviation noted $\delta\omega_{\text{PLL}}$. The sum of this frequency deviation and the nominal frequency ω_1 is integrated to obtain the angle of rotation θ_{PLL} . The corresponding transfer functions are:

$$\delta\omega_{\text{PLL}} = \left(K_p^{\text{PLL}} + \frac{K_i^{\text{PLL}}}{s} \right) \delta\theta_{\text{PLL}}, \quad (1.21a)$$

$$\theta_{\text{PLL}} = \frac{1}{s}(\omega_1 + \delta\omega_{\text{PLL}}), \quad (1.21b)$$

of which an equivalent state-space representation is given by:

$$\begin{cases} \frac{d\eta_{\text{PLL}}}{dt} = K_i^{\text{PLL}} \delta\theta_{\text{PLL}} \end{cases} \quad (1.22a)$$

$$\begin{cases} \frac{d\theta_{\text{PLL}}}{dt} = \omega_1 + \eta_{\text{PLL}} + K_p^{\text{PLL}} \delta\theta_{\text{PLL}}. \end{cases} \quad (1.22b)$$

The rotation angle can be expressed as:

$$\theta_{\text{PLL}} = \theta_1 + \theta_\epsilon \quad (1.23)$$

such that

$$\begin{cases} \frac{d\theta_1}{dt} = \omega_1 \end{cases} \quad (1.24a)$$

$$\begin{cases} \frac{d\theta_\epsilon}{dt} = \eta_{\text{PLL}} + K_p^{\text{PLL}} \delta\theta_{\text{PLL}}. \end{cases} \quad (1.24b)$$

Due to the constant term ω_1 in (1.24a), the angle θ_1 increases linearly with time and does not follow a periodic trajectory in steady state. Since this thesis is concerned with systems whose states can follow periodic trajectories, (1.22b) is replaced by (1.24b), and (1.24a) is replaced by its solution:

$$\theta_1 = \omega_1 t \quad (\text{assuming } \theta_1(0) = 0). \quad (1.25)$$

Next, the trigonometric functions of θ_{PLL} that are required in the PLL frame rotation can be retrieved as:

$$\cos \theta_{\text{PLL}} = \cos(\omega_1 t + \theta_\epsilon) = \cos(\omega_1 t) \cos \theta_\epsilon - \sin(\omega_1 t) \sin \theta_\epsilon \quad (1.26a)$$

$$\sin \theta_{\text{PLL}} = \sin(\omega_1 t + \theta_\epsilon) = \sin(\omega_1 t) \cos \theta_\epsilon + \sin \theta_\epsilon \cos(\omega_1 t), \quad (1.26b)$$

where $\cos(\omega_1 t)$ and $\sin(\omega_1 t)$ are then considered as known periodic parameters.

To close the loop, the $\alpha\beta$ components of the filtered positive-sequence alternating voltage are transformed into dq components via the direct frame rotation:

$$v_{gd}^{f+} = \cos \theta_{\text{PLL}} v_{g\alpha}^{f+} + \sin \theta_{\text{PLL}} v_{g\beta}^{f+} \quad (1.27a)$$

$$v_{gq}^{f+} = -\sin \theta_{\text{PLL}} v_{g\alpha}^{f+} + \cos \theta_{\text{PLL}} v_{g\beta}^{f+}. \quad (1.27b)$$

Active and reactive power control

The objective of the active and reactive power (PQ) controller is to control these quantities to their references by acting on the d - and q -axis alternating currents references (i_{sd}^* and i_{sq}^*). This is achieved by means of PI controllers with proportional and integral coefficients K_p^{PQ} and K_i^{PQ} , and whose transfer functions are:

$$i_{sd}^* = + \left(K_p^{\text{PQ}} + \frac{K_i^{\text{PQ}}}{s} \right) (p_g^* - p_g) \quad (1.28a)$$

$$i_{sq}^* = - \left(K_p^{\text{PQ}} + \frac{K_i^{\text{PQ}}}{s} \right) (q_g^* - q_g), \quad (1.28b)$$

where p_g^* , q_g^* are the active and reactive power references. An equivalent state-space representation is given by:

$$\begin{cases} \frac{d\eta_P}{dt} = +K_i^{\text{PQ}}(p_g^* - p_g) \\ \frac{d\eta_Q}{dt} = -K_i^{\text{PQ}}(q_g^* - q_g) \\ i_{sd}^* = \eta_P + K_p^{\text{PQ}}(p_g^* - p_g) \\ i_{sq}^* = \eta_Q - K_p^{\text{PQ}}(q_g^* - q_g). \end{cases} \quad (1.29)$$

Lastly, the $\alpha\beta$ components of the alternating current references are obtained via the inverse frame rotation:

$$i_{s\alpha}^* = \cos \theta_{\text{PLL}} i_{sd}^* - \sin \theta_{\text{PLL}} i_{sq}^* \quad (1.30a)$$

$$i_{s\beta}^* = \sin \theta_{\text{PLL}} i_{sd}^* + \cos \theta_{\text{PLL}} i_{sq}^*. \quad (1.30b)$$

Alternating current control

The objective of the alternating current (AC) controller is to control the alternating currents to their references by acting on the DM inserted voltage references ($v_{s\varphi}^*$). The control loops are implemented in the $\alpha\beta$ frame by means of a proportional resonant (PR) controller with a resonance at the fundamental frequency ω_1 , and with proportional and resonant coefficients K_p^{AC} and K_r^{AC} . A feedforward term consisting of the filtered alternating voltage $v_{g\varphi}^f$ (brought to the converter-side of the ideal transformer) aims at compensating for the disturbances related to the alternating voltage. The transfer function is:

$$v_{s\varphi}^* = \frac{1}{k} v_{g\varphi}^f + \left(K_p^{\text{AC}} + \frac{K_r^{\text{AC}} s}{s^2 + \omega_1^2} \right) (i_{s\varphi}^* - i_{s\varphi}). \quad (1.31a)$$

An equivalent state-space representation is given by:

$$\begin{cases} \frac{d\eta_{\text{AC}1\varphi}}{dt} = -\omega_1 \eta_{\text{AC}2\varphi} \\ \frac{d\eta_{\text{AC}2\varphi}}{dt} = \omega_1 \eta_{\text{AC}1\varphi} + K_r^{\text{AC}} (i_{s\varphi}^* - i_{s\varphi}) \\ v_{s\varphi}^* = \frac{1}{k} v_{g\varphi}^f + \eta_{\text{AC}2\varphi} + K_p^{\text{AC}} (i_{s\varphi}^* - i_{s\varphi}). \end{cases} \quad (1.32)$$

In the AC-grid-forming mode, the filtered alternating voltage $v_{g\varphi}^f$ in the feedforward term is replaced with the alternating voltage reference $v_{g\varphi}^*$.

Time delay

In this model of the MMC controller, the time delays caused by sampling, communication, calculation and modulation are represented by a single aggregated value [12, Ch.3]. This total delay is represented by a pure time-shift of the reference insertion indices in the abc frame:

$$n_{u\phi}(t) = n_{u\phi}^* (t - t_d), \quad n_{l\phi}(t) = n_{l\phi}^* (t - t_d), \quad (1.33)$$

where t_d is a constant delay value.

1.2.4 Closed-loop operation and steady-state waveforms

Closed-loop operation

The dynamic behaviour of the controlled MMC is described by the feedback connection of its power stage with its controller, which results in the *closed-loop*

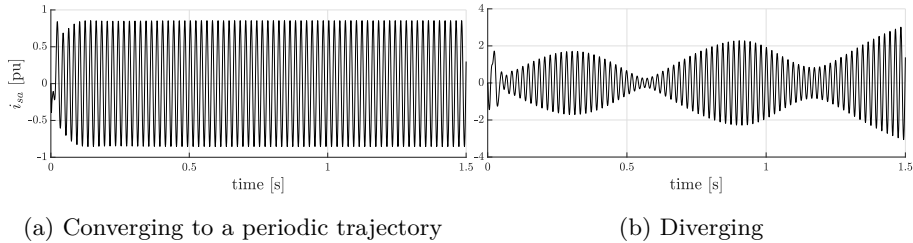


Figure 1.4: Illustrative examples of transient behaviours

MMC model. In state-space form, the closed-loop equations are obtained by considering the set of all circuit and control differential equations, in addition to the algebraic relationships (for instance, those associated with Clarke transformations and frame rotations).

For a given set of circuit parameters and external sources, and for a chosen set of control parameters and references, the differential equations are numerically integrated⁵ from an initial point. Two outcomes are typically observed: either the variables converge to a steady state where waveforms are constant or periodic, or they diverge. The two cases are illustrated in Fig. 1.4.

Research Questions 1 and 2 formally given in the Introduction can be reformulated as:

- What are efficient ways of calculating periodic trajectories, i.e. without having to numerically integrate differential equations through lengthy and potentially diverging transients?
- What are efficient ways of determining from which periodic trajectories the variables would diverge after a small perturbation, i.e. of determining their small-signal stability?

Steady-state waveforms

The steady-state waveforms of a selection of variables are provided in Fig. 1.5. The quantities are displayed in *per-unit* (pu), i.e. they are normalised with respect to constant representative quantities: the circulating currents in Fig. 1.5a are normalised by the rated direct current. Similarly, the sum-capacitor voltages in Fig. 1.5b are normalised by the rated direct voltage. Next, the alternating

⁵ The numerical integration is performed in Matlab with solvers such as `dde23` or `ode15s` according to the procedure described in Appendix C.2.

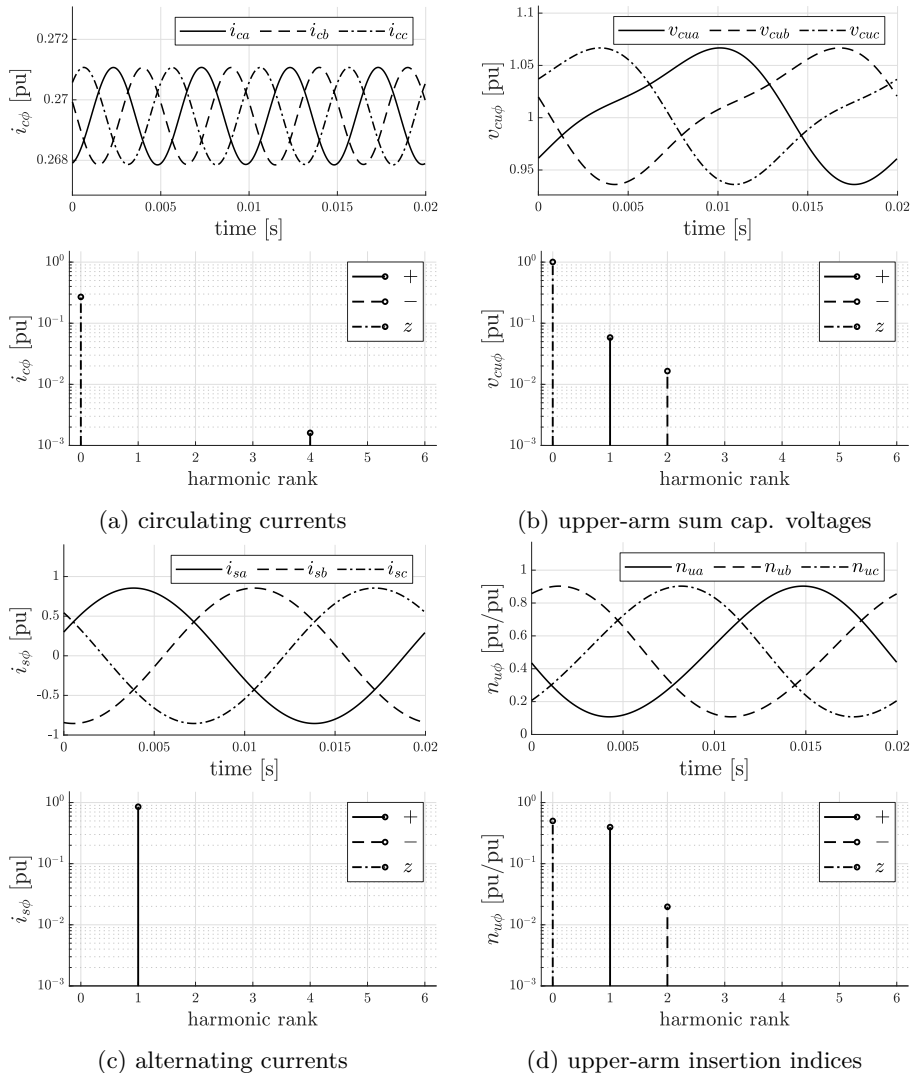


Figure 1.5: Complete MMC model: typical time-domain waveforms and sequence-harmonic spectra

currents in Fig. 1.5c are normalised by their rated peak value. Eventually, the insertion indices are unit-less since they are already normalised quantities.

The variables are displayed over one fundamental period (20 ms) along with the corresponding sequence-harmonic spectra⁶. All of the displayed variables present oscillatory components. For instance, in Fig. 1.5a, the circulating currents present a small 0.2% positive-sequence component at 200 Hz in addition to the constant component. It is observed that the second-harmonic circulating current suppression controller succeeds in eliminating the 100 Hz component that would otherwise naturally arise in these quantities. Furthermore, in Fig. 1.5b, the upper-arm sum-capacitor voltages present a 6% positive-sequence fundamental component and a 2% negative-sequence second-harmonic component, which form what is commonly referred to as the sum-capacitor voltage ripple.

From the above, it is clear that the steady-state trajectory of the presented MMC model is not described by a constant operating point, but by periodic waveforms with various harmonic and sequence contents. The challenges related to performing a small-signal stability assessment of such trajectories are further described in the following section, after briefly introducing a simplified MMC model used for illustrative purposes.

1.2.5 Simplified single-phase MMC model

Considering the number of differential equations describing the dynamic behaviour of the three-phase closed-loop MMC, but also bearing in mind the need for tractable examples to illustrate the methods covered in this thesis, a simplified model of the MMC is presented in this subsection. A single-phase converter is considered and its transformer is assumed to have a transformation ratio of unity. The uncompensated modulation approach is chosen as control strategy. The SOGI-PNSE, the PLL, the outer PQ control loops and the time

⁶ The sequence-harmonic spectra provides information about both sequence and harmonic content of three-phase variables. Practically, the harmonic spectra is determined first from the waveforms via a discrete Fourier transform (DFT). Next, Fortescue transformation is applied to the Fourier coefficients of the three-phase variables at every harmonic rank. It is added that, in such spectra displaying only positive harmonic ranks, the magnitude of the complex-valued Fourier coefficients of index $k \neq 0$ have been multiplied by two to match the amplitude of the corresponding sinusoidal waveforms in the time domain.

delays are disregarded for simplicity. The resulting equations are given by:

$$\left\{ \begin{array}{l} \frac{di_s}{dt} = f_1(\mathbf{x}, \mathbf{u}) = \frac{1}{L_e} \left(-R_e i_s - v_g - n_u \frac{v_{Cu}}{2} + n_l \frac{v_{Cl}}{2} \right) \\ \frac{di_c}{dt} = f_2(\mathbf{x}, \mathbf{u}) = \frac{1}{L_a} \left(-R_a i_c + \frac{v_d}{2} - n_u \frac{v_{Cu}}{2} - n_l \frac{v_{Cl}}{2} \right) \end{array} \right. \quad (1.34a)$$

$$\left. \begin{array}{l} \frac{dv_{Cu}}{dt} = f_3(\mathbf{x}, \mathbf{u}) = \frac{1}{C_a} n_u \left(i_c + \frac{i_s}{2} \right) \\ \frac{dv_{Cl}}{dt} = f_4(\mathbf{x}, \mathbf{u}) = \frac{1}{C_a} n_l \left(i_c - \frac{i_s}{2} \right) \end{array} \right. \quad (1.34c)$$

$$\left. \begin{array}{l} \frac{di_d^f}{dt} = f_5(\mathbf{x}, \mathbf{u}) = \omega_f (i_d - i_d^f) \\ \frac{d\eta_{AC1}}{dt} = f_6(\mathbf{x}, \mathbf{u}) = -\omega_1 \eta_{AC2} \end{array} \right. \quad (1.34e)$$

$$\left. \begin{array}{l} \frac{d\eta_{AC2}}{dt} = f_7(\mathbf{x}, \mathbf{u}) = \omega_1 \eta_{AC1} + K_r^{AC} (i_s^* - i_s) \\ \frac{d\eta_{CC1}}{dt} = f_8(\mathbf{x}, \mathbf{u}) = -2\omega_1 \eta_{CC2} \end{array} \right. \quad (1.34f)$$

$$\left. \begin{array}{l} \frac{d\eta_{CC2}}{dt} = f_9(\mathbf{x}, \mathbf{u}) = 2\omega_1 \eta_{CC1} - K_r^{CC} (i_d^f - i_c). \end{array} \right. \quad (1.34g)$$

$$\left. \begin{array}{l} \frac{di_s}{dt} = f_1(\mathbf{x}, \mathbf{u}) = \frac{1}{L_e} \left(-R_e i_s - v_g - \eta_{AC2} - K_p^{AC} (i_s^* - i_s) \right) \\ \frac{di_c}{dt} = f_2(\mathbf{x}, \mathbf{u}) = \frac{1}{L_a} \left(-R_a i_c + \frac{v_d}{2} - \eta_{AC2} - K_p^{AC} (i_s^* - i_s) \right) \\ \frac{dv_{Cu}}{dt} = f_3(\mathbf{x}, \mathbf{u}) = \frac{1}{C_a} n_u \left(i_c + \frac{i_s}{2} \right) \\ \frac{dv_{Cl}}{dt} = f_4(\mathbf{x}, \mathbf{u}) = \frac{1}{C_a} n_l \left(i_c - \frac{i_s}{2} \right) \\ \frac{di_d^f}{dt} = f_5(\mathbf{x}, \mathbf{u}) = \omega_f (i_d - i_d^f) \\ \frac{d\eta_{AC1}}{dt} = f_6(\mathbf{x}, \mathbf{u}) = -\omega_1 \eta_{AC2} \\ \frac{d\eta_{AC2}}{dt} = f_7(\mathbf{x}, \mathbf{u}) = \omega_1 \eta_{AC1} + K_r^{AC} (i_s^* - i_s) \\ \frac{d\eta_{CC1}}{dt} = f_8(\mathbf{x}, \mathbf{u}) = -2\omega_1 \eta_{CC2} \\ \frac{d\eta_{CC2}}{dt} = f_9(\mathbf{x}, \mathbf{u}) = 2\omega_1 \eta_{CC1} - K_r^{CC} (i_d^f - i_c). \end{array} \right. \quad (1.35a)$$

The expressions of the insertion indices are not substituted in the differential equations for clarity, and are given by:

$$n_u = \frac{1}{v_d} (v_d/2 + \eta_{CC2} - K_p^{CC} (i_c^* - i_c) - v_g - \eta_{AC2} - K_p^{AC} (i_s^* - i_s)) \quad (1.35a)$$

$$n_l = \frac{1}{v_d} (v_d/2 + \eta_{CC2} - K_p^{CC} (i_c^* - i_c) + v_g + \eta_{AC2} + K_p^{AC} (i_s^* - i_s)). \quad (1.35b)$$

In this particular example, the circulating current reference i_c^* is equal to the direct current⁷ processed with a first-order filter, resulting in the filtered direct current i_d^f . The state and input vectors are defined as:

$$\mathbf{x} = [i_s \quad i_c \quad v_{Cu} \quad v_{Cl} \quad i_d^f \quad \eta_{AC1} \quad \eta_{AC2} \quad \eta_{CC1} \quad \eta_{CC2}]^T \quad (1.36)$$

$$\mathbf{u} = [v_g \quad v_d \quad i_s^*]^T, \quad (1.37)$$

⁷ It is recalled from (1.9) that, in a single-phase application, the direct current i_d and the circulating current i_c are equal.

where superscript T indicates transposition.

In addition to the three-phase closed-loop MMC model and the simplified single-phase MMC model, an MMC-based point-to-point HVDC link connecting an offshore grid is detailed in Appendix B.4. This system and its sub-circuits also support the illustration of the methods discussed in this thesis.

1.3 Fundamentals of stability analysis

The closed-loop MMC models presented in the previous section are characterised by three important features from the perspective of stability assessments: (i) nonlinearity, (ii) periodic inputs, and (iii) time delays. This section is dedicated to setting a general mathematical background to describe systems with the first two features. Time delays are discussed later, briefly in Section 3.4 and more thoroughly in Chapter 4.

1.3.1 Nonlinear systems and linearisation

The described state-space model of the MMC and of its controller contains several types of nonlinear functions, such as the inverse tangent in the calculation of the PLL deviation angle $\delta\theta_{\text{PLL}}$ in (1.20), as well as sine and cosine functions applied to state variable θ_e in (1.26). Ratios of variables appear in e.g. (1.13) and (1.14), and a square root is used in (B.4). Lastly, products of variables occur in e.g. (1.10), in particular once the insertion indices are replaced with their complete expressions.

In this thesis, the formulation of continuous-time dynamic systems involving the above-mentioned types of nonlinearities relies on generic state and output functions noted \mathbf{f} and \mathbf{g} . Nonlinear systems characterised by n states $x_i(t)$, m inputs $u_i(t)$ and p outputs $y_i(t)$ can then be systematically described through the following general state-space form [35]:

$$\begin{cases} \frac{d\mathbf{x}(t)}{dt} = \mathbf{f}(t, \mathbf{x}(t), \mathbf{u}(t)) \\ \mathbf{y}(t) = \mathbf{g}(t, \mathbf{x}(t), \mathbf{u}(t)), \end{cases} \quad (1.38)$$

with $\mathbf{x}(t)$, $\mathbf{u}(t)$ and $\mathbf{y}(t)$ vectors of state, input and output variables:

$$\mathbf{x}(t) = [x_1(t) \quad x_2(t) \quad \dots \quad x_n(t)]^T, \quad (1.39a)$$

$$\mathbf{u}(t) = [u_1(t) \quad u_2(t) \quad \dots \quad u_m(t)]^T, \quad (1.39b)$$

$$\mathbf{y}(t) = [y_1(t) \quad y_2(t) \quad \dots \quad y_p(t)]^T, \quad (1.39c)$$

where numerical subscripts denote here the index of the scalar variables within the vectors. The values of state and output functions \mathbf{f} and \mathbf{g} depend on the values of the states and inputs, and may depend on time either directly or indirectly through the values of possibly time-varying parameters. The position $\mathbf{p}(t) = (\mathbf{x}(t), \mathbf{u}(t)) \in \mathbb{R}^n \times \mathbb{R}^m$ describes the *trajectory* of the system as t increases and, at a given time t , it is called a *point*.

In this thesis, the expression *input variables* is used to collectively refer to both control inputs and exogenous inputs, which model the interface between the system and its environment. Specifically, control inputs represent the commands that are intentionally applied to the system to influence its behaviour, while exogenous inputs encompass any external influences or disturbances that affect the system. For instance, the control inputs of the arm-averaged model of the three-phase MMC power stage in (1.6) are the six insertion indices. The exogenous inputs are the positive-pole and negative-pole voltages at the DC side, as well as the three-phase alternating voltages at the AC side. These voltages correspond to external sources representing the physical environment beyond the electrical connections of the converter.

Some classifications of dynamic systems

Dynamic systems such as (1.38) can be specified according to several classifications [35, 36]. A first distinction is made between *linear* and *nonlinear* systems, with as fundamental difference the fact that the latter feature nonlinear operations on the variables. A second distinction is made between *forced* and *unforced* systems: the former are explicitly subject to input variables while the latter are not. A third distinction is made between *time-invariant* and *time-varying* systems, sometimes also referred to as *autonomous* and *non-autonomous* systems [36, Ch.1]. Some confusion could arise at this point, since the states of any dynamic system are susceptible to change with time, hence "all systems should be time-varying". However, time-dependency of a system is not defined based on whether the trajectories of its states change with time or not, but according to whether these trajectories would have been different had they been initiated at another moment. In other words, a system is time-varying

if its response to an input disturbance depends on the instant at which this disturbance is applied. Otherwise, the system is time-invariant. In (1.38), time-variability is indicated by an explicit dependency of functions f and g on time t .

The definitions in e.g. [35, 36] further suggest that time-invariant systems are also unforced systems, thereby discarding the possibility of indirect time-dependency via the input variables. At first sight, this might seem conflicting with the generally accepted idea that a simple resistance-inductance-capacitance (RLC) circuit is a time-invariant system, even if it is supplied with an alternating voltage source. Reassuringly, [36] indicates that these seemingly imprecise distinctions are not set in stone, and that a system may well be seen as autonomous or non-autonomous depending on the context and on the way it is written. Nevertheless, in this thesis, it will be of particular interest to know whether a system has only constant coefficients or not. Consequently, it is chosen to rely on the following clarification: a system will be referred to as time-varying if its **parameters or coefficients** depend on time, and as time-invariant otherwise, regardless of whether its inputs are time-varying or not.

Among time-varying systems, time-periodic systems are characterised by a periodic variation of their parameters, whose fundamental period is noted T_1 . For instance, the arm-averaged model of the three-phase MMC power stage in (1.6) is nonlinear but time-invariant because all its parameters (R_g , L_g , etc.) are constant. Interestingly, the PLL model described by (1.20)-(1.27) is nonlinear and time-periodic, due to the presence of time-periodic coefficients $\sin(\omega_1 t)$ and $\cos(\omega_1 t)$ in the frame rotation. Frame rotations are also used to transform the dq current references from the outer loops into $\alpha\beta$ current references fed to the AC controller. These transformations make the complete closed-loop MMC model a nonlinear time-periodic system.

The distinctions between the concepts of linearity, nonlinearity, time-invariance and time-periodicity are illustrated in Table 1.1, where four simple expressions with two state variables correspond to four types of systems: linear time-invariant (LTI), nonlinear time-invariant (NTI), linear time-periodic (LTP) and nonlinear time-periodic (NTP) systems. Among these types of systems, LTI systems are the simplest and lend themselves to the application of stability analysis techniques relying on eigenvalues and transfer functions. It is emphasised that, for illustration purposes, nonlinearity takes the shape of products of variables in Table 1.1. There are, however, more types of nonlinear operations in the systems considered in this thesis, as listed at the start of this section.

| $f_i(t, \mathbf{x}(t))$ | time-invariant | time-periodic |
|-------------------------|--------------------------|---------------------------|
| linear | $\alpha x_1(t) + x_2(t)$ | $\beta(t)x_1(t) + x_2(t)$ |
| nonlinear | $\alpha x_1(t)x_2(t)$ | $\beta(t)x_1(t)x_2(t)$ |

Table 1.1: Illustrative classification of dynamic systems with α a constant parameter and $\beta(t)$ a periodic parameter.

Linearisation of nonlinear systems

Regardless of whether they are linear or nonlinear, forced or unforced, and time-invariant or time-periodic, dynamic systems may present solutions of different types, including non-periodic trajectories, periodic trajectories and/or constant trajectories, which are also referred to as constant operating points or equilibria.

Definition 1. A system is in **steady state** when its trajectory is constant or repeats itself periodically as long as it remains undisturbed.

According to Definition 1, a system operating at either a constant operating point or evolving along a periodic trajectory is considered to be in steady state. In this thesis, the upper-bar notation is used to refer to steady-state operation. The following assumptions are also introduced:

Assumption 5. The considered systems have an equilibrium point or a periodic trajectory $\bar{\mathbf{p}}(t) = (\bar{\mathbf{x}}(t), \bar{\mathbf{u}}(t))$ which can be determined analytically or numerically.

Assumption 6. Functions \mathbf{f} and \mathbf{g} are continuously differentiable at/along $\bar{\mathbf{p}}(t)$.

Under Assumptions 5 and 6, and according to the indirect Lyapunov method [37, Ch.5], the stability of a steady-state trajectory of a nonlinear system can be studied by considering the linear approximation of that system near the steady-state trajectory. The resulting linear approximation is generally only valid for small deviations of the variables with respect to the steady-state trajectory.

This paragraph presents the procedure of linearising a nonlinear system around a steady-state trajectory $\bar{\mathbf{p}}(t)$. We consider deviations $(\tilde{\mathbf{x}}(t), \tilde{\mathbf{u}}(t))$ of the variables with respect to $\bar{\mathbf{p}}(t)$:

$$\tilde{\mathbf{x}}(t) \triangleq \mathbf{x}(t) - \bar{\mathbf{x}}(t) \quad (1.40a)$$

$$\tilde{\mathbf{u}}(t) \triangleq \mathbf{u}(t) - \bar{\mathbf{u}}(t). \quad (1.40b)$$

These variables are referred to as *deviation variables*, indicated with the upper tilde notation. Their definition is used to replace the original variables $(\mathbf{x}(t), \mathbf{u}(t))$ in (1.38):

$$\begin{cases} \frac{d}{dt}(\bar{\mathbf{x}}(t) + \tilde{\mathbf{x}}(t)) = \mathbf{f}(t, \bar{\mathbf{x}}(t) + \tilde{\mathbf{x}}(t), \bar{\mathbf{u}}(t) + \tilde{\mathbf{u}}(t)) \\ \bar{\mathbf{y}}(t) + \tilde{\mathbf{y}}(t) = \mathbf{g}(t, \bar{\mathbf{x}}(t) + \tilde{\mathbf{x}}(t), \bar{\mathbf{u}}(t) + \tilde{\mathbf{u}}(t)). \end{cases} \quad (1.41)$$

Under small deviations, a linear approximation of \mathbf{f} and \mathbf{g} near $\bar{\mathbf{p}}(t)$ is obtained by applying Taylor's expansion limited to first-order terms:

$$\begin{cases} \frac{d}{dt}\bar{\mathbf{x}}(t) + \frac{d}{dt}\tilde{\mathbf{x}}(t) \approx \mathbf{f}(t, \bar{\mathbf{p}}(t)) + \frac{\partial \mathbf{f}}{\partial \mathbf{x}}(t, \bar{\mathbf{p}}(t))\tilde{\mathbf{x}}(t) + \frac{\partial \mathbf{f}}{\partial \mathbf{u}}(t, \bar{\mathbf{p}}(t))\tilde{\mathbf{u}}(t) \\ \bar{\mathbf{y}}(t) + \tilde{\mathbf{y}}(t) \approx \mathbf{g}(t, \bar{\mathbf{p}}(t)) + \frac{\partial \mathbf{g}}{\partial \mathbf{x}}(t, \bar{\mathbf{p}}(t))\tilde{\mathbf{x}}(t) + \frac{\partial \mathbf{g}}{\partial \mathbf{u}}(t, \bar{\mathbf{p}}(t))\tilde{\mathbf{u}}(t). \end{cases} \quad (1.42)$$

Under Assumption 6, the partial derivatives exist and are continuous, and the matrix coefficients of the state-space representation can be defined as:

$$\mathbf{A}(t) \triangleq \frac{\partial \mathbf{f}}{\partial \mathbf{x}}(t, \bar{\mathbf{p}}(t)) \quad \mathbf{B}(t) \triangleq \frac{\partial \mathbf{f}}{\partial \mathbf{u}}(t, \bar{\mathbf{p}}(t)) \quad (1.43a)$$

$$\mathbf{C}(t) \triangleq \frac{\partial \mathbf{g}}{\partial \mathbf{x}}(t, \bar{\mathbf{p}}(t)) \quad \mathbf{D}(t) \triangleq \frac{\partial \mathbf{g}}{\partial \mathbf{u}}(t, \bar{\mathbf{p}}(t)). \quad (1.43b)$$

Observing that

$$\begin{cases} \frac{d\bar{\mathbf{x}}(t)}{dt} = \mathbf{f}(t, \bar{\mathbf{p}}(t)) \\ \bar{\mathbf{y}}(t) = \mathbf{g}(t, \bar{\mathbf{p}}(t)), \end{cases} \quad (1.44)$$

system (1.42) is simplified by only retaining terms related to the small deviations, whose dynamics are described by the resulting linear system:

$$\begin{cases} \frac{d\tilde{\mathbf{x}}(t)}{dt} = \mathbf{A}(t)\tilde{\mathbf{x}}(t) + \mathbf{B}(t)\tilde{\mathbf{u}}(t) \\ \tilde{\mathbf{y}}(t) = \mathbf{C}(t)\tilde{\mathbf{x}}(t) + \mathbf{D}(t)\tilde{\mathbf{u}}(t). \end{cases} \quad (1.45)$$

It is clear from (1.43) that if functions \mathbf{f} and \mathbf{g} are time-invariant and if $\bar{\mathbf{p}}(t)$ is a constant operating point such that $\bar{\mathbf{p}}(t) = \mathbf{p}_0$ (where \mathbf{p}_0 refers to the average of $\mathbf{p}(t)$ over the fundamental period) then the matrix coefficients of the linear approximation are constant. In this case, the linearised system is LTI. On the contrary, if there are time-periodic parameters and/or if $\bar{\mathbf{p}}(t)$ is a periodic trajectory, then the matrix coefficients are periodic. In this case, the linearised

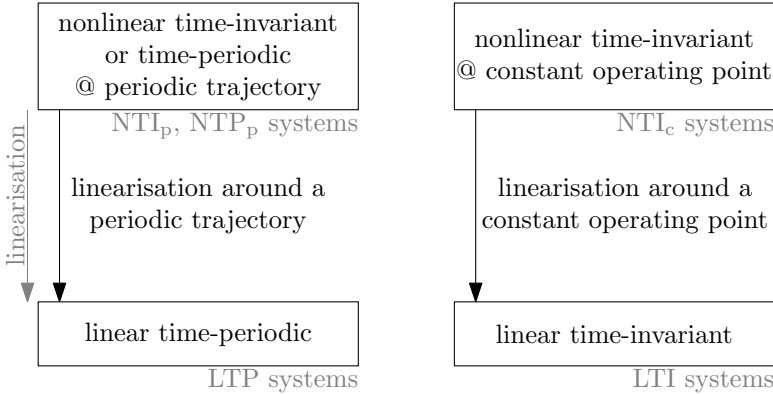


Figure 1.6: Overview of system types through the linearisation process

system is LTP. It is worth noting that the small deviations around a periodic trajectory ought not to be periodic themselves.

In this thesis, NTI systems operating at a constant operating point or following a periodic trajectory are referred to as NTI_c and NTI_p systems, respectively. Similarly, the abbreviation NTP_p is used for NTP systems following a periodic trajectory. This is indicated in Fig. 1.6, which gives an overview of system types and illustrates the relationship between nonlinear and linear systems.

Example: linearisation of a nonlinear time-invariant system

The linearisation procedure is applied to the simple NTI system from Table 1.1, where the dot (·) is an alternative notation for the time derivative:

$$\dot{x}_i(t) = f_i(\mathbf{x}(t)) = \alpha x_1(t)x_2(t). \quad (1.46)$$

- If $x_1(t)$ and $x_2(t)$ are constant in steady state, then the linearised system is linear time-invariant:

$$\dot{\tilde{x}}_i(t) \approx \alpha \bar{x}_1 \tilde{x}_2(t) + \alpha \bar{x}_2 \tilde{x}_1(t) \quad (1.47)$$

with \bar{x}_1 and \bar{x}_2 constant quantities describing the steady-state equilibrium point, and $\tilde{x}_1(t)$ and $\tilde{x}_2(t)$ small deviations with respect to the equilibrium.

- If $x_1(t)$ and $x_2(t)$ are periodic in steady state, then the linearised system is linear time-periodic, even though the original system was time-invariant:

$$\dot{\tilde{x}}_i(t) \approx \alpha \bar{x}_1(t) \tilde{x}_2(t) + \alpha \bar{x}_2(t) \tilde{x}_1(t) \quad (1.48)$$

with $\bar{x}_1(t)$ and $\bar{x}_2(t)$ periodic quantities describing the steady-state periodic trajectory, and $\tilde{x}_1(t)$ and $\tilde{x}_2(t)$ small deviations with respect to the periodic trajectory.

Remarks

1. LTP systems are on the edge between the realms of linear and nonlinear systems, as they present characteristics of both types of systems. For instance, they involve the product of time-varying quantities (the time-periodic coefficients and the deviations), which is not unlike the product of variables in a nonlinear system. Besides, both LTP systems and nonlinear systems display the mechanism of frequency coupling⁸, a phenomenon that does not arise in LTI systems.
2. To be precise, it should be kept in mind that stability is a property of operating conditions such as equilibria or periodic trajectories, not a property of a system. This is particularly important in the case of nonlinear systems, which may have multiple equilibria with different stability properties [37]. Some tolerated abuse of language may lead to talk about "system stability", with the implied meaning of "stability of its trajectory", when the context is sufficiently clear.
3. As observed in the above example, a time-invariant system will become time-periodic through the process of linearisation around a periodic trajectory. Hence the increased complexity of small-signal stability analyses brought by periodicity may seem to come from linearisation itself. More precisely, however, periodicity of variables in steady state is converted into periodicity of coefficients, not through linearisation, but through rewriting the equations in terms of deviations with respect to the periodic trajectory. For this reason, periodicity does not only arise in the context of small-signal stability assessments, but also in the more general context of nonlinear system theory, for instance when applying the direct Lyapunov method to an incremental model, see for instance [38].
4. The previous remark also implies that the stability analysis of periodic trajectories of a nonlinear system can be replaced with the stability analysis of an equilibrium of a nonlinear time-periodic system by means of a change of variables [35, Ch.8]. Linearising the first system around a periodic

⁸ Frequency coupling refers to the physical phenomenon in which an input oscillation at a given frequency produces an output oscillation at other frequencies. This phenomenon, which can be seen as an interaction between different frequencies, does not appear in LTI systems, in which an input oscillation at a given frequency can only produce output oscillations at the same frequency.

trajectory or the second around the corresponding equilibrium results in the same LTP system. Eventually, linearised systems expressed in terms of deviation variables possess an equilibrium at the origin, regardless of whether linearisation has been carried out near an equilibrium or a periodic trajectory.

Example: linearisation of the simplified single-phase MMC

Considering the simplified single-phase closed-loop MMC specifically, nonlinearity in the circuit equations (1.34a)-(1.34d) comes from the modulation of currents and voltages by the insertion indices, which depend on the input variables as well as on the alternating currents, circulating currents and the control states. All parameters are constant so the system is time-invariant.

The linearisation process leads to expressions of the form:

$$\left\{ \begin{array}{l} \frac{d\tilde{i}_s}{dt} \approx \frac{\partial f_1}{\partial i_s} \Big|_{\bar{\mathbf{p}}(t)} \tilde{i}_s + \frac{\partial f_1}{\partial i_c} \Big|_{\bar{\mathbf{p}}(t)} \tilde{i}_c + \frac{\partial f_1}{\partial v_{Cu}} \Big|_{\bar{\mathbf{p}}(t)} \tilde{v}_{Cu} + \dots \\ \frac{d\tilde{i}_c}{dt} \approx \frac{\partial f_2}{\partial i_s} \Big|_{\bar{\mathbf{p}}(t)} \tilde{i}_s + \frac{\partial f_2}{\partial i_c} \Big|_{\bar{\mathbf{p}}(t)} \tilde{i}_c + \frac{\partial f_2}{\partial v_{Cu}} \Big|_{\bar{\mathbf{p}}(t)} \tilde{v}_{Cu} + \dots \\ \vdots \end{array} \right. \quad (1.49)$$

The complete state matrix $\mathbf{A}(t)$ of the linearised state-space representation is given by:

$$\begin{bmatrix} \frac{\partial f_1}{\partial i_s} \Big|_{\bar{\mathbf{p}}} & \frac{\partial f_1}{\partial i_c} \Big|_{\bar{\mathbf{p}}} & \frac{\partial f_1}{\partial v_{Cu}} \Big|_{\bar{\mathbf{p}}} & \frac{\partial f_1}{\partial v_{Cl}} \Big|_{\bar{\mathbf{p}}} & \frac{\partial f_1}{\partial i_d^f} \Big|_{\bar{\mathbf{p}}} & 0 & \frac{\partial f_1}{\partial \eta_{AC2}} \Big|_{\bar{\mathbf{p}}} & 0 & \frac{\partial f_1}{\partial \eta_{CC2}} \Big|_{\bar{\mathbf{p}}} \\ \frac{\partial f_2}{\partial i_s} \Big|_{\bar{\mathbf{p}}} & \frac{\partial f_2}{\partial i_c} \Big|_{\bar{\mathbf{p}}} & \frac{\partial f_2}{\partial v_{Cu}} \Big|_{\bar{\mathbf{p}}} & \frac{\partial f_2}{\partial v_{Cl}} \Big|_{\bar{\mathbf{p}}} & \frac{\partial f_2}{\partial i_d^f} \Big|_{\bar{\mathbf{p}}} & 0 & \frac{\partial f_2}{\partial \eta_{AC2}} \Big|_{\bar{\mathbf{p}}} & 0 & \frac{\partial f_2}{\partial \eta_{CC2}} \Big|_{\bar{\mathbf{p}}} \\ \frac{\partial i_s}{\partial i_s} \Big|_{\bar{\mathbf{p}}} & \frac{\partial i_c}{\partial i_c} \Big|_{\bar{\mathbf{p}}} & 0 & 0 & \frac{\partial i_d^f}{\partial i_d^f} \Big|_{\bar{\mathbf{p}}} & 0 & \frac{\partial f_3}{\partial \eta_{AC2}} \Big|_{\bar{\mathbf{p}}} & 0 & \frac{\partial f_3}{\partial \eta_{CC2}} \Big|_{\bar{\mathbf{p}}} \\ \frac{\partial f_3}{\partial i_s} \Big|_{\bar{\mathbf{p}}} & \frac{\partial f_3}{\partial i_c} \Big|_{\bar{\mathbf{p}}} & 0 & 0 & \frac{\partial i_d^f}{\partial i_d^f} \Big|_{\bar{\mathbf{p}}} & 0 & \frac{\partial f_4}{\partial \eta_{AC2}} \Big|_{\bar{\mathbf{p}}} & 0 & \frac{\partial f_4}{\partial \eta_{CC2}} \Big|_{\bar{\mathbf{p}}} \\ \frac{\partial f_4}{\partial i_s} \Big|_{\bar{\mathbf{p}}} & \frac{\partial f_4}{\partial i_c} \Big|_{\bar{\mathbf{p}}} & 0 & 0 & \frac{\partial f_4}{\partial i_d^f} \Big|_{\bar{\mathbf{p}}} & 0 & \frac{\partial f_4}{\partial \eta_{AC2}} \Big|_{\bar{\mathbf{p}}} & 0 & \frac{\partial f_4}{\partial \eta_{CC2}} \Big|_{\bar{\mathbf{p}}} \\ 0 & \omega_1/5 & 0 & 0 & -\omega_1/5 & 0 & 0 & 0 & 0 \\ 0 & 0 & 0 & 0 & 0 & 0 & -\omega_1 & 0 & 0 \\ -K_r^{AC} & 0 & 0 & 0 & 0 & \omega_1 & 0 & 0 & 0 \\ 0 & 0 & 0 & 0 & 0 & 0 & 0 & 0 & -2\omega_1 \\ 0 & K_r^{CC} & 0 & 0 & -K_r^{CC} & 0 & 0 & 2\omega_1 & 0 \end{bmatrix} \quad (1.50)$$

where the first few partial derivatives read as:

$$\frac{\partial f_1}{\partial i_s} \Big|_{\bar{\mathbf{p}}(t)} = -\frac{1}{2L_e \bar{v}_d} (K_p^{\text{AC}} (\bar{v}_{Cl} + \bar{v}_{Cu}) + 2R_e \bar{v}_d) \quad (1.51\text{a})$$

$$\frac{\partial f_1}{\partial i_c} \Big|_{\bar{\mathbf{p}}(t)} = \frac{K_p^{\text{CC}}}{2L_e \bar{v}_d} (\bar{v}_{Cl} - \bar{v}_{Cu}) \quad (1.51\text{b})$$

$$\frac{\partial f_1}{\partial v_{Cu}} \Big|_{\bar{\mathbf{p}}(t)} = -\frac{1}{2L_e \bar{v}_d} \left(\bar{\eta}_{\text{CC2}} - \bar{\eta}_{\text{AC2}} + \frac{\bar{v}_d}{2} - \bar{v}_g + K_p^{\text{AC}} (\bar{i}_s - \bar{i}_s^*) + K_p^{\text{CC}} (\bar{i}_c - \bar{i}_d^f) \right) \quad (1.51\text{c})$$

The complete set of analytical expressions of the partial derivatives is provided in Appendix B.5. It is emphasised that these expressions depend on the type of controller used, since the converter is considered in closed-loop with its controller. While the expressions remain acceptably short for this simplified model and provide some insights into the impact of variables and parameters on system dynamics, the expressions corresponding to a complete three-phase closed-loop MMC model quickly become cumbersome. Yet, for the nonlinearities considered in this thesis, the analytical expressions of the state-space matrix coefficients $\mathbf{A}(t)$, $\mathbf{B}(t)$, $\mathbf{C}(t)$, and $\mathbf{D}(t)$ can be obtained straightforwardly with the help of automated symbolic computations, for instance by means of the Matlab symbolic toolbox, which is used wherever necessary throughout this thesis.

In (1.51), it is observed that the partial derivatives evaluated around the periodic trajectory of the MMC are periodic because they involve the time-periodic states and inputs. In (1.51c) specifically, there may be cancellations between variables under certain conditions. For instance, the steady-state control error $\bar{i}_s - \bar{i}_s^*$ is equal to zero for a perfect controller. However, such assumption is not made in this thesis. In non-ideal conditions, control errors may not be equal to zero over the whole spectrum and some harmonic components could propagate and be observed in the spectrum of the state-space coefficients. This motivates a review of stability analysis techniques dedicated to LTP systems.

1.3.2 Linear time-invariant systems

As will be clear from Chapters 2 and 3, the stability analysis of LTP systems often boils down to the study of an equivalent or approximate LTI system. Consequently, this section provides a brief presentation of LTI systems, which also serves as a point of reference for the subsequent presentation of LTP systems.

Following (1.45), an LTI system is described in state-space form by [39]:

$$\frac{d\mathbf{x}(t)}{dt} = \mathbf{A}\mathbf{x}(t) + \mathbf{B}\mathbf{u}(t) \quad (1.52a)$$

$$\mathbf{y}(t) = \mathbf{C}\mathbf{x}(t) + \mathbf{D}\mathbf{u}(t) \quad (1.52b)$$

where all matrix coefficients are constant and where, in comparison to (1.45), the small-signal tilde notation has been dropped since the considerations made in the following paragraphs are applicable to both linear and linearised time-invariant systems.

In the following paragraphs, a brief review of the time and frequency responses of LTI systems naturally leads to the discussion of stability criteria. For more information on the topics in this section, the reader is referred to [18, Ch.3].

Time response of LTI systems

The future values of the states of (1.52) beyond an initial time t_0 are called the total state response and consist of the superposition of the unforced state response $\mathbf{x}_u(t)$ and the forced state response $\mathbf{x}_f(t)$ [18, Eq.(3.4)]:

$$\mathbf{x}(t) = \mathbf{x}_u(t) + \mathbf{x}_f(t) \quad (1.53a)$$

with

$$\mathbf{x}_u(t) = e^{\mathbf{A}(t-t_0)}\mathbf{x}(t_0) \quad (1.53b)$$

$$\mathbf{x}_f(t) = \int_{t_0}^t e^{\mathbf{A}(t-\tau)}\mathbf{B}\mathbf{u}(\tau)d\tau. \quad (1.53c)$$

On the one hand, the unforced state response $\mathbf{x}_u(t)$ is the solution of the unforced differential equation:

$$\frac{d\mathbf{x}(t)}{dt} = \mathbf{A}\mathbf{x}(t) \quad (1.54)$$

which describes the evolution of the system from the initial state $\mathbf{x}(t_0)$ when the inputs are set to zero. On the other hand, the forced state response $\mathbf{x}_f(t)$ accounts for the effect of the inputs while the initial state is set to zero. Substituting (1.53a) into (1.52b) gives the total output response $\mathbf{y}(t)$.

As both the unforced and forced responses involve an exponential function of time, the total response may feature combinations of decaying, diverging and oscillatory terms. The prime purpose of a stability analysis is to identify any

diverging terms, which can be done by considering the modal decomposition⁹ of matrix \mathbf{A} :

$$\mathbf{A} = \mathbf{V}\Lambda\mathbf{W}, \quad \text{with} \quad \mathbf{W} = \mathbf{V}^{-1}, \quad (1.55)$$

where the columns of \mathbf{V} are the right eigenvectors, the rows of \mathbf{W} are the left eigenvectors and where Λ is a diagonal matrix with the eigenvalues λ_i of \mathbf{A} on its diagonal:

$$\Lambda = \begin{bmatrix} \lambda_1 & & & \\ & \lambda_2 & & \\ & & \ddots & \\ & & & \lambda_n \end{bmatrix}. \quad (1.56)$$

To establish the relationship between the eigenvalues of \mathbf{A} and stability, the following change of variables is applied to the unforced state response:

$$\mathbf{m}(t) = \mathbf{W}\mathbf{x}_u(t) \iff \mathbf{x}_u(t) = \mathbf{V}\mathbf{m}(t). \quad (1.57)$$

The elements of vector $\mathbf{m}(t)$ are called the *modes* of the system. Replacing $\mathbf{x}_u(t)$ by its expression from (1.53b) and assuming $t_0 = 0$ for simplicity, we obtain:

$$\mathbf{m}(t) = \mathbf{W}e^{\mathbf{A}t}\mathbf{x}(0) \quad (1.58a)$$

$$= \mathbf{W}\mathbf{V}e^{\Lambda t}\mathbf{W}\mathbf{x}(0) \quad (1.58b)$$

$$= e^{\Lambda t}\mathbf{m}(0) \quad (1.58c)$$

where we used the fact that, for a diagonalisable matrix \mathbf{A} with the modal decomposition in (1.55), we have $e^{\mathbf{A}t} = \mathbf{V}e^{\Lambda t}\mathbf{W}$ [41, Ch.7]. Substituting (1.58c) into (1.57), we obtain:

$$\mathbf{x}_u(t) = \mathbf{V}e^{\Lambda t}\mathbf{m}(0) \quad (1.59a)$$

$$= [\mathbf{v}_1 \quad \mathbf{v}_2 \quad \cdots \quad \mathbf{v}_n] \begin{bmatrix} e^{\lambda_1 t} & & & \\ & \ddots & & \\ & & e^{\lambda_n t} & \end{bmatrix} \begin{bmatrix} m_1(0) \\ m_2(0) \\ \vdots \\ m_n(0) \end{bmatrix} \quad (1.59b)$$

$$= \sum_{i=1}^n \mathbf{v}_i e^{\lambda_i t} m_i(0), \quad (1.59c)$$

⁹This assumes that matrix \mathbf{A} is diagonalisable, or non-defective, which is generally the case for the systems considered in this thesis. A square matrix is diagonalisable if it has n independent right eigenvectors. Consequently, it also has n independent left eigenvectors [40, Ch.7].

where \mathbf{v}_i are the right eigenvectors of \mathbf{A} . The last equation shows that the unforced state response can be written as a linear combination of the modes. Each mode is characterised by an exponential shape $e^{\lambda_i t}$ which can be rewritten as:

$$e^{\lambda_i t} = e^{(\sigma_i + j\omega_i)t} = e^{\sigma_i t} (\cos(\omega_i t) + j \sin(\omega_i t)). \quad (1.60)$$

The sign of the real part σ_i of eigenvalue λ_i defines the decaying or diverging aspect of the modal response, while the imaginary part ω_i defines the frequency of its oscillations. If one of the eigenvalues presents a strictly positive real part ($\exists \sigma_i > 0$), the response of the system to a small perturbation will diverge. On the contrary, the response will decay towards zero if all eigenvalues present a strictly negative real part ($\sigma_i < 0, \forall i$). A third possibility arises when one or more eigenvalues have a zero real part ($\exists \sigma_i = 0$), in which case linearisation fails to determine the stability properties of the equilibrium [35, Ch.4] and more elaborate methods must be considered to study the behaviour of the nonlinear system around that equilibrium. For all other cases, the stability of the equilibrium of an autonomous linearised time-invariant system such as (1.54) is determined by the state matrix \mathbf{A} , and more specifically by the real part of its eigenvalues.

Equation (1.59c) shows that the components of the right eigenvectors quantify the weight of the modes in the behaviour of the states. Likewise, the components of the left eigenvectors quantify the weight of the states in the behaviour of the modes. The weights can be combined into single factors called *participation factors* [42, Ch.12], defined as:

$$p_{ij} \triangleq \frac{|v_{ij}w_{ij}|}{\sum_{i=1}^n |v_{ij}w_{ij}|} \quad (1.61)$$

with v_{ij} the j^{th} element of right eigenvector \mathbf{v}_i and w_{ij} the j^{th} element of left eigenvector \mathbf{w}_i . As eigenvectors may be complex-valued, the participation is essentially quantified by the magnitude of the $v_{ij}w_{ij}$ quantities. Participation factor p_{ij} is a measure of the relationship between the j^{th} mode and the i^{th} state variable. For ease of interpretation, the participation factors are normalised in such a way that $\sum_{i=1}^n p_{ij} = 1$. Consequently, a factor $p_{ij} = 1$ indicates that the i^{th} state is the only contributor to the j^{th} mode, while a factor $p_{ij} = 0$ indicates that the i^{th} state does not contribute to the j^{th} mode.

The ability to relate modes with states makes modal analysis a highly insightful method. In particular, for poorly damped or unstable modes, participation factors allow determining which of the states are involved, and suggest which differential equation(s) should be modified, for instance by changing its parameters, in order to increase the damping and resolve instabilities.

Frequency response of LTI systems

The frequency response of a system describes the way in which oscillations are magnified and phase-shifted from the input to the output. In the context of LTI systems, the frequency response can be obtained by considering a complex exponential as input signal:

$$\mathbf{u}(t) = \hat{\mathbf{u}}e^{st}, \quad \text{with } s = \sigma + j\omega. \quad (1.62)$$

The imaginary part of parameter s defines the angular frequency of the input signal and $\hat{\mathbf{u}}$ is a vector of complex amplitudes. With this particular input, the forced state response in (1.53c) becomes:

$$\mathbf{x}_f(t) = \int_0^t e^{\mathbf{A}(t-\tau)} \mathbf{B} \hat{\mathbf{u}} e^{s\tau} d\tau \quad (1.63a)$$

$$= e^{\mathbf{A}t} \int_0^t e^{(sI - \mathbf{A})\tau} d\tau \mathbf{B} \hat{\mathbf{u}} \quad (1.63b)$$

$$= e^{\mathbf{A}t} (e^{(sI - \mathbf{A})t} - I)(sI - \mathbf{A})^{-1} \mathbf{B} \hat{\mathbf{u}} \quad (1.63c)$$

where we used the fact that

$$\int_0^t e^{(sI - \mathbf{A})\tau} d\tau = \left[e^{(sI - \mathbf{A})\tau} \right]_{\tau=0}^{\tau=t} (sI - \mathbf{A})^{-1} \quad (1.64a)$$

$$= (e^{(sI - \mathbf{A})t} - I)(sI - \mathbf{A})^{-1}. \quad (1.64b)$$

Adding the forced response from (1.63c) to the unforced response in (1.53b), the total state response becomes [18, Ch.3]:

$$\mathbf{x}(t) = \underbrace{e^{\mathbf{A}t} (\mathbf{x}(0) - (sI - \mathbf{A})^{-1} \mathbf{B} \hat{\mathbf{u}})}_{\mathbf{x}_{tr}(t)} + \underbrace{(sI - \mathbf{A})^{-1} \mathbf{B} \hat{\mathbf{u}} e^{st}}_{\mathbf{x}_{ss}(t)} \quad (1.65)$$

where a transient response $\mathbf{x}_{tr}(t)$ and a steady-state response $\mathbf{x}_{ss}(t)$ can be identified. Eventually, the steady-state output response of the LTI system to the complex exponential input is:

$$\mathbf{y}_{ss}(t) = \mathbf{C} \mathbf{x}_{ss}(t) + \mathbf{D} \hat{\mathbf{u}} e^{st} \quad (1.66a)$$

$$= (\mathbf{C}(sI - \mathbf{A})^{-1} \mathbf{B} + \mathbf{D}) \hat{\mathbf{u}} e^{st}. \quad (1.66b)$$

It is noted that the output $\mathbf{y}_{ss}(t)$ is itself a vector of complex exponentials of the same frequency as the input, but with possibly different amplitudes and

phase angles. Writing $\mathbf{y}_{ss}(t)$ as $\hat{\mathbf{y}}e^{st}$ allows seeing (1.66b) as a mapping between the complex amplitudes of the input and output complex exponentials:

$$\hat{\mathbf{y}} = (\mathbf{C}(sI - \mathbf{A})^{-1}\mathbf{B} + \mathbf{D})\hat{\mathbf{u}}. \quad (1.67)$$

This leads to the definition of the transfer function, i.e. the operator that defines the gain and the phase shift of the system as a function of frequency [39]:

$$\mathbf{H}(s) \triangleq \mathbf{C}(sI - \mathbf{A})^{-1}\mathbf{B} + \mathbf{D}, \quad (1.68)$$

where the inverse of $(sI - \mathbf{A})$ can be expressed in terms of its adjoint matrix and its determinant:

$$\mathbf{H}(s) = \mathbf{C} \frac{\text{adj}(sI - \mathbf{A})}{\det(sI - \mathbf{A})} \mathbf{B} + \mathbf{D}. \quad (1.69)$$

The determinant $\det(sI - \mathbf{A})$ appears at the denominator and its roots, also called *characteristic roots*, are the poles of the transfer function. Interestingly, $\det(sI - \mathbf{A})$ is also the characteristic polynomial of matrix \mathbf{A} , whose roots are the eigenvalues of \mathbf{A} [43, Ch.8]. Consequently, in such non-delayed system, the poles of the transfer function are equal to the eigenvalues of \mathbf{A} and the equilibrium point of the system is asymptotically stable if and only if all the poles have a strictly negative real part [37, Ch.5].

Despite the equivalence between transfer function poles and state matrix eigenvalues (in non-delayed systems), stability is rarely assessed based on a calculation of the poles. In fact, the roots of polynomials are highly sensitive to small numerical errors in their coefficients. When the transfer function of a given system is obtained by means of successive feedback connections of the transfer functions of its subsystems, such numerical errors are susceptible to accumulate, possibly resulting in large errors in the values of the poles. Instead, in the frequency domain, stability is generally assessed by identifying the loop gain of two interconnected subsystems and applying the Nyquist criterion to determine whether their closed-loop interconnection is stable [44].

In the next section, the discussion is extended to LTP systems.

1.3.3 Linear time-periodic systems

According to (1.45), an LTP system is described in state-space form by:

$$\left\{ \begin{array}{l} \frac{d\mathbf{x}(t)}{dt} = \mathbf{A}(t)\mathbf{x}(t) + \mathbf{B}(t)\mathbf{u}(t) \\ \mathbf{y}(t) = \mathbf{C}(t)\mathbf{x}(t) + \mathbf{D}(t)\mathbf{u}(t), \end{array} \right. \quad \begin{aligned} & (1.70a) \\ & (1.70b) \end{aligned}$$

where the matrix coefficients are periodic of fundamental period T_1 :

$$\begin{bmatrix} \mathbf{A}(t) & \mathbf{B}(t) \\ \mathbf{C}(t) & \mathbf{D}(t) \end{bmatrix} = \begin{bmatrix} \mathbf{A}(t + T_1) & \mathbf{B}(t + T_1) \\ \mathbf{C}(t + T_1) & \mathbf{D}(t + T_1) \end{bmatrix}, \quad (1.71)$$

and where, in comparison to (1.45), the small-signal tilde notation has again been dropped.

In the following paragraphs, a brief review of the time and frequency responses of LTP systems reveals their similarities and differences with respect to LTI systems, and shows why the stability criteria of LTI systems cannot be applied directly to LTP systems. For more information on the topics in this section, the reader is referred to [18, Ch.2].

Time response of LTP systems

Just as for LTI systems, the total state response is the sum of unforced and forced responses, and the unforced response is the solution of the unforced equation:

$$\frac{d\mathbf{x}(t)}{dt} = \mathbf{A}(t)\mathbf{x}(t). \quad (1.72)$$

Despite the similarities between (1.54) and (1.72), the main difference between LTI and LTP systems is related to the fact that the state matrix $\mathbf{A}(t)$ is not constant, and neither are its eigenvalues in general. The real parts of the eigenvalues of a periodic matrix such as $\mathbf{A}(t)$ may take both positive and negative values over the fundamental period with, at first sight, no apparent connection to stability. Similarly, the periodic state matrix could have all its eigenvalues constant and in the left-hand plane and the system could still be unstable [35, Ch.4]. Consequently, the study of systems with time-varying parameters requires a more general approach than that followed in Section 1.3.2, and the concept of *fundamental matrix* is introduced in this context.

Specifically, a fundamental matrix refers to any matrix $\Psi(t)$ written as

$$\Psi(t) = [\psi_1(t) \quad \cdots \quad \psi_n(t)], \quad (1.73)$$

whose columns correspond to n linearly independent vectors $\psi_i(t)$ that satisfy the unforced differential equation [45, Ch.11]:

$$\frac{d\psi_i(t)}{dt} = \mathbf{A}(t)\psi_i(t), \quad i = 1, \dots, n. \quad (1.74)$$

This implies that matrix $\Psi(t)$ also satisfies the unforced equation:

$$\frac{d\Psi(t)}{dt} = \mathbf{A}(t)\Psi(t). \quad (1.75)$$

In other words, each vector $\psi_i(t)$ is a solution of the unforced equation that corresponds to one of n linearly independent initial conditions $\psi_1(t_0), \dots, \psi_n(t_0)$. At time t_0 , the fundamental matrix is given by:

$$\Psi(t_0) = [\psi_1(t_0) \ \cdots \ \psi_n(t_0)]. \quad (1.76)$$

Since the initial matrix $\Psi(t_0)$ is invertible, the product $\Psi(t)\Psi^{-1}(t_0)$ also satisfies the unforced equation:

$$\frac{d}{dt} \left(\Psi(t)\Psi^{-1}(t_0) \right) = \mathbf{A}(t) \left(\Psi(t)\Psi^{-1}(t_0) \right). \quad (1.77)$$

Replacing t_0 with τ for generality, such product of matrices is referred to as the *state transition matrix* between times τ and t :

$$\Phi(t, \tau) \triangleq \Psi(t)\Psi^{-1}(\tau). \quad (1.78)$$

The state transition matrix is therefore also a fundamental matrix. It has the property of being equal to the identity matrix when $\tau = t$:

$$\Phi(t, t) = \mathbf{I}. \quad (1.79)$$

Additionally, the state transition matrix of an LTP system is periodic:

$$\Phi(t, \tau) = \Phi(t + T_1, \tau + T_1), \quad (1.80)$$

with T_1 the fundamental period of $\mathbf{A}(t)$. The state transition matrix allows expressing the unforced and forced state responses as [18, Ch.2]:

$$\mathbf{x}_u(t) = \Phi(t, t_0)\mathbf{x}(t_0) \quad (1.81a)$$

$$\mathbf{x}_f(t) = \int_{t_0}^t \Phi(t, \tau)\mathbf{B}(\tau)\mathbf{u}(\tau)d\tau, \quad (1.81b)$$

with their sum giving the total state response:

$$\mathbf{x}(t) = \mathbf{x}_u(t) + \mathbf{x}_f(t). \quad (1.81c)$$

Eventually, the state transition matrix $\Phi(t, t_0)$ can be seen as a generalisation of the matrix $e^{\mathbf{A}(t-t_0)}$ involved in the time response of LTI systems. Since there is a relationship between $e^{\mathbf{A}(t-t_0)}$ and the stability of LTI systems, the next paragraphs make a step towards establishing the relationship between the state transition matrix $\Phi(t, t_0)$ and the stability of LTP systems.

According to the Floquet-Lyapunov theory, the state transition matrix of an LTP system can be expressed as [18, Ch.2]:

$$\Phi(t, \tau) = \mathbf{P}(t)e^{\mathbf{Q}(t-\tau)}\mathbf{P}^{-1}(\tau), \quad (1.82)$$

| system | LTI | LTP |
|-----------------------|--|---|
| unforced response | $e^{\mathbf{A}(t-t_0)}\mathbf{x}(t_0)$ | $\mathbf{P}(t)e^{\mathbf{Q}(t-t_0)}\mathbf{x}(t_0)$ |
| stability information | eigenvalues of \mathbf{A} | eigenvalues of \mathbf{Q} |

Table 1.2: Similarities between LTI and LTP systems

with \mathbf{Q} a constant matrix called the *Floquet matrix*, and $\mathbf{P}(t)$ a periodic matrix of fundamental period T_1 such that $\mathbf{P}(t_0) = \mathbf{P}(t_0 + T_1) = \mathbf{I}$. Both $\mathbf{P}(t)$ and \mathbf{Q} may be complex-valued.

Relying on (1.82), the unforced state response becomes:

$$\mathbf{x}_u(t) = \Phi(t, t_0)\mathbf{x}(t_0) \quad (1.83a)$$

$$= \mathbf{P}(t)e^{\mathbf{Q}(t-t_0)}\mathbf{P}^{-1}(t_0)\mathbf{x}(t_0) \quad (1.83b)$$

$$= \mathbf{P}(t)e^{\mathbf{Q}(t-t_0)}\mathbf{x}(t_0). \quad (1.83c)$$

Just as for LTI systems, the unforced response of LTP systems involves an exponential matrix of the form $e^{\mathbf{Q}(t-t_0)}$. Mirroring the conclusions that were obtained for LTI systems, the Floquet matrix \mathbf{Q} is therefore a matrix whose eigenvalues define whether the equilibrium of the periodic system is stable.

The similarities between LTI and LTP systems are summarised in Table 1.2. As far as LTP systems are concerned, it is worthwhile observing that the relationship between periodicity and stability is essentially contained within the relationship between periodic matrix $\mathbf{A}(t)$ and the eigenvalues of the constant Floquet matrix \mathbf{Q} . Despite knowing that a constant matrix \mathbf{Q} exists for any LTP system, (1.82) does not provide a way of calculating it, at least at first sight, since matrix $\mathbf{P}(t)$ is also unknown. Consequently, the application of modal analysis to LTP systems via a direct eigenvalue calculation is not possible *a priori*. These aspects are further discussed in Section 2.2.

Frequency response of LTP systems

Similarly to LTI systems, insights into the frequency response of LTP systems can be obtained by considering a complex exponential $\hat{\mathbf{u}}e^{s(t-t_0)}$ as input signal. With this particular input, the forced state response in (1.81b) becomes:

$$\mathbf{x}_f(t) = \int_{t_0}^t \Phi(t, \tau)\mathbf{B}(\tau)\hat{\mathbf{u}}e^{s(\tau-t_0)}d\tau. \quad (1.84)$$

Recalling the expression of the state transition matrix from (1.82), we obtain:

$$\mathbf{x}_f(t) = \int_{t_0}^t \underbrace{\mathbf{P}(t)e^{\mathbf{Q}(t-\tau)}\mathbf{P}^{-1}(\tau)}_{\Phi(t,\tau)} \mathbf{B}(\tau)\hat{\mathbf{u}}e^{s(\tau-t_0)}d\tau \quad (1.85a)$$

$$= \mathbf{P}(t)e^{\mathbf{Q}(t-t_0)} \int_{t_0}^t e^{-\mathbf{Q}(\tau-t_0)} \underbrace{\mathbf{P}^{-1}(\tau)\mathbf{B}(\tau)}_{\triangleq \bar{\mathbf{B}}(\tau)} \hat{\mathbf{u}}e^{s(\tau-t_0)}d\tau \quad (1.85b)$$

where we used the fact that $e^{\mathbf{Q}(t-\tau)} = e^{\mathbf{Q}(t-t_0)}e^{-\mathbf{Q}(\tau-t_0)}$. Since both matrices $\mathbf{P}(t)$ and $\mathbf{B}(t)$ are periodic, the defined quantity $\bar{\mathbf{B}}(\tau)$ is also periodic and can be written as the following Fourier series:

$$\bar{\mathbf{B}}(\tau) = \sum_{k=-\infty}^{+\infty} \bar{\mathbf{B}}_k e^{jk\omega_1(\tau-t_0)}. \quad (1.86)$$

Including this expression in (1.85b), the forced response becomes:

$$\mathbf{x}_f(t) = \mathbf{P}(t)e^{\mathbf{Q}(t-t_0)} \overbrace{\int_{t_0}^t e^{-\mathbf{Q}(\tau-t_0)} \sum_{k=-\infty}^{+\infty} (\bar{\mathbf{B}}_k e^{jk\omega_1(\tau-t_0)}) \hat{\mathbf{u}}e^{s(\tau-t_0)}d\tau}^{\bar{\mathbf{B}}(\tau)} \quad (1.87a)$$

$$= \mathbf{P}(t)e^{\mathbf{Q}(t-t_0)} \sum_{k=-\infty}^{+\infty} \int_{t_0}^t e^{(s_k \mathbf{I} - \mathbf{Q})(\tau-t_0)} d\tau \bar{\mathbf{B}}_k \hat{\mathbf{u}} \quad (1.87b)$$

$$= \mathbf{P}(t)e^{\mathbf{Q}(t-t_0)} \sum_{k=-\infty}^{+\infty} \left(e^{(s_k \mathbf{I} - \mathbf{Q})(t-t_0)} - I \right) (s_k \mathbf{I} - \mathbf{Q})^{-1} \bar{\mathbf{B}}_k \hat{\mathbf{u}} \quad (1.87c)$$

where s_k is defined as $s_k \triangleq s + jk\omega_1$ and where we used the fact that

$$\int_{t_0}^t e^{(s_k \mathbf{I} - \mathbf{Q})(\tau-t_0)} d\tau = \left[e^{(s_k \mathbf{I} - \mathbf{Q})(\tau-t_0)} \right]_{\tau=t_0}^{\tau=t} (s_k \mathbf{I} - \mathbf{Q})^{-1} \quad (1.88a)$$

$$= \left(e^{(s_k \mathbf{I} - \mathbf{Q})(t-t_0)} - I \right) (s_k \mathbf{I} - \mathbf{Q})^{-1}. \quad (1.88b)$$

Adding the forced response from (1.87c) to the unforced response in (1.81a), the total state response becomes:

$$\begin{aligned} \mathbf{x}(t) &= \underbrace{\Phi(t, t_0) \left(\mathbf{x}(t_0) - \sum_{k=-\infty}^{+\infty} (s_k \mathbf{I} - \mathbf{Q})^{-1} \bar{\mathbf{B}}_k \hat{\mathbf{u}} \right)}_{\mathbf{x}_{tr}(t)} \\ &\quad + \underbrace{\mathbf{P}(t) \sum_{k=-\infty}^{+\infty} (s_k \mathbf{I} - \mathbf{Q})^{-1} \bar{\mathbf{B}}_k \hat{\mathbf{u}} e^{s_k(t-t_0)}}_{\mathbf{x}_{ss}(t)}, \end{aligned} \quad (1.89)$$

where a transient response $\mathbf{x}_{tr}(t)$ and a steady-state response $\mathbf{x}_{ss}(t)$ can be identified. The steady-state response can be written in a more compact form by defining a time-periodic matrix $\mathbf{L}(t, s)$ as:

$$\mathbf{L}(t, s) \triangleq \sum_{k=-\infty}^{+\infty} (s_k \mathbf{I} - \mathbf{Q})^{-1} \bar{\mathbf{B}}_k e^{jk\omega_1(t-t_0)}, \quad (1.90)$$

which gives:

$$\mathbf{x}_{ss}(t) = \mathbf{P}(t) \mathbf{L}(t, s) \hat{\mathbf{u}} e^{s(t-t_0)}. \quad (1.91)$$

Matrix $\mathbf{L}(t, s)$ can be seen as a scaled version of the quantity $\bar{\mathbf{B}}(t) = \mathbf{P}^{-1}(t) \mathbf{B}(t)$, with a complex-valued frequency-dependent scaling factor $(s_k \mathbf{I} - \mathbf{Q})^{-1}$. Eventually, the steady-state output response of the LTP system to the complex exponential input is:

$$\mathbf{y}_{ss}(t) = \mathbf{C}(t) \mathbf{x}_{ss}(t) + \mathbf{D}(t) \hat{\mathbf{u}} e^{s(t-t_0)} \quad (1.92a)$$

$$= (\mathbf{C}(t) \mathbf{P}(t) \mathbf{L}(t, s) + \mathbf{D}(t)) \hat{\mathbf{u}} e^{s(t-t_0)}. \quad (1.92b)$$

By analogy with the transfer functions of LTI systems, the *periodic transfer operator* [46, Ch.2] is defined as:

$$\mathbf{G}(t, s) \triangleq \mathbf{C}(t) \mathbf{P}(t) \mathbf{L}(t, s) + \mathbf{D}(t). \quad (1.93)$$

$\mathbf{G}(t, s)$ being a periodic function of time, it can be written as the following Fourier series:

$$\mathbf{G}(t, s) = \sum_{k=-\infty}^{+\infty} \mathbf{G}_k(s) e^{jk\omega_1(t-t_0)}, \quad (1.94)$$

where the Fourier coefficients $\mathbf{G}_k(s)$ are constant but frequency-dependent. The steady-state output response can finally be rewritten as:

$$\mathbf{y}_{ss}(t) = \sum_{k=-\infty}^{+\infty} \mathbf{G}_k(s) \hat{\mathbf{u}} e^{(s+jk\omega_1)(t-t_0)}. \quad (1.95)$$

In the case of LTI systems, it was observed that applying a complex exponential input perturbation at a given frequency led to a complex exponential output component with possibly different magnitude and phase, but with the same frequency. According to (1.95), applying the same perturbation to an LTP system leads to not only one, but multiple (possibly, an infinite number of) complex exponential components at the output. Noting ω_p the frequency of the input oscillation, the output oscillations are located at frequencies $\{\omega_p + k\omega_1\}$, $k \in \mathbb{Z}$. This is the consequence of the frequency coupling phenomenon in LTP systems.

Setting $t_0 = 0$ and defining $\mathbf{y}_k(s) \triangleq \mathbf{G}_k(s)\hat{\mathbf{u}}$, (1.95) can be rewritten as:

$$\mathbf{y}_{ss}(t) = \sum_{k=-\infty}^{+\infty} \mathbf{y}_k(s) e^{(s+jk\omega_1)t} \quad (1.96a)$$

$$= \sum_{k=-\infty}^{+\infty} \underbrace{\mathbf{y}_k(s)e^{st}}_{\triangleq \mathbf{y}_k(t,s)} e^{jk\omega_1 t} = \sum_{k=-\infty}^{+\infty} \mathbf{y}_k(t,s) e^{jk\omega_1 t}, \quad (1.96b)$$

as well as:

$$\mathbf{y}_{ss}(t) = \underbrace{\left(\sum_{k=-\infty}^{+\infty} \mathbf{y}_k(s) e^{jk\omega_1 t} \right)}_{\triangleq \mathbf{y}_p(t,s)} e^{st} = \mathbf{y}_p(t,s) e^{st}. \quad (1.96c)$$

The above shows that the steady-state output response can be interpreted as both a Fourier series with time- and frequency-dependent Fourier coefficients in (1.96b), and as a time-periodic signal $\mathbf{y}_p(t,s) = \mathbf{y}_p(t+T_1, s)$ of fundamental frequency $\omega_1 = 2\pi/T_1$ modulated by a complex exponential e^{st} in (1.96c). The latter is referred to as an exponentially-modulated periodic (EMP) signal [18, Ch.3], which will come again into play in Chapter 3.

Remarks

While it is straightforward to describe the input-output behaviour of LTI systems by means of a transfer function and to establish a relationship between the poles of the transfer function and stability of LTI systems, the relationship between the periodic transfer operator and stability of LTP systems is not directly apparent, which hints towards the fact that stability analysis based on transfer functions is not directly applicable to LTP systems. It is also recalled that no conclusion on stability can be drawn directly from the eigenvalues of the periodic state matrix $\mathbf{A}(t)$.

Overall, traditional stability analysis methods dedicated to LTI systems are not readily applicable to LTP systems. For this reason, several approaches exist to analyse the small-signal stability of periodic trajectories. These approaches, only briefly introduced here, are described in detail in the following chapters.

- A first approach stems from the idea that transformations can be used to convert periodic variables into constant variables. In this context, a first category of transformations consists in applying a periodic change of variables such that the studied periodic trajectory is transformed into an equilibrium point. Such transformations enable linearising the modified nonlinear equations around the resulting equilibrium point, in which case the process may result in an LTI system instead of an LTP system. Frame rotations and dynamic phasors are such transformations that, in specific cases, can be applied to the variables of nonlinear systems to make them constant in steady state [34]. Frame rotations are presented in Section 2.4 and dynamic phasors are briefly covered in Section 3.2.4.
- As an alternative to transforming periodic trajectories, other approaches are applied instead on the LTP system that results from linearisation around a periodic trajectory. The idea consists in transforming the local LTP approximation into an LTI approximation. In this case, the objective is not to transform the periodic variables of nonlinear systems to make them constant in steady state, but to transform the periodic coefficients of the LTP approximation into constant coefficients. Such transformations of the coefficients enable the application of stability analysis techniques of LTI systems onto LTP systems, albeit indirectly. Frequency-lifting and, to some extent, the Floquet transformation, are examples of such transformations. The Floquet transformation is presented in Section 2.2, while the harmonic state space and harmonic transfer function methods, which rely on frequency-lifting, are presented in Chapter 3.
- Given the apparent complexity of accounting for the oscillatory components of periodic coefficients of an LTP system in its small-signal stability assessment, it is relevant to consider the possibility of simply neglecting these oscillatory components, which results in an approximate LTI system. This approach, referred to as the *averaging technique*, is investigated in Section 2.3.
- Instead of transforming or approximating LTP systems into LTI systems, an additional approach consist in addressing the LTP systems *as such*, e.g. by calculating characteristic matrices such as the Floquet matrix or the monodromy matrix, whose eigenvalues are constant and characterise the stability of LTP systems. These matrices are further discussed in Section 2.2.

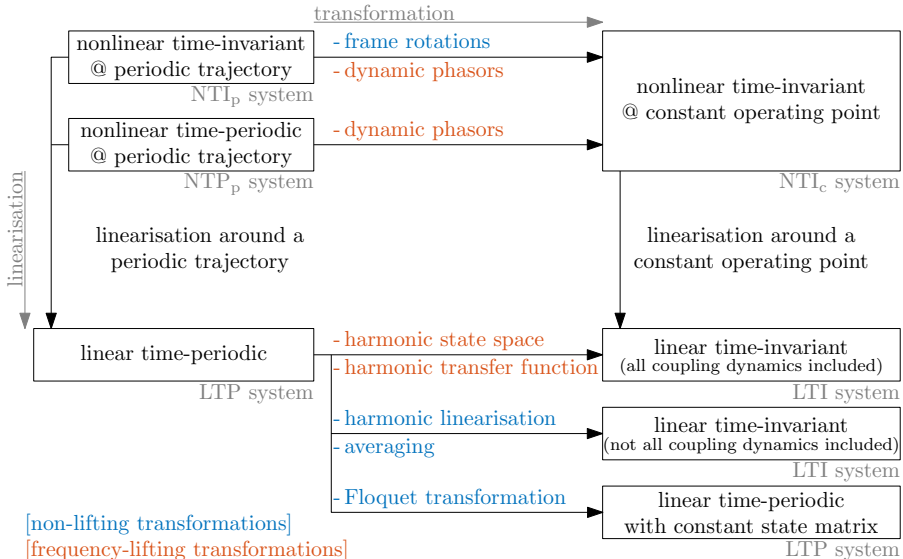


Figure 1.7: Overview of system types and transformations

The different options are depicted in Fig. 1.7, which revisits Fig. 1.6. It is shown that, in the case of NTI_p systems, one path consists in first transforming the periodic trajectory into a constant operating point, and then linearising the resulting NTI_c system to obtain an LTI formulation. The same option exists for NTP_p systems, however periodic parameters must also be addressed in the transformation to obtain an NTI_c system. Alternatively, NTI_p and NTP_p systems may be linearised around their periodic trajectories to obtain LTP representations. The latter can either be transformed into another LTP system but with a constant state matrix, or into LTI systems in which the impact of frequency couplings can be depicted to different levels of accuracy.

1.4 Chapter conclusion

This chapter presented a stationary-frame arm-averaged dynamic model of the three-phase MMC as well as a set of control equations. Typical waveforms showed that the state variables display oscillatory components in steady-state. Consequently, the system does not operate at a constant operating point but follows a periodic trajectory in steady state. To understand the stability characteristics of such periodic trajectories when they are subject to small

perturbations, it was shown that the linearised equations of the stationary-frame MMC model correspond to an LTP system, which has periodic coefficients.

The fundamentals of LTI and LTP systems have been reviewed, highlighting the fact that the traditional stability analysis methods of LTI systems are not directly applicable to LTP systems. Several alternatives have been identified. The simplest option *a priori* consists in neglecting the oscillatory components through an averaging technique. Otherwise, accounting for the oscillatory components is possible, either by transforming the periodic trajectory into a constant operating point, or by transforming the periodic coefficients of LTP systems into constant coefficients. These options are covered in detail in Chapters 2 and 3.

Chapter 2

Non-lifting transformation methods

2.1 Introduction

This chapter is dedicated to reviewing existing transformations of nonlinear systems following periodic trajectories, such as the MMC, into linear time-invariant systems. This review fulfils Objective 2.

Firstly, Section 2.2 continues the description of Floquet-Lyapunov theory started in Section 1.3. It presents the monodromy matrix, a keystone in the study of LTP systems. Next, the Floquet transformation is presented as a way of converting an LTP system into an equivalent linear system, still time-periodic but with a constant state matrix. The Floquet transformation delivers essential insights into the behaviour of LTP systems.

Secondly, Section 2.3 is dedicated to developing a mathematical criterion theoretically capable of determining conditions under which oscillatory components of the periodic coefficients of LTP systems can be safely neglected in a stability analysis, which fulfils Objective 3. This simplification, which relies on an averaging technique, is a form of transformation since it results in an LTI system, albeit an approximation instead of an equivalent representation of the initial LTP system.

Lastly, Section 2.4 presents frame rotations as a way of transforming periodic trajectories into constant operating points. This section also presents the necessary steps and assumptions leading towards a model of the MMC developed

in [47] and known as the multiple synchronously-rotating reference frames model. It is shown that the numerous advantages of frame rotations make them the preferred transformation approach in a large number of cases, unless there is a need to account for single-phase systems, for unbalanced multi-phase systems, or simply for a wider spectrum of periodic trajectories.

2.2 Floquet-Lyapunov theory

Floquet-Lyapunov theory provides two main approaches for the stability assessment of LTP systems. On the one hand, Floquet-Lyapunov theory shows that the stability information is contained within the monodromy matrix, which characterises the dynamic behaviour of LTP systems from one period to the next, and whose eigenvalues define whether the system is stable or not. On the other hand, the theory shows that an LTP system can be transformed into an equivalent system whose state matrix is constant, and whose eigenvalues also define whether the system is stable. Both approaches are presented in this section. For more information on these topics, the reader is referred to [18, Ch.2] and [48, Ch.3].

2.2.1 The monodromy matrix

A useful trick in the stability analysis of periodic systems is to study their dynamic behaviour "from one period to the next", i.e. from instant t to instant $t + T_1$. In this context, we rely on the concept of state transition matrix to obtain a time-invariant equivalent of the unforced LTP system:

$$\frac{d\mathbf{x}(t)}{dt} = \mathbf{A}(t)\mathbf{x}(t). \quad (2.1)$$

As presented in Section 1.3.3, the state transition matrix $\Phi(t, t_0)$ of an LTP system is a solution of the unforced differential equation and can be written as a function of a periodic matrix $\mathbf{P}(t)$ and the constant Floquet matrix \mathbf{Q} :

$$\frac{d}{dt}\Phi(t, t_0) = \mathbf{A}(t)\Phi(t, t_0) \quad (2.2a)$$

$$\Phi(t, \tau) = \mathbf{P}(t)e^{\mathbf{Q}(t-\tau)}\mathbf{P}^{-1}(\tau). \quad (2.2b)$$

Recalling (1.83a), the unforced state response $\mathbf{x}_u(t)$ can be written by means of the state transition matrix as:

$$\mathbf{x}_u(t) = \Phi(t, t_0)\mathbf{x}(t_0). \quad (2.3)$$

After one fundamental period, at $t = t_0 + T_1$, the unforced response becomes:

$$\mathbf{x}_u(t_0 + T_1) = \Phi(t_0 + T_1, t_0)\mathbf{x}(t_0) \quad (2.4a)$$

$$= \mathbf{P}(t_0 + T_1)e^{\mathbf{Q}(t_0 + T_1 - t_0)}\mathbf{P}(t_0)\mathbf{x}(t_0) \quad (2.4b)$$

$$= e^{T_1\mathbf{Q}}\mathbf{x}(t_0), \quad (2.4c)$$

where we used the fact that $\mathbf{P}(t_0 + T_1) = \mathbf{P}(t_0) = \mathbf{I}$.

The state transition matrix from t_0 to $t_0 + T_1$ is called the *monodromy matrix at time t_0* and is noted Ψ :

$$\Psi \triangleq \Phi(t_0 + T_1, t_0) = e^{T_1\mathbf{Q}}. \quad (2.5)$$

The monodromy matrix at time t is periodic [48, Ch.3], i.e.

$$\Phi(t + T_1, t) = \Phi(t + 2T_1, t + T_1), \quad \forall t. \quad (2.6)$$

Remarkably, the eigenvalues of the monodromy matrix, which are called the *Floquet multipliers*, are constant, i.e. they do not depend on t [48, Ch.3]. The time at which the monodromy matrix is considered is thus not important for eigenvalue-based analyses. Consequently, in this thesis, the monodromy matrix will be considered at time t_0 and will be simply referred to as the *monodromy matrix*.

After k fundamental periods ($k \in \mathbb{N}$), the unforced response becomes:

$$\mathbf{x}_u(t_0 + kT_1) = e^{kT_1\mathbf{Q}}\mathbf{x}(t_0) = \Psi^k\mathbf{x}(t_0). \quad (2.7)$$

The above equation can be interpreted as the result of discretising the unforced LTP system with a time step equal to the fundamental period T_1 . It can be seen that, as k grows, the unforced state response will diverge if Ψ has at least one Floquet multiplier with a modulus strictly larger than 1. If all Floquet multipliers lie within the unit circle in the complex plane, then the origin of the LTP system is asymptotically stable [18, Ch.2].

Worthwhile noting is that the monodromy matrix describing the periodic solutions of autonomous systems always has a trivial Floquet multiplier equal to 1 with a corresponding eigenvector along the direction of the periodic trajectory $\bar{p}(t)$ [49]. However, the LTP systems covered here are non-autonomous and all their Floquet multipliers are non-trivial. A preliminary step to their calculation is to obtain the monodromy matrix, which is considered next.

Determination of the monodromy matrix via numerical integration

Considering that the monodromy matrix is the state transition matrix from t_0 to $t_0 + T_1$, one approach to its calculation consists in solving the linearised

unforced differential equations for n linearly-independent initial conditions over $[t_0, t_0 + T_1]$. Each solution then forms one column of the state transition matrix. To obtain the state transition matrix and not any fundamental matrix, the initial condition $\Phi(t_0, t_0) = \mathbf{I}$ must be satisfied, which means that the i^{th} initial condition $\psi_i(t_0)$ is a unit vector corresponding to the i^{th} column of the identity matrix, noted δ_i . In summary, the following initial value problem

$$\begin{cases} \frac{d\psi_i(t)}{dt} = \mathbf{A}(t)\psi_i(t) \\ \psi_i(t_0) = \delta_i \end{cases} \quad (2.8)$$

is solved for $i = 1, \dots, n$ and the monodromy matrix is given by:

$$\Psi = \Phi(t_0 + T_1, t_0) = \begin{bmatrix} \psi_1(t_0 + T_1) & \dots & \psi_n(t_0 + T_1) \end{bmatrix}. \quad (2.9)$$

Eventually, the Floquet multipliers are retrieved as the eigenvalues of Ψ .

While this method benefits from its simplicity, solving differential equations is not always the most efficient approach. Even more, this approach amounts to solving n times the complete system (equivalently, n^2 differential equations) over the fundamental period. Additionally, the results of numerical integration for the purpose of determining the monodromy matrix may be ill-conditioned [50]. Alternative approaches such as shooting and multiple-shooting methods, for instance the one covered in [51], are capable of delivering the monodromy matrix as a by-product of a periodic trajectory calculation. However, shooting methods also rely on numerical integration which still limits their computational efficiency. Other approaches based on polynomial-based collocation methods would be preferred in that regard, as the monodromy matrix can be obtained as a by-product of a periodic trajectory calculation without relying on numerical integration of the differential equations [52, 53].

2.2.2 Floquet transformation

The second topic from Floquet-Lyapunov theory covered in this section is the Floquet transformation. The principle behind this transformation is to apply a periodic change of variables to the LTP system. First, a necessary preliminary result is given, after what the Floquet transformation is presented specifically.

Preliminary result

The preliminary step consists in establishing the relationship between matrices $\mathbf{P}(t)$, \mathbf{Q} and $\mathbf{A}(t)$. Starting from the state transition matrix with $t_0 = 0$, $\mathbf{P}(t)$

and its time derivative can be expressed as:

$$\mathbf{P}(t) = \Phi(t, 0)e^{-\mathbf{Q}t} \quad (2.10a)$$

$$\dot{\mathbf{P}}(t) = \dot{\Phi}(t, 0)e^{-\mathbf{Q}t} - \Phi(t, 0)e^{-\mathbf{Q}t}\mathbf{Q} \quad (2.10b)$$

$$= \dot{\Phi}(t, 0)e^{-\mathbf{Q}t} - \mathbf{P}(t)\mathbf{Q}. \quad (2.10c)$$

Recalling that the state transition matrix is a solution of the unforced equation, its time derivative is given by $\dot{\Phi}(t, 0) = \mathbf{A}(t)\Phi(t, 0)$. This leads to:

$$\dot{\mathbf{P}}(t) = \mathbf{A}(t)\Phi(t, 0)e^{-\mathbf{Q}t} - \mathbf{P}(t)\mathbf{Q} \quad (2.11a)$$

$$= \mathbf{A}(t)\mathbf{P}(t) - \mathbf{P}(t)\mathbf{Q}. \quad (2.11b)$$

Isolating Floquet matrix \mathbf{Q} , we obtain:

$$\mathbf{Q} = \mathbf{P}^{-1}(t) (\mathbf{A}(t)\mathbf{P}(t) - \dot{\mathbf{P}}(t)), \quad (2.12)$$

which is the sought relationship between matrices $\mathbf{P}(t)$, \mathbf{Q} and $\mathbf{A}(t)$.

Floquet transformation

We consider the generic state-space representation of LTP systems:

$$\begin{cases} \dot{\mathbf{x}}(t) = \mathbf{A}(t)\mathbf{x}(t) + \mathbf{B}(t)\mathbf{u}(t) \\ \mathbf{y}(t) = \mathbf{C}(t)\mathbf{x}(t) + \mathbf{D}(t)\mathbf{u}(t). \end{cases} \quad (2.13)$$

To transform the LTP system into an equivalent system with a constant state matrix, the Floquet transformation relies on a periodic change of variables involving the periodic matrix $\mathbf{P}(t)$:

$$\mathbf{x}(t) = \mathbf{P}(t)\mathbf{v}(t) \iff \mathbf{v}(t) = \mathbf{P}^{-1}(t)\mathbf{x}(t). \quad (2.14)$$

Using the chain rule, the time derivative of $\mathbf{x}(t)$ is expressed as:

$$\dot{\mathbf{x}}(t) = \dot{\mathbf{P}}(t)\mathbf{v}(t) + \mathbf{P}(t)\dot{\mathbf{v}}(t). \quad (2.15)$$

Substituting the expressions of $\mathbf{x}(t)$ and $\dot{\mathbf{x}}(t)$ into (2.13), we obtain:

$$\begin{cases} \dot{\mathbf{P}}(t)\mathbf{v}(t) + \mathbf{P}(t)\dot{\mathbf{v}}(t) = \mathbf{A}(t)\mathbf{P}(t)\mathbf{v}(t) + \mathbf{B}(t)\mathbf{u}(t) \\ \mathbf{y}(t) = \mathbf{C}(t)\mathbf{P}(t)\mathbf{v}(t) + \mathbf{D}(t)\mathbf{u}(t). \end{cases} \quad (2.16)$$

Reorganising the differential equation, we have:

$$\begin{cases} \dot{\mathbf{v}}(t) = \underbrace{\mathbf{P}^{-1}(t) (\mathbf{A}(t)\mathbf{P} - \dot{\mathbf{P}}(t))}_{= \mathbf{Q}} \mathbf{v}(t) + \mathbf{P}^{-1}(t)\mathbf{B}(t)\mathbf{u}(t) \\ \mathbf{y}(t) = \mathbf{C}(t)\mathbf{P}(t)\mathbf{v}(t) + \mathbf{D}(t)\mathbf{u}(t) \end{cases} \quad (2.17)$$

where \mathbf{Q} can be identified according to the preliminary result. Defining also $\bar{\mathbf{B}}(t) \triangleq \mathbf{P}^{-1}(t)\mathbf{B}(t)$ and $\bar{\mathbf{C}}(t) \triangleq \mathbf{C}(t)\mathbf{P}(t)$, the LTP system eventually becomes:

$$\begin{cases} \dot{\mathbf{v}}(t) = \mathbf{Q}\mathbf{v}(t) + \bar{\mathbf{B}}(t)\mathbf{u}(t) \\ \mathbf{y}(t) = \bar{\mathbf{C}}(t)\mathbf{v}(t) + \mathbf{D}(t)\mathbf{u}(t). \end{cases} \quad (2.18)$$

Although the resulting system is still time-periodic, the new state matrix is the Floquet matrix \mathbf{Q} , which is constant. The eigenvalues of \mathbf{Q} are called the *Floquet exponents* and can be used to assess the stability of the LTP system. Specifically, if all Floquet exponents have a strictly negative real part, then the origin of the LTP system is asymptotically stable.

Remarks

- An advantage of the Floquet transformation is that it accounts precisely for the oscillatory components of $\mathbf{A}(t)$: no assumption or simplification of the harmonic content is involved.
- The input-output behaviour of the system is not impacted by the Floquet transformation since the change of variables concerns only the states. This can be seen as a disadvantage since the input-output behaviour is still time-dependent: the periodic transfer operator of the system remains unchanged and, at this point of the discussion, no time-invariant transfer function can be obtained for the transformed system.
- A limitation to the use of the Floquet transformation as a way of obtaining an LTI form of the unforced system is that matrix $\mathbf{P}(t)$ is generally unknown. This limitation hinders the application of the Floquet transformation to practical cases, which motivates the discussion of alternative methods that do not depend on prior knowledge of this matrix.
- The Floquet transformation can be interpreted as a time-varying coordinate transformation, providing a new set of coordinates for the states. Similarly, the technique of frame rotations relies on periodic transformation matrices composed of sinusoidal waves at selected frequencies to convert periodic quantities into constant quantities. Unlike

the Floquet transformation, frame rotations involve known transformation matrices. The technique of frame rotations is discussed in Section 2.4.

Relationship between Floquet multipliers and Floquet exponents

The definition of the monodromy matrix Ψ in (2.5) gives its relationship to the Floquet matrix Q :

$$\Psi = e^{T_1 Q}. \quad (2.19)$$

This relationship allows calculating one possible matrix Q from the monodromy matrix:

$$Q = \frac{1}{T_1} (\ln(\Psi) + 2jk\pi I) = f_1 \ln(\Psi) + jk\omega_1 I, \quad \forall k \in \mathbb{Z} \quad (2.20)$$

where $\ln(\Psi)$ refers to a matrix logarithm of Ψ , and I is the identity matrix of size n . The result is non-unique, as the matrix logarithm is defined up to a factor $jk\omega_1$, with $\omega_1 = 2\pi/T_1$. This shows that, unlike the Floquet multipliers (eigenvalues of Ψ) which are uniquely defined for a given LTP system, the Floquet exponents (eigenvalues of Q) are not unique. This particular feature of the Floquet exponents implies that it is not possible to determine the exact oscillatory frequency of the modes based on the eigenvalues of the monodromy matrix or of the Floquet matrix with the approach of (2.20), which is thus a limitation to their use in the context of small-signal stability studies. This observation will come again into play when discussing the eigenvalues of frequency-lifted systems in Section 3.2.4.

2.2.3 Conclusion

Floquet-Lyapunov theory provides fundamental insights into LTP systems as well as two particular options for stability assessments: the monodromy matrix and the Floquet transformation.

On the one hand, the monodromy matrix describes the evolution of a periodic system from one period to the next. Its eigenvalues are constant and contain information about stability. Numerical integration of the unforced LTP differential equation was briefly presented as a way of determining the monodromy matrix. However, numerical integration may be computationally intensive and, for the purpose of stability assessments, its results may be ill-conditioned for the calculation of eigenvalues. Additionally, identifying the precise oscillation frequency of the modes is complicated by the fact that this information is only defined up to an integer multiple of the fundamental frequency.

On the other hand, the Floquet transformation relies on a time-periodic similarity transformation to convert the periodic state matrix of an LTP system into a constant state matrix (the Floquet matrix). Despite the advantage of generality, the Floquet transformation is not directly applicable since the necessary periodic transformation matrix is generally unknown. This limitation motivates the introduction of alternative methods capable of accounting for the oscillatory components in the small-signal stability assessment of periodic trajectories. In this context, frame rotations will be presented in Section 2.4 as a transformation method which, unlike the Floquet transformation, involves known periodic matrices.

Before discussing frame rotations, the following section is dedicated to exploring an averaging technique, in which the link between monodromy matrix and stability is harnessed to establish a sufficient stability criterion for LTP systems based on LTI approximations.

2.3 Averaging technique

Considering the objective of obtaining LTI counterparts of LTP systems in order to facilitate the stability analysis of their equilibria, this section touches upon an averaging technique in which the periodic coefficients of an LTP system are simply approximated by their constant part¹, while the oscillatory components are neglected.

Intuitively, this may be a valid approach as long as the oscillatory components are "small enough". This intuition is formally covered by the theory of averaging described for instance in [35, Ch.10] and [37, Ch.6], where theorems are formulated in the general context of nonlinear systems. These theorems support the idea that, for systems with particular structures and under particular assumptions, there exist parameters such that stability of an equilibrium of the nonlinear system can be inferred from the stability of the averaged system. However, in general, the available theorems only ensure that such parameters exist, but do not provide a way of determining their values.

This section addresses this limitation and aims to establish a criterion for the averaging of LTP systems specifically, with the capability of quantifying parameters such that the averaging principle is applicable. The idea stems from a similar criterion given for discrete-time systems in [46, Proposition 3.4].

¹ It is noted that considering the constant part of the coefficients of an LTP system is not generally equivalent to considering the constant part of the periodic variables of the original nonlinear system. The reason is that the coefficients of the linearised equations may be nonlinear functions of the steady-state variables.

The original contribution of this section is thus the derivation of a counterpart specifically for continuous-time systems².

2.3.1 Problem statement and existing result

We consider the unforced LTP system with the following differential equation and initial condition:

$$\begin{cases} \dot{\mathbf{x}}(t) = \mathbf{A}(t)\mathbf{x}(t) \\ \mathbf{x}(0) = \mathbf{x}_{\text{init}}. \end{cases} \quad (2.21)$$

We define \mathbf{A}_0 as the constant part of $\mathbf{A}(t)$, i.e. its average value over the fundamental period, which is also its index-0 Fourier coefficient. Next, we consider the LTI system that has \mathbf{A}_0 as state matrix, the initial condition remaining the same:

$$\dot{\mathbf{x}}(t) = \mathbf{A}_0\mathbf{x}(t). \quad (2.22)$$

In this context, the differential equation in (2.21) can be seen as a disturbed version of (2.22) and is equivalent to:

$$\dot{\mathbf{x}}(t) = \mathbf{A}_0\mathbf{x}(t) + \underbrace{(\mathbf{A}(t) - \mathbf{A}_0)}_{\triangleq \mathbf{E}(t)}\mathbf{x}(t). \quad (2.23)$$

Nonlinear systems with a structure close to that of (2.23) have been studied in e.g. [35, Section 10.3]:

$$\dot{\mathbf{x}}(t) = \mathbf{f}(\mathbf{x}(t)) + \epsilon\mathbf{g}(t, \mathbf{x}(t), \epsilon). \quad (2.24)$$

According to Theorem 10.3 in [35], if \mathbf{f} and \mathbf{g} in (2.24) are bounded and sufficiently smooth, if the origin is an exponentially stable equilibrium of $\dot{\mathbf{x}}(t) = \mathbf{f}(\mathbf{x}(t))$, if $\mathbf{g}(t, \mathbf{x}(t), \epsilon)$ is time-periodic and if $\mathbf{g}(t, \mathbf{0}, \epsilon) = \mathbf{0}$, then there exist a sufficiently small ϵ such that the origin is also an exponentially stable equilibrium of (2.24). Associating $\mathbf{A}_0\mathbf{x}(t)$ to $\mathbf{f}(\mathbf{x}(t))$ and $\mathbf{E}(t)\mathbf{x}(t)$ to $\epsilon\mathbf{g}(t, \mathbf{x}(t), \epsilon)$, the same theorem ensures that (2.23) is exponentially stable if (2.22) is exponentially stable and if $\mathbf{E}(t)\mathbf{x}(t)$ is small enough.

In this section, the objective is to find a condition on the size of $\mathbf{E}(t)$ specifically, such that if (2.22) is stable, then (2.21) is stable too. It is emphasised that no particular attention is given in this section to the exact harmonic content of $\mathbf{E}(t)$, which potentially contains oscillatory components from the fundamental frequency up to an arbitrarily-large harmonic rank.

² The author warmly thanks Dr. Katrien De Cock for her careful proofreading of this section and her help with the establishment of a relationship between the state transition matrix and the periodic disturbance in Section 2.3.2.

2.3.2 Preliminary considerations

Three preliminary considerations are introduced before establishing the criterion in the next subsection.

Relationship between state transition matrix and periodic disturbance

It is recalled that, according to (1.81a), the solution of (2.21) can be expressed by means of the state transition matrix $\Phi(t, 0)$ and the initial state $x(0)$:

$$x(t) = \Phi(t, 0)x(0). \quad (2.25)$$

It is also recalled from (1.77) that the state transition matrix satisfies the unforced differential equation, with the identity matrix as initial condition:

$$\begin{cases} \dot{\Phi}(t, 0) = A(t)\Phi(t, 0) \\ \Phi(0, 0) = I. \end{cases} \quad (2.26)$$

The first preliminary step consists in establishing a relationship between the state transition matrix $\Phi(t, 0)$ and the disturbance $E(t)$, for which the following reasoning is used. Matrix $B(t)$ (temporarily unrelated to the input matrix of state-space representations) is defined as:

$$B(t) \triangleq \exp(-A_0 t)\Phi(t, 0), \quad (2.27)$$

where $\exp(\cdot)$ is an alternative notation for $e^{(\cdot)}$. Being a function of time, $B(t)$ can also be expressed as the definite integral of its time derivative:

$$B(t) = B(0) + \int_0^t \dot{B}(\tau) d\tau. \quad (2.28)$$

To find $\dot{B}(\tau)$, we take the time derivative of (2.27) and use the chain rule:

$$\dot{B}(\tau) = \frac{d}{d\tau} (\exp(-A_0 \tau)\Phi(\tau, 0)) \quad (2.29a)$$

$$= -\exp(-A_0 \tau)A_0\Phi(\tau, 0) + \exp(-A_0 \tau)\dot{\Phi}(\tau, 0). \quad (2.29b)$$

Noting from (2.26) that $\dot{\Phi}(\tau, 0) = A(\tau)\Phi(\tau, 0)$, we have:

$$\dot{B}(\tau) = -\exp(-A_0 \tau)A_0\Phi(\tau, 0) + \exp(-A_0 \tau)A(\tau)\Phi(\tau, 0) \quad (2.30a)$$

$$= \exp(-A_0 \tau)(A(\tau) - A_0)\Phi(\tau, 0) \quad (2.30b)$$

$$= \exp(-A_0 \tau)E(\tau)\Phi(\tau, 0). \quad (2.30c)$$

Now substituting $\dot{\mathbf{B}}(\tau)$ in (2.28) and equating it to (2.27), we have:

$$\exp(-\mathbf{A}_0 t) \Phi(t, 0) = \mathbf{B}(0) + \int_0^t \exp(-\mathbf{A}_0 \tau) \mathbf{E}(\tau) \Phi(\tau, 0) d\tau. \quad (2.31)$$

Additionally, from (2.26) and (2.27), we obtain:

$$\mathbf{B}(0) = \exp(0) \Phi(0, 0) = \mathbf{I}. \quad (2.32)$$

Consequently,

$$\exp(-\mathbf{A}_0 t) \Phi(t, 0) = \mathbf{I} + \int_0^t \exp(-\mathbf{A}_0 \tau) \mathbf{E}(\tau) \Phi(\tau, 0) d\tau \quad (2.33a)$$

$$\implies \Phi(t, 0) = \exp(\mathbf{A}_0 t) + \exp(\mathbf{A}_0 t) \int_0^t \exp(-\mathbf{A}_0 \tau) \mathbf{E}(\tau) \Phi(\tau, 0) d\tau \quad (2.33b)$$

$$\implies \Phi(t, 0) = \exp(\mathbf{A}_0 t) + \int_0^t \exp(\mathbf{A}_0(t - \tau)) \mathbf{E}(\tau) \Phi(\tau, 0) d\tau. \quad (2.33c)$$

Eq. (2.33c) provides the sought relationship between the state transition matrix $\Phi(t, 0)$ and the disturbance $\mathbf{E}(t)$.

Norms of matrices and stability of linear time-periodic systems

The second preliminary step consists in defining the norm $\|\mathbf{M}\|$ of a square matrix \mathbf{M} as its spectral norm, in accordance with [46, Ch.3]. The spectral norm is equivalent to the largest singular value of the matrix and has the property that

$$\|\mathbf{M}\mathbf{N}\| \leq \|\mathbf{M}\| \|\mathbf{N}\|, \quad (2.34)$$

with \mathbf{N} another arbitrary square matrix with same dimension as \mathbf{M} . Based on this norm, an LTP system with state transition matrix $\Phi(t, 0)$ is globally asymptotically stable if

$$\|\Phi(T_1, 0)\| = \|\Psi\| < 1, \quad (2.35)$$

with Ψ the monodromy matrix and T_1 the fundamental period. Indeed, if the largest singular value of Ψ is less than 1, then all eigenvalues of Ψ have a modulus smaller than 1. This is a consequence of the fact that the magnitude of all eigenvalues of a square matrix is bounded by its largest singular value [54, Theorem 5.6.9]. According to the discussion in Section 2.2, condition (2.35) ensures global asymptotic stability of the LTP system.

A property of matrices of norm less than unity

The third and last preliminary step recalls the following property from [46, Ch.3]. If all eigenvalues of a square matrix \mathbf{M} have a modulus strictly smaller than 1, then there exist two parameters λ and K such that

$$\begin{cases} 0 < \lambda < 1 \\ K \geq 1 \\ \|\mathbf{M}^t\| \leq K\lambda^t, \quad \forall t \geq 0. \end{cases} \quad (2.36)$$

We consider next a diagonalisable matrix \mathbf{N} such that $\mathbf{M} = \exp(\mathbf{N})$. If all eigenvalues of matrix \mathbf{N} have a strictly negative real part, then all eigenvalues of \mathbf{M} have a modulus strictly smaller than 1. Consequently, the above result is valid for the matrix-exponential of \mathbf{N} and there exist two parameters λ and K such that

$$\begin{cases} 0 < \lambda < 1 \\ K \geq 1 \end{cases} \quad (2.37a)$$

$$\begin{cases} 0 < \lambda < 1 \\ K \geq 1 \end{cases} \quad (2.37b)$$

$$\begin{cases} 0 < \lambda < 1 \\ K \geq 1 \\ \|\exp(\mathbf{N})^t\| = \|\exp(\mathbf{N}t)\| \leq K\lambda^t, \quad \forall t \geq 0. \end{cases} \quad (2.37c)$$

2.3.3 Establishing a sufficient stability criterion

In this subsection, the objective is to rely on the three preliminary steps to find a condition on the disturbance $\mathbf{E}(t)$ such that, if the averaged LTI approximation is stable, then the original LTP system is stable. This task is accomplished by obtaining an upper bound for the norm of the monodromy matrix. Using the triangle inequality on the sum and then on the integral in (2.33c), we have:

$$\|\Phi(t, 0)\| = \left\| \exp(\mathbf{A}_0 t) + \int_0^t \exp(\mathbf{A}_0(t - \tau)) \mathbf{E}(\tau) \Phi(\tau, 0) d\tau \right\| \quad (2.38a)$$

$$\begin{aligned} &\leq \|\exp(\mathbf{A}_0 t)\| + \underbrace{\left\| \int_0^t \exp(\mathbf{A}_0(t - \tau)) \mathbf{E}(\tau) \Phi(\tau, 0) d\tau \right\|}_{\leq \int_0^t \|\exp(\mathbf{A}_0(t - \tau)) \mathbf{E}(\tau) \Phi(\tau, 0)\| d\tau}. \end{aligned} \quad (2.38b)$$

Applying (2.34) twice, we also have

$$\|\exp(\mathbf{A}_0(t-\tau))\mathbf{E}(\tau)\Phi(\tau, 0)\| \leq \|\exp(\mathbf{A}_0(t-\tau))\mathbf{E}(\tau)\|\|\Phi(\tau, 0)\| \quad (2.39a)$$

$$\leq \|\exp(\mathbf{A}_0(t-\tau))\|\|\mathbf{E}(\tau)\|\|\Phi(\tau, 0)\|. \quad (2.39b)$$

Overall,

$$\|\Phi(t, 0)\| \leq \|\exp(\mathbf{A}_0 t)\| + \int_0^t \|\exp(\mathbf{A}_0(t-\tau))\|\|\mathbf{E}(\tau)\|\|\Phi(\tau, 0)\|d\tau. \quad (2.40)$$

Assuming that all eigenvalues of \mathbf{A}_0 have negative real part, there exist parameters K and λ satisfying (2.37):

$$\|\exp(\mathbf{A}_0 t)\| \leq K\lambda^t, \quad \forall t \geq 0. \quad (2.41)$$

Similarly,

$$\|\exp(\mathbf{A}_0(t-\tau))\| \leq K\lambda^{t-\tau}, \quad \forall t \geq \tau. \quad (2.42)$$

Consequently, it is deduced from (2.40) that:

$$\|\Phi(t, 0)\| \leq K\lambda^t + \int_0^t K\lambda^{t-\tau}\|\mathbf{E}(\tau)\|\|\Phi(\tau, 0)\|d\tau \quad (2.43a)$$

$$\leq K\lambda^t + \lambda^t \int_0^t K\lambda^{-\tau}\|\mathbf{E}(\tau)\|\|\Phi(\tau, 0)\|d\tau. \quad (2.43b)$$

Equivalently, since λ is strictly positive,

$$\frac{\|\Phi(t, 0)\|}{\lambda^t} \leq K + \int_0^t K\|\mathbf{E}(\tau)\| \frac{\|\Phi(\tau, 0)\|}{\lambda^\tau} d\tau. \quad (2.44)$$

Finding an upper bound for $\|\Phi(t, 0)\|$ is not obvious since the inequality is implicit with respect to this quantity. To solve this issue, the following theorem is presented according to [55, Ch.1], see also [35, App.A].

Theorem 1 (Grönwall's inequality). *Let $K \geq 0$ and T_1 be constant parameters. Let $\mathbf{F}(t) \geq 0$ and $\mathbf{G}(t)$ be continuous functions on $[0, T_1]$.*

If

$$\mathbf{F}(t) \leq K + \int_0^t \mathbf{F}(\tau)\mathbf{G}(\tau)d\tau \quad \forall 0 \leq t \leq T_1, \quad (2.45)$$

then

$$\mathbf{F}(t) \leq K \exp\left(\int_0^t \mathbf{G}(\tau)d\tau\right) \quad \forall 0 \leq t \leq T_1. \quad (2.46)$$

Grönwall's inequality can now be used to find an upper bound for $\|\Phi(t, 0)\|$. Defining functions $\mathbf{F}(t)$ and $\mathbf{G}(t)$ such that

$$\begin{cases} \mathbf{F}(t) \triangleq \frac{\|\Phi(t, 0)\|}{\lambda^t} \\ \mathbf{G}(t) \triangleq K\|\mathbf{E}(t)\|, \end{cases} \quad (2.47)$$

Eq. (2.44) can be rewritten as in Theorem 1:

$$\mathbf{F}(t) \leq K + \int_0^t \mathbf{G}(\tau) \mathbf{F}(\tau) d\tau. \quad (2.48)$$

Then, according to Grönwall's inequality,

$$\mathbf{F}(t) \leq K \exp \left(\int_0^t \mathbf{G}(\tau) d\tau \right), \quad \forall 0 \leq t \leq T_1. \quad (2.49)$$

Returning to the previous notation, taking the natural logarithm of both sides and considering the integral for t over $[0, T_1]$, we have:

$$\frac{\|\Phi(t, 0)\|}{\lambda^t} \leq K \exp \left(\int_0^t K\|\mathbf{E}(\tau)\| d\tau \right) \quad (2.50a)$$

$$\implies \ln \left(\frac{\|\Psi\|}{K\lambda^{T_1}} \right) \leq K \int_0^{T_1} \|\mathbf{E}(\tau)\| d\tau. \quad (2.50b)$$

If parameters λ and K can be found such that

$$K \int_0^{T_1} \|\mathbf{E}(\tau)\| d\tau < \ln \left(\frac{1}{K\lambda^{T_1}} \right), \quad (2.51)$$

then combining (2.50b) and (2.51) gives:

$$\ln \left(\frac{\|\Psi\|}{K\lambda^{T_1}} \right) < \ln \left(\frac{1}{K\lambda^{T_1}} \right) \quad (2.52)$$

which is equivalent to:

$$\|\Psi\| < 1, \quad (2.53)$$

thereby ensuring that the LTP system is stable according to the preliminary considerations. The above developments, specifically (2.41) and (2.51), lead to the following proposition which states the sought sufficient stability criterion.

Proposition 1. If all eigenvalues of \mathbf{A}_0 have a strictly negative real part, and if parameters $0 < \lambda < 1$ and $K \geq 1$ can be found such that

$$\left\{ \begin{array}{l} \|\exp(\mathbf{A}_0 t)\| \leq K \lambda^t, \quad t \geq 0 \\ \int_0^{T_1} \|\mathbf{E}(\tau)\| d\tau < \frac{1}{K} \ln \left(\frac{1}{K \lambda^{T_1}} \right), \end{array} \right. \quad (2.54a)$$

$$\int_0^{T_1} \|\mathbf{E}(\tau)\| d\tau < \frac{1}{K} \ln \left(\frac{1}{K \lambda^{T_1}} \right), \quad (2.54b)$$

then the origin of (2.21) is globally asymptotically stable.

To simplify the discussion, the following notation is introduced:

$$\delta(t) \triangleq \|\exp(\mathbf{A}_0 t)\| \leq \delta_{up}(t) \triangleq K \lambda^t \quad (2.55a)$$

$$\epsilon \triangleq \int_0^{T_1} \|\mathbf{E}(\tau)\| d\tau < \epsilon_{up} \triangleq \frac{1}{K} \ln \left(\frac{1}{K \lambda^{T_1}} \right). \quad (2.55b)$$

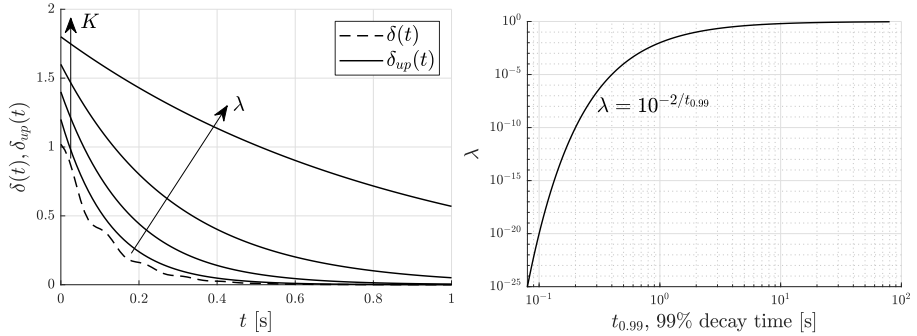
Besides, for a practical application of the criterion, it is noted that the oscillatory part $\mathbf{E}(t)$ can be calculated as:

$$\mathbf{E}(t) = \sum_{\substack{k=-h_m \\ k \neq 0}}^{h_m} \mathbf{A}_k e^{jk\omega_1 t}, \quad (2.56)$$

with \mathbf{A}_k the Fourier coefficients of state matrix $\mathbf{A}(t)$, and with h_m a sufficiently-large rank such that all non-negligible harmonic components in $\mathbf{A}(t)$ are taken into account in the Fourier series. Eventually, the value of ϵ in (2.55b) is determined by means of a numerical integration of $\|\mathbf{E}(t)\|$ over $[0, T_1]$.

2.3.4 Criterion analysis and choice of parameters

Condition (2.54a) expresses the fact that, for the original LTP system to be stable, its LTI approximation should not only be stable, but "stable enough". In other words, it should be characterised by a sufficiently fast decay. In the proposition, the decay of the LTI system is expressed by the evolution of $\delta(t)$ as t increases from 0. To assess whether this decay is sufficiently fast, an upper bound must be found and is defined by $\delta_{up}(t)$, an exponential decay with base λ and initial value K . Fig. 2.1a shows the evolution of $\delta(t)$ for an illustrative LTI system as well as a set of upper bounds $\delta_{up}(t)$ for several values of K and λ . It is observed that, for every value of $t \geq 0$, $\delta_{up}(t)$ increases with increasing K and λ .



(a) Effect of parameters K and λ when determining an upper bound for the decay (b) Parameter λ as a function of the 99% decay time

Figure 2.1: Stability criterion: analysis of Condition (2.54a)

The selection of parameters K and λ is facilitated by a preliminary inspection of the curve of $\delta(t)$. For the illustrative example in Fig. 2.1a, the maximum value of $\delta(t)$ is its initial value, which is equal to 1. In general, however, the maximum value is not necessarily the initial value $\delta(0)$ and may be reached at strictly-positive time values, e.g. for non-minimum phase systems. Another helpful characteristic of the $\delta(t)$ curve is its 99% decay time, i.e. the time at which this quantity has decreased to 1% of its maximum value. A visual inspection of Fig. 2.1a helps estimating this 99% decay time to about 0.6 s.

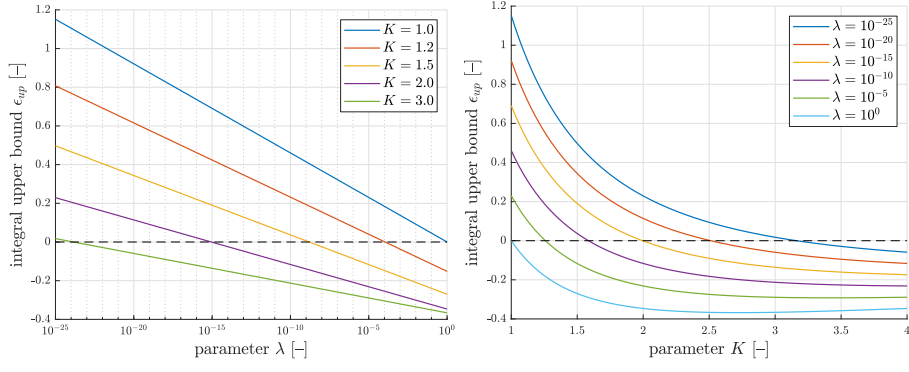
A good first choice for K would be the maximum value of $\delta(t)$, or a slightly larger value. As for parameter λ , it can be chosen in such a way that $\delta(t)$ and $\delta_{up}(t)$ have comparable 99% decay times. The value of λ can be related to the 99% decay time $t_{0.99}$ of $\delta_{up}(t)$ by requiring that δ_{up} must reach 1% of its initial value K at $t_{0.99}$:

$$0.01K = K\lambda^{t_{0.99}} \implies t_{0.99} = \log_\lambda(0.01) = \frac{\log_{10}(0.01)}{\log_{10}(\lambda)} \quad (2.57a)$$

$$\implies \lambda = 10^{-2/t_{0.99}}. \quad (2.57b)$$

This relation is displayed in Fig. 2.1b. For $t_{0.99} \approx 0.6$ s, then a good first choice for λ would be about 10^{-4} .

Condition (2.54b) expresses the fact that, for the LTP system to be stable, the periodic disturbance $\mathbf{E}(t)$ should be sufficiently small. More precisely, the size of the disturbance is noted ϵ and is quantified by the integral of the norm of $\mathbf{E}(t)$ over one fundamental period. According to the proposition, the periodic disturbance is sufficiently small if ϵ is strictly smaller than the upper bound



(a) Integral upper bound ϵ_{up} as a function of λ , for several values of K (b) Integral upper bound ϵ_{up} as a function of K , for various values of λ

Figure 2.2: Stability criterion: analysis of Condition (2.54b)

ϵ_{up} , which is a function of the same parameters K and λ . Fig. 2.2 illustrates the behaviour of the upper bound ϵ_{up} as a function of K and λ . Specifically, Fig. 2.2a plots ϵ_{up} as a function of λ for several values of K , and Fig. 2.2b plots ϵ_{up} as a function of K for several values of λ . Over the range of values of λ and K that make physical sense, i.e. such that $\epsilon_{up} \geq 0$, ϵ_{up} is strictly decreasing with respect to both parameters.

Intuitively, increasing the parameters allows for less stable systems (slower decays) but smaller oscillatory components. Decreasing the parameters makes more room for the periodic disturbance, but requires a faster decay for the criterion to be satisfied. Overall, the two conditions are opposing each other and a compromise must be found. Consequently, the suggested guideline is to find λ and K as small as possible while satisfying Condition (2.54a). Once the two parameters are determined, the value of ϵ_{up} is fixed and it is known directly whether Condition (2.54b) is satisfied or not for the given system.

2.3.5 Numerical applications

The criterion is applied to two illustrative examples: a two-level converter (TLC) and an MMC.

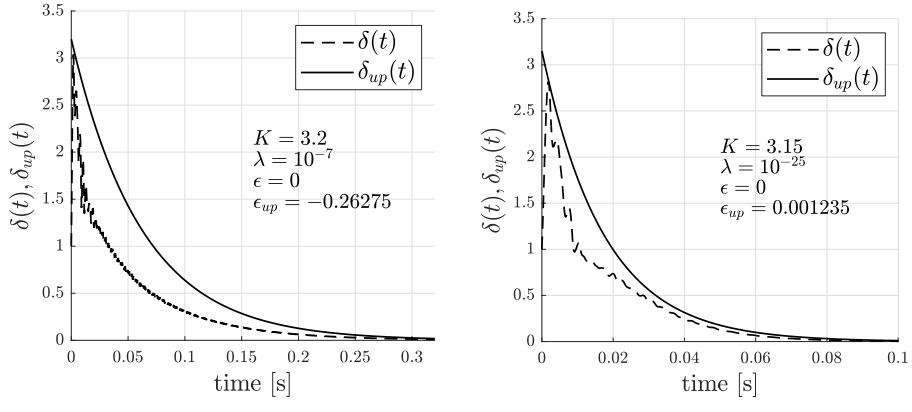


Figure 2.3: Stability criterion: application to the TLC

Application to the two-level converter

The NTI_c *dq*-frame model of a TLC described in Appendix B.3.2 is considered. This illustrative case is rather simple since the system operates at a constant operating point in steady state and the linearisation of its differential equations around this operating point results in a LTI system: the state matrix $\mathbf{A}(t)$ is constant and equal to \mathbf{A}_0 . This implies that the periodic disturbance $\mathbf{E}(t)$ is zero and so is the integral ϵ in Condition (2.54b). Consequently, there is no approximation in assessing the stability of the system based on the constant part of the state matrix of the linearised model. Nevertheless, the application of the criterion to this model provides valuable insights into its working principle.

The eigenvalues of matrix \mathbf{A}_0 have strictly negative real parts and the decay $\delta(t)$ that corresponds to this system is displayed in Fig. 2.3a. Values of K and λ are found which satisfy Condition 2.54a and are also displayed in Fig. 2.3a. However, these parameters result in a negative value for ϵ_{up} , implying that Condition 2.54b is not satisfied and that the criterion is inconclusive. For the sake of illustration, several circuit and control parameters such as resistances R_t , R_f , as well as PLL and PQ control loop bandwidths are increased to somewhat less realistic values than those initially considered: both the original and the altered values are given in Table 2.1. This results in a new matrix \mathbf{A}_0 , with all eigenvalues still in the left-hand plane, and a new $\delta(t)$ presented in Fig. 2.3b. New values of K and λ can be found which both satisfy Condition 2.54a and give a positive value for ϵ_{up} . Consequently, Condition 2.54b is also satisfied.

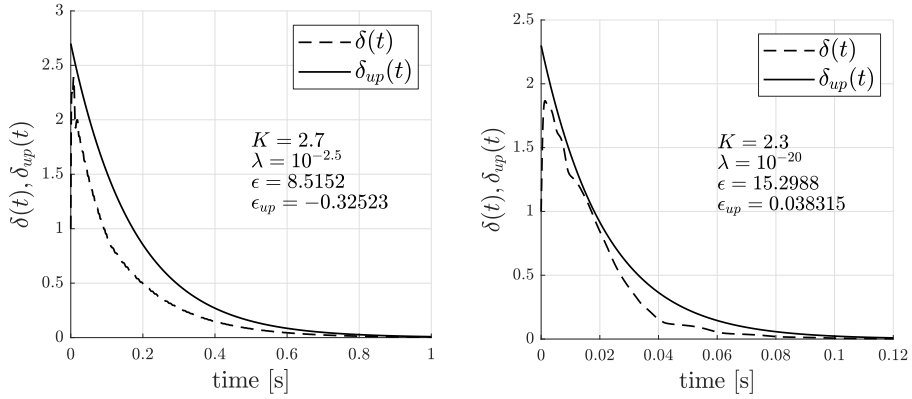


Figure 2.4: Stability criterion: application to the simplified single-phase MMC

The conclusion of the above reasoning is that the LTI approximation is stable with the modified parameters, which is obvious as this was already known from the eigenvalues of \mathbf{A}_0 . This first example shows that the criterion is rather conservative, which was also noted concerning its counterpart for discrete-time systems in [46, Ch.3].

Application to the modular multilevel converter

The simplified single-phase MMC presented in Section 1.2.5 is considered with the circuit and control parameters of Appendix B.2. The nonlinear differential equations are linearised around a periodic trajectory, which results in an LTP approximation. Just as for the TLC model, the averaging technique results in a stable LTI approximation. However, this time, the periodic disturbance $\mathbf{E}(t)$ is non-zero and ϵ has a strictly positive value. For this system, Condition (2.54a) is satisfied with the parameter values displayed in Fig. 2.4a, however these values are such that ϵ_{up} is negative, hence Condition (2.54b) is not satisfied. Several circuit and control parameters are modified to somewhat less realistic values according to Table 2.1, which results in a faster decay displayed in Fig. 2.4b. New values of K and λ satisfy Condition (2.54a) and lead to a positive value of ϵ_{up} . However, ϵ_{up} is still significantly smaller than ϵ and Condition (2.54b) remains unsatisfied. Further modifying circuit and control parameters would bring the system too far from realistic values. Overall, the criterion cannot be satisfied for this particular model of the single-phase MMC: even though the

| TLC | original | modified | MMC | original | modified |
|---------------------|----------|----------|--------------------|----------|----------|
| R_f | 0.01 pu | 0.055 pu | R_g | 0.005 pu | 0.06 pu |
| R_t | 0.01 pu | 0.055 pu | R_a | 0.01 pu | 0.06 pu |
| ω_{bw}^{PLL} | 10 Hz | 12 Hz | L_a | 48 mH | 30 mH |
| ω_{bw}^{PQ} | 5 Hz | 12 Hz | C_s | 13 mF | 8 mF |
| | | | ω_{bw}^{AC} | 150 Hz | 300 Hz |
| | | | ω_{bw}^{CC} | 150 Hz | 300 Hz |

Table 2.1: Relevant TLC and MMC circuit and control parameters

averaged LTI approximation is stable, it cannot be concluded that the LTP approximation is stable too.

2.3.6 Discussion

Although quite conservative, it is emphasised that Proposition 1 is only a *sufficient* criterion. The inability to find parameters K and λ such that both conditions of the proposition are satisfied does not imply that the oscillatory components of the periodic coefficients cannot be neglected. Yet, the fact that no conclusion can be drawn based on Proposition 1 for the particular models covered in this section further motivates reviewing and developing other methods capable of accounting for oscillatory components when assessing the small-signal stability of periodic trajectories.

Despite the fact that the criterion remains inconclusive for the tested examples, it is expected that its conditions could be fulfilled for other systems, in which case the criterion can also be used as a way of determining which harmonic components within $\mathbf{E}(t)$ should be taken into account for accurate small-signal stability assessments. Specifically, transformation methods such as frame rotations, which are discussed next, could be used to convert some of the oscillatory components into constant components. Proposition 1 would be applied afterwards to determine whether the remaining oscillatory components can be safely neglected.

2.4 Frame rotations

In the field of electrical power systems, frame rotations are the most common form of transformation used to convert three-phase sinusoidal variables into constant variables, e.g. for the purpose of control design or for the

reduction of the computational cost of time-domain simulations. Additionally, frame rotations are also used in combination with linearisation in order to transform NTI_p systems into LTI systems, thereby enabling small-signal stability assessments of their trajectories by means of traditional methods of linear systems theory.

In this section, the theory of frame rotations is reviewed to better understand their underlying assumptions and delimit the cases in which alternative transformation methods have to be considered. Although LTI systems do not need to be transformed for stability assessments, the case of LTI systems is considered first to introduce the basic concepts and the notation. Next, the more complex case of nonlinear systems is discussed. The multiple *dq*-frame method developed in [47] is revisited and applied to the MMC.

2.4.1 Transformation of linear time-invariant systems

Transforming a periodic trajectory into a constant operating point is carried out in two steps. Firstly, the change of variables is defined to express a new set of variables in terms of the old ones. Secondly, the differential equations governing the dynamics of the new variables are determined.

At this stage, a notation similar to that proposed for nonlinear systems in Section 1.3 is introduced for linear systems: LTI systems operating at an equilibrium in steady state are referred to as LTI_c systems, while those evolving along periodic trajectories are referred to as LTI_p systems. While such distinction is not necessary from a stability analysis perspective, it allows presenting the technique of frame rotations on simple equations before addressing nonlinear systems.

In the next paragraphs, Park transformation is applied to transform the periodic trajectory of an LTI_p system into the constant operating point of an equivalent LTI_c system. To that end, Park transformation is split into two successive changes of variables: the Clarke transformation of *abc* variables into $\alpha\beta z$ variables, and the frame rotation of $\alpha\beta z$ variables into *dqz* variables. These transformations are defined in Appendix A.2.

The following unforced LTI_p system is considered:

$$\frac{d}{dt} \mathbf{x}_{abc}(t) = \mathbf{A} \mathbf{x}_{abc}(t), \quad (2.58)$$

where $\mathbf{x}_{abc}(t)$ is a vector of three-phase variables with, *a priori*, each variable having a possibly different harmonic spectrum populated at multiple frequencies.

In the following, the dependence of \mathbf{x}_{abc} on t is not explicitly shown to keep the notation simple.

Clarke transformation

The first step consists in expressing the relationship between abc variables and $\alpha\beta z$ variables, which relies on the direct Clarke transformation:

$$\mathbf{x}_{\alpha\beta z} = \mathbf{T}\mathbf{x}_{abc}. \quad (2.59)$$

The differential equations governing the $\alpha\beta z$ variables are given by:

$$\frac{d\mathbf{x}_{\alpha\beta z}}{dt} = \frac{d}{dt}(\mathbf{T}\mathbf{x}_{abc}) = \mathbf{T}\frac{d\mathbf{x}_{abc}}{dt} \quad (2.60a)$$

$$= \mathbf{T}\mathbf{A}\mathbf{x}_{abc} = \mathbf{T}\mathbf{A}\mathbf{T}^{-1}\mathbf{x}_{\alpha\beta z}. \quad (2.60b)$$

where we used the fact that \mathbf{T} is constant and can thus be taken out of the time derivative. Defining the constant matrix $\mathbf{A}_T \triangleq \mathbf{T}\mathbf{A}\mathbf{T}^{-1}$, the new LTI system is given by:

$$\frac{d\mathbf{x}_{\alpha\beta z}}{dt} = \mathbf{A}_T\mathbf{x}_{\alpha\beta z}. \quad (2.61)$$

The effect of Clarke transformation is to separate initial abc variables into $\alpha\beta$ variables, which contain the positive-sequence and negative-sequence components of all frequencies, and the z variable which represents the zero-sequence components, also covering the whole frequency spectrum. At this point, all variables may still follow a periodic trajectory.

Frame rotation for positive- or negative-sequence components

A frame rotation at an arbitrary frequency ω is introduced as a transformation of $\alpha\beta z$ variables into dqz variables, where the zero-sequence variable is left unchanged:

$$\mathbf{x}_{dqz} = \mathbf{R}_\omega(t)\mathbf{x}_{\alpha\beta z}. \quad (2.62)$$

This change of variables leads to constant dq variables under the following assumption and condition, which are also explained in intuitive terms in Appendix A.1.

Assumption 7. *In addition to a possible zero-sequence component, the three-phase variables consist of a single-frequency component being either a positive-sequence or a negative-sequence component.*

Condition 1. *The chosen frequency and direction of the frame rotation $\mathbf{R}_\omega(t)$ correspond precisely to the frequency and sequence direction of the $\alpha\beta$ components it transforms.*

The dynamics of the dqz variables are obtained as:

$$\frac{d\mathbf{x}_{dqz}}{dt} = \frac{d}{dt}(\mathbf{R}_\omega(t)\mathbf{x}_{\alpha\beta z}) = \mathbf{R}_\omega(t)\frac{d\mathbf{x}_{\alpha\beta z}}{dt} + \frac{d\mathbf{R}_\omega(t)}{dt}\mathbf{x}_{\alpha\beta z} \quad (2.63a)$$

$$= \mathbf{R}_\omega(t)\mathbf{A}_T\mathbf{x}_{\alpha\beta z} + \frac{d\mathbf{R}_\omega(t)}{dt}\mathbf{x}_{\alpha\beta z} \quad (2.63b)$$

$$= \left(\mathbf{R}_\omega(t)\mathbf{A}_T\mathbf{R}_\omega^{-1}(t) + \frac{d\mathbf{R}_\omega(t)}{dt}\mathbf{R}_\omega^{-1}(t) \right) \mathbf{x}_{dqz}, \quad (2.63c)$$

where the chain rule was used to account for the fact that $\mathbf{R}_\omega(t)$ depends on time. The notation can be simplified by defining the following matrix \mathbf{J}_ω :

$$\mathbf{J}_\omega \triangleq \mathbf{R}_\omega(t)\frac{d\mathbf{R}_\omega^{-1}(t)}{dt} = -\frac{d\mathbf{R}_\omega(t)}{dt}\mathbf{R}_\omega^{-1}(t) = \begin{bmatrix} 0 & -\omega & 0 \\ \omega & 0 & 0 \\ 0 & 0 & 0 \end{bmatrix}. \quad (2.64)$$

The system can then be rewritten as:

$$\frac{d\mathbf{x}_{dqz}}{dt} = (\mathbf{R}_\omega(t)\mathbf{A}_T\mathbf{R}_\omega^{-1}(t) - \mathbf{J}_\omega)\mathbf{x}_{dqz}. \quad (2.65)$$

Under Assumption 7 and Condition 1, the frame rotation successfully transforms periodic $\alpha\beta$ variables into constant dq variables. It is noticed that, for a general matrix \mathbf{A}_T , coefficient $\mathbf{R}_\omega(t)\mathbf{A}_T\mathbf{R}_\omega^{-1}(t)$ is time-periodic and the resulting set of equations is LTP. The following assumption is introduced:

Assumption 8. *The three-phase system is balanced.*

Note that Assumption 8 is concerned with the parameters of the system, not its variables, since a balanced system may have unbalanced states under unbalanced excitation. Under Assumption 8, a three-phase system has the following properties:

1. The impedance matrix is symmetric, which means that the impedance between two phases does not depend on the order in which these phases are considered.
2. The diagonal elements of the impedance matrix represent the self impedance of each phase. In a balanced three-phase system, the three self impedances are equal.

3. The off-diagonal elements of the impedance matrix represent the mutual impedance between two phases. In a balanced three-phase system, the mutual impedances are equal.

As far as system (2.58) is concerned, Assumption 8 implies that matrix \mathbf{A} has the form:

$$\mathbf{A} = \begin{bmatrix} A & B & B \\ B & A & B \\ B & B & A \end{bmatrix}, \quad (2.66)$$

with A and B scalar parameters, and Clarke transformation results in \mathbf{A}_T being a diagonal matrix:

$$\mathbf{A}_T = \mathbf{T} \mathbf{A} \mathbf{T}^{-1} = \begin{bmatrix} A - B & & \\ & A - B & \\ & & A + 2B \end{bmatrix}. \quad (2.67)$$

Additionally, the particular structure of rotation matrices implies that

$$\mathbf{R}_\omega(t) \mathbf{A}_T \mathbf{R}_\omega^{-1}(t) = \mathbf{A}_T. \quad (2.68)$$

Eventually, the dynamic system becomes:

$$\frac{d\mathbf{x}_{dqz}}{dt} = (\mathbf{A}_T - \mathbf{J}_\omega) \mathbf{x}_{dqz}. \quad (2.69)$$

This system is LTI and operates at a constant operating point, unless the zero-sequence variable is not constant.

Although not a prerequisite to the application of frame rotations, an additional assumption is considered:

Assumption 9. *The three-phase system is decoupled.*

If in addition to being balanced (Assumption 8), the system is also decoupled (Assumption 9), then $B = 0$ and \mathbf{A} is a scalar matrix³:

$$\mathbf{A} = \begin{bmatrix} A & & \\ & A & \\ & & A \end{bmatrix} = A \mathbf{I} \quad (2.70)$$

with \mathbf{I} the identity matrix. This implies that

$$\mathbf{A}_T = \mathbf{T} \mathbf{A} \mathbf{T}^{-1} = \mathbf{T} \mathbf{I} \mathbf{T}^{-1} \mathbf{A} = \mathbf{A}, \quad (2.71)$$

³ A scalar matrix is a diagonal matrix with all elements on the diagonal being the same.

and also that

$$\mathbf{R}_\omega(t) \mathbf{A}_T \mathbf{R}_\omega^{-1}(t) = \mathbf{R}_\omega(t) \mathbf{R}_\omega^{-1}(t) \mathbf{A} = \mathbf{A}. \quad (2.72)$$

In this case, the dynamic system becomes:

$$\frac{d\mathbf{x}_{dqz}}{dt} = (\mathbf{A} - \mathbf{J}_\omega) \mathbf{x}_{dqz}. \quad (2.73)$$

It is emphasised once more that Assumption 9, unlike Assumptions 7 and 8, is not a necessary condition for frame rotations to be applicable. However, the MMC power stage is generally modelled with decoupled phases, in which case the assumption is verified and the related simplifications are valid.

Frame rotation for zero-sequence components

If the zero-sequence component x_z is not constant, the resulting set of dqz variables still describes a periodic trajectory and a follow-up step is needed. Relying on [47], the trick is to generate an additional virtual variable leading or lagging the zero-sequence variable x_z by $\pi/2$ rad.

Precisely, the original zero-sequence variable is assimilated to an α variable and is noted $x_{z\alpha}$, while the virtual variable is assimilated to a β variable and is noted $x_{z\beta}$.

Assumption 10. *The zero sequence consists of a single-frequency component.*

Under Assumption 10, $x_{z\alpha}$ can be expressed as:

$$x_{z\alpha}(t) = x_{zd} \cos(\omega_z t) - x_{zq} \sin(\omega_z t), \quad (2.74)$$

with ω_z the (unique) frequency of the zero-sequence component. The corresponding β variable forming a positive-sequence is deduced as:

$$x_{z\beta}(t) = x_{zd} \sin(\omega_z t) + x_{zq} \cos(\omega_z t). \quad (2.75)$$

Eventually, a frame rotation at frequency ω_z and in the positive-sequence direction results in constant x_{zd} and x_{zq} components:

$$\mathbf{x}_{zd,zq} = \mathbf{R}_{\omega_z}(t) \mathbf{x}_{z\alpha,z\beta}. \quad (2.76)$$

Overall, under Assumptions 7, 8 and 10, frame rotations successfully transform the periodic trajectory of a three-phase LTI_p system into a constant operating point without introducing periodic coefficients into the dynamic equations.

It is emphasised that Assumptions 7 and 10 together imply that the initial *abc* variables consist of at most one single-frequency positive or negative sequence, and one single-frequency zero sequence, with the positive- or negative-sequence frequency possibly different from that of the zero sequence.

2.4.2 Transformation of nonlinear time-invariant systems

The extension of the above-described procedure to NTI_P systems in general, and to the MMC in particular, is motivated by the perspective of linearisation around a constant operating point. Yet, not all nonlinear systems can be made time-invariant by means of Clarke transformation and frame rotations. For simplicity, all other forms of nonlinearities than products of variables are discarded for the rest of this section, which corresponds to the following assumption:

Assumption 11. *System nonlinearity consists of at most products of two variables.*

In this thesis, systems satisfying Assumption 11 are referred to as *quadratic systems*. Under Assumption 11, the differential equations may contain both linear and quadratic operations, as described by the following generic equation:

$$\frac{d\mathbf{u}_\phi}{dt} = \mathbf{A}\mathbf{u}_\phi + \mathbf{B}(\mathbf{v}_\phi \odot \mathbf{w}_\phi) \quad (2.77)$$

where \mathbf{u} , \mathbf{v} , \mathbf{w} are generic quantities, where \odot denotes the element-wise product, and where subscript ϕ refers to *abc* variables. Additionally, \mathbf{A} and \mathbf{B} are scalar matrices, i.e. they are assumed to represent decoupled and balanced three-phase impedances.

For the sake of illustration, a particular case satisfying Assumptions 7 and 10 is considered, where variables \mathbf{u} and \mathbf{v} are assumed to both have a positive sequence at ω_1 and possibly a zero sequence at $3\omega_1$. Variable \mathbf{w} is assumed to have a negative sequence at $2\omega_1$ and a constant zero sequence. Park transformation being the combination of Clarke transformation and a frame rotation, we have:

$$\mathbf{P}_\omega(t) = \mathbf{R}_\omega(t)\mathbf{T}. \quad (2.78)$$

Each set of variables is transformed into *dqz* components using a Park transformation at the frequency that makes their positive-sequence or negative-sequence constant, i.e. satisfying Condition 1. This results in:

$$\frac{d\mathbf{u}_{dqz}}{dt} = (\mathbf{A} - \mathbf{J}_{\omega_1})\mathbf{u}_{dqz} + \underbrace{\mathbf{B} \mathbf{P}_{\omega_1}(t) \left((\mathbf{P}_{\omega_1}^{-1}(t)\mathbf{v}_{dqz}) \odot (\mathbf{P}_{-\omega_2}^{-1}(t)\mathbf{w}_{dqz}) \right)}_{\triangleq \Psi_{dqz}}. \quad (2.79)$$

Because of the element-wise product, the direct Park transformation cannot be brought within the parentheses and the expression of the quantity defined as

Ψ_{dqz} cannot be simplified. In this specific case, Ψ_{dqz} is given by:

$$\begin{bmatrix} \Psi_d \\ \Psi_q \\ \Psi_z \end{bmatrix} = \begin{bmatrix} \frac{1}{2}v_d w_d + v_d w_z - \frac{1}{2}v_q w_q + v_z w_q \sin(3\omega_1 t) + v_z w_d \cos(3\omega_1 t) \\ v_q w_z - \frac{1}{2}v_q w_d - \frac{1}{2}v_d w_q - v_z w_d \sin(3\omega_1 t) + v_z w_q \cos(3\omega_1 t) \\ v_z w_z + \frac{1}{2}(v_d w_q - v_q w_d) \sin(3\omega_1 t) + \frac{1}{2}(v_d w_d + v_q w_q) \cos(3\omega_1 t) \end{bmatrix}. \quad (2.80)$$

At this point, all of the dq components of variables \mathbf{u}_ϕ , \mathbf{v}_ϕ and \mathbf{w}_ϕ are constant. However, v_z may present a third-harmonic component, which implies that the operating trajectory has not yet been transformed into a constant operating point. Additionally, the combinations of Park transformations at ω_1 and $-2\omega_1$ lead to third-harmonic sine and cosine coefficients, which make (2.79) a time-periodic equation. To resolve this issue, two options are proposed in [47]:

1. In the expressions of Ψ_d and Ψ_q , the trigonometric functions are always multiplied by v_z . If v_z is null, Ψ_d and Ψ_q are constant in steady state. If v_z consists of a non-zero third-harmonic component, the products with sines and cosines at $3\omega_1$ lead to both constant components and components at $6\omega_1$. For the particular MMC model under consideration in [47], the resulting sixth-harmonic components were neglected.
2. The previous considerations do not apply to the expression of Ψ_z since the sines and cosines are multiplied with constant d and q components. In this specific case, little can be done to make the equation time-invariant unless it is considered that the zero sequence term u_z is null, in which case its differential equation is simply disregarded. Otherwise, if v_z is null instead, then the differential equation can be written in the following form:

$$\frac{du_z}{dt} = Au_z + B(\Psi_{z_d} \cos(3\omega_1 t) - \Psi_{z_q} \sin(3\omega_1 t)) \quad (2.81)$$

where u_z contains a third-harmonic component, and where Ψ_{z_d} and Ψ_{z_q} are given by:

$$\Psi_{z_d} \triangleq \frac{1}{2}(v_d w_d + v_q w_q), \quad \Psi_{z_q} \triangleq -\frac{1}{2}(v_d w_q - v_q w_d). \quad (2.82)$$

To make the dynamics of u_z time-invariant, u_z is redefined as u_{z_α} and a virtual variable u_{z_β} is introduced into the system:

$$\begin{cases} \frac{du_{z_\alpha}}{dt} = Au_{z_\alpha} + B(\Psi_{z_d} \cos(3\omega_1 t) - \Psi_{z_q} \sin(3\omega_1 t)) \\ \frac{du_{z_\beta}}{dt} = Au_{z_\beta} + B(\Psi_{z_d} \sin(3\omega_1 t) + \Psi_{z_q} \cos(3\omega_1 t)). \end{cases} \quad (2.83)$$

A frame rotation at $3\omega_1$ eventually brings the two equations to a time-invariant form:

$$\begin{cases} \frac{du_{z_d}}{dt} = Au_{z_d} + 3\omega_1 u_{z_q} + B\Psi_{z_d} \\ \frac{du_{z_q}}{dt} = Au_{z_q} - 3\omega_1 u_{z_d} + B\Psi_{z_q}. \end{cases} \quad (2.84)$$

As illustrated with this example, the use of Clarke transformation and frame rotations generally requires a case-specific selection of rotation frequencies and directions. At times, further simplifications may be needed to transform a periodic trajectory into an equilibrium while retaining the time-invariant property of the differential equations. The complete procedure is sometimes referred to as the multiple dq -frame method, the multiple synchronously-rotating reference frames method, or simply the multi-Park transformation [34].

2.4.3 Application to the MMC

The multiple dq -frame method is applied to a three-phase model of the MMC, with the very same assumptions as those supporting the simplified single-phase MMC model of Section 1.2.5, aside from the number of phases. The control equations of this simplified system being linear, they are not displayed and can be transformed according to the procedure presented in Section 2.4.1. The power-stage dynamic equations are:

$$\begin{cases} L_e \frac{d\mathbf{i}_{s\phi}}{dt} = -R_e \mathbf{i}_{s\phi} - \mathbf{v}_{g\phi} - \frac{\mathbf{v}_{c\phi}^* - \mathbf{v}_{s\phi}^*}{v_d} \odot \frac{\mathbf{v}_{Cu\phi}}{2} + \frac{\mathbf{v}_{c\phi}^* + \mathbf{v}_{s\phi}^*}{v_d} \odot \frac{\mathbf{v}_{Cl\phi}}{2} \\ L_a \frac{d\mathbf{i}_{c\phi}}{dt} = -R_a \mathbf{i}_{c\phi} + \frac{v_d}{2} \mathbf{1}_3 - \frac{\mathbf{v}_{c\phi}^* - \mathbf{v}_{s\phi}^*}{v_d} \odot \frac{\mathbf{v}_{Cu\phi}}{2} - \frac{\mathbf{v}_{c\phi}^* + \mathbf{v}_{s\phi}^*}{v_d} \odot \frac{\mathbf{v}_{Cl\phi}}{2} \\ C_a \frac{d\mathbf{v}_{Cu\phi}}{dt} = \frac{\mathbf{v}_{c\phi}^* - \mathbf{v}_{s\phi}^*}{v_d} \odot \left(\mathbf{i}_{c\phi} + \frac{\mathbf{i}_{s\phi}}{2} \right) \\ C_a \frac{d\mathbf{v}_{Cl\phi}}{dt} = \frac{\mathbf{v}_{c\phi}^* + \mathbf{v}_{s\phi}^*}{v_d} \odot \left(\mathbf{i}_{c\phi} - \frac{\mathbf{i}_{s\phi}}{2} \right), \end{cases} \quad (2.85)$$

where three-phase variables are written as vectors, e.g. $\mathbf{i}_{s\phi} = [i_{sa} \ i_{sb} \ i_{sc}]^T$, and where $\mathbf{1}_3 \triangleq [1 \ 1 \ 1]^T$.

| | | |
|-----------------------------|---------------------------|------------------------------------|
| $\mathbf{i}_{s\phi}$ | ω_1 | positive sequence |
| $\mathbf{i}_{c\phi}$ | 0 $4\omega_1$ | zero sequence positive sequence |
| $\mathbf{v}_{C\phi}^\Sigma$ | 0 $2\omega_1$ | zero sequence negative sequence |
| $\mathbf{v}_{C\phi}^\Delta$ | ω_1 $3\omega_1$ | positive sequence zero sequence |

Table 2.2: Frequency and sequence content of abc variables**Frequency content and sequences requirements**

The system under consideration has balanced parameters across the three phases, and it contains at most products of variables since the direct voltage v_d is considered a constant parameter: Assumptions 8 and 11 are satisfied. Besides, although not a prerequisite, the system does not present couplings across phases and Assumption 9 is also verified.

However, not all sets of three-phase variables satisfy the requirements related to frequency content and sequences: under ideal positive-sequence excitation by $\mathbf{v}_{g\phi}$ at the fundamental frequency, the sum-capacitor voltages $\mathbf{v}_{Cu\phi}$ and $\mathbf{v}_{Cl\phi}$ have a constant zero sequence, a fundamental-frequency positive sequence and a second-harmonic negative sequence (see also the typical waveforms and spectra in Fig. 1.5 of Chapter 1). Rearranging the first two equations and taking linear combinations of the last two gives:

$$\left. \begin{aligned} L_e \frac{d\mathbf{i}_{s\phi}}{dt} &= -R_e \mathbf{i}_{s\phi} - \mathbf{v}_{g\phi} + \frac{1}{v_d} (\mathbf{v}_{s\phi}^* \odot \mathbf{v}_{C\phi}^\Sigma - \mathbf{v}_{c\phi}^* \odot \mathbf{v}_{C\phi}^\Delta) \end{aligned} \right\} \quad (2.86a)$$

$$L_a \frac{d\mathbf{i}_{c\phi}}{dt} = -R_a \mathbf{i}_{c\phi} + \frac{v_d}{2} \mathbf{1}_3 + \frac{1}{v_d} (\mathbf{v}_{s\phi}^* \odot \mathbf{v}_{C\phi}^\Delta - \mathbf{v}_{c\phi}^* \odot \mathbf{v}_{C\phi}^\Sigma) \quad (2.86b)$$

$$C_a v_d \frac{d\mathbf{v}_{C\phi}^\Sigma}{dt} = \mathbf{v}_{c\phi}^* \odot \mathbf{i}_{c\phi} - \mathbf{v}_{s\phi}^* \odot \frac{\mathbf{i}_{s\phi}}{2} \quad (2.86c)$$

$$C_a v_d \frac{d\mathbf{v}_{C\phi}^\Delta}{dt} = -\mathbf{v}_{s\phi}^* \odot \mathbf{i}_{c\phi} + \mathbf{v}_{c\phi}^* \odot \frac{\mathbf{i}_{s\phi}}{2}, \quad (2.86d)$$

where common-mode and differential-mode sum-capacitor voltages are defined as:

$$\mathbf{v}_{C\phi}^\Sigma \triangleq \frac{\mathbf{v}_{Cu\phi} + \mathbf{v}_{Cl\phi}}{2} \quad \mathbf{v}_{C\phi}^\Delta \triangleq \frac{\mathbf{v}_{Cu\phi} - \mathbf{v}_{Cl\phi}}{2}. \quad (2.87)$$

The harmonic and sequence content of the new set of state variables is determined with a periodic trajectory calculation and the results are displayed in Table 2.2: the frequency content and sequences requirements of Assumptions 7 and 10 are now satisfied.

Multiple frame transformations

The procedure presented with the generic quadratic differential equation is now applied to the MMC. Every set of three-phase abc variables is transformed into its dqz counterpart, relying on the inverse Park transformation satisfying Condition 1. One exception to this guideline concerns the circulating currents, which contain fourth-harmonic positive-sequence components but for which a Park transformation at twice the fundamental frequency in the negative-sequence direction is used. The fourth-harmonic components are thus transformed into sixth-harmonic components. While this choice does not enable a conversion of the fourth-harmonic components into constant components, it contributes to introducing only third-harmonic coefficients in the DM sum-capacitor dynamics. This point is further clarified and motivated in the following paragraphs.

The procedure gives:

$$\left\{ \begin{array}{l} L_e \left(\frac{d}{dt} + \mathbf{J}_{\omega_1} \right) \mathbf{i}_{s,dqz} = -R_e \mathbf{i}_{s,dqz} - \mathbf{v}_{g,dqz} + \dots \\ \frac{1}{v_d} \mathbf{P}_{\omega_1} \left(\mathbf{P}_{\omega_1}^{-1} \mathbf{v}_{s,dqz}^* \odot \mathbf{P}_{-2\omega_1}^{-1} \mathbf{v}_{C,dqz}^\Sigma - \mathbf{P}_{-2\omega_1}^{-1} \mathbf{v}_{c,dqz}^* \odot \mathbf{P}_{\omega_1}^{-1} \mathbf{v}_{C,dqz}^\Delta \right) \end{array} \right. \quad (2.88a)$$

$$\left. \begin{array}{l} L_a \left(\frac{d}{dt} + \mathbf{J}_{-2\omega_1} \right) \mathbf{i}_{c,dqz} = -R_a \mathbf{i}_{c,dqz} + \frac{v_d}{2} \boldsymbol{\delta}_z + \dots \\ \frac{1}{v_d} \mathbf{P}_{-2\omega_1} \left(\mathbf{P}_{\omega_1}^{-1} \mathbf{v}_{s,dqz}^* \odot \mathbf{P}_{\omega_1}^{-1} \mathbf{v}_{C,dqz}^\Delta - \mathbf{P}_{-2\omega_1}^{-1} \mathbf{v}_{c,dqz}^* \odot \mathbf{P}_{-2\omega_1}^{-1} \mathbf{v}_{C,dqz}^\Sigma \right) \end{array} \right. \quad (2.88b)$$

$$\left\{ \begin{array}{l} C_a \left(\frac{d}{dt} + \mathbf{J}_{-2\omega_1} \right) \mathbf{v}_{C,dqz}^\Sigma = \dots \\ \frac{1}{v_d} \mathbf{P}_{-2\omega_1} \left(\mathbf{P}_{-2\omega_1}^{-1} \mathbf{v}_{c,dqz}^* \odot \mathbf{P}_{-2\omega_1}^{-1} \mathbf{i}_{c,dqz} - \mathbf{P}_{\omega_1}^{-1} \mathbf{v}_{s,dqz}^* \odot \mathbf{P}_{\omega_1}^{-1} \frac{\mathbf{i}_{s,dqz}}{2} \right) \end{array} \right. \quad (2.88c)$$

$$\left. \begin{array}{l} C_a \left(\frac{d}{dt} + \mathbf{J}_{\omega_1} \right) \mathbf{v}_{C,dqz}^\Delta = \dots \\ \frac{1}{v_d} \mathbf{P}_{\omega_1} \left(-\mathbf{P}_{\omega_1}^{-1} \mathbf{v}_{s,dqz}^* \odot \mathbf{P}_{-2\omega_1}^{-1} \mathbf{i}_{c,dqz} + \mathbf{P}_{-2\omega_1}^{-1} \mathbf{v}_{c,dqz}^* \odot \mathbf{P}_{\omega_1}^{-1} \frac{\mathbf{i}_{s,dqz}}{2} \right) \end{array} \right. \quad (2.88d)$$

$$\underbrace{\frac{1}{v_d} \mathbf{P}_{\omega_1} \left(-\mathbf{P}_{\omega_1}^{-1} \mathbf{v}_{s,dqz}^* \odot \mathbf{P}_{-2\omega_1}^{-1} \mathbf{i}_{c,dqz} + \mathbf{P}_{-2\omega_1}^{-1} \mathbf{v}_{c,dqz}^* \odot \mathbf{P}_{\omega_1}^{-1} \frac{\mathbf{i}_{s,dqz}}{2} \right)}_{\triangleq \mathbf{i}_{t,dqz}}$$

To facilitate a visual examination of these equations, time-dependency is not shown and matrices associated with Park transformations and their time

derivatives are written in grey. In (2.88b), $\boldsymbol{\delta}_z \triangleq [0 \ 0 \ 1]^T$, and in (2.88d), the defined intermediate quantity $\dot{\boldsymbol{i}}_{t,dqz}$ has units of current.

The trajectory of this system is still periodic, not only because of the sixth-harmonic components in the circulating currents, which are a consequence of using a Park transformation at $-2\omega_1$ instead of $4\omega_1$, but also because the DM sum-capacitor voltages $\mathbf{v}_{C,dqz}^\Delta$ still have a third-harmonic zero-sequence component. The latter can be written as a z_α variable expressed in terms of constant z_d and z_q components. A corresponding z_β virtual variable is introduced too:

$$\begin{cases} v_{C,z}^\Delta = v_{C,z_\alpha}^\Delta = v_{C,z_d}^\Delta \cos(3\omega_1 t) - v_{C,z_q}^\Delta \sin(3\omega_1 t) \\ v_{C,z_\beta}^\Delta = v_{C,z_d}^\Delta \sin(3\omega_1 t) + v_{C,z_q}^\Delta \cos(3\omega_1 t). \end{cases} \quad (2.89)$$

Likewise, the zero-sequence component and associated virtual variable of the intermediate current i_t in (2.88d) are written as:

$$\begin{cases} i_{t,z} = i_{t,z_\alpha} = i_{t,z_d} \cos(3\omega_1 t) - i_{t,z_q} \sin(3\omega_1 t) \\ i_{t,z_\beta} = i_{t,z_d} \sin(3\omega_1 t) + i_{t,z_q} \cos(3\omega_1 t), \end{cases} \quad (2.90)$$

where i_{t,z_d} and i_{t,z_q} are identified by developing (2.88d):

$$\begin{cases} i_{t,z_d} = -2i_{cd}v_{sd}^* + i_{sd}v_{cd}^* - 2i_{cq}v_{sq}^* + i_{sq}v_{cq}^* \\ i_{t,z_q} = -2i_{cd}v_{sq}^* - i_{sd}v_{cq}^* + 2i_{cq}v_{sd}^* + i_{sq}v_{cd}^*. \end{cases} \quad (2.91)$$

A frame rotation at $3\omega_1$ concludes the transformation of the zero-sequence dynamics of the DM sum-capacitor voltages:

$$C_a \left(\frac{d}{dt} + \mathbf{J}_{3\omega_1}^{2 \times 2} \right) \mathbf{v}_{C,z_d z_q}^\Delta = \dot{\boldsymbol{i}}_{t,z_d z_q}, \quad (2.92)$$

where $\mathbf{J}_{3\omega_1}^{2 \times 2}$ is the upper-left 2×2 block of matrix $\mathbf{J}_{3\omega_1}$:

$$\mathbf{J}_{3\omega_1}^{2 \times 2} \triangleq \begin{bmatrix} 0 & -\omega \\ \omega & 0 \end{bmatrix}. \quad (2.93)$$

The above manipulations rely on the presence of third-harmonic coefficients in (2.88d), which are a consequence of the Park transformations at ω_1 and $-\omega_2$. Using instead a Park transformation at $4\omega_1$ to transform the circulating currents leads to both third-harmonic and sixth-harmonic coefficients to appear, which complicate the process. This illustrates the challenge of finding a compromise between transforming the periodic trajectory into a constant point while also

bearing in mind the objective of obtaining NTI equations instead of NTP equations.

Precisely, in the case of (2.88)-(2.92), all dynamic equations of the resulting model are NTI as they do not present time-varying coefficients, except the dynamic equations of i_{sd} , i_{sq} , i_{cd} , i_{cq} , v_{Cd}^Σ and v_{Cq}^Σ . In these equations, the trigonometric functions from the frame rotations do not compensate one another and remain part of the system in the form of sines and cosines at $6\omega_1$. The resulting system is therefore NTP, unless further simplifications are considered. For instance, neglecting the remaining oscillatory coefficients gives a NTI system, which approximates the NTP system. This approximation admits an equilibrium as operating point around which the equations can be linearised. The corresponding developments are not provided, however the procedure would be similar to that presented in [47].

2.4.4 Discussion and conclusion

Using Clarke transformation and frame rotations to transform NTI_p systems into NTI_c systems allows linearising the resulting differential equations around a constant operating point. This method can be applied to balanced systems that contain at most products of two variables, and have an excitation such that the resulting periodic trajectories contain a sufficiently simple harmonic and sequence content. When these requirements are satisfied, frame rotations are a convenient approach enabling stability assessments by means of the traditional methods of linear systems theory.

However, in the case of the three-phase MMC model, frame rotations result in an NTI_c representation only when remaining oscillatory coefficients are neglected. The challenge of rigorously assessing the validity of an averaged model⁴ for small-signal stability assessments persists. Comparing the outcomes of the stability study with a reliable independent approach (often, a numerical integration) increases the confidence in the validity of the eventual LTI approximation, however the process remains largely case-dependent.

Furthermore, the assumptions underlying the application of frame rotations become limitations when it comes to studying systems with unbalanced phases, unbalanced or disturbed excitation, and/or with other nonlinearities than the products of two variables. A selection of cases not covered by frame rotations is identified:

⁴ In the sense of the averaging technique discussed in Section 2.3.

- To design control features such as active harmonic filters [56], it becomes relevant to carry out stability assessments where undesired oscillatory components are too large to be regarded as small perturbations, in particular when the active harmonic filter is unable to perform its intended task. Power-electronic converters subject to harmonic disturbances at their AC side would typically not satisfy Assumption 7.
- The importance of stable operation under unbalanced and fault conditions is justified by the need of preventing the propagation of disturbances from the AC-side to the DC-side, and vice-versa. Problematic conditions on one side of a power-electronic converter should ideally not jeopardise the operation on the other side [57, 58]. However, any system operating under unbalanced excitation does not satisfy Assumption 7. Similarly, models accounting for unbalanced phase parameters do not satisfy Assumption 8.
- In MMC control structures relying on e.g. the compensated modulation strategy presented in Section 1.2, the insertion indices are normalised by the sum-capacitor voltages, which introduces nonlinearity with respect to state variables in the differential equations. This implies that Assumption 11 is not satisfied. This issue has been circumvented by multiplying the differential equations describing the sum-capacitor voltage dynamics by the sum-capacitor voltages themselves, thereby obtaining equations that describe the dynamics of upper- and lower-arm energies [59]. However, this approach is only applicable to non-delayed systems.

Another common source of nonlinearity in controllers of power-electronic converters is the PLL. With ideal filtering and under balanced conditions or ideal sequence separation, PLL control variables are constant and the PLL equations can be linearised around an equilibrium. However, under unbalanced conditions or harmonic disturbance without perfect filters, internal PLL variables may not be constant and the corresponding oscillatory components must be handled as a time-periodic trajectory. The presence of nonlinearity other than the product of variables implies that frame rotations are not directly applicable in this case to tackle a possible time-periodicity of PLL variables.

The selection of above examples motivates the presentation of alternative methods capable of opening the way towards stability assessments of systems and trajectories not covered by Assumptions 7, 8, 10, or 11.

2.5 Chapter conclusion

This chapter presented a selection of non-lifting transformations and an approximation based on the averaging technique.

Firstly, the presentation of Floquet-Lyapunov theory showed that the monodromy matrix has constant eigenvalues which contain information about the stability of LTP systems. However, its calculation by means of numerical integration is not particularly computationally efficient and alternative approaches to its determination are necessary. Also supported by the Floquet-Lyapunov theory, the Floquet transformation delivers valuable insights into the characteristics of LTP systems. Relying on a periodic change of variables, it transforms the periodic state matrix of an LTP system into a constant state matrix, thereby resulting in an LTI representation if only the unforced dynamics are considered. However, its applicability to practical cases is limited as it relies on an *a priori* unknown transformation matrix.

Secondly, a stability criterion relying on the averaging technique and on the properties of the monodromy matrix was introduced to determine whether oscillatory components within the coefficients of LTP systems can be disregarded in a stability assessment. The application of this criterion to the MMC remained inconclusive, which further motivated the presentation of more-elaborate methods capable of addressing the periodic nature of steady-state trajectories of the MMC.

Lastly, frame rotations were presented as a way of transforming periodic trajectories into constant operating points, thereby enabling the derivation of LTI models as well as the application of traditional methods of stability analysis. It was concluded that the assumptions underlying frame rotations become a limitation to its application when considering systems with unbalanced phases, unbalanced or harmonically disturbed excitation, and/or other nonlinear operations than products of two variables.

To address the limitations of the presented methods, the following chapter is dedicated to describing the technique of frequency-lifting, which allows studying the stability of arbitrary periodic trajectories followed by models not necessarily covered by the assumptions of balanced and quadratic differential equations. Besides, facing the increased sophistication of the models of power-electronic converters such as the MMC, it is beneficial to opt for transformations that are model-agnostic, thereby reducing the number of required assumptions and simplifications involved in small-signal stability assessments.

Chapter 3

Frequency-lifting transformation methods

3.1 Introduction

Continuing the discussion of transformation methods initiated in Chapters 1 and 2, this chapter is dedicated to further fulfilling Objective 2. Precisely, the aim is to present a technique known as *frequency-lifting*, which relies on the *harmonic balance principle*, to transform time-periodic systems into time-invariant systems. Both frequency-lifting and the harmonic balance principle are defined in this chapter.

Throughout the last decades, methods based on the harmonic balance principle have been introduced in the literature under various forms and names [60], among others the harmonic state space (HSS) [18], the harmonic transfer function (HTF) [18, 48], dynamic phasors (of which the generalised averaging method [61] is considered to lay the foundations), the extended harmonic domain [62] as well as harmonic linearisation (HL) [63] and multi-harmonic linearisation [17]. Although the exact procedures and goals vary somewhat from one method to the next, harmonic balance remains the common underlying principle.

A selection of the aforementioned methods was displayed in Fig. 1.7 and showed that frequency-lifting methods can be used to tackle periodicity in two main ways: either by transforming periodic trajectories into constant operating points, or by transforming periodic coefficients of LTP systems into constant coefficients of LTI systems. As dynamic phasors and their application as a frequency-lifting

method have been thoroughly covered in recent works such as [64], this chapter focuses more specifically on the path that consists in transforming LTP systems into LTI systems with the HSS and HTF methods. Being respectively time-domain and frequency-domain counterparts, they are referred jointly to as the HSS/HTF framework. The main milestones in the development of the HSS/HTF framework are the following ones.

The work by Norman M. Wereley in the years 1990 presents the HSS/HTF framework as an alternative to the Floquet transformation [18]. His work is often cited as the first formal presentation of such models. Although Wereley does not refer to frequency-lifting under this name, he refers to the harmonic balance principle, which had been previously presented in e.g. [65] and several references therein.

Another notable contribution to the development of the HSS/HTF framework is the work of Erik Möllerstedt in the years 2000 [48]. Relying partly on Wereley's publications, Möllerstedt focuses primarily on the frequency-domain approach, i.e. on the HTF representation. In his PhD thesis, Möllerstedt gives an additional independent derivation of the HTF representation starting from the principles of the impulse response of LTP systems. Another fundamental step forward made by Möllerstedt is to highlight the relationship between the HSS/HTF framework and the concept of frequency-lifting, which was in fact developed prior to Wereley's work, see for instance [66].

In 2008, the concept of frequency-lifting was brought to the world of textbooks by Sergio Bittanti and Patrizio Colaneri. Although focusing primarily on discrete-time systems, their book "Periodic Systems" [46] covers the topic in great detail and introduces the HSS/HTF framework as a frequency-lifted formulation.

This chapter is structured as followed.

- Section 3.2 presents the fundamental concepts of frequency-lifting and harmonic balance in the time domain through the lens of the HSS method. Since the original formulation of HSS covers only ordinary differential equations (ODEs), delays are neglected at this stage. This section also delivers a broader overview and further clarification on the topic of frequency-lifting transformations by comparing the HSS method with rotating frames, dynamic phasors and the Floquet transformation.
- Section 3.3 is dedicated to describing the HL method. Although this method does not result in a frequency-lifted representation, it is covered in this chapter as it relies on the harmonic balance principle and corresponds to a subset of the HTF. The relationship between HL and the well-known frequency-scan method is highlighted and insights based on the concept

of frequency coupling are provided, which largely support the description of the HTF method in the next section.

- Section 3.4 describes the HTF as the frequency-domain counterpart of HSS and revisits its derivation from the impulse response of LTP systems. The HTF is also presented as a generalisation of HL, which clarifies the relationship between these two methods. Leveraging the natural capacity of frequency-domain models to account for irrational transfer functions, exact delays are introduced in the HTF framework as complex exponential transfer functions.

In this chapter, all periodic trajectories are once more assumed to be known *a priori*. Their calculation is addressed in Chapter 5.

3.2 Frequency-lifting and the harmonic state space

This section begins with an introduction of the notation and of the frequency-lifting technique. It is shown how fundamental mathematical operations translate into a frequency-lifted framework. The HSS approach is described next. The section ends with numerical applications and a comparison with other transformation methods.

3.2.1 Mathematical operations in a frequency-lifted framework

Let $\mathbf{x}(t)$ be a vector of n scalar signals that are functions of time:

$$\mathbf{x}(t) = \begin{bmatrix} x^{(1)}(t) \\ x^{(2)}(t) \\ \vdots \\ x^{(n)}(t) \end{bmatrix}. \quad (3.1)$$

Unlike the initial notation from Chapter 1, the index of the scalar variables within the vector is from now on denoted with superscripts in parentheses. The Fourier series representation of $\mathbf{x}(t)$ is given by [67]:

$$\mathbf{x}(t) = \sum_{k=-\infty}^{+\infty} \mathbf{x}_k(t) e^{jk\omega t}, \quad (3.2)$$

where $\omega = 2\pi/T$ is the fundamental angular frequency, T being the fundamental period, and where $\mathbf{x}_k(t)$ are vectors of complex-valued Fourier coefficients, whose indices are denoted with subscripts:

$$\mathbf{x}_k(t) = \begin{bmatrix} x_k^{(1)}(t) \\ x_k^{(2)}(t) \\ \vdots \\ x_k^{(n)}(t) \end{bmatrix}, \quad \forall k \in \mathbb{Z}. \quad (3.3)$$

When sufficiently clear from the context, these vectors are simply referred to as Fourier coefficients. It is noted that the Fourier coefficients are not constant in general, unless $\mathbf{x}(t)$ is a periodic quantity, and unless T is an integer multiple of its fundamental period $T_1 = 2\pi/\omega_1$, in which case its Fourier coefficients are constant and (3.2) becomes:

$$\bar{\mathbf{x}}(t) = \sum_{k=-\infty}^{+\infty} \mathbf{x}_k e^{jk\omega_1 t}. \quad (3.4)$$

The same series can be written for periodic matrix quantities.

The harmonic balance principle and frequency-lifting

The following definitions are provided for the harmonic balance principle and frequency-lifting according to [18, 46].

Definition 2. *The harmonic balance principle describes the fact that two equal quantities have the same Fourier coefficients at the same harmonic ranks.*

The harmonic balance principle is a consequence of the fact that, in a Fourier series, the sinusoidal or complex exponential basis functions form an orthonormal basis over the fundamental period [18, Ch.2].

Definition 3. *Frequency-lifting refers to the representation of a given quantity by the set of its Fourier coefficients.*

As will be shown in this section, the application of the harmonic balance principle to a given differential equation results in a frequency-lifted system.

Practically, frequency-lifting a scalar quantity consists in replacing it by a vector of its Fourier coefficients:

$$\mathcal{K}\{x(t)\} \triangleq \boldsymbol{x}(t) \triangleq \begin{bmatrix} \vdots \\ x_{-1}(t) \\ x_0(t) \\ x_1(t) \\ \vdots \end{bmatrix}, \quad (3.5)$$

where $\mathcal{K}\{\}$ indicates frequency-lifting. By extension, frequency-lifting also replaces a vector quantity by a vector of its Fourier coefficients, in which case these Fourier coefficients are themselves vectors:

$$\mathcal{K}\{\boldsymbol{x}(t)\} = \boldsymbol{x}(t) = \begin{bmatrix} \vdots \\ \boldsymbol{x}_{-1}(t) \\ \boldsymbol{x}_0(t) \\ \boldsymbol{x}_1(t) \\ \vdots \end{bmatrix}. \quad (3.6)$$

In this thesis, such vectors of Fourier coefficients are referred to as *harmonic vectors*. They are denoted with round lowercase letters, and for simplicity, this same notation is used for both frequency-lifted scalars and frequency-lifted vectors. It is worth noting that since Fourier coefficients of arbitrary signals are time-dependent quantities, harmonic vectors are, in spite of their name, also time-domain quantities. Lastly, the non-lifted variables are referred to as *original variables*.

Replacing original variables by harmonic vectors has a number of consequences concerning the way in which mathematical operations are applied. The following operations are considered, relying on (3.2) as well as [18, Ch.2]:

- (1) multiplication of a signal by a constant scalar parameter;
- (2) addition of two signals;
- (3) multiplication of two scalar signals;
- (4) multiplication of a signal by a periodic matrix;
- (5) time derivation of a signal.

Unless otherwise mentioned, the operations involve quantities that are not necessarily periodic.

Multiplication of a signal by a constant scalar parameter

The multiplication of a signal $\mathbf{x}(t)$ by a constant scalar parameter α is given by:

$$\alpha\mathbf{x}(t) = \alpha \sum_{k=-\infty}^{+\infty} \mathbf{x}_k(t) e^{jk\omega_1 t} = \sum_{k=-\infty}^{+\infty} (\alpha \mathbf{x}_k(t)) e^{jk\omega_1 t}. \quad (3.7)$$

Consequently, the harmonic vector of $\alpha\mathbf{x}(t)$ is simply obtained as:

$$\mathcal{K}\{\alpha\mathbf{x}(t)\} = \alpha\mathcal{K}\{\mathbf{x}(t)\} = \alpha\mathbf{x}(t), \quad (3.8)$$

which follows from the linearity of the Fourier series.

Addition of two signals

The sum of two signals $\mathbf{x}(t)$ and $\mathbf{y}(t)$ is given by:

$$\mathbf{x}(t) + \mathbf{y}(t) = \left(\sum_{k=-\infty}^{+\infty} \mathbf{x}_k(t) e^{jk\omega_1 t} \right) + \left(\sum_{k=-\infty}^{+\infty} \mathbf{y}_k(t) e^{jk\omega_1 t} \right) \quad (3.9a)$$

$$= \sum_{k=-\infty}^{+\infty} (\mathbf{x}_k(t) + \mathbf{y}_k(t)) e^{jk\omega_1 t}. \quad (3.9b)$$

Consequently, the harmonic vector of $\mathbf{x}(t) + \mathbf{y}(t)$ is obtained as:

$$\mathcal{K}\{\mathbf{x}(t) + \mathbf{y}(t)\} = \mathcal{K}\{\mathbf{x}(t)\} + \mathcal{K}\{\mathbf{y}(t)\} = \mathbf{x}(t) + \mathbf{y}(t) \quad (3.10)$$

where $\mathbf{x}(t)$ and $\mathbf{y}(t)$ are the harmonic vectors related to $\mathbf{x}(t)$ and $\mathbf{y}(t)$, respectively. This result also follows from the linearity of the Fourier series.

Multiplication of two scalar signals

The product of two scalar signals $x(t)$ and $y(t)$ is given by:

$$x(t)y(t) = \left(\sum_{l=-\infty}^{+\infty} x_l(t) e^{jl\omega_1 t} \right) \left(\sum_{h=-\infty}^{+\infty} y_h(t) e^{jh\omega_1 t} \right) \quad (3.11a)$$

$$= \sum_{h=-\infty}^{+\infty} \sum_{l=-\infty}^{+\infty} x_l(t) y_h(t) e^{j(l+h)\omega_1 t}. \quad (3.11b)$$

Defining $k \triangleq h + l$ and observing that, for every value of h , k goes from $-\infty$ to $+\infty$ as l goes from $-\infty$ to $+\infty$, we have:

$$x(t)y(t) = \sum_{h=-\infty}^{+\infty} \sum_{k=-\infty}^{+\infty} x_{k-h}(t)y_h(t)e^{jk\omega_1 t}. \quad (3.12)$$

Rearranging, we obtain:

$$x(t)y(t) = \sum_{k=-\infty}^{+\infty} \left(\sum_{h=-\infty}^{+\infty} x_{k-h}(t)y_h(t) \right) e^{jk\omega_1 t}. \quad (3.13)$$

This result is also known as the Cauchy product of infinite series [68, Ch.8]. The resulting Fourier coefficients are discrete convolution products of the Fourier coefficients of $x(t)$ and $y(t)$. Consequently, the harmonic vector of $x(t)y(t)$ is given by:

$$\mathcal{K}\{x(t)y(t)\} = \begin{bmatrix} \vdots \\ \sum_h x_{-1-h}(t)y_h(t) \\ \sum_h x_{0-h}(t)y_h(t) \\ \sum_h x_{1-h}(t)y_h(t) \\ \vdots \end{bmatrix}. \quad (3.14)$$

The convolution products can also be carried out by means of a matrix multiplication as follows:

$$\mathcal{K}\{x(t)y(t)\} = \underbrace{\begin{bmatrix} \ddots & & \vdots & & \ddots \\ \cdots & x_0(t) & x_{-1}(t) & x_{-2}(t) & \cdots \\ \cdots & x_1(t) & x_0(t) & x_{-1}(t) & \cdots \\ & x_2(t) & x_1(t) & x_0(t) & \cdots \\ \ddots & & \vdots & & \ddots \end{bmatrix}}_{\triangleq \mathbf{X}(t)} \underbrace{\begin{bmatrix} \vdots \\ y_{-1}(t) \\ y_0(t) \\ y_1(t) \\ \vdots \end{bmatrix}}_{= \mathbf{y}(t)}. \quad (3.15)$$

The above-defined matrix $\mathbf{X}(t)$ is a matrix of infinite dimension in which the terms are constant along descending diagonals and are equal to the Fourier coefficients of the original signal $x(t)$. The particular structure of such a matrix is known as the Toeplitz structure [46, 69], and the relationship between the Fourier coefficients of $x(t)$ and $\mathbf{X}(t)$ is noted

$$\mathbf{X}(t) = \mathcal{T}\{x_k(t) : k \in \mathbb{Z}\}, \quad (3.16)$$

where $\mathcal{T}\{\}$ stands for Toeplitz. In this document, Toeplitz and block-Toeplitz matrices made of Fourier coefficients are denoted with round uppercase letters¹.

¹ Notable exceptions to this guideline are matrices \mathcal{N} and \mathcal{E}_{T_d} , which are involved in the calculation of time derivatives and time delays in the frequency-lifted framework. Although the round upper-case notation is used, these matrices do not have a Toeplitz structure.

It is worth noting that the harmonic vector of $x(t)y(t)$ can also be obtained by means of a Toeplitz matrix $\mathcal{Y}(t) = \mathcal{T}\{y_k(t) : k \in \mathbb{Z}\}$:

$$\mathcal{K}\{x(t)y(t)\} = \mathcal{A}(t)\mathbf{y}(t) = \mathcal{Y}(t)\mathbf{x}(t). \quad (3.17)$$

Multiplication of a signal by a periodic matrix

The product of a periodic matrix $\mathbf{A}(t) = \mathbf{A}(t + T_1)$ with a signal $\mathbf{x}(t)$ is given by:

$$\mathbf{A}(t)\mathbf{x}(t) = \left(\sum_{l=-\infty}^{+\infty} \mathbf{A}_l e^{j l \omega_1 t} \right) \left(\sum_{h=-\infty}^{+\infty} \mathbf{x}_h(t) e^{j h \omega_1 t} \right) \quad (3.18a)$$

$$= \sum_{k=-\infty}^{+\infty} \left(\sum_{h=-\infty}^{+\infty} \mathbf{A}_{k-h} \mathbf{x}_h(t) \right) e^{j k \omega_1 t} \quad (3.18b)$$

where the Cauchy product of infinite series was used. Here, the Fourier coefficients of $\mathbf{A}(t)$ are constant matrices since $\mathbf{A}(t)$ is a periodic matrix of fundamental period T_1 . The block-Toeplitz matrix \mathcal{A} is defined as:

$$\mathcal{A} \triangleq \mathcal{T}\{\mathbf{A}_k : k \in \mathbb{Z}\} = \begin{bmatrix} \ddots & & \vdots & & \ddots \\ & \mathbf{A}_0 & \mathbf{A}_{-1} & \mathbf{A}_{-2} & \\ \cdots & \mathbf{A}_1 & \mathbf{A}_0 & \mathbf{A}_{-1} & \cdots \\ & \mathbf{A}_2 & \mathbf{A}_1 & \mathbf{A}_0 & \\ \ddots & & \vdots & & \ddots \end{bmatrix}. \quad (3.19)$$

In a similar way to (3.15), the harmonic vector of $\mathbf{A}(t)\mathbf{x}(t)$ is eventually obtained as:

$$\mathcal{K}\{\mathbf{A}(t)\mathbf{x}(t)\} = \mathcal{A}\mathbf{x}(t). \quad (3.20)$$

Time derivative of a signal

Using the chain rule, the time derivative of $\mathbf{x}(t)$ is given by:

$$\dot{\mathbf{x}}(t) = \frac{d}{dt} \sum_{k=-\infty}^{+\infty} \mathbf{x}_k(t) e^{j k \omega_1 t} = \sum_{k=-\infty}^{+\infty} \left(e^{j k \omega_1 t} \frac{d}{dt} \mathbf{x}_k(t) + \mathbf{x}_k(t) \frac{d}{dt} e^{j k \omega_1 t} \right) \quad (3.21a)$$

$$= \sum_{k=-\infty}^{+\infty} \left(\frac{d}{dt} \mathbf{x}_k(t) + j k \omega_1 \mathbf{x}_k(t) \right) e^{j k \omega_1 t}. \quad (3.21b)$$

Consequently, the harmonic vector of $\dot{\mathbf{x}}(t)$ is obtained as:

$$\mathcal{K}\{\dot{\mathbf{x}}(t)\} = \begin{bmatrix} \vdots \\ \dot{\mathbf{x}}_{-1}(t) \\ \dot{\mathbf{x}}_0(t) \\ \dot{\mathbf{x}}_1(t) \\ \vdots \end{bmatrix} + \underbrace{\begin{bmatrix} \ddots & & & & \\ & -j\omega_1 \mathbf{I} & & & \\ & & \mathbf{0} & & \\ & & & j\omega_1 \mathbf{I} & \\ & & & & \ddots \end{bmatrix}}_{\triangleq \mathcal{N}} \begin{bmatrix} \vdots \\ \mathbf{x}_{-1}(t) \\ \mathbf{x}_0(t) \\ \mathbf{x}_1(t) \\ \vdots \end{bmatrix}, \quad (3.22)$$

with \mathbf{I} and $\mathbf{0}$ the identity and zero matrices of size n , respectively. With the above-defined diagonal matrix \mathcal{N} , the harmonic vector of $\dot{\mathbf{x}}(t)$ is also written as:

$$\mathcal{K}\{\dot{\mathbf{x}}(t)\} = \dot{\mathbf{x}}(t) + \mathcal{N}\mathbf{x}(t). \quad (3.23)$$

3.2.2 Derivation of the harmonic state-space representation

The HSS framework relies on frequency-lifting to transform LTP systems into LTI systems of higher dimensions. The starting point is the generic LTP state-space representation:

$$\begin{cases} \dot{\mathbf{x}}(t) = \mathbf{A}(t)\mathbf{x}(t) + \mathbf{B}(t)\mathbf{u}(t) \\ \mathbf{y}(t) = \mathbf{C}(t)\mathbf{x}(t) + \mathbf{D}(t)\mathbf{u}(t) \end{cases} \quad (3.24)$$

where all matrix coefficients are periodic of fundamental period T_1 .

Transformation of LTP systems into HSS systems

Recalling the procedure presented by Wereley in [18, Ch.3], frequency-lifting is carried out in two steps: first, replacing quantities with their Fourier series, and next, applying the harmonic balance principle. In the first step, the Fourier series have time-dependent Fourier coefficients if they are used to replace variables, since the variables themselves are not necessarily periodic. On the contrary, constant Fourier coefficients are used in the Fourier series that replace periodic matrices.

For simplicity, these two steps are illustrated in the case of the unforced LTP equation:

$$\dot{\mathbf{x}}(t) = \mathbf{A}(t)\mathbf{x}(t). \quad (3.25)$$

According to (3.18b) and (3.21b), replacing signals with their Fourier series leads to:

$$\sum_{k=-\infty}^{+\infty} \left(\frac{d\mathbf{x}_k(t)}{dt} + jk\omega_1 \mathbf{x}_k(t) \right) e^{jk\omega_1 t} = \sum_{k=-\infty}^{+\infty} \left(\sum_{h=-\infty}^{+\infty} \mathbf{A}_{k-h} \mathbf{x}_h(t) \right) e^{jk\omega_1 t}. \quad (3.26)$$

Next, the harmonic balance principle ensures that

$$\frac{d\mathbf{x}_k(t)}{dt} + jk\omega_1 \mathbf{x}_k(t) = \sum_{h=-\infty}^{+\infty} \mathbf{A}_{k-h} \mathbf{x}_h(t), \quad \forall k \in \mathbb{Z}. \quad (3.27)$$

According to (3.27), the harmonic balance principle transforms the n -dimensional system (3.25) into an infinite set of n -dimensional systems. Specifically, there is one such n -dimensional system per harmonic index $k \in \mathbb{Z}$. Relying on the notation introduced previously, the same result is obtained by equating the harmonic vectors of $\dot{\mathbf{x}}(t)$ and $\mathbf{A}(t)\mathbf{x}(t)$:

$$\dot{\mathbf{x}}(t) + \mathcal{N}\mathbf{x}(t) = \mathbf{A}\mathbf{x}(t). \quad (3.28)$$

The idea is generalised to obtain the equivalent HSS representation of the complete LTP system (3.24):

$$\begin{cases} \dot{\mathbf{x}}(t) = (\mathbf{A} - \mathcal{N})\mathbf{x}(t) + \mathbf{B}\mathbf{u}(t) \\ \mathbf{y}(t) = \mathbf{C}\mathbf{x}(t) + \mathbf{D}\mathbf{u}(t), \end{cases} \quad (3.29)$$

where $\mathbf{x}(t)$, $\mathbf{u}(t)$ and $\mathbf{y}(t)$ are the infinite harmonic vectors related to vectors $\mathbf{x}(t)$, $\mathbf{u}(t)$ and $\mathbf{y}(t)$, and where matrices \mathbf{A} , \mathbf{B} , \mathbf{C} , \mathbf{D} are infinite block-Toeplitz matrices:

$$\mathbf{A} \triangleq \mathcal{T}\{\mathbf{A}_k : k \in \mathbb{Z}\} \quad \mathbf{B} \triangleq \mathcal{T}\{\mathbf{B}_k : k \in \mathbb{Z}\} \quad (3.30)$$

$$\mathbf{C} \triangleq \mathcal{T}\{\mathbf{C}_k : k \in \mathbb{Z}\} \quad \mathbf{D} \triangleq \mathcal{T}\{\mathbf{D}_k : k \in \mathbb{Z}\}. \quad (3.31)$$

According to (3.29), frequency-lifting successfully leads to a system representation where all matrix coefficients are constant, making it an LTI state-space model whose stability can be assessed based on the eigenvalues of the new state matrix $\mathbf{A} - \mathcal{N}$.

It is underlined that the HSS derivation relies only on Assumptions 5 and 6, i.e. on the fact that there exist a steady-state trajectory around which the nonlinear system can be linearised. No other assumptions have been made, nor are necessary, concerning the initial equations or their variables. Consequently, frequency-lifting in the form of HSS is capable of addressing the

periodicity of linear and linearised systems, regardless of the physical nature and characteristics of the original nonlinear equations: they can describe balanced as well as unbalanced phases and excitation. Besides, the exact type of converter does not come into play and can consist of an arbitrary number of phases. It is emphasised that the precise type of nonlinear operations is unimportant, as long as a linearisation around the periodic trajectory is possible and relevant. All nonlinear operations involved in the closed-loop MMC model of Section 1.2 are covered by this generic approach.

Truncation of HSS representations

In theory, vectors and matrices of the HSS formulation are of infinite dimensions. In practice, numerical analyses require truncating the vectors and matrices to finite dimensions that can be processed on a computer. A distinction is made between three indices:

- The **periodic rank** h_m is defined in this thesis as the maximum harmonic index needed to accurately describe the periodic matrix coefficients $\mathbf{A}(t)$, $\mathbf{B}(t)$, $\mathbf{C}(t)$ and $\mathbf{D}(t)$ up to an arbitrarily small error ϵ . The Fourier series of these matrices are truncated to the periodic rank and all Fourier coefficients of rank higher than h_m are assumed to be zero or negligible. Eventually, in a system with periodic rank h_m , the periodic matrices are described with a total of $n_{h_m} \triangleq 2h_m + 1$ Fourier coefficients covering indices $-h_m$ to h_m .

Mathematically, the accuracy related to a given periodic rank can be expressed in several ways. One option quantifies the error globally:

$$\left\| \mathbf{M}(t) - \sum_{k=-h_m}^{h_m} \mathbf{M}_k e^{jk\omega_1 t} \right\| \leq \epsilon, \quad \forall t, \quad (3.32)$$

with $\mathbf{M}(t)$ a periodic matrix and $\|\cdot\|$ the norm². Another option quantifies the error as an upper bound for each neglected Fourier coefficient:

$$\|\mathbf{M}_k\| \leq \epsilon, \quad \forall k \in \mathbb{Z}, |k| > h_m. \quad (3.33)$$

For quadratic systems, i.e. systems satisfying Assumption 11, the periodic rank is also the maximum harmonic index needed to accurately describe the periodic trajectory $\bar{\mathbf{p}}(t) = (\bar{\mathbf{x}}(t), \bar{\mathbf{u}}(t))$. Indeed, linearising the product $x^{(1)}x^{(2)}$ around the periodic trajectory $(\bar{\mathbf{x}}^{(1)}, \bar{\mathbf{x}}^{(2)})$ gives:

$$x^{(1)}x^{(2)} \longrightarrow \bar{x}^{(2)}\tilde{x}^{(1)} + \bar{x}^{(1)}\tilde{x}^{(2)}, \quad (3.34)$$

² It is recalled from Section 2.3 that, in this thesis, the norm of a matrix \mathbf{M} is chosen to be its spectral norm, i.e. its largest singular value $\sigma_1(\mathbf{M})$.

where time-dependency is not shown for simplicity, and where the harmonic content of the coefficients $\bar{x}^{(1)}$ and $\bar{x}^{(2)}$ is of course equal to the harmonic content of $(\bar{x}^{(1)}, \bar{x}^{(2)})$. In general, however, the periodic rank of the trajectory can be different from the periodic rank of the state-space coefficients. Considering the following linearisation:

$$\frac{x^{(1)}}{x^{(2)}} \longrightarrow \frac{1}{\bar{x}^{(2)}} \tilde{x}^{(1)} - \frac{\bar{x}^{(1)}}{(\bar{x}^{(2)})^2} \tilde{x}^{(2)}, \quad (3.35)$$

it is clear that the spectrum of the coefficients $\frac{1}{\bar{x}^{(2)}}$ and $-\frac{\bar{x}^{(1)}}{(\bar{x}^{(2)})^2}$ is not equal to the spectrum of $(\bar{x}^{(1)}, \bar{x}^{(2)})$. Consequently, truncating the Fourier series of the trajectory could lead to inaccurate harmonic content in the periodic coefficients of the linearised model. This is avoided in this thesis by truncating the Fourier series of the periodic coefficients and not the Fourier series of the periodic trajectory.

As far as modal analysis is concerned, it is sufficient to take h_m such that at least matrix $\mathbf{A}(t)$ is accurately described by its truncated Fourier series, since the other matrices are not involved in the eigenvalues calculation.

- The **truncation rank** h_t is the maximum harmonic rank included in the harmonic vectors $\boldsymbol{x}(t)$, $\boldsymbol{u}(t)$ and $\boldsymbol{y}(t)$ of a frequency-lifted system, which also corresponds to a truncation of the infinite block-Toeplitz matrices to block-size (n_{h_t}, n_{h_t}) , with $n_{h_t} \triangleq 2h_t + 1$. Consequently, index h_t defines the block-dimension of the HSS vectors and matrices. *A priori*, the truncation rank h_t and the periodic rank h_m do not necessarily have the same value.
 - The **forced periodic rank** h_f is similar to the periodic rank h_m as it describes the truncation of the Fourier series of the periodic matrix coefficients. However, unlike the periodic rank h_m , the choice of forced periodic rank is not guided by the need to accurately describe the periodic quantity. More precisely, the forced periodic rank is used to disregard all Fourier coefficients of index larger than h_f , regardless of the resulting error. Distinguishing the forced periodic rank h_f from the periodic rank h_m is thus particularly convenient when assessing the impact of purposely neglecting potentially non-negligible Fourier coefficients in a stability assessment. The choice of h_f is thus completely independent from the values actually taken by h_m and chosen for h_t . Normally, the impact of neglecting Fourier coefficients should only be noticeable if $h_f < h_m$, whereas taking $h_f \geq h_m$ should not have any noticeable impact on the representation of the periodic quantity.
- Unless otherwise mentioned, the forced periodic rank is considered equal to the periodic rank h_m .

Although the periodic rank h_m is essentially dictated by the physics of the system under consideration, the choice of truncation rank h_t ought to be made in such a way that the truncated HSS model remains a sufficiently-accurate depiction of the original LTP system. This is illustrated by means of the frequency-lifted representation of $\mathbf{A}(t)\mathbf{x}(t)$. For example, with $h_m = 4$ and $h_t = 1$, we have:

$$\mathbf{Ax}(t) = \begin{bmatrix} \mathbf{A}_0 & \mathbf{A}_{-1} & \mathbf{A}_{-2} \\ \mathbf{A}_1 & \mathbf{A}_0 & \mathbf{A}_{-1} \\ \mathbf{A}_2 & \mathbf{A}_1 & \mathbf{A}_0 \end{bmatrix} \begin{bmatrix} \mathbf{x}_{-1}(t) \\ \mathbf{x}_0(t) \\ \mathbf{x}_1(t) \end{bmatrix}. \quad (3.36)$$

In this case, the truncation rank is too small and some information about the original LTP system is lost due to truncation. Precisely, Fourier coefficients $\mathbf{A}_{\pm 3}$ and $\mathbf{A}_{\pm 4}$ are non-zero (since $h_m = 4$) but do not appear in (3.36). Keeping h_m and h_t to the same values, the forced periodic rank is lowered to $h_f = 0$, which gives:

$$\mathbf{Ax}(t) = \begin{bmatrix} \mathbf{A}_0 & \mathbf{0} & \mathbf{0} \\ \mathbf{0} & \mathbf{A}_0 & \mathbf{0} \\ \mathbf{0} & \mathbf{0} & \mathbf{A}_0 \end{bmatrix} \begin{bmatrix} \mathbf{x}_{-1}(t) \\ \mathbf{x}_0(t) \\ \mathbf{x}_1(t) \end{bmatrix}. \quad (3.37)$$

This corresponds to accounting for the constant part of $\mathbf{A}(t)$ only, and thus neglecting Fourier coefficients from $\mathbf{A}_{\pm 1}$ up to $\mathbf{A}_{\pm 4}$. This is a similar approach to that of the averaging technique in Section 2.3.

With $h_m = h_f = 1$ and $h_t = 2$, we have:

$$\mathbf{Ax}(t) = \begin{bmatrix} \mathbf{A}_0 & \mathbf{A}_{-1} & \mathbf{0} & \mathbf{0} & \mathbf{0} \\ \mathbf{A}_1 & \mathbf{A}_0 & \mathbf{A}_{-1} & \mathbf{0} & \mathbf{0} \\ \mathbf{0} & \mathbf{A}_1 & \mathbf{A}_0 & \mathbf{A}_{-1} & \mathbf{0} \\ \mathbf{0} & \mathbf{0} & \mathbf{A}_1 & \mathbf{A}_0 & \mathbf{A}_{-1} \\ \mathbf{0} & \mathbf{0} & \mathbf{0} & \mathbf{A}_1 & \mathbf{A}_0 \end{bmatrix} \begin{bmatrix} \mathbf{x}_{-2}(t) \\ \mathbf{x}_{-1}(t) \\ \mathbf{x}_0(t) \\ \mathbf{x}_1(t) \\ \mathbf{x}_2(t) \end{bmatrix}. \quad (3.38)$$

In this case, no information about the LTP system is lost in the truncation process: all non-zero Fourier coefficients of $\mathbf{A}(t)$ appear in the block-Toeplitz matrix \mathbf{A} .

It is important to note that block-Toeplitz matrices truncated to rank h_t can technically involve Fourier coefficients up to rank $2h_t$. Overall, for the HSS framework, it is sensible to use a truncation rank at least equal to the periodic rank: $h_t \geq h_m$. This point is further discussed in the remainder of this section.

In summary, the truncation of HSS models is necessary for numerical analyses and should be carried out in a way that all frequency components relevant to the studied case are preserved. The next paragraphs present practical examples of modal analysis based on HSS models.

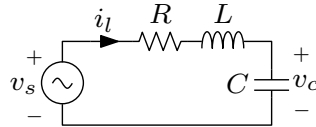


Figure 3.1: Simple RLC circuit diagram

3.2.3 Numerical application: HSS-based modal analysis

In the HSS framework, modal analysis relies on the eigenvalues and eigenvectors of the state matrix $\mathbf{A} - \mathbf{N}$. Considering for instance $h_m = h_t = 2$, this matrix takes the form:

$$\mathbf{A} - \mathbf{N} = \begin{bmatrix} \mathbf{A}_0 + 2j\omega_1 \mathbf{I} & \mathbf{A}_{-1} & \mathbf{A}_{-2} & & \\ \mathbf{A}_1 & \mathbf{A}_0 + j\omega_1 \mathbf{I} & \mathbf{A}_{-1} & \mathbf{A}_{-2} & \\ \mathbf{A}_2 & \mathbf{A}_1 & \mathbf{A}_0 & \mathbf{A}_{-1} & \mathbf{A}_{-2} \\ & \mathbf{A}_2 & \mathbf{A}_1 & \mathbf{A}_0 - j\omega_1 \mathbf{I} & \mathbf{A}_{-1} \\ & & \mathbf{A}_2 & \mathbf{A}_1 & \mathbf{A}_0 - 2j\omega_1 \mathbf{I} \end{bmatrix}. \quad (3.39)$$

Although it is unnecessary to apply frequency-lifting to study the stability of LTI systems, HSS models can also be established in this case and their analysis provides fundamental insights into the properties of frequency-lifted systems. For this reason, the HSS model of a simple LTI system is considered first, and the HSS model of LTP systems is analysed next.

Application to an LTI system: simple RLC circuit

The resistance-inductance-capacitance (RLC) circuit³ displayed in Fig. 3.1 is modelled with the following LTI differential equations:

$$\begin{cases} \frac{di_l}{dt} = \frac{1}{L}(-Ri_l - v_c + v_s) \\ \frac{dv_c}{dt} = \frac{1}{C}i_l \end{cases} \quad (3.40)$$

with i_l the inductor current, v_c the capacitor voltage and v_s the source voltage. This system has two state variables and its state matrix is constant and given by:

$$\mathbf{A}(t) = \mathbf{A}_0 = \begin{bmatrix} -R/L & -1/L \\ 1/C & 0 \end{bmatrix}. \quad (3.41)$$

³ $R = 0.8 \Omega$, $L = 1 \text{ H}$, $C = 1 \text{ mF}$.

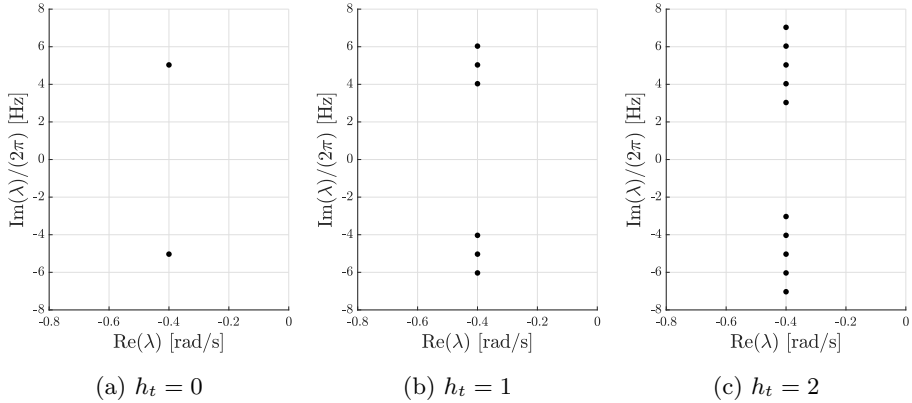


Figure 3.2: Simple RLC circuit: impact of truncation on HSS eigenvalues ($h_m = 0$)

Only the Fourier coefficient of index $k = 0$ is needed to accurately describe the state matrix. Consequently, the periodic rank is $h_m = 0$, regardless of the harmonic content of the input and state variables. If a truncation rank equal to the periodic rank is chosen ($h_t = h_m = 0$), then the HSS state matrix is equal to the state matrix of the LTI system ($\mathcal{A} - \mathcal{N} = \mathbf{A}_0$). The two complex-conjugate eigenvalues of this matrix are displayed in Fig. 3.2a.

If the truncation rank is increased to $h_t = 1$, the HSS state matrix takes the form:

$$\mathcal{A} - \mathcal{N} = \begin{bmatrix} \mathbf{A}_0 + j\omega_1 \mathbf{I} & & \\ & \mathbf{A}_0 & \\ & & \mathbf{A}_0 - j\omega_1 \mathbf{I} \end{bmatrix} \quad (3.42)$$

with ω_1 arbitrarily⁴ set to 2π rad/s. The six eigenvalues of this matrix are displayed in Fig. 3.2b, where it is observed that the four new eigenvalues appear as duplicated versions of the two original ones, shifted along the imaginary axis by increments of $\pm j\omega_1$. This is further illustrated in Fig. 3.2c for a truncation rank $h_t = 2$, where the additional eigenvalues (with respect to $h_t = 0$) are again duplicated versions of the original ones, this time shifted by increments of $\pm j\omega_1$ and $\pm 2j\omega_1$. In general terms, choosing a truncation rank h_t results in $n \cdot n_{h_t}$ eigenvalues forming vertical lines in the complex plane. Their values are given by $\lambda_i + jk\omega_1$ ($k = -h_t, \dots, h_t$), where λ_i ($i = 1, \dots, n$) correspond to the n eigenvalues of \mathbf{A}_0 . In this thesis, such vertical lines are referred to as *sets* or *eigensets*. Every eigenset comprises n_{h_t} eigenvalues.

⁴ This choice is in fact unimportant for LTI systems since their state matrix is constant.

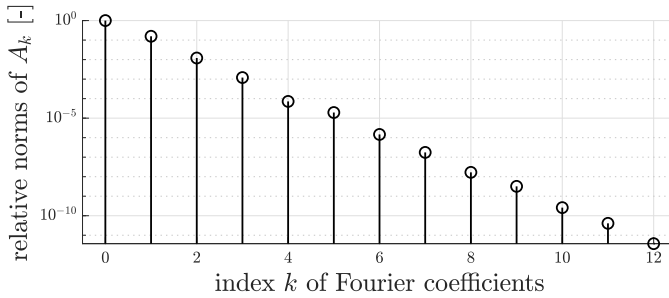


Figure 3.3: LTP model of the simplified MMC: relative norm of state matrix Fourier coefficients

Application to an LTP system: the linearised single-phase MMC

The more general case of LTP systems is now considered, relying on the linearised model of the single-phase MMC presented in Section 1.2.5.

The periodic trajectory followed by the states for the set of parameters and inputs given in Appendix B.2 is determined first and the analytical expression of the state matrix $\mathbf{A}(t)$ is evaluated numerically over one fundamental period of the trajectory. Next, the discrete Fourier transform (DFT) is applied to $\mathbf{A}(t)$, which delivers the Fourier coefficients \mathbf{A}_k , $k \in \mathbb{Z}$. Here, a possible approach to determine the periodic rank h_m consists in observing the relative norms of the Fourier coefficients \mathbf{A}_k . In this example, the norm of \mathbf{A}_0 is taken as reference to calculate the relative norm of the other coefficients, thus given by $\|\mathbf{A}_k\|/\|\mathbf{A}_0\|$.

In Fig. 3.3, it is observed that the relative norm of the Fourier coefficients of $\mathbf{A}(t)$ decreases at an exponential rate (linear on the logarithmic scale) with respect to the harmonic rank k . For this system, the periodic rank is thus arbitrarily taken to be $h_m = 6$, which ensures that the relative norm of all Fourier coefficients with index $k > h_m$ is smaller than 10^{-6} .

The eigenvalues of the $\mathcal{A} - \mathcal{N}$ state matrix of the HSS model are displayed in Fig. 3.4 for different truncation ranks. In Fig. 3.4a, $h_t = 20$ is used (not all eigenvalues are visible). Visually, this representation is closest to the theoretical infinite-dimensional case without truncation, where the complex plane contains n infinite eigensets. In Figs. 3.4b and 3.4c, lower truncation ranks $h_t = 6$ and $h_t = 3$ are used, respectively. Although the eigensets still form vertical lines for the most part, it is observed that some eigenvalues near the ends of the vertical lines are not aligned. This shift of some eigenvalues along the real axis is a purely mathematical artefact that occurs as a consequence of truncation of the HSS state matrix [70, Ch.3]. Unlike the LTI case, the HSS state matrix of

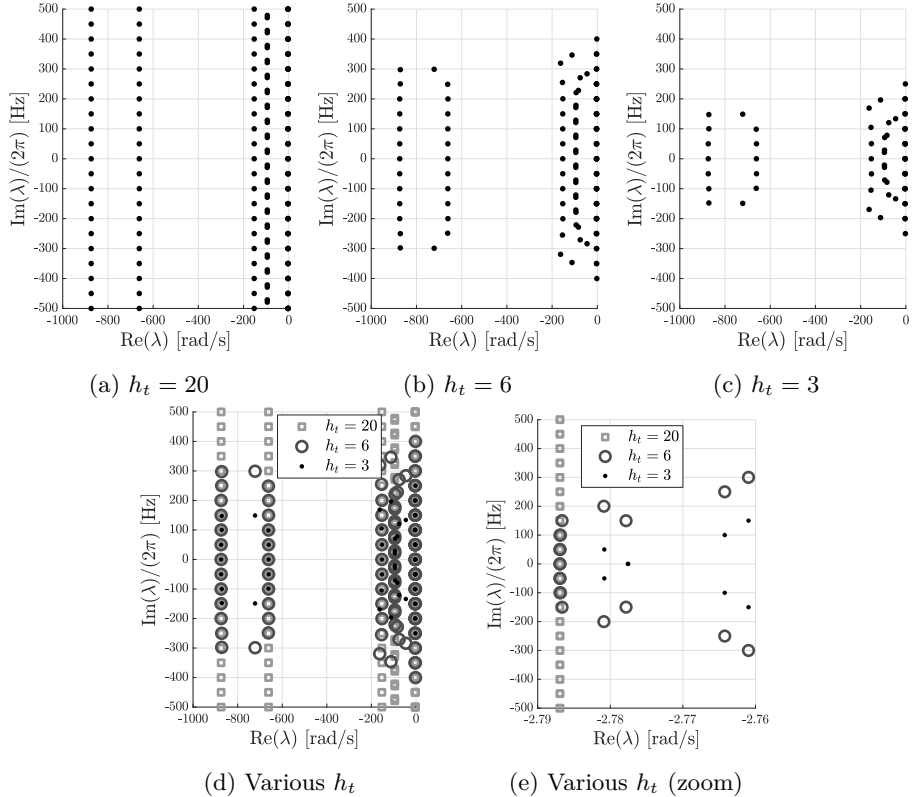


Figure 3.4: Simplified single-phase MMC: impact of truncation on HSS eigenvalues ($h_m = 6$)

an LTP system also involves non-zero off-diagonal block elements. Intuitively, truncation causes the repeated patterns of the block-Toeplitz multi-diagonal structure to be incomplete at the upper-left and lower-right corners of the truncated matrices as illustrated in Fig. 3.5. This results in a distorted pattern of the vertical eigensets.

The eigenvalues that are clearly misaligned are referred to as *spurious eigenvalues*. Their location within the complex plane has no physical meaning and they should thus be ignored in modal analyses of truncated frequency-lifted systems [70, Ch.3]. It is recalled that the theoretical HSS models are infinite-dimensional, in which case the vertical lines have no end and thus no spurious eigenvalues. It is noted that $h_t = 20$ also leads to spurious eigenvalues in Fig. 3.4a. These are simply not visible as the limits of the eigensets are not shown.

$$\begin{bmatrix} A_0 + 3j\omega_1 I & A_{-1} & A_{-2} \\ A_1 & A_0 + 2j\omega_1 I & A_{-1} & A_{-2} \\ A_2 & A_1 & A_0 + j\omega_1 I & A_{-1} & A_{-2} \\ & A_2 & A_1 & A_0 & A_{-1} & A_{-2} \\ & & A_2 & A_1 & A_0 - j\omega_1 I & A_{-1} & A_{-2} \\ & & & A_2 & A_1 & A_0 - 2j\omega_1 I & A_{-1} \\ & & & & A_2 & A_1 & A_0 - 3j\omega_1 I \end{bmatrix}$$

Figure 3.5: HSS model of an LTP system: the truncation of the state matrix results in incomplete patterns of the block-Toeplitz multi-diagonal structure

In Fig. 3.4d, the eigensets obtained with different truncation ranks are superimposed, showing that the main effect of truncation is to change the number of eigenvalues in each set and thus the length of the vertical lines.

A horizontal zoom of Fig. 3.4d is given in Fig. 3.4e and shows that, for truncation ranks significantly smaller than the periodic rank (e.g. $h_t = 3$), the disturbed ends of the vertical lines are qualitatively close to the centremost eigenvalue. This implies that most, if not all eigenvalues within the set are spurious and misaligned. With $h_t = 3$, the real-part of the centremost eigenvalue has not converged to its true value. This motivates choosing a truncation rank such that the stability assessment can be based on eigensets in which the real part of the centremost eigenvalues has converged.

Remarks on spurious eigenvalues

- It is observed in Fig. 3.4b that not all vertical lines present spurious eigenvalues. Intuitively, some dynamics of LTP systems are in fact time-invariant, e.g. governed exclusively by constant circuit parameters, and are thus not impacted by truncation.
- It may happen that spurious eigenvalues appear in the right-half plane while their corresponding eigenset lies within the left-half plane. When such spurious eigenvalues lead to uncertainty regarding the true stability of the system, the focus should be set on determining the converged eigenvalues of the corresponding eigenset, for instance by increasing the truncation rank h_t .

Application to an LTP system: the linearised HVDC link

The procedure applied earlier to the simplified single-phase MMC is now applied to an MMC-based point-to-point HVDC link. This system, which is described



Figure 3.6: LTP model of the MMC-based HVDC link: relative norm of state matrix Fourier coefficients

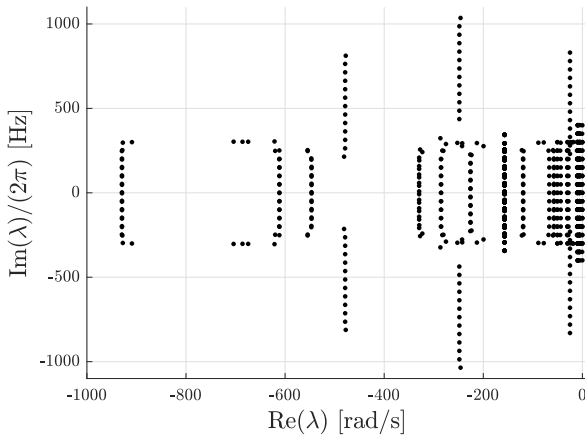


Figure 3.7: MMC-based HVDC link: HSS eigenvalues ($h_m = 6$, $h_t = 6$)

in Appendix B.4, is considered in this section with all delays set to zero. After determining the steady-state periodic trajectory over one fundamental period and linearising the equations, the Fourier coefficients of the periodic state matrix are obtained. According to Fig. 3.6, a periodic rank $h_m = 6$ corresponds to neglecting Fourier coefficients with a maximum relative norm of about 10^{-6} . Next, the HSS model is retrieved with a truncation rank $h_t = h_m = 6$ and the eigenvalues of the HSS state matrix $\mathcal{A} - \mathcal{N}$ are calculated and displayed in Fig. 3.7.

The HSS framework allows analysing the impact of accounting or not for specific harmonic components of $\mathcal{A}(t)$. This is done by adjusting the forced periodic rank, thereby disregarding non-zero Fourier coefficients of ranks larger than h_f .

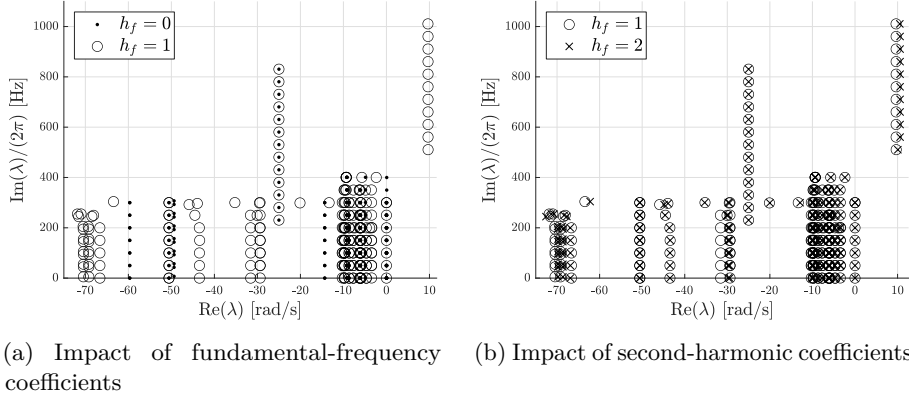


Figure 3.8: MMC-based HVDC link: Upper-half plane HSS eigenvalues with $\text{Re}(\lambda) > -75 \text{ rad/s}$ ($h_t = 6$)

First, the HVDC system is pushed towards an unstable behaviour by increasing the bandwidth of the direct voltage controller in MMC_1 from 5 Hz to 65 Hz. The new eigenvalues of $\mathcal{A} - \mathcal{N}$ are displayed in Fig. 3.8 for different values of the forced periodic rank h_f (the truncation rank h_t remains unchanged). Being symmetrical, only the upper-half plane is shown for clarity. Moreover, only dominant eigenvalues of real-part larger than -75 rad/s are displayed.

Fig. 3.8a compares the results obtained with $h_f = 0$ and $h_f = 1$. It shows the impact of including fundamental-frequency Fourier coefficients with respect to the case in which only the index-0 coefficient is used. It appears that disregarding fundamental-frequency components is too rough of a simplification. In particular, the resonance located near 760 Hz (according to the centremost eigenvalue of the unstable eigenset) is only captured when the fundamental-frequency components are considered.

Next, Fig. 3.8b compares the results obtained with $h_f = 1$ and $h_f = 2$. It shows the impact of including second-harmonic Fourier coefficients with respect to the case in which only the constant and fundamental-frequency coefficients are considered. Here, the improvement in accuracy is more subtle but not negligible, as it reveals that the centremost eigenvalues of several eigensets, in particular the unstable eigenset, had not converged for $h_f = 1$. Further increasing the forced periodic rank does not significantly change the results for this particular case.

This analysis describes the impact of accounting for harmonic components of periodic coefficients in a stability assessment. Precisely, the assessment can become incorrect or inaccurate if some non-negligible harmonic components

are not taken into account. Considering the fact that different values of the forced periodic rank h_f does not significantly change the computational cost of the eigenvalue calculation for a given truncation rank h_t , it is sensible to include all harmonic components below the identified periodic rank ($h_f = h_m$) for eigenvalue-based stability analyses relying on HSS models.

3.2.4 Comparisons with other transformation methods

The HSS framework is here briefly compared with dynamic phasors, frame rotations and the Floquet transformation.

Comparison of HSS with dynamic phasors⁵

The expression *dynamic phasor* refers to time-varying Fourier coefficients $x_k(t)$, $k \in \mathbb{Z}$, however commonly noted $\langle x \rangle_k$. Originally, dynamic phasors have been introduced as a way of relaxing the steady-state assumption on which the concept of phasor relies. By allowing for time-dependency, dynamic phasors have been used to express the variation of phase and magnitude of sinusoidal waveforms over time. By extension, several dynamic phasors can be employed to describe waveforms of more than one frequency component, and whose amplitudes or phase angles present time-varying characteristics. Due to the fact that a signal undergoing a transient does not have a unique representation with two or more time-dependent Fourier coefficients⁶, dynamic phasors are calculated in such a way that they are each typically related to limited portions of the frequency spectrum [72].

In steady-state, dynamic phasors related to harmonic components of a periodic quantity are constant and the concept of band-limited dynamic phasors can be rethought into dynamic phasors associated with specific harmonic frequencies. In the context of small-signal stability analyses, dynamic phasors have thus also been used as a way of transforming NTI_P and NTP_P systems into NTI_C systems that can be linearised around a constant operating point, in a way similar to that of frame rotations.

Establishing a small-signal dynamic-phasor-based representation of a nonlinear system following a periodic trajectory relies on the three following steps:

⁵ The comparison of HSS with dynamic phasors relies on published article [71], see also the List of Publications.

⁶ For example, a 100 Hz oscillatory component can be represented by a 50 Hz oscillation of a 50 Hz Fourier coefficient, as well as by a constant 100 Hz Fourier coefficient.

1. Replacing the variables (and time-periodic parameters, if any) with their Fourier series;
2. Applying the principle of harmonic balance to obtain one differential equation per harmonic index;
3. Linearising around the resulting constant operating point.

A first observation is that the steps are similar to those used for the derivation of the HSS formulation. The main difference is that, in the case of HSS, the nonlinear equations are linearised first. In fact, the HSS approach and the dynamic-phasor approach rely on the very same transformation (i.e. frequency-lifting) and, when applied to the same initial nonlinear model and under the same truncation assumptions, the two approaches result in LTI models with similar state matrices (i.e. matrices that have the same eigenvalues).

A second observation is that, just as with frame rotations, carrying out the first two steps is only possible for quadratic systems, i.e. systems satisfying Assumption 11, and the proposed approach does not result in a NTI_c system if nonlinearities other than the product of two variables are present. While this is a limitation of the dynamic-phasor approach, this is not an issue for the HSS approach, which addresses time-periodicity of the linearised system instead.

For quadratic systems, the first two steps result in a collection of generic sets of differential equations, each set being related to a harmonic index $k \in \mathbb{Z}$. The generic set of index- k equations is directly obtained by replacing the states $x^{(i)}(t)$, inputs $u^{(i)}(t)$ and outputs $y^{(i)}(t)$ by their index- k dynamic phasors $\langle x \rangle_k^{(i)}$, $\langle u \rangle_k^{(i)}$ and $\langle y \rangle_k^{(i)}$. Additionally, time derivatives and products of variables are transformed as:

$$\frac{dx(t)}{dt} \xrightarrow{k} \frac{d\langle x \rangle_k}{dt} + jk\omega_1 \langle x \rangle_k \quad (3.43)$$

$$u(t)v(t) \xrightarrow{k} \sum_{l=-\infty}^{+\infty} \langle u \rangle_l \langle v \rangle_{k-l}. \quad (3.44)$$

Just as with HSS, harmonic balance in the context of dynamic phasors results in a theoretically infinite set of dynamic equations. In practice, sets of equations are considered only up to a maximum harmonic rank. Furthermore, it is common practice to include, in each set, only the differential equations related to harmonic components that are known (or assumed) to be non-zero [64]. This is a fundamental difference with respect to the HSS approach, in which all indices below the periodic rank are usually considered, regardless of whether they correspond to null Fourier coefficients. Aside from resulting in systems of

smaller dimensions, the main impact of not including all harmonic indices below the truncation rank in dynamic-phasor-based systems is that not all eigenvalues within the eigensets are visible in the complex plane, which may complicate the identification of the eigensets, of their centremost eigenvalue, and of spurious eigenvalues.

Comparison of HSS and frame rotations

As the application of frame rotations does not rely on the harmonic balance principle, frame rotations do not result in a frequency-lifted system. Consequently, an important difference between frequency-lifting and frame rotations is the dimension of the resulting system, since lifting naturally leads to higher-dimensional systems. This is not the case of frame-rotation-based methods, where the number of states is kept constant, unless virtual variables are introduced to transform zero-sequence components. This is a major advantage of frame rotations, which do not result in theoretically infinite-dimensional systems. No truncation is needed, therefore the approach does not lead to apparition of spurious eigenvalues. As a consequence, the ensuing stability assessment is simpler.

On the other hand, frequency-lifting in the form of HSS has the advantage of relying on few to no assumptions on the nature of the considered equations, and thus benefits from a wider range of applicability. In particular, no preliminary assumption on the harmonic or sequence content of the variables is required. Unlike frame rotations, frequency-lifting is also applicable to systems that do not necessarily satisfy Assumptions 7, 8, 10, or 11.

Comparison of HSS and Floquet transformation

Applying the Floquet transformation directly to the HSS representation delivers valuable insights into their relationship. Such developments were introduced in [18, Lemma 3.17] and are revisited in the following paragraphs.

The starting point is the HSS representation (3.29) repeated here for convenience:

$$\begin{cases} \dot{\mathbf{x}}(t) = (\mathcal{A} - \mathcal{N})\mathbf{x}(t) + \mathcal{B}\mathbf{u}(t) \\ \mathbf{y}(t) = \mathcal{C}\mathbf{x}(t) + \mathcal{D}\mathbf{u}(t). \end{cases} \quad (3.45)$$

First, the frequency-lifted form of the Floquet transformation described by (2.14) is considered:

$$\mathcal{K}\{\mathbf{x}(t) = \mathbf{P}(t)\mathbf{v}(t)\} \implies \mathbf{x}(t) = \mathcal{P}\mathbf{v}(t), \quad (3.46)$$

with $\mathcal{P} = \mathcal{T}\{\mathbf{P}_k : k \in \mathbb{Z}\}$ and \mathbf{P}_k the Fourier coefficients of periodic matrix $\mathbf{P}(t)$ introduced in (1.82). Applying this change of variables, the HSS system becomes:

$$\begin{cases} \mathcal{P}\dot{\mathbf{v}}(t) = (\mathcal{A} - \mathcal{N})\mathcal{P}\mathbf{v}(t) + \mathcal{B}\mathbf{u}(t) \\ \mathbf{y}(t) = \mathcal{C}\mathcal{P}\mathbf{v}(t) + \mathcal{D}\mathbf{u}(t). \end{cases} \quad (3.47)$$

Rearranging the differential equation results in:

$$\begin{cases} \dot{\mathbf{v}}(t) = \mathcal{P}^{-1}(\mathcal{A} - \mathcal{N})\mathcal{P}\mathbf{v}(t) + \mathcal{P}^{-1}\mathcal{B}\mathbf{u}(t) \\ \mathbf{y}(t) = \mathcal{C}\mathcal{P}\mathbf{v}(t) + \mathcal{D}\mathbf{u}(t). \end{cases} \quad (3.48)$$

The notation is simplified by defining matrices $\bar{\mathcal{B}} \triangleq \mathcal{P}^{-1}\mathcal{B}$ and $\bar{\mathcal{C}} \triangleq \mathcal{C}\mathcal{P}$:

$$\begin{cases} \dot{\mathbf{v}}(t) = \mathcal{P}^{-1}(\mathcal{A} - \mathcal{N})\mathcal{P}\mathbf{v}(t) + \bar{\mathcal{B}}\mathbf{u}(t) \\ \mathbf{y}(t) = \bar{\mathcal{C}}\mathbf{v}(t) + \mathcal{D}\mathbf{u}(t). \end{cases} \quad (3.49)$$

Next, the relationship between matrices $\mathbf{A}(t)$, $\mathbf{P}(t)$ and \mathbf{Q} is recalled from (2.12), also repeated here for convenience:

$$\mathbf{A}(t)\mathbf{P}(t) = \mathbf{P}(t)\mathbf{Q} + \dot{\mathbf{P}}(t), \quad (3.50)$$

with frequency-lifted counterparts given by:

$$\mathcal{K}\{\mathbf{A}(t)\mathbf{P}(t)\} = \mathcal{A}\mathcal{P} \quad (3.51a)$$

$$\mathcal{K}\{\mathbf{P}(t)\mathbf{Q}\} = \mathcal{P}\mathbf{Q} \quad (3.51b)$$

$$\mathcal{K}\{\dot{\mathbf{P}}(t)\} = \mathcal{N}\mathcal{P} - \mathcal{P}\mathcal{N}, \quad (3.51c)$$

which are proven in [18, Ch.2]⁷. Recalling that \mathbf{Q} is a constant matrix, the block-Toeplitz matrix \mathbf{Q} is block-diagonal:

$$\mathbf{Q} = \text{blkdiag}\{[\cdots \quad \mathbf{Q} \quad \mathbf{Q} \quad \mathbf{Q} \quad \cdots]\}. \quad (3.52)$$

Relying on the expressions above, the frequency-lifted form of (3.50) becomes:

$$\mathcal{A}\mathcal{P} = \mathcal{P}\mathbf{Q} + \mathcal{N}\mathcal{P} - \mathcal{P}\mathcal{N} \iff (\mathcal{A} - \mathcal{N})\mathcal{P} = \mathcal{P}(\mathbf{Q} - \mathcal{N}) \quad (3.53a)$$

$$\iff \mathcal{P}^{-1}(\mathcal{A} - \mathcal{N})\mathcal{P} = \mathbf{Q} - \mathcal{N} \quad (3.53b)$$

⁷ See Theorem 2.5 in [18]. In particular, the proof of (3.51c) may not be straightforward at first sight, but comes from the fact that $\mathbf{P}(t)$ is a matrix and not a vector.

Substituting the last result into (3.49) gives:

$$\begin{cases} \dot{\mathbf{v}}(t) = (\bar{\mathbf{Q}} - \bar{\mathbf{N}})\mathbf{v}(t) + \bar{\mathbf{B}}\mathbf{u}(t) \\ \mathbf{y}(t) = \bar{\mathbf{C}}\mathbf{v}(t) + \mathbf{D}\mathbf{u}(t). \end{cases} \quad (3.54)$$

This system is precisely the frequency-lifted form of (2.18), which was the non-lifted system resulting from the Floquet transformation in Section 2.2.2.

The above procedure is essentially summarised in the observation that, according to (3.53b), matrix $\bar{\mathbf{Q}} \triangleq \mathbf{Q} - \mathbf{N}$ is the similarity transformation of matrix $\bar{\mathbf{A}} \triangleq \mathbf{A} - \mathbf{N}$ by matrix \mathbf{P} . Recalling that the eigenvalues of a matrix are not changed by a similarity transformation, $\bar{\mathbf{Q}}$ and $\bar{\mathbf{A}}$ have the same eigenvalues. Furthermore, $\bar{\mathbf{Q}}$ is a block-diagonal matrix:

$$\bar{\mathbf{Q}} = \mathbf{Q} - \mathbf{N} = \begin{bmatrix} \ddots & & & & \\ & \mathbf{Q} + j\omega_1 \mathbf{I} & & & \\ & & \mathbf{Q} & & \\ & & & \mathbf{Q} - j\omega_1 \mathbf{I} & \\ & & & & \ddots \end{bmatrix}. \quad (3.55)$$

Since the eigenvalues of a block-diagonal matrix are composed of the set of eigenvalues of every block taken separately, the set of eigenvalues of $\bar{\mathbf{A}}$ is given by

$$\{\lambda(\bar{\mathbf{A}})\} = \{\lambda(\mathbf{Q}); \quad \lambda(\mathbf{Q}) \pm j\omega_1; \quad \lambda(\mathbf{Q}) \pm 2j\omega_1; \quad \dots\}, \quad (3.56)$$

where $\lambda(\mathbf{Q})$ are (one set of) the Floquet exponents of the original LTP system, as explained in Section 2.2.2. Consequently, the eigenvalues of the state matrix of an HSS system are the duplicated and shifted versions of the Floquet exponents.

In conclusion, frequency-lifting in the form of HSS is a rather direct way of calculating the Floquet exponents once the harmonic content of the coefficients of an LTP system is known. Besides, an advantage of retrieving the Floquet exponents as the eigenvalues of $\mathbf{A} - \mathbf{N}$ is that the centremost eigenvalue of every eigenset provides direct information regarding the oscillatory frequency of the corresponding mode. This information, although particularly relevant in the context of stability and interaction studies, is seemingly less straightforward to retrieve based on the Floquet multipliers (i.e. the eigenvalues of the monodromy matrix) or based on the Floquet exponents when these are obtained from the logarithm of the monodromy matrix, as in (2.20). This is a consequence of the fact that the oscillatory mode frequency of the Floquet multipliers is only defined up to an integer multiple of the fundamental frequency.

3.2.5 Conclusion

Frequency-lifting, in the form of HSS, is a generic and flexible way of transforming LTP systems into LTI systems. This transformation method, which relies on the idea of representing periodic quantities by the set of their Fourier coefficients, can be interpreted as the projection of LTP systems onto a higher-dimensional space where these systems are time invariant. The fact that HSS models can be established from the linearised equations of the initial nonlinear system and from the harmonic content of the periodic matrix coefficients, gives this approach the significant advantage of relying on few to no simplifying assumptions on the nature of the studied system. Nevertheless, the stability assessment of the resulting HSS system differs somewhat from that of traditional, i.e. non-lifted LTI systems, in particular due to the fact that the eigenvalues of HSS representations appear as vertical lines in the complex plane, and rely on the truncation of theoretically infinite matrices to enable numerical evaluations.

In the next section, the presentation of frequency-domain models based on the harmonic balance principle starts with a description of the harmonic linearisation method.

3.3 Harmonic linearisation

Harmonic linearisation (HL) is a transformation method that focuses on establishing an input-output description of dynamic systems in the frequency domain, and eventually results in a transfer function or a frequency-response representation. The main idea behind this technique is to determine how the system impacts the magnitude and the phase angle of a small-signal perturbation, from its application at the input and at a given frequency to its manifestation at the output and at the same frequency.

The expression *harmonic linearisation* hides two aspects of this method, which addresses first nonlinearity, and then periodicity. When applied to a NTI_p system or a NTP_p system, the equations are linearised around the periodic trajectory, which results in an LTP system. Next, the LTP system is transformed into an LTI system, which is naturally reminiscent of the HSS procedure described in the previous section. HL can also be applied to NTI_c systems, in which case it is equivalent to linearisation and directly results in an LTI system. If directly applied to LTP systems, the linearisation step is unnecessary and only the transformation to a time-invariant system is relevant.

In this section, both numerical and analytical approaches to HL are presented.

3.3.1 Numerical approach: frequency scans

The numerical application of HL is referred to as a *frequency scan* or a *frequency sweep*. The procedure for both nonlinear and linear systems is the same and consists in adding a small sinusoidal perturbation $\tilde{u}(t) = \hat{u} \sin(\omega_p t)$ to the steady-state value or trajectory of an input variable, and measuring the resulting output perturbation $\tilde{y}(t)$ at frequency ω_p [63]. Considering directly the frequency-domain complex-valued components as a function of ω_p , we have:

$$u(j\omega_p) = \bar{u}(j\omega_p) + \tilde{u}(j\omega_p) \quad (3.57a)$$

$$y(j\omega_p) = \bar{y}(j\omega_p) + \tilde{y}(j\omega_p) \quad (3.57b)$$

where $u(j\omega_p)$, $y(j\omega_p)$ are the disturbed input and output large-signal components, $\bar{u}(j\omega_p)$, $\bar{y}(j\omega_p)$ are the undisturbed input and output large-signal components in steady state, and $\tilde{u}(j\omega_p)$, $\tilde{y}(j\omega_p)$ are the input and output small-signal disturbances, respectively.

The input perturbation is characterised by its frequency ω_p and has a sufficiently small amplitude for the small-signal assumption to hold. In the specific cases of nonlinear systems and of LTP systems, frequency couplings arise. This implies that applying the input perturbation at ω_p may not only result in output perturbations at the same frequency ω_p , but also at other frequencies. In HL, these additional output components at other frequencies than the perturbation frequency are normally disregarded and only the output perturbation at the same frequency ω_p is collected. In that regard, the resulting system is a simplification of the initial system.

Clearly, such simplification is sometimes unacceptable. The following LTP system is considered for example:

$$y(t) = \sin(\omega_1 t)u(t). \quad (3.58)$$

In this system, an input perturbation at non-zero frequency ω_p is never mapped to the same frequency at the output. In this case, HL would simply result in a null transfer function.

Otherwise, when relevant and applicable, HL results in an input-output representation in the frequency domain, in which an input perturbation at one frequency leads to an output perturbation at the same frequency: the outcome of HL has the characteristics of an LTI system.

Once the disturbed system reaches steady state, the single-input single-output (SISO) frequency response at the perturbation frequency ω_p is given by:

$$H(j\omega_p) \triangleq \frac{\tilde{y}(j\omega_p)}{\tilde{u}(j\omega_p)}, \quad (3.59)$$

which is equivalent to:

$$H(j\omega_p) = \frac{y(j\omega_p) - \bar{y}(j\omega_p)}{u(j\omega_p) - \bar{u}(j\omega_p)}. \quad (3.60)$$

In the case of systems operating at equilibrium points, $\bar{u}(j\omega_p)$ and $\bar{y}(j\omega_p)$ are equal to zero at all values of ω_p except perhaps at $\omega_p = 0$. In the case of nonlinear systems following periodic trajectories of fundamental period T_1 , $\bar{u}(j\omega_p)$ and $\bar{y}(j\omega_p)$ may be non-zero when the perturbation frequency is equal to harmonic frequencies $\omega_p = k\omega_1$, $k \in \mathbb{Z}$. The described procedure is repeated for all frequencies of interest, generally covering a range from a few hertz to a few kilohertz.

In order to speed up the above procedure, it may be tempting to apply perturbations at every frequency of interest simultaneously. However, this is only acceptable for systems that are not subject to frequency couplings, i.e. it is acceptable for LTI systems. In the case of nonlinear and LTP systems, the safest approach is to carry out a scan frequency per frequency. In this case, it is ensured that a perturbation appearing in the output variable at frequency ω_p (if any) is the consequence of the input perturbation at the same frequency ω_p , and not the consequence of an input perturbation at another frequency ω'_p being coupled to the output at the target frequency ω_p . An exception to this guideline is possible in frequency ranges where it can be verified that frequency couplings can be neglected.

Numerical HL is often carried out in a simulation environment or via measurements on a physical system as a system identification technique, e.g. for the validation of frequency responses obtained from analytical models.

Generalised forms of harmonic linearisation

Generalisations of HL are possible, where the input-output representation also accounts for output perturbations at other frequencies than that of the input perturbation, which would be necessary to accurately model systems such as (3.58). Specifically, in numerical HL, the following ratios can also be measured or simulated:

$$H_k(j\omega_p) \triangleq \frac{\tilde{y}(j\omega_p + jk\omega_1)}{\tilde{u}(j\omega_p)}, \quad k \in \mathbb{Z}. \quad (3.61)$$

These ratios describe the relationships between an input perturbation at frequency ω_p and the resulting perturbations at output frequencies $\omega_p + k\omega_1$. In the case of SISO systems, such generalised HL approach results in a single-input multi-output (SIMO) system due to the fact that the resulting transfer function maps an input perturbation to multiple output perturbations.

3.3.2 Analytical approach

While the numerical HL is widely used in practice, further insights into its underlying mechanisms are provided in this section by means of an analytical approach. Starting with NTI_p or NTP_p systems, the linearisation step within the HL approach is carried out by means of an analytical linearisation, which results in an LTP system. The description of the frequency response of LTP systems initiated in Section 1.3.3 is continued next.

Frequency response of LTP systems (continued)

In Section 1.3.3, it was shown that the steady-state output response of an LTP system to an input perturbation $\tilde{\mathbf{u}}(t) = \hat{\mathbf{u}}e^{st}$ can be written as (1.95), repeated here for convenience (with $t_0 = 0$):

$$\tilde{\mathbf{y}}_{ss}(t) = \sum_{k=-\infty}^{+\infty} \mathbf{G}_k(s) \hat{\mathbf{u}} e^{(s+jk\omega_1)t}, \quad (3.62)$$

where $\mathbf{G}_k(s)$ are the Fourier coefficients of $\mathbf{G}(t, s)$, which is defined as:

$$\mathbf{G}(t, s) \triangleq \mathbf{C}(t)\mathbf{P}(t)\mathbf{L}(t, s) + \mathbf{D}(t), \quad (3.63a)$$

with

$$\mathbf{L}(t, s) \triangleq \sum_{k=-\infty}^{+\infty} (s_k \mathbf{I} - \mathbf{Q})^{-1} \bar{\mathbf{B}}_k e^{jk\omega_1 t}, \quad (3.63b)$$

also recalling that $s_k = s + jk\omega_1$. The expression of the steady-state output response $\tilde{\mathbf{y}}_{ss}(t)$ shows that, as a consequence of frequency couplings, the output perturbations appear as duplicated and frequency-shifted versions of the input perturbation, each copy being multiplied by a complex-valued gain $\mathbf{G}_k(s)$. Equivalently, the steady-state output response can be rewritten as:

$$\tilde{\mathbf{y}}_{ss}(t) = \mathbf{G}_0(s) \hat{\mathbf{u}} e^{st} + \sum_{\substack{k=-\infty \\ k \neq 0}}^{+\infty} \mathbf{G}_k(s) \hat{\mathbf{u}} e^{(s+jk\omega_1)t}, \quad (3.64)$$

where the output component corresponding to $k = 0$ has been brought out. This component is not shifted in frequency and is the one that is normally identified in the HL process, while all other components ($k \neq 0$) are normally disregarded. The resulting model is given by:

$$\tilde{\mathbf{y}}(j\omega_p) = \mathbf{H}(j\omega_p)\tilde{\mathbf{u}}(j\omega_p) \quad (3.65)$$

with $\mathbf{H}(j\omega_p) = \mathbf{G}_0(j\omega_p)$. At this point, it is recalled that $\mathbf{G}_0(s)$ is the average value of the periodic quantity $\mathbf{G}(t, s) = \mathbf{C}(t)\mathbf{P}(t)\mathbf{L}(t, s) + \mathbf{D}(t)$. However, it is important to note that $\mathbf{G}_0(s)$ is not equal to the products and sums of average values, i.e. it is not equal to $\mathbf{C}_0\mathbf{P}_0\mathbf{L}_0(s) + \mathbf{D}_0$.

To illustrate this point as well as the transfer and frequency-coupling principles involved in the calculation of $\mathbf{G}_0(s)$, the process is represented by the multiplication of an input perturbation by three time-periodic quantities:

$$\tilde{y}(t) = \mathbf{C}(t)\mathbf{P}(t)\mathbf{L}(t)\tilde{u}(t), \quad (3.66)$$

where for simplicity with respect to the complete expression of $\mathbf{G}(t, s)$, the contribution of matrix $\mathbf{D}(t)$ is disregarded, the dependency of $\mathbf{L}(t, s)$ on s is not shown and the SISO scalar case is considered instead of the multi-input multi-output (MIMO) matrix case. Equivalently, relying on intermediate signals $\tilde{a}(t)$ and $\tilde{b}(t)$, we have:

$$\begin{cases} \tilde{a}(t) = \mathbf{L}(t)\tilde{u}(t) \\ \tilde{b}(t) = \mathbf{P}(t)\tilde{a}(t) \\ \tilde{y}(t) = \mathbf{C}(t)\tilde{b}(t). \end{cases} \quad (3.67)$$

The three steps are displayed horizontally in Fig. 3.9. At each step, the multiplication of the signal by a periodic quantity causes the perturbation(s) to be mapped onto components at multiple frequencies. These components are written $\tilde{x}|_k(t)$, with x standing for any of the signals involved. In this notation, subscript k refers to the frequency at which the components appear, i.e. $\omega_p + k\omega_1$, $k \in \mathbb{Z}$. In particular, it is considered that the input perturbation $\tilde{u}|_0(t)$ is applied at ω_p only, i.e. at $k = 0$.

In Fig. 3.9a, the input-output transfer indicated in blue is incomplete: since successive products of periodic quantities are involved, there are in fact multiple paths that could link inputs and outputs of same frequencies. This is illustrated in Fig. 3.9b, where at each step, a selection of paths connecting the input perturbation to the output perturbation at the same frequency are indicated in red. Not all possible paths are shown: in theory, each node could be leading to an infinite number of arrows. The paths that are actually enabled by frequency couplings depend on the specific harmonic content of the periodic quantities $\mathbf{L}(t)$, $\mathbf{P}(t)$ and $\mathbf{C}(t)$.

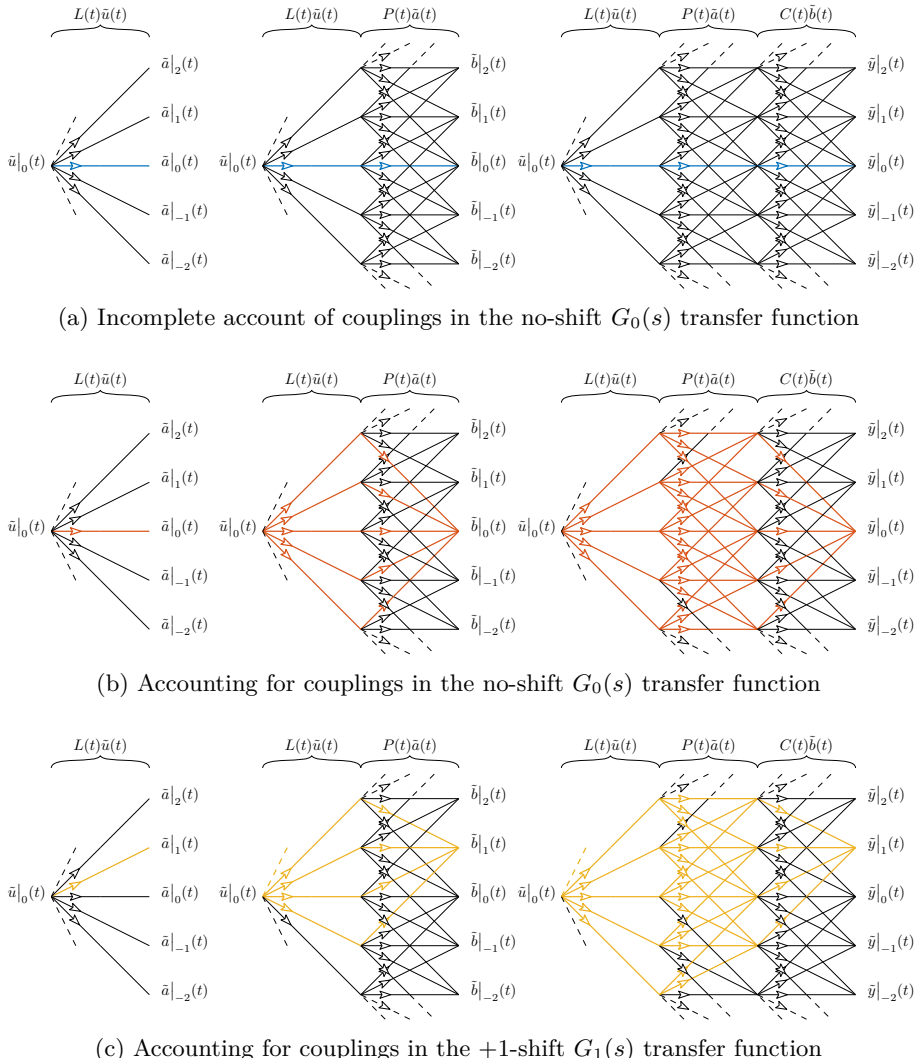


Figure 3.9: Frequency coupling mechanism in harmonic linearisation

The input-output transfer function $\mathbf{G}_0(s)$ illustrated in Fig. 3.9b relates input and output components of the same frequency. It corresponds to the *no-shift* transfer function of the periodic system, to be understood in the sense of *no input-output frequency-shift* transfer function. The illustration in Fig. 3.9b shows that, even though the *no-shift* model resulting from HL does not display apparent consequences of frequency couplings (i.e. output components at frequencies different from ω_p), internal frequency couplings are indeed taken into account.

The presence of frequency couplings implies that *shift* transfer functions can also be determined by considering the paths linking input and output perturbations of different frequencies. For instance, Fourier coefficient $G_1(s)$ of the complete input-output transfer operator (3.66) relates the input $\tilde{u}|_0(t)$ at ω_p to the output $\tilde{y}|_1(t)$ at $\omega_p + \omega_1$. This case is illustrated in Fig. 3.9c, where a selection of paths connecting the input perturbation to the output perturbation at the specified frequencies are indicated in yellow.

Although the presented analytical considerations give insights into the mechanisms behind frequency couplings and HL, they do not provide a practical tool to carry out an analytical derivation for an actual set of equations, especially because matrix $\mathbf{P}(t)$ is rarely available in analytical form. The remainder of this section briefly describes the analytical application of HL to practical models.

Analytical harmonic linearisation for practical models

In practice, the analytical application of HL relies on the following successive steps [63, 73, 74]:

- 1. Establishing the initial set of dynamic equations**

The initial set of dynamic equations is represented as linear or nonlinear differential equations, and/or transfer functions.

- 2. Identifying the input and output variables** $u(t)$ and $y(t)$ between which the input-output representation must be retrieved. Their corresponding deviations are noted $\tilde{u}|_k(t)$ and $\tilde{y}|_l(t)$ where, generally, $(k, l) = (0, 0)$ to retrieve the *no-shift* frequency response.

- 3. Specifying the operating trajectory**

Before linearisation, the steady-state operating point or periodic trajectory is determined. Specifically, the steady-state harmonic spectrum of all variables must be known.

- 4. Harmonic linearisation**

Harmonic linearisation is decomposed into the following steps:

- 4.1 Analytical linearisation of the equations to obtain an LTP system: the variables of the linearised equations are small-signal deviations and the coefficients are periodic quantities, functions of the undisturbed steady-state variables.
- 4.2 Application of the harmonic balance principle to obtain time-invariant relationships between the frequency components of the small-signal deviations.
- 4.3 Extraction of the relationship between the input perturbation $\tilde{u}|_k(t)$ and the output deviation $\tilde{y}|_l(t)$ as a function of ω_p by successive elimination of all other intermediate small-signal variables.

Steps 4.2 and 4.3 are now illustrated by means of a simple LTP system, where the output is given by $\tilde{x}(t)$ processed by a low-pass filter of bandwidth ω_f :

$$\left\{ \begin{array}{l} \frac{d\tilde{x}(t)}{dt} = a(t)\tilde{x}(t) + \tilde{u}(t) \end{array} \right. \quad (3.68a)$$

$$\left\{ \begin{array}{l} \tilde{y}(s) = \frac{\omega_f}{s + \omega_f}\tilde{x}(s), \end{array} \right. \quad (3.68b)$$

with $a(t) = 2 \cos(\omega_1 t)$. Additionally, $\tilde{x}(s)$ and $\tilde{y}(s)$ correspond to the Laplace transforms of $\tilde{x}(t)$ and $\tilde{y}(t)$, respectively. For simplicity, the same letters are used for variables in time and Laplace domains, the difference being shown by means of their argument. The following input perturbation is considered:

$$\tilde{u}(t) = \tilde{u}|_0(t) = \hat{u}|_0 e^{j\omega_p t} \quad (3.69)$$

where $\hat{u}|_0$ is a complex number accounting for the magnitude and phase angle of $\tilde{u}|_0(t)$. Intuitively, state perturbations are expected at least at frequencies ω_p and $\omega_p \pm \omega_1$:

$$\tilde{x}(t) = \hat{x}|_0 e^{j\omega_p t} + \hat{x}|_{-1} e^{j(\omega_p - \omega_1)t} + \hat{x}|_1 e^{j(\omega_p + \omega_1)t}. \quad (3.70)$$

Rewriting also $a(t)$ as $a(t) = e^{j\omega_1 t} + e^{-j\omega_1 t}$, (3.68a) becomes:

$$\frac{d}{dt} \left(\hat{x}|_0 e^{j\omega_p t} + \hat{x}|_{-1} e^{j(\omega_p - \omega_1)t} + \hat{x}|_1 e^{j(\omega_p + \omega_1)t} \right) \quad (3.71)$$

$$= (e^{j\omega_1 t} + e^{-j\omega_1 t}) \left(\hat{x}|_0 e^{j\omega_p t} + \hat{x}|_{-1} e^{j(\omega_p - \omega_1)t} + \hat{x}|_1 e^{j(\omega_p + \omega_1)t} \right) + \hat{u}|_0 e^{j\omega_p t}$$

$$= \left(\hat{x}|_0 e^{j(\omega_p + \omega_1)t} + \hat{x}|_0 e^{j(\omega_p - \omega_1)t} + (\hat{x}|_{-1} + \hat{x}|_1) e^{j\omega_p t} + \dots \right. \\ \left. \hat{x}|_{-1} e^{j(\omega_p - 2\omega_1)t} + \hat{x}|_1 e^{j(\omega_p + 2\omega_1)t} \right) + \hat{u}|_0 e^{j\omega_p t}. \quad (3.72)$$

Evaluating the time derivative, applying the harmonic balance principle and, for simplicity, neglecting the oscillations at $\omega_p \pm 2\omega_1$, gives:

$$\left. j\omega_p \hat{x} \right|_0 = \hat{x}|_{-1} + \hat{x}|_1 + \hat{u}|_0 \quad (3.73a)$$

$$\left. j(\omega_p - \omega_1) \hat{x} \right|_{-1} = \hat{x}|_0 \quad (3.73b)$$

$$\left. j(\omega_p + \omega_1) \hat{x} \right|_1 = \hat{x}|_0. \quad (3.73c)$$

Eliminating the intermediate perturbations $\hat{x}|_{-1}$ and $\hat{x}|_1$ gives:

$$j\omega_p \hat{x}|_0 = \frac{\hat{x}|_0}{j(\omega_p - \omega_1)} + \frac{\hat{x}|_0}{j(\omega_p + \omega_1)} + \hat{u}|_0. \quad (3.74)$$

Relying successively on (3.68b) and (3.74), the output perturbation at ω_p is given by:

$$\hat{y}|_0 = \frac{\omega_f}{j\omega_p + \omega_f} \hat{x}|_0 \quad (3.75a)$$

$$= \underbrace{\frac{\omega_f}{j\omega_p + \omega_f} \left(j\omega_p + \frac{2j\omega_p}{(\omega_p - \omega_1)(\omega_p + \omega_1)} \right)^{-1}}_{\triangleq H_0(j\omega_p)} \hat{u}|_0, \quad (3.75b)$$

with $H_0(j\omega_p)$ the sought frequency-domain model.

In the literature, analytical HL has often been carried out "by hand" as in the example above: in step 4.2, Fourier coefficients of periodic quantities and small-signal perturbations have generally been selected on an intuitive per-variable basis. In step 4.3, successive substitutions have generally been carried out variable per variable. Although tractable for this simple illustrative example, this "by-hand" process applied at equation level to elaborate systems such as the closed-loop three-phase MMC is rather tedious and naturally model-dependent (hence not provided in this thesis, but the process has been described in e.g. [74]). The complexity of the corresponding developments might have prevented the identification of similarities between HL and system-level approaches⁸ such as the HSS and the HTF [75].

⁸In this thesis, *system-level* refers to an approach where a set of differential equations is treated as a whole, in contrast with an *equation-level* approach where the differential equations are handled individually.

Comparison of HL with HSS

From the above procedure and illustrative example, it becomes evident that the HL approach is highly similar to the HSS approach [75]: both rely on the application of the harmonic balance principle to an LTP system, which results in an LTI representation. The main difference between the two approaches is that the outcome of HL is a frequency-domain model, while that of HSS is a time-domain model.

Another difference between the two methods is that the HSS is *a priori* only applicable to state-space models, while HL is applicable to models whose dynamics are also described with transfer functions. However, the application of HL to such systems faces the additional difficulty of dealing with both time-periodic characteristics in the time domain and dynamics described by transfer functions in the frequency domain. To some extent, HL can be seen an attempt at addressing problems that are more straightforwardly and comprehensively solved within the formalism of frequency-lifting. Hence, there is a need for a more elaborate description of frequency-lifting in the frequency domain.

This motivates the presentation of the HTF in the next section, not only as the frequency-domain counterpart of HSS, but also as a generalisation (or a formalisation) of the HL approach.

3.3.3 Conclusion

This section was dedicated to presenting the HL method, a transformation method relying on linearisation and on the harmonic balance principle to convert LTP models into LTI models.

Both the numerical and the analytical HL have been discussed. On the one hand, the numerical application of HL consists in performing a frequency scan of the studied system, a widely-used technique for the extraction of numerical small-signal models from nonlinear systems. On the other hand, the analytical application of HL shows how internal frequency couplings are taken into account in the HL process. Besides, the analytical approach highlights similarities with the HSS approach and hints towards the fact that the tedious "by-hand" application of HL to elaborate systems involving both periodicity in the time domain as well as dynamics described by transfer functions in the frequency domain could be simplified by the system-level formalism of frequency-lifting. This motivates the presentation of the HTF method in the next section.

3.4 The harmonic transfer function

This section is dedicated to presenting the HTF through three lenses. First, the HTF is obtained from the HSS formulation. Next, the HTF is obtained from the impulse response of LTP systems. Lastly, the HTF approach is presented as a generalisation of the HL method. The section ends with numerical applications, including a comparison of the results of the HTF approach with frequency scans.

3.4.1 The HTF from the HSS formulation

According to [18, 48], the HTF can be simply and directly obtained by applying the Laplace transform to the time-domain HSS system (3.29), which results in:

$$\begin{cases} s\mathbf{x}(s) = (\mathcal{A} - \mathcal{N})\mathbf{x}(s) + \mathcal{B}\mathbf{u}(s) \\ \mathbf{y}(s) = \mathcal{C}\mathbf{x}(s) + \mathcal{D}\mathbf{u}(s) \end{cases} \quad (3.76)$$

with s the Laplace variable. Additionally, $\mathbf{x}(s) = \mathcal{L}\{\mathbf{x}(t)\}$ and similarly for the input and output variables, with $\mathcal{L}\{\cdot\}$ denoting the Laplace transform. Here again, the same letters are used for corresponding variables in time and Laplace domains. Since only the steady-state response is of interest here, the initial conditions are disregarded in the transformation. Eliminating the state vector $\mathbf{x}(s)$ leads to the HTF representation:

$$\mathbf{y}(s) = \mathcal{H}(s)\mathbf{u}(s) \quad (3.77)$$

where

$$\mathcal{H}(s) \triangleq \mathcal{C}(s\mathcal{I} - \mathcal{A} + \mathcal{N})^{-1}\mathcal{B} + \mathcal{D}, \quad (3.78)$$

with \mathcal{I} the infinite-dimensional identity matrix.

In [18, Ch.3], the same formula is obtained by relying on the concept of exponentially-modulated periodic (EMP) signals. Intuitively, this can be seen as a way of specifying how time-dependent Fourier coefficients could vary over time, thereby also giving insights into the nature of signals $\mathbf{u}(s)$, $\mathbf{x}(s)$ and $\mathbf{y}(s)$ in the frequency domain. In this context, is it relevant to make a step back and consider again the non-lifted LTP system (3.24) and, as in Section 3.2, the unforced LTP equation is retained for simplicity:

$$\dot{\mathbf{x}}(t) = \mathbf{A}(t)\mathbf{x}(t). \quad (3.79)$$

The state vector is written in the form of an EMP signal as [18, Ch.3]:

$$\mathbf{x}(t) = \left(\sum_{k=-\infty}^{+\infty} \mathbf{x}_k(s)e^{jk\omega_1 t} \right) e^{st} = \sum_{k=-\infty}^{+\infty} \mathbf{x}_k(s)e^{(s+jk\omega_1)t} \quad (3.80)$$

where the values of \mathbf{x}_k possibly depend on s . The time derivative of $\mathbf{x}(t)$ is given by:

$$\dot{\mathbf{x}}(t) = \sum_{k=-\infty}^{+\infty} (s + jk\omega_1) \mathbf{x}_k(s) e^{(s+jk\omega_1)t}. \quad (3.81)$$

Replacing $\mathbf{A}(t)$ with its Fourier series and using the Cauchy product of infinite series, (3.79) becomes:

$$\sum_{k=-\infty}^{+\infty} (s + jk\omega_1) \mathbf{x}_k(s) e^{(s+jk\omega_1)t} = \sum_{k=-\infty}^{+\infty} \left(\sum_{h=-\infty}^{+\infty} \mathbf{A}_{k-h} \mathbf{x}_h(s) \right) e^{(s+jk\omega_1)t}. \quad (3.82)$$

The harmonic balance principle gives:

$$(s + jk\omega_1) \mathbf{x}_k(s) e^{st} = \left(\sum_{h=-\infty}^{+\infty} \mathbf{A}_{k-h} \mathbf{x}_h(s) \right) e^{st}, \quad \forall k \in \mathbb{Z}. \quad (3.83)$$

Further eliminating e^{st} on both sides and defining

$$\mathbf{x}(s) \triangleq [\dots \quad \mathbf{x}_{-1}^T(s) \quad \mathbf{x}_0^T(s) \quad \mathbf{x}_1^T(s) \quad \dots]^T, \quad (3.84)$$

Eq. (3.83) can be written in matrix form:

$$s\mathbf{x}(s) = (\mathcal{A} - \mathcal{N})\mathbf{x}(s), \quad (3.85)$$

which can also be generalised to fall back onto (3.76), i.e. on the frequency-domain representation of the complete LTP system.

From (3.77) and (3.78), the HTF $\mathcal{H}(s)$ is an infinite matrix such that

$$\begin{bmatrix} \vdots \\ \mathbf{y}_{-1}(s) \\ \mathbf{y}_0(s) \\ \mathbf{y}_1(s) \\ \vdots \end{bmatrix} = \begin{bmatrix} \ddots & & \vdots & & \ddots \\ & \mathbf{H}_{-1,-1}(s) & \mathbf{H}_{-1,0}(s) & \mathbf{H}_{-1,1}(s) & \cdots \\ \cdots & \mathbf{H}_{0,-1}(s) & \mathbf{H}_{0,0}(s) & \mathbf{H}_{0,1}(s) & \cdots \\ & \mathbf{H}_{1,-1}(s) & \mathbf{H}_{1,0}(s) & \mathbf{H}_{1,1}(s) & \cdots \\ \ddots & & \vdots & & \ddots \end{bmatrix} \begin{bmatrix} \vdots \\ \mathbf{u}_{-1}(s) \\ \mathbf{u}_0(s) \\ \mathbf{u}_1(s) \\ \vdots \end{bmatrix} \quad (3.86)$$

where $\mathbf{u}_k(s)$ and $\mathbf{y}_l(s)$, $(k, l) \in \mathbb{Z}^2$, are the Laplace-domain counterparts of Fourier coefficients $\mathbf{u}_k(t)$ and $\mathbf{y}_l(t)$, and where matrices $\mathbf{H}_{l,k}(s)$ are referred to as the *shift* transfer functions⁹. The frequency response $\mathbf{H}_{l,k}(j\omega_p)$ is thus the complex gain from a complex-exponential perturbation applied on $\mathbf{u}_k(t)$ at frequency ω_p to the perturbation measured on $\mathbf{y}_l(t)$ at that same frequency ω_p .

⁹ To be general, the set of shift transfer functions encompasses the set of no-shift transfer functions.

Equivalently, $\mathbf{H}_{l,k}(j\omega_p)$ is also the complex gain from a complex-exponential perturbation applied on the original signal $\mathbf{u}(t)$ at frequency $\omega_p + k\omega_1$ to the perturbation measured on the original signal $\mathbf{y}(t)$ at frequency $\omega_p + l\omega_1$.

The transfer functions $\mathbf{H}_{l,l}(s)$ on the main diagonal of the HTF are referred to as *no-shift* transfer functions, as they describe input-output dynamics that do not result in an apparent frequency shift. In particular, the centremost transfer function $\mathbf{H}_{0,0}(s)$ is the *no-shift* transfer function generally retrieved via the HL approach. The structure of the HTF is further described next by relying on the concept of impulse response.

3.4.2 The HTF from the impulse response

To introduce the concepts and notation, the calculation of the transfer function from the impulse response is first reviewed in the case of LTI systems, which helps to better grasp the case of LTP systems afterwards. For simplicity, the SISO case is considered, but the extension to MIMO systems is straightforward. For more information on the topics in this section, the reader is referred to [48].

Impulse response and transfer function of LTI systems

The impulse response $h(t, \tau)$ of a linear SISO dynamic system is its response at time t to a unit impulse applied at time τ . When the impulse response is known, the response $y(t)$ of the system to a more general input function $u(t)$ can be written as the convolution between the impulse response and the input of interest [39]:

$$y(t) = \int_{-\infty}^{+\infty} h(t, \tau)u(\tau)d\tau = \int_0^{+\infty} h(t, \tau)u(\tau)d\tau, \quad (3.87)$$

where the second equality reflects the fact that the input is considered to be zero for negative times. For LTI systems, the value of $h(t, \tau)$ depends only on the elapsed time since the impulse was applied, i.e. on $t - \tau$. For this reason, the impulse response of LTI systems can (with some overloading of notation) also be written as:

$$h(t, \tau) = h(t - \tau, 0) = h(t - \tau). \quad (3.88)$$

Additionally, it is recalled that the transfer function $H(s)$ of an LTI system is obtained as the (one-sided) Laplace transform of the impulse response $h(t)$ [39]:

$$H(s) = \int_0^{+\infty} e^{-st} h(t) dt. \quad (3.89)$$

The Laplace transform of the output $y(t)$ in (3.87) is then given by:

$$y(s) = \int_0^{+\infty} e^{-st} y(t) dt \quad (3.90a)$$

$$= \int_{t=0}^{+\infty} e^{-st} \int_{\tau=0}^{+\infty} h(t, \tau) u(\tau) d\tau dt \quad (3.90b)$$

$$= \int_{\tau=0}^{+\infty} \int_{t=\tau}^{+\infty} e^{-st} h(t - \tau) dt u(\tau) d\tau \quad (3.90c)$$

For causal systems, $h(t - \tau) = 0$ when $t < \tau$. Consequently,

$$y(s) = \int_{\tau=0}^{+\infty} \int_{t=\tau}^{+\infty} e^{-st} h(t - \tau) dt u(\tau) d\tau. \quad (3.91)$$

The following change of variables is applied:

$$r \triangleq t - \tau \implies dt = dr \quad (\text{for every given } \tau) \quad (3.92a)$$

$$t = \tau \implies r = 0 \quad (3.92b)$$

$$t = +\infty \implies r = +\infty, \quad (3.92c)$$

and leads to:

$$\int_{t=\tau}^{+\infty} e^{-st} h(t - \tau) dt = \int_{r=0}^{+\infty} e^{-sr} e^{-s\tau} h(r) dr \quad (3.93a)$$

$$= e^{-s\tau} \int_{r=0}^{+\infty} e^{-sr} h(r) dr \quad (3.93b)$$

$$= e^{-s\tau} H(s). \quad (3.93c)$$

The input-output relationship (3.91) becomes:

$$y(s) = \int_0^{+\infty} e^{-s\tau} H(s)u(\tau)d\tau = H(s) \int_0^{+\infty} e^{-s\tau} u(\tau)d\tau = H(s)u(s), \quad (3.94)$$

where $u(s)$ was recognised as the Laplace transform of $u(t)$. This procedure, which results in the traditional transfer function description of LTI systems in the frequency domain, is now transposed to LTP systems.

Impulse response and transfer function of LTP systems

For LTP systems, (3.87) still holds. However, the impulse response does not only depend on the elapsed time $r = t - \tau$, but also on the time at which the impulse is applied, i.e. on τ (or equivalently, on t for a given r). Additionally, the impulse response of LTP systems is periodic in both t and τ [48, Ch.4]:

$$h(t, \tau) = h(t + T_1, \tau + T_1), \quad (3.95)$$

with T_1 the fundamental period of the LTP system. Substituting $\tau = t - r$, the impulse response is periodic in t for a given r and can be written as a Fourier series whose Fourier coefficients only depend on the elapsed time $r = t - \tau$ [48, Ch.4]:

$$h(t, \tau) = h(t, t - r) = \sum_{k=-\infty}^{+\infty} h_k(r) e^{jk\omega_1 t}. \quad (3.96)$$

The Laplace transform of the output $y(t)$ is once more given by:

$$y(s) = \int_0^{+\infty} e^{-st} y(t) dt = \int_{t=0}^{+\infty} e^{-st} \int_{\tau=0}^{+\infty} h(t, \tau) u(\tau) d\tau dt. \quad (3.97)$$

Replacing the impulse response with (3.96) and rearranging gives:

$$y(s) = \int_{t=0}^{+\infty} e^{-st} \int_{\tau=0}^{+\infty} \sum_{k=-\infty}^{+\infty} h_k(t - \tau) e^{jk\omega_1 t} u(\tau) d\tau dt \quad (3.98a)$$

$$= \int_{\tau=0}^{+\infty} \int_{t=\tau}^{+\infty} e^{-st} \sum_{k=-\infty}^{+\infty} h_k(t - \tau) e^{jk\omega_1 t} dt u(\tau) d\tau. \quad (3.98b)$$

Using the change of variables $r = t - \tau$, we have:

$$\int_{t=\tau}^{+\infty} e^{-st} \sum_{k=-\infty}^{+\infty} h_k(t-\tau) e^{jk\omega_1 t} dt = \int_{r=0}^{+\infty} \sum_{k=-\infty}^{+\infty} h_k(r) e^{-(s-jk\omega_1)(r+\tau)} dr \quad (3.99a)$$

$$= \sum_{k=-\infty}^{+\infty} e^{-(s-jk\omega_1)\tau} \int_0^{+\infty} h_k(r) e^{-(s-jk\omega_1)r} dr \quad (3.99b)$$

$$= \sum_{k=-\infty}^{+\infty} e^{-(s-jk\omega_1)\tau} H_k(s - jk\omega_1), \quad (3.99c)$$

where the transfer functions $H_k(s)$ were identified as the Laplace transforms of the Fourier coefficients $h_k(r)$ of the impulse response, and where the frequency-shift property of the Laplace transform was used. Substituting the last result in (3.98b), $y(s)$ becomes:

$$y(s) = \int_0^{+\infty} \sum_{k=-\infty}^{+\infty} e^{-(s-jk\omega_1)\tau} H_k(s - jk\omega_1) u(\tau) d\tau \quad (3.100a)$$

$$= \sum_{k=-\infty}^{+\infty} H_k(s - jk\omega_1) \int_0^{+\infty} e^{-(s-jk\omega_1)\tau} u(\tau) d\tau \quad (3.100b)$$

$$= \sum_{k=-\infty}^{+\infty} H_k(s - jk\omega_1) u(s - jk\omega_1) \quad (3.100c)$$

where the shift property of the Laplace transform was used again. Eq. (3.100c) shows that, for LTP systems, the output spectrum $y(s)$ is equal to the superposition of duplicated and shifted versions of the input spectrum $u(s)$, each multiplied by a different transfer function $H_k(s)$. The result obtained for LTI systems can be retrieved as a particular case of the last equation in which the sum is reduced to a single term with $k = 0$.

At this point, it is convenient to write the relationship in matrix form. To do so, the output spectrum $y(s)$ is duplicated and shifted using $s \rightarrow s + jn\omega_1$, $n \in \mathbb{Z}$, which gives:

$$y(s + jn\omega_1) = \sum_{k=-\infty}^{+\infty} H_k(s + j(n-k)\omega_1) u(s + j(n-k)\omega_1), \quad \forall n \in \mathbb{Z}. \quad (3.101)$$

Further defining $m \triangleq n - k$, we obtain:

$$y(s + jn\omega_1) = \sum_{m=-\infty}^{+\infty} H_{n-m}(s + jm\omega_1)u(s + jm\omega_1), \quad \forall n \in \mathbb{Z}. \quad (3.102)$$

Eventually, the corresponding infinite-dimensional matrix formulation is:

$$\begin{bmatrix} \vdots \\ y(s - j\omega_1) \\ \vdots \\ y(s) \\ \vdots \\ y(s + j\omega_1) \\ \vdots \end{bmatrix} = \underbrace{\begin{bmatrix} \ddots & & & & & & \\ & H_0(s - j\omega_1) & H_{-1}(s) & H_{-2}(s + j\omega_1) & & & \\ & H_1(s - j\omega_1) & H_0(s) & H_{-1}(s + j\omega_1) & \cdots & & \\ & H_2(s - j\omega_1) & H_1(s) & H_0(s + j\omega_1) & & & \\ & & & \vdots & & & \\ & & & & \ddots & & \end{bmatrix}}_{\triangleq \mathcal{H}(s)} \begin{bmatrix} \vdots \\ u(s - j\omega_1) \\ \vdots \\ u(s) \\ \vdots \\ u(s + j\omega_1) \\ \vdots \end{bmatrix} \quad (3.103)$$

where the SISO notation has been adjusted to MIMO systems, and where $\mathcal{H}(s)$ is identified as the HTF of the initial LTP system.

So far, the HTF has been obtained from two independent approaches, first by application of the Laplace transform to the HSS model, and then by relying on the impulse response of LTP systems. The formulation derived from HSS, with its specific notation, is repeated here for convenience:

$$\begin{bmatrix} \vdots \\ y_{-1}(s) \\ y_0(s) \\ y_1(s) \\ \vdots \end{bmatrix} = \begin{bmatrix} \ddots & & & & & & \\ & H_{-1,-1}(s) & H_{-1,0}(s) & H_{-1,1}(s) & & & \\ & H_{0,-1}(s) & H_{0,0}(s) & H_{0,1}(s) & \cdots & & \\ & H_{1,-1}(s) & H_{1,0}(s) & H_{1,1}(s) & & & \\ & & & \vdots & & & \\ & & & & \ddots & & \end{bmatrix} \begin{bmatrix} \vdots \\ u_{-1}(s) \\ u_0(s) \\ u_1(s) \\ \vdots \end{bmatrix}. \quad (3.104)$$

Although not necessarily obvious¹⁰, the two HTFs are equivalent [18, 46, 48, 76].

¹⁰ Applying the Laplace transform to a Fourier series with time-dependent coefficients gives:

$$u(s) = \mathcal{L}\{u(t)\} = \int_0^{+\infty} e^{-st} \left(\sum_k u_k(t) e^{jk\omega_1 t} \right) dt \quad (3.105a)$$

$$= \sum_k \int_0^{+\infty} u_k(t) e^{-(s-jk\omega_1)t} dt = \sum_k u_k(s - jk\omega_1), \quad (3.105b)$$

which implies that the vectors mapped by (3.103) and those mapped by (3.104) are not equivalent. While the HTF in (3.104) maps complex amplitudes of input and output EMP signals, the HTF in (3.103) maps shifted spectra of input and output signals. Despite taking the form of mappings between *a priori* different quantities, it appears that both approaches are valid ways of obtaining the HTF [76]. Yet, further research might be necessary to help fully bridging the identified gap between the different derivations of the HTF.

As a consequence, (3.103) gives additional insights into the structure of (3.104). In particular, every descending block-diagonal of the HTF is actually composed of the same transfer function, but shifted along the imaginary axis by an integer multiple of the fundamental frequency.

It is noted that LTI systems, which do not feature frequency couplings, have a frequency-lifted HTF with only diagonal terms consisting of duplicated and shifted versions of the LTI transfer function $H_0(s)$:

$$\begin{bmatrix} \vdots \\ \mathbf{y}(s - j\omega_1) \\ \mathbf{y}(s) \\ \mathbf{y}(s + j\omega_1) \\ \vdots \end{bmatrix} = \begin{bmatrix} \ddots & & & & \\ & \mathbf{H}_0(s - j\omega_1) & & & \\ & & \mathbf{H}_0(s) & & \\ & & & \mathbf{H}_0(s + j\omega_1) & \\ & & & & \ddots \end{bmatrix} \begin{bmatrix} \vdots \\ \mathbf{u}(s - j\omega_1) \\ \mathbf{u}(s) \\ \mathbf{u}(s + j\omega_1) \\ \vdots \end{bmatrix} \quad (3.106)$$

Building upon the above developments, the derivation of the HTF of NTP_P systems with dynamics expressed as transfer functions is presented next.

3.4.3 The HTF as a generalisation of harmonic linearisation

In this subsection, the concepts of frequency-lifting in the Laplace domain and in the time domain are combined to show how the linearisation of nonlinear systems around a periodic trajectory can be made LTI when their dynamics are expressed by means of transfer functions. While the approach is different from that followed in the development of the HSS formulation in Section 3.2.2, the results are equivalent, except for the presence of pure time delays which are taken into account in this section in the form of complex exponential transfer functions. The main reason for including delays at this stage is the simple fact that it is possible and straightforward, as will be clear from the following paragraphs. It also serves the purpose of introducing the need for a discussion of delays not only in models based on transfer functions, but also in state-space models, which is done in detail in the next chapter.

The procedure developed in this section can be seen as a system-level reformulation of the HL method and is an original contribution of this thesis¹¹. It allows following the same principles while preventing tedious analytical manipulations at equation level.

¹¹ This section relies on published article [77], see also the List of Publications.

Initial nonlinear-TF model

Although applicable to elaborate systems such as the three-phase closed-loop MMC and MMC-based systems, the procedure is illustrated by means of the simplified single-phase MMC model presented in Section 1.2.5. It is written as:

$$\left. \begin{aligned} L_e \frac{di_s(t)}{dt} &= -R_e i_s(t) - v_g(t) - n_u(t) \frac{v_{Cu}(t)}{2} + n_l(t) \frac{v_{Cl}(t)}{2} \end{aligned} \right\} \quad (3.107a)$$

$$\left. \begin{aligned} L_a \frac{di_c(t)}{dt} &= -R_a i_c(t) + \frac{v_d(t)}{2} - n_u(t) \frac{v_{Cu}(t)}{2} - n_l(t) \frac{v_{Cl}(t)}{2} \end{aligned} \right\} \quad (3.107b)$$

$$\left. \begin{aligned} C_a \frac{dv_{Cu}(t)}{dt} &= n_u(t) \left(i_c(t) + \frac{i_s(t)}{2} \right) \end{aligned} \right\} \quad (3.107c)$$

$$\left. \begin{aligned} C_a \frac{dv_{Cl}(t)}{dt} &= n_l(t) \left(i_c(t) - \frac{i_s(t)}{2} \right) \end{aligned} \right\} \quad (3.107d)$$

$$\left. \begin{aligned} v_c^*(s) &= - \left(K_p^{CC} + \frac{K_r^{CC}s}{s^2 + (2\omega_1)^2} \right) (i_c^*(s) - i_c(s)) \end{aligned} \right\} \quad (3.107e)$$

$$\left. \begin{aligned} v_s^*(s) &= \left(K_p^{AC} + \frac{K_r^{AC}s}{s^2 + \omega_1^2} \right) (i_s^*(s) - i_s(s)) \end{aligned} \right\} \quad (3.107f)$$

$$\left. \begin{aligned} n_u(s) &= e^{-st_d} \frac{v_c^*(s) + v_d(s)/2 - v_s^*(s) - v_g(s)}{v_d(s)} \end{aligned} \right\} \quad (3.107g)$$

$$\left. \begin{aligned} n_l(s) &= e^{-st_d} \frac{v_c^*(s) + v_d(s)/2 + v_s^*(s) + v_g(s)}{v_d(s)} \end{aligned} \right\} \quad (3.107h)$$

where v_c^* and v_s^* have been temporarily redefined in such a way that the feedforward terms $v_d(s)/2$ and $v_g(s)$ do not appear in (3.107e) and (3.107f), but directly in the expressions of the insertion indices in (3.107g) and (3.107h). Additionally, pure time delays have now been included in these last equations in the form of e^{-st_d} . The system is rewritten concisely by defining the following transfer functions:

$$M_1(s) \triangleq (R_e + sL_e)^{-1} \quad M_5(s) \triangleq - \left(K_p^{CC} + \frac{K_r^{CC}s}{s^2 + (2\omega_1)^2} \right) \quad (3.108)$$

$$M_2(s) \triangleq (R_a + sL_a)^{-1} \quad M_6(s) \triangleq K_p^{AC} + \frac{K_r^{AC}s}{s^2 + \omega_1^2} \quad (3.109)$$

$$M_3(s) = M_4(s) \triangleq (sC_a)^{-1} \quad M_7(s) = M_8(s) \triangleq e^{-st_d} \quad (3.110)$$

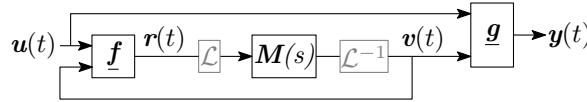


Figure 3.10: Nonlinear-TF model: block diagram with explicit direct and inverse Laplace transforms (\mathcal{L} , \mathcal{L}^{-1})

as well as matrix transfer function $\mathbf{M}(s)$ that gathers all SISO functions on its main diagonal:

$$\mathbf{M}(s) \triangleq \begin{bmatrix} M_1(s) & & & \\ & M_2(s) & & \\ & & \ddots & \\ & & & M_8(s) \end{bmatrix}. \quad (3.111)$$

Relying on this notation, the MMC model, and more generally NTP_p systems, can be represented by the following generic formulation referred to as the nonlinear-transfer function (TF) model, also displayed in Fig. 3.10:

$$\mathbf{v}(s) = \mathbf{M}(s)\mathbf{r}(s) \quad (3.112a)$$

$$\mathbf{r}(t) = \underline{\mathbf{f}}(t, \mathbf{v}(t), \mathbf{u}(t)) \quad (3.112b)$$

$$\mathbf{y}(t) = \underline{\mathbf{g}}(t, \mathbf{v}(t), \mathbf{u}(t)), \quad (3.112c)$$

where system dynamics are expressed by means of transfer functions in (3.112a) and algebraic relationships in (3.112b) and (3.112c). The direct and inverse Laplace transforms are shown in Fig. 3.10 but not in the equations. The particular structure of this model originates from the observation that the input vector \mathbf{r} of matrix $\mathbf{M}(s)$ can be expressed as functions of the system inputs \mathbf{u} and of the outputs \mathbf{v} of $\mathbf{M}(s)$. The system outputs \mathbf{y} can also be written as functions of the elements of \mathbf{u} and \mathbf{v} . Once more, the same letters are used for variables in time and Laplace domains. Lastly, the under-bar notation is used to emphasise the fact that functions $\underline{\mathbf{f}}$ and $\underline{\mathbf{g}}$ are different from other functions \mathbf{f} and \mathbf{g} used throughout the thesis.

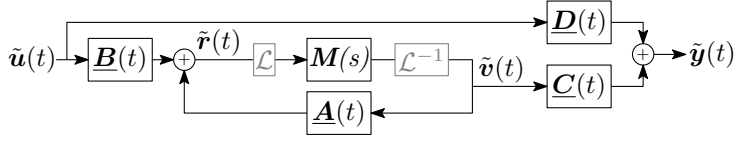


Figure 3.11: LTP-TF model: block diagram

For the example under consideration, vectors $\mathbf{r}(t)$, $\mathbf{v}(t)$ and $\mathbf{u}(t)$ are defined as:

$$\mathbf{r}(t) \triangleq \begin{bmatrix} -v_g - \frac{1}{2}n_u v_{Cu} + \frac{1}{2}n_l v_{Cl} \\ +\frac{1}{2}v_d - \frac{1}{2}n_u v_{Cu} - \frac{1}{2}n_l v_{Cl} \\ n_u (i_c + \frac{1}{2}i_s) \\ n_l (i_c - \frac{1}{2}i_s) \\ -i_c \\ -i_s \\ (v_c^* + v_d/2 - v_s^* - v_g) / v_d \\ (v_c^* + v_d/2 + v_s^* + v_g) / v_d \end{bmatrix}, \quad \mathbf{v}(t) \triangleq \begin{bmatrix} i_s \\ i_c \\ v_{Cu} \\ v_{Cl} \\ v_c^* \\ v_s^* \\ n_u \\ n_l \end{bmatrix}, \quad \mathbf{u}(t) \triangleq \begin{bmatrix} v_g \\ v_d \\ i_c^* \\ i_s^* \end{bmatrix}. \quad (3.113)$$

Linearisation of the nonlinear-TF model

While the set of transfer functions in $\mathbf{M}(s)$ relates to LTI system dynamics, functions \mathbf{f} and \mathbf{g} may be NTP. Linearisation around a periodic trajectory $\bar{\mathbf{p}}(t) = (\bar{\mathbf{u}}(t), \bar{\mathbf{v}}(t))$ results in an LTP system whose dynamics are expressed as transfer functions, therefore referred to as the LTP-TF representation:

$$\begin{cases} \tilde{\mathbf{v}}(s) = \mathbf{M}(s)\tilde{\mathbf{r}}(s) \\ \tilde{\mathbf{r}}(t) = \underline{\mathbf{A}}(t)\tilde{\mathbf{v}}(t) + \underline{\mathbf{B}}(t)\tilde{\mathbf{u}}(t) \\ \tilde{\mathbf{y}}(t) = \underline{\mathbf{C}}(t)\tilde{\mathbf{v}}(t) + \underline{\mathbf{D}}(t)\tilde{\mathbf{u}}(t) \end{cases} \quad (3.114)$$

with

$$\underline{\mathbf{A}}(t) \triangleq \frac{\partial \underline{\mathbf{f}}}{\partial \underline{\mathbf{v}}}(t, \bar{\mathbf{p}}(t)) \quad \underline{\mathbf{B}}(t) \triangleq \frac{\partial \underline{\mathbf{f}}}{\partial \underline{\mathbf{u}}}(t, \bar{\mathbf{p}}(t)) \quad (3.115a)$$

$$\underline{\mathbf{C}}(t) \triangleq \frac{\partial \underline{\mathbf{g}}}{\partial \underline{\mathbf{v}}}(t, \bar{\mathbf{p}}(t)) \quad \underline{\mathbf{D}}(t) \triangleq \frac{\partial \underline{\mathbf{g}}}{\partial \underline{\mathbf{u}}}(t, \bar{\mathbf{p}}(t)), \quad (3.115b)$$

and where the tilde notation refers to small deviations around the periodic trajectory. The linearised system is displayed in Fig. 3.11. In the following paragraph, the system is made time-invariant by eliminating the time-dependency of the periodic matrix coefficients.

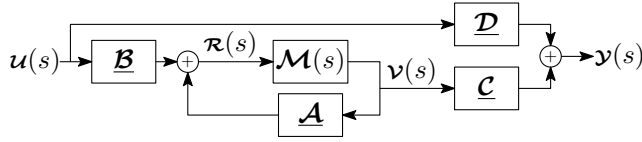


Figure 3.12: Frequency-lifted HTF representation

Transformation of LTP-TF into HTF formulation

Omitting the tilde notation for simplicity, frequency-lifting is applied to (3.114). The periodic matrices are replaced with the block-Toeplitz matrices made of their Fourier coefficients:

$$\underline{\mathcal{A}} \triangleq \mathcal{T}\{\underline{\mathcal{A}}_k : k \in \mathbb{Z}\} \quad \underline{\mathcal{B}} \triangleq \mathcal{T}\{\underline{\mathcal{B}}_k : k \in \mathbb{Z}\} \quad (3.116)$$

$$\underline{\mathcal{C}} \triangleq \mathcal{T}\{\underline{\mathcal{C}}_k : k \in \mathbb{Z}\} \quad \underline{\mathcal{D}} \triangleq \mathcal{T}\{\underline{\mathcal{D}}_k : k \in \mathbb{Z}\}. \quad (3.117)$$

Additionally, vectors \mathbf{u} , \mathbf{r} , \mathbf{v} and \mathbf{y} are replaced with their harmonic vectors: \mathbf{u} , \mathbf{r} , \mathbf{v} and \mathbf{y} . Lastly, the frequency-lifted version of the matrix transfer function $\mathbf{M}(s)$ is obtained according to (3.106), where the resulting block-diagonal matrix expresses the fact that the original LTI dynamics described by $\mathbf{M}(s)$ do not cause any frequency couplings:

$$\mathbf{M}(s) = \begin{bmatrix} \ddots & & & \\ & \mathbf{M}(s - j\omega_1) & & \\ & & \mathbf{M}(s) & \\ & & & \mathbf{M}(s + j\omega_1) \\ & & & \ddots \end{bmatrix}. \quad (3.118)$$

The frequency-lifted system is now LTI and the Laplace transform can be applied to the remaining time-domain signals, resulting in the following model, also displayed in Fig. 3.12:

$$\begin{cases} \mathbf{v}(s) = \mathbf{M}(s)\mathbf{r}(s) \\ \mathbf{r}(s) = \underline{\mathcal{A}}\mathbf{v}(s) + \underline{\mathcal{B}}\mathbf{u}(s) \\ \mathbf{y}(s) = \underline{\mathcal{C}}\mathbf{v}(s) + \underline{\mathcal{D}}\mathbf{u}(s). \end{cases} \quad (3.119)$$

The HTF representation $\mathcal{H}(s)$ of the whole system is obtained by eliminating intermediate variables $\mathbf{r}(s)$ and $\mathbf{v}(s)$:

$$\mathbf{y}(s) = \mathcal{H}(s)\mathbf{u}(s), \quad (3.120a)$$

$$\mathcal{H}(s) \triangleq \underline{\mathcal{C}}(\mathcal{I} - \mathbf{M}(s)\underline{\mathcal{A}})^{-1}\mathbf{M}(s)\underline{\mathcal{B}} + \underline{\mathcal{D}}. \quad (3.120b)$$

From (3.120b), it can be understood that, although matrix $\mathbf{M}(s)$ is block-diagonal, the resulting HTF $\mathbf{H}(s)$ presents off-diagonal blocks as a consequence of the fact that matrices $\underline{\mathbf{A}}$, $\underline{\mathbf{B}}$, $\underline{\mathbf{C}}$ and $\underline{\mathbf{D}}$ are not necessarily block-diagonal.

Truncation of HTF representations

Like the HSS model, the infinite-dimensional HTF matrix must be truncated for practical applications. Three aspects ought to be considered: the truncation of the Fourier series of periodic coefficients, the truncation of the infinite-dimensional matrices resulting from frequency-lifting, and the truncation of the resulting HTF matrix itself.

- The truncation of the Fourier series consists in identifying the periodic rank h_m of coefficients $\underline{\mathbf{A}}(t)$, $\underline{\mathbf{B}}(t)$, $\underline{\mathbf{C}}(t)$ and $\underline{\mathbf{D}}(t)$ in (3.114). The challenges are the same as those discussed for the HSS in Section 3.2 and are thus not repeated here.
- The truncation of the infinite-dimensional matrices resulting from frequency-lifting consists in selecting a truncation rank h_t for the system. In practical cases, the HTF can be obtained from either (3.78) or (3.120b). The former is chosen to support the discussion and is repeated here for convenience:

$$\mathbf{H}(s) = \mathbf{C}(s\mathcal{I} - \mathbf{A} + \mathbf{N})^{-1}\mathbf{B} + \mathbf{D}. \quad (3.121)$$

Disregarding \mathbf{D} for simplicity, the HTF can be calculated as the product of three matrices, specifically \mathbf{C} , $(s\mathcal{I} - \mathbf{A} + \mathbf{N})^{-1}$ and \mathbf{B} . Let us temporarily assume that these matrices have non-zero Fourier coefficients only up to h_m . Then, their product may lead to couplings up to $3h_m$. However, if the block-Toeplitz matrices are truncated to $h_t = h_m$, then their product allows for coefficients only up to $2h_m$. Consequently, it is expected that a truncation rank larger than h_m should be used in order to preserve all possible frequency couplings between the inputs and the outputs of the system.

The inverse matrix operation complicates the matter further. In particular, if \mathbf{A} contains non-zero Fourier coefficients up to h_m , then it is easily verified that matrix $(s\mathcal{I} - \mathbf{A} + \mathbf{N})^{-1}$ can display non-zero Fourier coefficients above h_m .

When the objective is the calculation of the no-shift transfer function $\mathbf{H}_0(s)$, which is the centremost transfer function in block-matrix $\mathbf{H}(s)$, the choice of a truncation rank can rely on the following reasoning. Considering again the product of matrices \mathbf{C} , $(s\mathcal{I} - \mathbf{A} + \mathbf{N})^{-1}$ and \mathbf{B} , a perturbation can only be shifted away from its original frequency by at most $h_m\omega_1$, for

it to be shifted back to its original frequency at the output¹². From this perspective, it is sufficient to use matrices truncated to $h_t = h_m$ for an accurate calculation of the no-shift transfer function $\mathbf{H}_0(s)$.

- Further truncating the resulting HTF matrix itself is an additional step without a counterpart in the HSS approach. Whether it is sound or not to focus only on function $\mathbf{H}_0(s)$ and eventually neglect all other *shift* transfer functions, as customarily done in HL, depends on the physics of the studied system. For LTP systems in general, all shift transfer functions are relevant in theory. For systems such as power-electronic converters, and the MMC in particular, it is generally verified that harmonic components become less and less significant at higher frequencies. Consequently, the largest frequency shifts, which are caused by multiplications of the input perturbation with harmonic components of the highest ranks, are also characterised by the smallest gains. This explains why transfer functions describing large input-output frequency shifts weigh less on the system dynamics than the ones describing small input-output frequency shifts.

The above argument is illustrated numerically in the following subsection. Convergence properties of the HTF are also discussed in [48, 76].

3.4.4 Numerical applications

In this subsection, the HTF approach is applied to the three-phase closed-loop MMC model.

Evaluation of shift transfer functions

Shift frequency responses of the MMC are obtained by first calculating the complete HTF $\mathcal{H}(s)$ with truncation and periodic ranks $h_t = h_m = 12$. Next, the shift transfer functions $\mathbf{H}_k(s)$, $k \in \mathbb{N}$, are retrieved. The corresponding frequency responses are obtained by evaluating the functions over a vector of frequency values.

For the MMC, two types of input-output relationships are calculated, namely the AC-side and DC-side admittances. At the AC side, the transfer functions are three-phase admittances, i.e. 3-by-3 MIMO transfer functions relating the alternating voltages $v_{g\phi}$ to the alternating currents $i_{s\phi}$, $\phi \in \{a, b, c\}$. The norms

¹²An abstraction of this problem, whose visualisation may be supported by Fig. 3.9b, can be stated as follows: the objective is that of starting from rank 0 and coming back to rank 0 in three steps. The first and last steps allow motion by at most $\pm h_m$ ranks at a time. The highest intermediate rank that can be reached under these constraints is h_m .

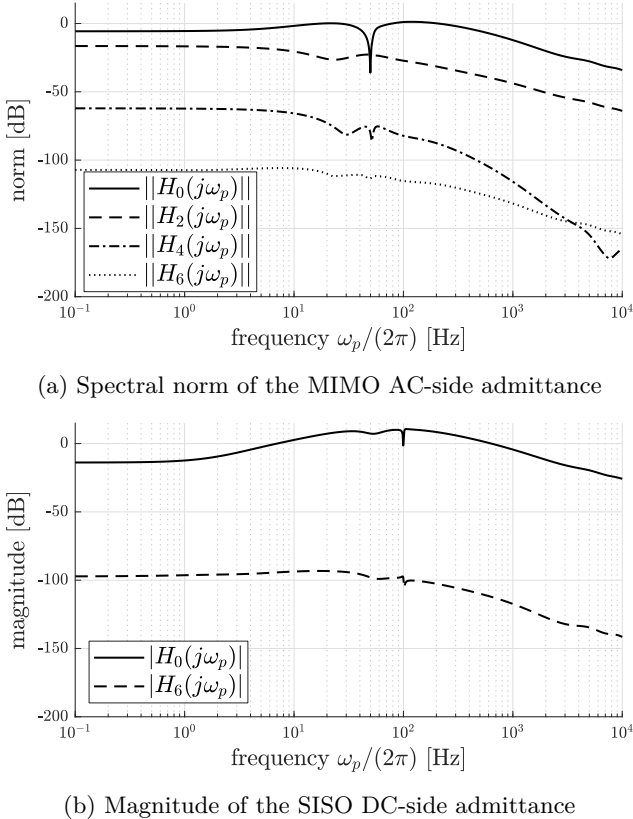


Figure 3.13: Complete MMC model: non-zero shift transfer functions corresponding to AC and DC admittances

(i.e. the maximum singular value) of the shift frequency responses are given in Fig. 3.13a. All responses from the no-shift response $\mathbf{H}_0(j\omega)$ to the +6-shift response $\mathbf{H}_6(j\omega)$ are considered. However, only those that are non-zero are displayed. It is observed that only even shifts are non-zero in this particular case, and that the amplitude of the shift frequency responses decreases significantly with increasing shifts.

At the DC side, the transfer functions are SISO admittances relating the direct voltage v_d to the direct current i_d . In this case, the magnitude of the frequency responses is provided in Fig. 3.13b. The observations made for the AC side hold for the DC side, aside from the fact that functions $\mathbf{H}_2(s)$ and $\mathbf{H}_4(s)$ are also null in this particular case. The latter observation suggests that the HL simplification is particularly justified for DC-side studies.

Comparison of HTF-based frequency response with frequency scans

Being the most significant component of its HTF, the no-shift frequency response of the MMC is considered further and compared in Fig. 3.14 with a frequency scan, i.e. HL based on numerical integration. Both the AC-side and DC-side admittances of the MMC are calculated with a delay value of 250 μs .

At the AC-side, the positive-sequence admittance¹³ is provided and is calculated from the three-phase abc -admittance according to [77]. The frequency scans are performed with small perturbations of 0.1% of rated voltage values. The numerical integration is carried out over 150 fundamental periods. The first 100 periods ensure that a steady-state is reached. The DFT is applied to the remaining 50 periods, which results in a frequency resolution of 1 Hz.

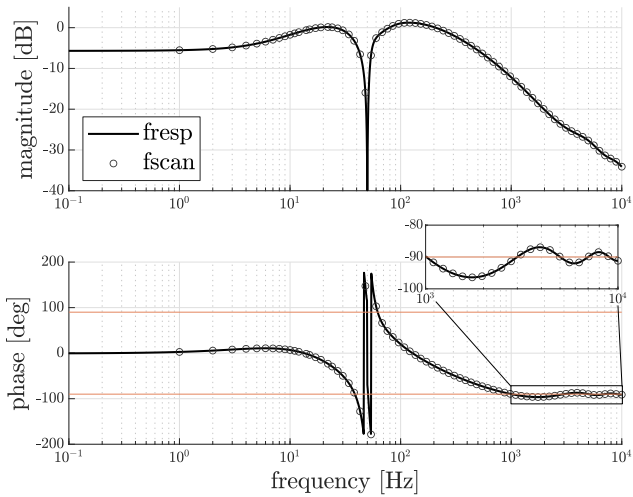
A visual inspection reveals a remarkable alignment between the HTF-based frequency responses and the integration-based frequency scans, which is expected since the results rely on the same models, simply solved with different methods. Discernible discrepancies, if any, can be attributed to the numerical accuracy of the solvers rather than inherent differences between the methods. The main difference between the two approaches is the computation time, which is typically significantly longer for the frequency scans. Exact calculation times depend, among others, on the size of the system, on the requested accuracies and resolutions in the frequency domain, on the solvers used, as well as on the available computational power.

The capability of the HTF approach to retrieve frequency responses with high accuracy over a large frequency range, but without relying on numerical integration, is a significant advantage of this method.

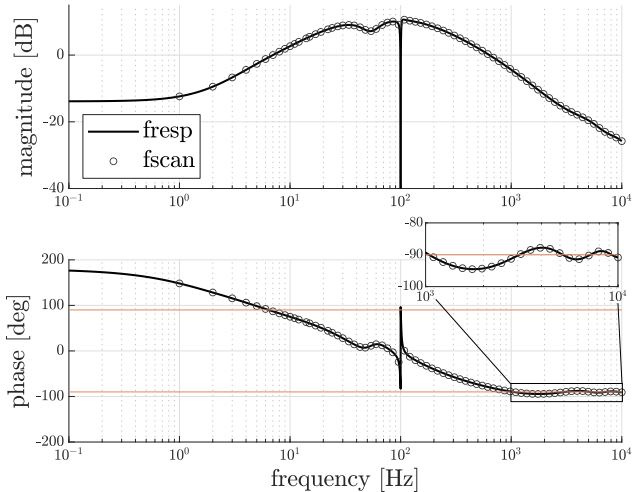
Impact of harmonic content on frequency response

The HTF allows studying the impact of oscillatory components in the periodic coefficients of LTP systems on their frequency responses. Both the AC-side and DC-side admittances of the MMC are again considered. To observe the impact of accounting for more or less harmonic components exclusively, and not the potential impact of truncation, the truncation rank h_t of the block-Toeplitz matrices is kept constant during the HTF calculations ($h_t = h_m = 6$). Only the forced periodic rank h_f is modified.

¹³ More precisely, the considered admittance is the positive-sequence to positive-sequence admittance, relating a positive-sequence disturbance on the alternating voltage $v_{g\phi}$ to a positive-sequence disturbance on the alternating current $i_{s\phi}$, $\phi \in \{a, b, c\}$, which is thus a SISO transfer function.



(a) AC-side positive-sequence admittance



(b) DC-side admittance

Figure 3.14: Validation of HTF-based frequency response (fresp) against numerical integration (fscan)

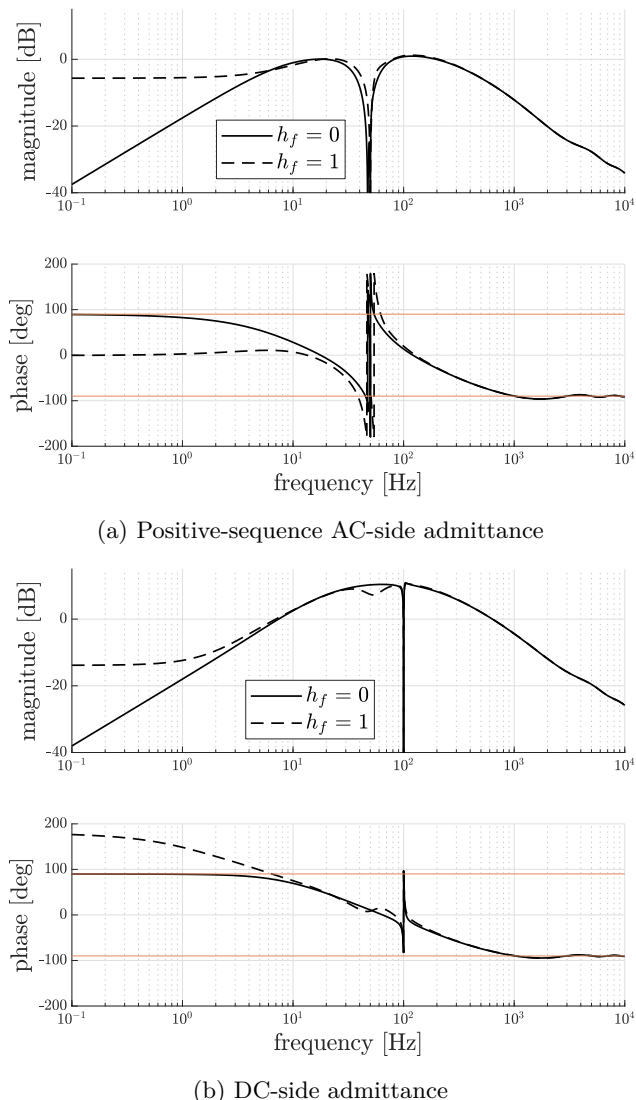


Figure 3.15: No-shift frequency response: impact of increasing the forced periodic rank from 0 to 1 ($h_t = h_m = 12$)

The results are provided in Fig. 3.15. In line with intuitive expectations, it is observed that accounting for the fundamental-frequency components greatly modifies the shape of the admittances, and confirms the importance of at least accounting for fundamental-frequency oscillatory components in small-signal models of the MMC. The impact of higher-order harmonic components is quantified in Fig. 3.16 in terms of the relative error $\epsilon(h_f)$ with respect to the most accurate curve available:

$$\epsilon(h_f) \triangleq \frac{|H_0[h_f] - H_0[h_m]|}{|H_0[h_m]|} \quad (3.122)$$

where $H_0[h]$ corresponds to $H_0(j\omega_p)$ calculated with a forced periodic rank equal to the argument h . For the particular case under consideration, the relative error decreases with every increment on the forced periodic rank h_f . It is emphasised that these numerical results are only valid for the specific case under study and no generic conclusions can be drawn.

3.4.5 Discussion and conclusion

This section was dedicated to presenting the HTF approach, which is the frequency-domain counterpart of the HSS approach and corresponds to a generalisation of the HL method. On the one hand, the HTF approach delivers not only the no-shift transfer function, which describes the transfer dynamics with same input and output frequencies, but also the shift transfer functions that result from frequency couplings. On the other hand, unlike the often laborious "manual" application of HL, the HTF approach benefits from the flexibility achieved by distinguishing the transformation framework from the particular model under consideration, which makes it the recommended approach when developing frequency-domain models of MMC-based systems.

The HTF being a frequency-lifted model, truncation is a necessary step to its utilisation and can be considered under three different aspects. First, the Fourier series representing the periodic state-space coefficients must be truncated in such a way that all relevant harmonic components are taken into account (Identification of the periodic rank). Next, the block-Toeplitz matrices resulting from frequency-lifting must be truncated in such a way that the relevant couplings between the selected harmonics are correctly depicted (Selection of a truncation rank). It is suggested that this requirement is fulfilled for the centremost no-shift transfer function if the truncation rank is at least equal to the periodic rank. Lastly, once the calculations have been carried out, the commonly adopted approach consists in further truncating the HTF matrix to only consider the no-shift transfer function in subsequent frequency-domain stability assessments. This simplification is supported by the observation

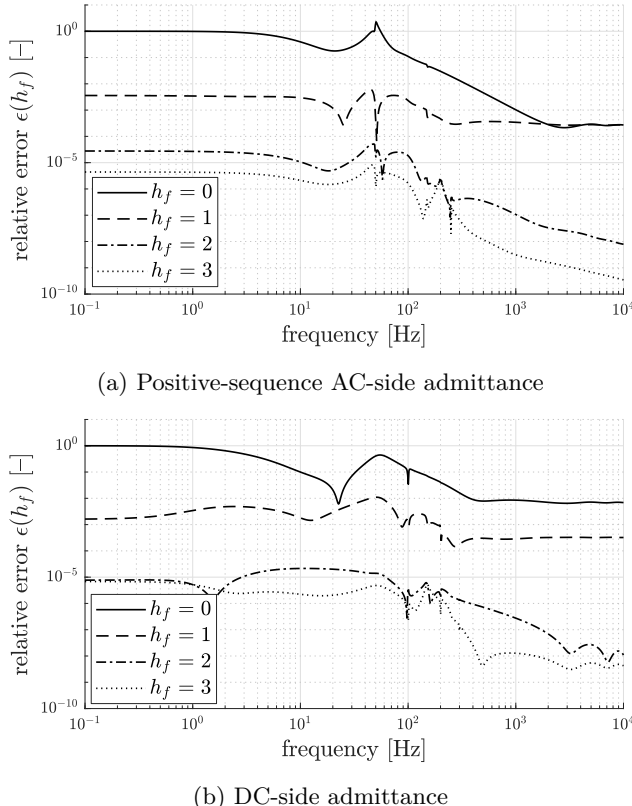


Figure 3.16: Relative error on the no-shift frequency response with increasing forced periodic rank ($h_t = h_m = 12$)

that, for the tested numerical cases, the no-shift transfer function is the most significant component of the HTF. Nevertheless, further research would be necessary to unveil conditions under which instability in MMC-based systems cannot be revealed unless a larger selection of the shift transfer functions is also included in the analysis.

3.5 Chapter conclusion

This chapter presented methods dedicated to the transformation of nonlinear systems following periodic trajectories into LTI systems that are suitable for small-signal stability assessments by means of traditional methods. The

| method | applicability | outcome | domain |
|------------------------|------------------|------------------|--|
| Floquet transformation | LTP | LTP ¹ | \mathbb{C}^n time |
| averaging ² | LTP | LTI | \mathbb{R}^n time |
| frame rotations | NTP ³ | LTI | \mathbb{R}^n time |
| harmonic balance | HL | LTI | \mathbb{C}^n frequency |
| | HSS | LTP | fr.-lifted LTI \mathbb{C}^∞ time |
| | HTF | LTP | fr.-lifted LTI \mathbb{C}^∞ frequency |
| | dynamic phasors | NTP ⁴ | fr.-lifted LTI \mathbb{C}^∞ time |

¹with a constant state matrix ²as described in Section 2.3

³satisfying Assumptions 7, 8, 10, and 11 ⁴satisfying Assumption 11

Table 3.1: Overview of transformation methods, considering that all initial systems have \mathbb{R}^n as state space

transformations rely on frequency-lifting, a technique that essentially consists in replacing variables with the set of their Fourier coefficients, which are constant in steady state.

Two main frequency-lifted methods were presented, specifically the HSS method, which results in a state-space representation in the time domain, and the HTF method, which results in a block-matrix of transfer functions in the frequency domain. The HSS and HTF are regarded as the most general formulations of frequency-lifting, which gives them the upper-hand in terms of flexibility of application. Both representations have infinite dimensions in theory and require truncation for numerical applications.

The HL approach, whose numerical application corresponds to the well-known frequency-scan method, was also presented. In its traditional application, HL delivers the no-shift transfer function, i.e. the centremost transfer function of the HTF representation, which is also the predominant component for the tested closed-loop MMC model. Being typically carried out at equation level, the HL procedure offers insights into the principles of frequency couplings, however it may quickly become intractable for elaborate systems. This is unlike the more systematic HTF approach introduced in this chapter for nonlinear systems with transfer functions, which benefits from a streamlined formalism comparable to that of HSS for time-domain models.

Summarised overview of transformation methods

All transformation methods discussed so far in Chapters 2 and 3 are displayed in Table 3.1, along with the types of systems to which they can be applied ("applicability"), the type of the resulting system and the state space on which

it relies ("outcome"). Lastly, the domain specifies whether the resulting system is a time-domain or a frequency-domain model.

The type of system to which a transformation method is applied is essentially determined by the order in which linearisation and transformation are used. When linearisation is considered in the first place, the transformation methods are necessarily applied to linearised systems, which are in this context also time-periodic. On the contrary, when transformation is considered first, the targeted sets of equations are generally nonlinear and possibly also time-periodic. This is the main difference between the dynamic-phasor approach, generally used to transform periodic trajectories of nonlinear systems, and the HSS approach, which addresses the periodic coefficients of a linearised set of equations. Bearing in mind the fact that transformations cannot easily address all types of nonlinear operations, starting with linearisation benefits from the advantage of generality.

Among the methods in Table 3.1, those relying on the harmonic balance principle, such as the HSS, HTF and the dynamic-phasor approach, typically result in frequency-lifted representations with infinite dimensions prior to truncation. The HL approach departs from this general rule as it does not result in a frequency-lifted model. A distinct advantage of techniques based on harmonic balance is their capability of covering a broad range of systems and operating conditions, including single-phase systems, unbalanced three-phase systems and systems subject to harmonically distorted excitation. Methods not involving frequency-lifting, such as the Floquet transformation, the averaging technique of Section 2.3 and frame rotations, do not normally increase the size of the system through the transformation process. While frame rotations may rely on additional virtual states to address the transformation of zero-sequence components, the corresponding increase in system size remains low.

A similarity between the Floquet transformation and frame rotations is that they both rely on a time-periodic change of variables to convert periodic quantities into constant quantities. Interestingly, the Floquet transformation is the only covered method that results in an LTP system, however with a constant state matrix. In practice, a limitation to the application of the Floquet transformation is that the suitable time-periodic transformation matrix is generally unknown *a priori*. On the contrary, frame rotations rely on common rotation matrices at predefined frequencies.

It is worthwhile noting that most transformation techniques resulting in time-domain models deliver in fact the same information about stability, albeit in different forms. The eigenvalues of the Floquet matrix, which results from the Floquet transformation, are (one set of) the Floquet exponents. Likewise, the eigensets of the state matrix of HSS models are the duplicated and shifted versions of the same Floquet exponents. Furthermore, dynamic phasors and

HSS result in equivalent sets of eigenvalues when applied to the same system satisfying Assumptions 7, 8, 10, and 11, and when the same truncation ranks are considered.

Lastly, among frequency-lifting techniques, an advantage of the HTF method over the HSS is its capability of seamlessly including exact delay representations in the form of complex exponential transfer functions. Consequently, the HTF is suitable for stability assessments of delayed systems by means of the Nyquist criterion. Yet, it is commonly accepted that such frequency-domain analyses lack the insights delivered by eigenvalue-based analyses, for instance the straightforward identification of the oscillation frequency of poorly-damped modes and their relation to specific states by means of participation factors. The original ODE-based HSS formulation presented in Section 3.2, however, does not currently support modal analysis when exact delays are taken into account. The following chapter addresses this limitation by generalising the HSS approach to also account for exact delays in modal analyses.

Chapter 4

Modal analysis of frequency-lifted delayed systems

4.1 Introduction

Chapter 3 was dedicated to the presentation of the frequency-lifting transformation method through the lens of two main approaches, namely the time-domain harmonic state space (HSS) and the frequency-domain harmonic transfer function (HTF). While the HSS is generally used for modal analysis based on eigenvalues calculations, the HTF lends itself to transfer-function-based stability assessments typically relying on Nyquist criterion.

The core idea of this chapter relies on the observation that, while exact delays are naturally included in the frequency domain and thus in HTF models, the original ordinary differential equation (ODE)-based HSS formulation does not currently support modal analysis when exact delays are taken into account. Consequently, this chapter builds upon the outcome of Objective 2 to address Objective 4. Precisely, the aim is to rely on frequency-lifting to analyse the small-signal stability of periodic trajectories followed by nonlinear delayed systems. Accounting for exact delays in HSS representations for the purpose of modal analysis is an original contribution of this thesis.

This chapter starts with a presentation of delay modelling for modal analysis in Section 4.2, showing the limitations of rational polynomial approximations

of exact delays and highlighting the challenges of modal analysis in delayed periodic systems. In Section 4.3, the fundamentals of delayed systems are reviewed, after what the original HSS formulation is generalised to account for exact delays in Section 4.4. The chapter ends with a numerical application in Section 4.5, providing a complete stability assessment of an MMC-based test system, relying on frequency-lifting in both time and frequency domains.

4.2 Delay modelling for modal analysis

The presence of time delays in the differential equations of the MMC implies that these equations are not ODEs but delay differential equations (DDEs). In state-space form, an unforced nonlinear time-invariant (NTI) delayed system can be expressed as:

$$\frac{d\mathbf{x}(t)}{dt} = \mathbf{f}(\mathbf{x}(t), \mathbf{x}(t - t_{d1}), \dots, \mathbf{x}(t - t_{dd})). \quad (4.1)$$

In such systems, the dynamics do not only depend on the value of \mathbf{x} at time t , but also on some past values $\mathbf{x}(t - t_{d1}), \dots, \mathbf{x}(t - t_{dd})$, where $0 < t_{d1} < \dots < t_{dd}$ are d discrete and constant delay values¹. After linearisation around an equilibrium point, the unforced system becomes [78, Ch.1]:

$$\frac{d\tilde{\mathbf{x}}(t)}{dt} = \mathbf{A}_{d0}\tilde{\mathbf{x}}(t) + \sum_{i=1}^d \mathbf{A}_{di}\tilde{\mathbf{x}}(t - t_{di}), \quad (4.2)$$

where the di subscripts refer to matrices related to specific delay values, and not to Fourier coefficients. It appears that the stability information of DDEs is not only contained in matrix \mathbf{A}_{d0} , as is the case with ODEs, but also in matrices \mathbf{A}_{di} , $\forall i = 1, \dots, d$. Consequently, calculating the eigenvalues of \mathbf{A}_{d0} is not sufficient to assess the stability of DDEs equilibria, and more elaborate methods must be used to calculate instead the characteristic roots² of the differential equations. Yet, to avoid using more-elaborate methods, it is common practice to approximate the DDEs by ODEs. First, the time-shift property of the Laplace transform allows expressing delays in the frequency domain with a complex exponential transfer function [39], as was already briefly introduced in

¹ The interest of accounting for more than one delay value lies in the capability of modelling power-electronic converters with scattered (i.e. not aggregated) delays, as well as systems comprising multiple converters with different aggregated delays, and combinations thereof.

² The notion of characteristic roots was shortly introduced in Section 1.3.2 for non-delayed systems, for which they are equivalent to the eigenvalues of the (unique) state matrix. The characteristic roots of delayed systems are still the roots of the characteristic polynomial but are not equal to the eigenvalues of any of the state matrices.

Section 3.4:

$$\mathcal{L}\{\boldsymbol{x}(t - \tau)\} = e^{-\tau s} \boldsymbol{x}(s). \quad (4.3)$$

In (4.3), the exponential transfer function can be approximated with a rational transfer function, for instance a Padé approximation [40, Ch.11]:

$$e^s \approx \frac{N_{pq}(s)}{D_{pq}(s)} \quad (4.4)$$

where $N_{pq}(s)$ and $D_{pq}(s)$ are polynomials of orders p and q respectively:

$$N_{pq}(s) = \sum_{k=0}^p \frac{(p+q-k)!}{(p+q)!} \frac{p!}{(p-k)!} \frac{s^k}{k!} \quad (4.5a)$$

$$D_{pq}(s) = \sum_{k=0}^q \frac{(p+q-k)!}{(p+q)!} \frac{q!}{(q-k)!} \frac{(-s)^k}{k!}. \quad (4.5b)$$

For simplicity, in this thesis, Padé approximations such that $p = q$ are considered. In this case, the order of the polynomials is referred to as the order of the approximation. This choice implies that the magnitude of the complex exponential is preserved, since the magnitude of the rational approximation is then equal to 1. The Padé approximation of the delay transfer function is obtained by evaluating the rational approximation at $-\tau s$. For instance, the third-order approximation is given by:

$$e^{-\tau s} \approx \frac{-(\tau s)^3 + 12(\tau s)^2 - 60\tau s + 120}{(\tau s)^3 + 12(\tau s)^2 + 60\tau s + 120}. \quad (4.6)$$

Once the rational transfer function is known, equivalent state-space realisations of the Padé approximation can be retrieved, thereby successfully replacing the original DDE by a set of first-order ODEs. In this thesis, modal canonical realisations are used as they benefit from better scaling properties than e.g. companion forms [79]. For instance, a state-space Padé approximation for the delay of the MMC's phase- a upper-arm insertion index can be written as:

$$n_{ua}(t) = n_{ua}^*(t - t_d) \quad (4.7a)$$

\implies

$$\begin{cases} \frac{d}{dt} \boldsymbol{\eta}_{\text{PAD}}(t) = \mathbf{A}_{\text{PAD}} \boldsymbol{\eta}_{\text{PAD}}(t) + \mathbf{B}_{\text{PAD}} n_{ua}^*(t) \end{cases} \quad (4.7b)$$

$$n_{ua}(t) = \mathbf{C}_{\text{PAD}} \boldsymbol{\eta}_{\text{PAD}}(t) + \mathbf{D}_{\text{PAD}} n_{ua}^*(t) \quad (4.7c)$$

with $\boldsymbol{\eta}_{\text{PAD}}$ a state vector of length equal to the order of the Padé approximation. For the third-order approximation with a delay of e.g. $250 \mu\text{s}$, modal canonical state-space matrices are given by:

$$\boldsymbol{A}_{\text{PAD}} = \begin{bmatrix} -1.471 & 1.404 & 0 \\ -1.404 & -1.471 & 0 \\ 0 & 0 & -1.858 \end{bmatrix} \cdot 10^4 \quad \boldsymbol{B}_{\text{PAD}} = \begin{bmatrix} 392.6 \\ 268.5 \\ 452.7 \end{bmatrix} \quad (4.8a)$$

$$\boldsymbol{C}_{\text{PAD}} = [-425.9 \quad 128.1 \quad 505.5] \quad \boldsymbol{D}_{\text{PAD}} = [-1]. \quad (4.8b)$$

Remarks

- The error of the approximation can be characterised by the phase angle difference between the exponential transfer function and the rational approximation, which is displayed in Fig. 4.1. Precisely, Figs. 4.1a and 4.1b show the approximation error for delays of $250 \mu\text{s}$ and $500 \mu\text{s}$ respectively. Several approximation orders are shown. It can be seen that the error is initially close to zero before increasing quickly above a threshold, referred here to as the *limit frequency*. The limit frequency can be identified more precisely by setting a limit on the acceptable approximation error. For instance, Figs. 4.2a and 4.2b display limit frequencies below which the error remains smaller than 1° and 5° respectively. The curves are given as a function of the delay value and for several approximation orders. For example, a 7th-order approximation guarantees errors smaller than 1° below 5 kHz if the delay is equal to $300 \mu\text{s}$. For each order, the space above the curve corresponds to frequency ranges where Padé approximations result in inaccurate delay models.

Hence, a Padé approximation is only valid at low frequencies [80], i.e. at frequencies below the limit frequency, which depends on the delay and on the order of the approximation.

- The poles of high-order Padé approximations are very sensitive to numerical errors in the coefficients [80], and it is recommended to avoid high-order Padé approximations for the calculation of characteristic roots. Reference [80] recommends avoiding Padé approximations of order larger than 10, even though numerical errors may already start to appear with such high orders. In the literature, the study of delays in power-electronic converters typically relies on approximations of orders 2 to 5, with a maximum order of 8 noted in [81]. Consequently, in this thesis, Padé approximations are considered up to the 9th order, which is a compromise fulfilling the intention of maximising Padé approximation accuracy at high frequencies (hence relying on a rather high approximation order) while preserving a sufficient numerical robustness of the results.

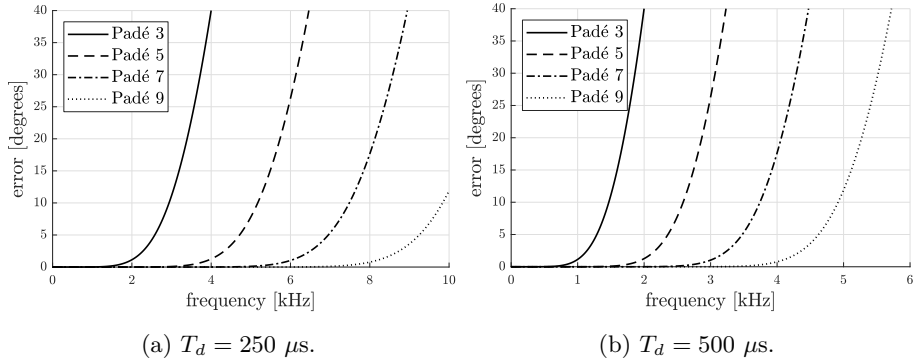


Figure 4.1: Padé approximation errors for different approximation orders

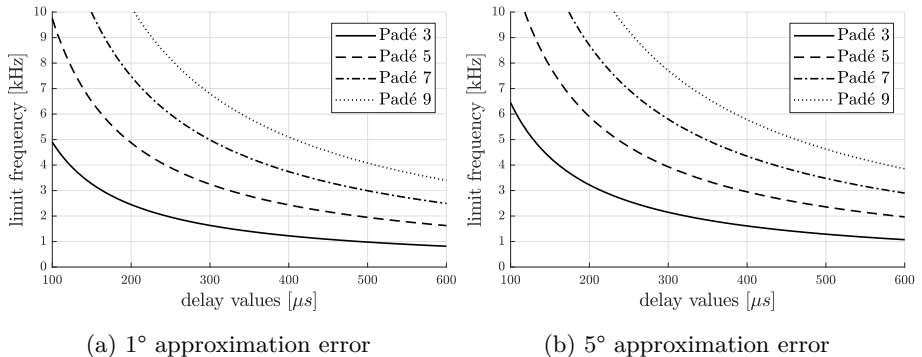


Figure 4.2: Limit frequencies for different approximation orders

It is worthwhile noting that a p -order approximation results in p additional states for every variable subjected to a delay. In the context of frequency-lifting, each state is represented by n_{h_t} Fourier coefficients. For a three-phase MMC with each of the six insertion indices subjected to a delay, using a 7th-order Padé approximation results in 294 additional states if frequency-lifting is used with a truncation order $h_t = 3$. Limiting the order of Padé approximations is thus not only a way of limiting the risk of numerical errors in eigenvalues calculations, but also a way of limiting the size of the eigenvalue system to solve [23], even more so with frequency-lifted systems.

To avoid the use of approximations, stability analyses can be carried out in the frequency domain, where exact delays can be included in the form of complex exponential transfer functions. However, frequency-domain stability assessments,

for instance by means of the Nyquist criterion, do not benefit from the insights delivered by modal analysis (e.g. identification of modal oscillation frequencies, participation factors, etc.). Additionally, the application of the Nyquist criterion relies on splitting the studied system into subsystems and requires preliminary knowledge of the number of unstable poles of these subsystems [44, 82]. This can be problematic when the subsystems have delays. Practically, this means that a complete stability analysis based on the Nyquist criterion may well require a repeated application of the criterion on subsystems of subsystems, which can be regarded as a limitation of frequency-domain studies in general and of the HTF approach in particular. Modal analyses of state-space models do not suffer from this limitation. This motivates the introduction of numerical methods capable of obtaining characteristic roots of DDEs with the aim of carrying out modal analyses, but without resorting to Padé approximations. In the context of nonlinear delayed systems following a periodic trajectory, an additional complexity arises when both periodic and delayed aspects are addressed simultaneously. To solve this problem, two possible approaches are identified:

Approach 1 A first approach relies on linearising the original nonlinear DDEs around a periodic trajectory to obtain LTP-DDEs. The delay is kept in its exact form during this procedure. Next, the focus is set on determining the monodromy operator of the LTP-DDEs. Intuitively, the monodromy operator is a generalisation of the monodromy matrix suitable to describe delayed periodic systems. Methods presented in e.g. [83, Ch.6] and [84] are capable of retrieving a discretisation of the monodromy operator, whose eigenvalues correspond to (a subset of) the characteristic roots of the LTP-DDEs.

Approach 2 A second approach relies on transforming the LTP-DDEs of Approach 1 into LTI-DDEs. Specifically, a transformation method is applied to make the periodic system time-invariant. The delay is also kept in its exact form during this procedure. Eventually, dedicated algorithms such as those presented in [85, 86] can be applied to the resulting LTI-DDEs to retrieve their characteristic roots.

An advantage of the second approach over the first is that the complete input-output system is made time-invariant in the process. Consequently, this approach not only enables the calculation of characteristic roots thanks to the state-space formalism, but also allows obtaining a transfer-function representation by application of the Laplace transform. For this reason, the second approach is presented in this section.

The main original contribution of this chapter is to describe the transformation of LTP-DDEs into LTI-DDEs by means of frequency-lifting. More precisely, a generalisation of the HSS formulation to delayed systems is proposed and

referred to as the delayed harmonic state space (DHSS) formulation. Before introducing the DHSS formulation, the fundamentals of delayed systems are presented in the following section, with the aim of showing how characteristic roots of LTI-DDEs can be calculated.

4.3 Fundamentals of delayed systems

The unforced LTI-DDE (4.2) is considered and is repeated here for convenience:

$$\frac{d\mathbf{x}(t)}{dt} = \mathbf{A}_{d0}\mathbf{x}(t) + \sum_{i=1}^d \mathbf{A}_{di}\mathbf{x}(t - t_{di}), \quad (4.9)$$

where the tilde notation has been dropped for simplicity. For more information on the topics in this section, the reader is referred to [78, Ch.1].

4.3.1 Characteristic roots of LTI-DDEs

Looking for solutions of (4.9) in the form of a complex exponential $\mathbf{x}(t) = \hat{\mathbf{x}}e^{st}$, the equation becomes:

$$s\hat{\mathbf{x}}e^{st} = \mathbf{A}_{d0}\hat{\mathbf{x}}e^{st} + \sum_{i=1}^d \mathbf{A}_{di}\hat{\mathbf{x}}e^{s(t-t_{di})} \quad (4.10a)$$

$$= \mathbf{A}_{d0}\hat{\mathbf{x}}e^{st} + \hat{\mathbf{x}}e^{st} \sum_{i=1}^d \mathbf{A}_{di}e^{-st_{di}}, \quad (4.10b)$$

$$\Rightarrow \left(s\mathbf{I} - \mathbf{A}_{d0} - \sum_{i=1}^d \mathbf{A}_{di}e^{-st_{di}} \right) \hat{\mathbf{x}}e^{st} = \mathbf{0} \quad (4.10c)$$

The quantity between parentheses is the characteristic matrix, noted \mathbf{M}_λ :

$$\mathbf{M}_\lambda \triangleq \lambda\mathbf{I} - \mathbf{A}_{d0} - \sum_{i=1}^d \mathbf{A}_{di}e^{-\lambda t_{di}}, \quad (4.11)$$

with the corresponding characteristic equation:

$$\det(\mathbf{M}_\lambda) = \det \left(\lambda\mathbf{I} - \mathbf{A}_{d0} - \sum_{i=1}^d \mathbf{A}_{di}e^{-\lambda t_{di}} \right) = 0, \quad (4.12)$$

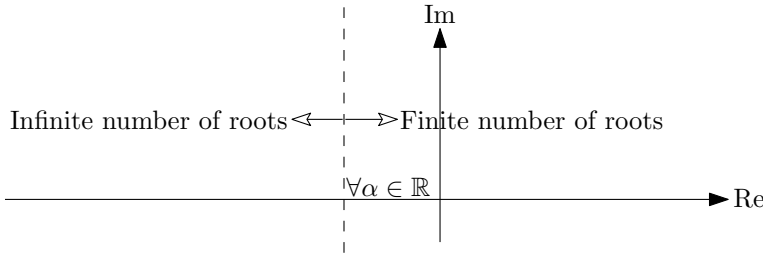


Figure 4.3: Delay differential equations: number of roots in the complex plane

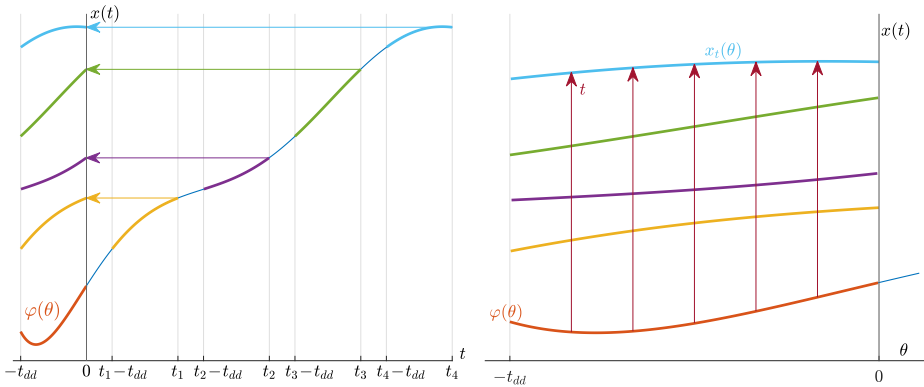
where $\det()$ gives the determinant of the matrix. The solutions of (4.12) are noted λ_j and are called the characteristic roots of the DDE. Their set is also referred to as its *spectrum*. Just as for LTI-ODEs, the equilibrium of the system is stable if all roots λ_j have a strictly negative real part, and is unstable if there exist a root λ_j such that $\text{Re}\{\lambda_j\} > 0$ [78, Ch.1-2].

In the case of n^{th} -order ODEs, the characteristic equation is a polynomial of degree n , in which case the fundamental theorem of algebra ensures the existence of exactly n roots in \mathbb{C} . On the contrary, the exponential term in (4.12) implies that the characteristic equation of DDEs has an infinite number of roots. The following property from [78, Ch.1] is helpful in that regard:

Property 1. *The number of DDE characteristic roots to the right of any vertical line in the complex plane, i.e. the number of roots λ_j such that $\text{Re}\{\lambda_j\} > \alpha$, $\alpha \in \mathbb{R}$, is finite.*

Property 1, which is illustrated in Fig. 4.3, ensures that calculating all roots with a real part larger than a given value is equivalent to calculating only a finite number of roots. The dominant roots would naturally be part of the calculated set and would thus be sufficient in assessing the stability of equilibria of delayed systems.

In practice, the spectrum is not generally found by directly solving the characteristic equation, but by determining a matrix whose eigenvalues correspond to (a finite subset of) the characteristic roots. Such matrix can be introduced from the concept of *infinitesimal generator*, which is presented in the following paragraphs. For simplicity, the notions are described for first-order systems, i.e. with scalar equations in \mathbb{C} . However, the generalisation to higher-order systems is straightforward.



(a) The DDE states can be visualised as pieces of functions defined over $[-t_{dd}, 0]$

(b) The abstract Cauchy problem describes the evolution of the DDE states

Figure 4.4: DDE states and abstract Cauchy problem: intuitive illustrations. Subfigure (b) corresponds to a zoomed version of subfigure (a) over $[-t_{dd}, 0]$.

4.3.2 States and state space of delay differential equations

As mentioned, at any time t , the future evolution of a delayed system depends not only on the current value of $x(t)$ but also on past values going as far back as $t - t_{dd}$. Consequently, while the state of a (first-order) ODE at time t is a point $x(t)$ in \mathbb{C} , the state of a (first-order) DDE at time t is the continuum of values taken by $x(t)$ from $t - t_{dd}$ to t . This continuum of values is called a *function segment*, and is noted

$$x_t(\theta) \triangleq x(t + \theta), \quad \text{with} \quad \theta \in [-t_{dd}, 0]. \quad (4.13)$$

It is emphasised that function segments are defined here on the interval $[-t_{dd}, 0]$, hence the particular notation $x_t(\theta)$. Mathematically,

$$x_t : \theta \in [-t_{dd}, 0] \mapsto x_t(\theta) \in \mathbb{C}. \quad (4.14)$$

Intuitively, function segment $x_t(\theta)$ can be seen as the state $x(t + \theta)$ at time t shifted over $[-t_{dd}, 0]$, as illustrated in Fig. 4.4a. Furthermore, for the problems considered in this thesis, the state space of a (first-order) DDE is the set X of continuous functions defined over $[-t_{dd}, 0]$ and taking values in \mathbb{C} . Mathematically,

$$X \triangleq C([-t_{dd}, 0]; \mathbb{C}). \quad (4.15)$$

The following subsections rely on the notion of function segments to provide general insights into the concept of infinitesimal generator and its discretisation,

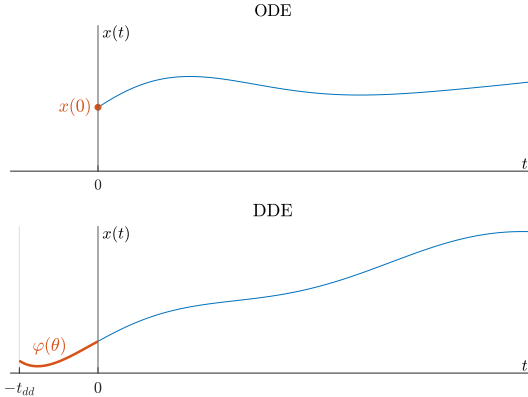


Figure 4.5: Notions of initial value (ODE) and initial function segment (DDE)

which allows calculating characteristic roots of delayed systems as the eigenvalues of the state matrix of a non-delayed system.

4.3.3 Infinitesimal generator

The following first-order Cauchy problem is considered:

$$\left\{ \begin{array}{l} \frac{dx(t)}{dt} = f(x(t), x(t - t_{d1}), \dots, x(t - t_{dd})) \\ x_{t=0}(\theta) = \varphi(\theta), \quad \theta \in [-t_{dd}, 0], \end{array} \right. \quad (4.16a)$$

$$(4.16b)$$

where (4.16a) describes how a point $x(t)$ evolves according to its current and past values. It is also noted that, while the initial value $x(0)$ of a first-order ODE is a point in \mathbb{C} , the initial value $x_{t=0}(\theta)$ in (4.16b) is an initial function segment $\varphi(\theta)$, as illustrated in Fig. 4.5.

Further relying on the concept of function segments, (4.16) can be represented by an equivalent Cauchy problem called *abstract* Cauchy problem [78, Ch.1]:

$$\left\{ \begin{array}{l} \frac{dx_t(\theta)}{dt} = F(x_t(\theta)) \\ x_{t=0}(\theta) = \varphi(\theta), \end{array} \right. \quad (4.17a)$$

$$(4.17b)$$

where (4.17a), unlike (4.16a), is not a DDE but an ODE: it describes how every state $x_t(\theta)$ evolves according to its *current value* only—which is a function segment.

In DDE (4.16a), function f maps points in \mathbb{C} onto points in \mathbb{C} . In ODE (4.17a), F maps function segments in X onto function segments in X , and is referred to as the *infinitesimal generator*. The way in which (4.17a) and the infinitesimal generator describe how the DDE states evolve in time is illustrated in Fig. 4.4b.

Mathematically, the *domain* of the infinitesimal generator F is expressed as:

$$\mathcal{D}(F) = \left\{ \phi \in X, \text{ i.e. } \phi : \theta \in [-t_{dd}, 0] \mapsto \phi(\theta) \in \mathbb{C}, \right. \quad (4.18a)$$

$$\text{such that } \frac{d\phi}{dt} \in X, \quad (4.18b)$$

$$\left. \text{and such that } \frac{d\phi}{d\theta}(0) = f(\phi(0), \phi(-t_{d1}), \dots, \phi(-t_{dd})) \right\}. \quad (4.18c)$$

In other words, the domain of F is the set of function segments whose time derivatives are also function segments, and whose time derivative at the right-end point of $[-t_{dd}, 0]$ (i.e. at $\theta = 0$) is related to past values within $[-t_{dd}, 0]$ as described by f in (4.16a). It is helpful to observe that, while (4.18a) and (4.18b) deal with function segments, (4.18c) deals with points in \mathbb{C} .

The *action* of the infinitesimal generator is expressed as:

$$F(\phi) = \frac{d\phi}{d\theta}. \quad (4.19)$$

By formulating the system dynamics in terms of function segments instead of points, the abstract Cauchy problem does not rely on the notion of *past values*, hence does not involve delays and corresponds to a formulation close to that of classical ODEs. One way of finding the characteristic roots of the original DDE is: (i) to find a matrix approximation of the infinitesimal generator F , and (ii) to calculate the eigenvalues of that matrix. The general idea behind finding a matrix approximation of the infinitesimal generator is presented next.

4.3.4 Matrix approximation of the infinitesimal generator

A matrix approximation of the infinitesimal generator is presented for the linearised form of (4.16):

$$\left\{ \begin{aligned} \frac{dx(t)}{dt} &= A_{d0}x(t) + \sum_{i=1}^d A_{di}x(t - t_{di}) \\ x_{t=0}(\theta) &= \varphi(\theta), \end{aligned} \right. \quad (4.20a)$$

$$(4.20b)$$

Relying on [78, Ch.2], the interval $[-t_{dd}, 0]$ can be discretised into a finite amount of $N + 1$ points $\{\theta_r\}$, $r = 0, \dots, N$, with for instance $\theta_0 = 0$ and $\theta_N = -t_{dd}$. We assume that the values of $x_t(\theta)$ at those points can be interpolated by a known function, e.g. a polynomial p_N of degree N :

$$x_t(\theta) \approx p_N(\theta) = \sum_{r=0}^N l_r(\theta) x_t(\theta_r) \quad (4.21)$$

where $l_r(\theta)$ are known Lagrange basis functions (see e.g. [87, Ch.3] for their expressions and underlying theory) and $x_t(\theta_r)$ are unknown coefficients, except at $t = 0$, where $x_{t=0}(\theta) = \varphi(\theta)$ is given. The derivative of the polynomial interpolation along θ is expressed as:

$$\frac{dp_N(\theta)}{d\theta} = \sum_{r=0}^N l'_r(\theta) x_t(\theta_r) \quad (4.22)$$

with $l'_r(\theta)$ the derivative of $l_r(\theta)$ with respect to θ . At position $\theta_k \in \{\theta_r\}$, the variation of $x_t(\theta) = x(t + \theta)$ along t is equal to its variation along θ (which is also implied by the combination of (4.17a) and (4.19)), hence:

$$\frac{dx_t(\theta_k)}{dt} = \frac{dx_t(\theta_k)}{d\theta}, \quad \forall k = 0, \dots, N. \quad (4.23)$$

Consequently,

$$F(x_t(\theta_k)) = \frac{dx_t(\theta_k)}{dt} = \frac{dx_t(\theta_k)}{d\theta} \quad (4.24a)$$

$$\approx \frac{dp_N(\theta_k)}{d\theta} = \sum_{r=0}^N l'_r(\theta_k) x_t(\theta_r), \quad \forall k = 0, \dots, N. \quad (4.24b)$$

For the particular value $k = 0$, also recalling that $\theta_0 = 0$, we have:

$$F(x_t(\theta_0)) = \frac{dx_t(\theta_0)}{dt} = \frac{dx(t)}{dt} \quad (4.25a)$$

$$= A_{d0}x(t) + \sum_{i=1}^d A_{di}x(t - t_{di}). \quad (4.25b)$$

Relying on (4.21), $x(t) = x_t(0) \approx p_N(0)$ and $x(t - t_{di}) = x_t(-t_{di}) \approx p_N(-t_{di})$. Consequently,

$$F(x_t(\theta_0)) \approx A_{d0} \sum_{r=0}^N l_r(0)x_t(\theta_r) + \sum_{i=1}^d A_{di} \sum_{r=0}^N l_r(-t_{di})x_t(\theta_r) \quad (4.26a)$$

$$\approx \sum_{r=0}^N \underbrace{\left(A_{d0}l_r(0) + \sum_{i=1}^d A_{di}l_r(-t_{di}) \right)}_{\triangleq L_r} x_t(\theta_r). \quad (4.26b)$$

In summary, (4.26b) provides a relationship for $k = 0$, and (4.24b) provides N more relationships for $k = 1, \dots, N$. Their combination gives:

$$\begin{cases} F(x_t(\theta_0)) \approx \sum_{r=0}^N L_r x_t(\theta_r) \\ F(x_t(\theta_k)) \approx \sum_{r=0}^N l'_r(\theta_k) x_t(\theta_r), \quad k = 1, \dots, N. \end{cases} \quad (4.27)$$

The above relationships describe the behaviour of the infinitesimal generator over the discretised interval, and (4.17a) can be approximated by:

$$\frac{d\mathbf{x}_N}{dt} \approx \mathbf{A}_N \mathbf{x}_N, \quad (4.28)$$

with

$$\mathbf{A}_N \triangleq \begin{bmatrix} L_0 & L_1 & \cdots & L_N \\ l'_0(\theta_1) & l'_1(\theta_1) & \cdots & l'_N(\theta_1) \\ \vdots & \vdots & \ddots & \vdots \\ l'_0(\theta_N) & l'_1(\theta_N) & \cdots & l'_N(\theta_N) \end{bmatrix}, \quad \mathbf{x}_N \triangleq \begin{bmatrix} x_t(\theta_0) \\ x_t(\theta_1) \\ \vdots \\ x_t(\theta_N) \end{bmatrix}. \quad (4.29)$$

The approximated eigenvalue problem becomes:

$$\mathbf{A}_N \mathbf{x}_N = \lambda \mathbf{x}_N, \quad (4.30)$$

the solutions of which are estimations of the characteristic roots of the original LTI-DDE in (4.20).

Over the last few decades, research on delayed systems theory has enabled the development of new algorithms and computer toolboxes which largely automate the process of discretising the infinitesimal generator and calculating

its eigenvalues. Available methods vary with the type of discretisation (number and location of discretisation points), the type of interpolating functions, the type of algorithm used to obtain the eigenvalues of \mathbf{A}_N , etc. In [86], a method is proposed to automate the choice of the number of discretisation points. Additionally, the eigenvalues obtained from \mathbf{A}_N are used as starting points to solve the nonlinear characteristic equation (4.12) via a Newton-based root finding algorithm (RFA). In [85], the approach distinguishes itself by the way in which the eigenvalues of \mathbf{A}_N are obtained, specifically by means of a procedure called the *delay Arnoldi algorithm*. The latter method is employed to extract characteristic roots of delayed systems in the numerical applications covered in this chapter (see Section 4.5).

Despite the fact that the eigenvalues resulting from the application of the delay Arnoldi algorithm are still estimations of (a finite subset of) the true DDE characteristic roots, the advantage of such an elaborate method is its ability to deliver results that are more accurate than those of Padé approximations, in particular above their limit frequency. In the case of the delay Arnoldi algorithm, a series of iterations is executed, where each iteration results in an additional eigenvalue being calculated. In this process, the eigenvalues of small modulus converge first. Retrieving a sufficiently large number N_{tot} of characteristic roots can ensure convergence of eigenvalues up to an arbitrarily large modulus. A convergence test is presented in Section 4.3.6.

4.3.5 Scaling and shifting the eigenvalue problem

This subsection and the next cover a number of practical points related to the use of the delay Arnoldi algorithm³. The delay Arnoldi algorithm requires that matrix $\mathbf{A}_{d0} + \mathbf{A}_{d1} + \dots + \mathbf{A}_{dd}$ be invertible, i.e. that it does not have an eigenvalue at 0. When this requirement is not satisfied, the system can be shifted by a quantity $\rho \in \mathbb{R}$, using the following change of variables:

$$\mu = \lambda + \rho. \quad (4.31)$$

In this case, the characteristic matrix \mathbf{M}_λ in (4.11) becomes:

$$\mathbf{M}_\mu = \mu \mathbf{I} - (\mathbf{A}_{d0} + \rho \mathbf{I}) - \sum_{i=1}^d \mathbf{A}_{di} e^{\rho t_{di}} e^{-\mu t_{di}}. \quad (4.32)$$

³ The content of this subsection and the next relies exclusively on the help provided by Prof. Wim Michiels and his team at the NUMA research group within the Department of Computer Science, KU Leuven, whom the author thanks warmly.

To enhance numerical properties, it is also recommended to scale the system such that the largest delay becomes equal to 1, using a second change of variables:

$$\nu = \mu t_{dd}, \quad (4.33)$$

with t_{dd} the largest delay of the original unscaled system. The characteristic matrix \mathbf{M}_μ becomes:

$$\mathbf{M}_\nu = \nu \mathbf{I} - \underbrace{(\mathbf{A}_{d0} + \rho \mathbf{I})t_{dd}}_{\triangleq \mathbf{A}'_{d0}} - \sum_{i=1}^d \underbrace{\mathbf{A}_{di} e^{\rho t_{di}} t_{dd}}_{\triangleq \mathbf{A}'_{di}} e^{-\mu t_{di}/t_{dd}}, \quad (4.34)$$

where the defined \mathbf{A}'_{di} , $i = 0, \dots, d$, are the scaled and shifted state matrices, with corresponding scaled delays $t'_{di} = t_{di}/t_{dd}$, $i = 1, \dots, d$. After solving for the scaled and shifted characteristic roots ν_j , the original characteristic roots λ_j are obtained as:

$$\lambda_j = \frac{\nu_j}{t_{dd}} - \rho, \quad \forall j = 1, \dots, N_{tot} \quad (4.35)$$

with N_{tot} the number of calculated characteristic roots.

4.3.6 Eigenvectors calculation and eigenvalue convergence test

One way of obtaining the eigenvectors related to the calculated characteristic roots consists in considering the characteristic matrix evaluated at solution λ_j , i.e. \mathbf{M}_{λ_j} :

$$\mathbf{M}_{\lambda_j} = \lambda_j \mathbf{I} - \mathbf{A}_{d0} - \sum_{i=1}^d \mathbf{A}_{di} e^{-\lambda_j t_{di}}, \quad \forall j = 1, \dots, N_{tot}. \quad (4.36)$$

The singular vector corresponding to the smallest singular value σ_n of \mathbf{M}_{λ_j} is the eigenvector corresponding to characteristic root λ_j .

The singular value decomposition of \mathbf{M}_{λ_j} also provides a way of assessing the convergence of the calculated characteristic roots. Specifically, it is considered that λ_j has converged within a radius of arbitrary magnitude $\epsilon \in \mathbb{R}$ if the ratio between the smallest and largest singular values of \mathbf{M}_{λ_j} is smaller than ϵ :

$$\frac{\sigma_n(\mathbf{M}_{\lambda_j})}{\sigma_1(\mathbf{M}_{\lambda_j})} < \epsilon \implies \lambda_j \text{ has converged.} \quad (4.37)$$

4.4 Generalised HSS framework for delayed systems

Having described the way in which characteristic roots of LTI-DDEs can be obtained, this section⁴ extends the application of frequency-lifting to LTP-DDEs by generalising the original ODE-based HSS formulation of [18]. The starting point is a generic state-space representation of NTP-DDEs, written as [88]:

$$\dot{\mathbf{x}}(t) = \mathbf{f}(t, \mathbf{x}(t), \mathbf{u}(t), \mathbf{w}(t)) \quad (4.38a)$$

$$\mathbf{y}(t) = \mathbf{g}(t, \mathbf{x}(t), \mathbf{u}(t), \mathbf{w}(t)) \quad (4.38b)$$

$$\mathbf{z}(t) = \mathbf{h}(t, \mathbf{x}(t), \mathbf{u}(t), \mathbf{w}(t)) \quad (4.38c)$$

$$\mathbf{w}(t) = \mathbf{z}(t, \mathbf{t}_d) \quad (4.38d)$$

with \mathbf{x} , \mathbf{u} and \mathbf{y} the state, input and output variables respectively. Additionally, (4.38d) is introduced to express the relationship between intermediate variables \mathbf{z} and delayed variables \mathbf{w} , and function \mathbf{h} in (4.38c) expresses the intermediate variables \mathbf{z} in terms of all other variables. In (4.38d), we consider a vector of d discrete and constant delay values:

$$\mathbf{t}_d \triangleq \begin{bmatrix} t_{d1} \\ \vdots \\ t_{dd} \end{bmatrix}. \quad (4.39)$$

Lastly, vector $\mathbf{z}(t)$ has length d and, with a slight overloading of notation, the element-wise delay of $\mathbf{z}(t)$ by the values in \mathbf{t}_d is expressed as:

$$\mathbf{z}(t, \mathbf{t}_d) \triangleq \begin{bmatrix} z^{(1)}(t - t_{d1}) \\ \vdots \\ z^{(d)}(t - t_{dd}) \end{bmatrix}. \quad (4.40)$$

Relying on this notation, we also have:

$$\mathbf{z}(t, \mathbf{0}) = \mathbf{z}(t), \quad (4.41)$$

with $\mathbf{0}$ the zero vector of length d .

In the next paragraphs, system (4.38) is first linearised around a periodic trajectory. Next, the resulting LTP-DDE system is transformed into an LTI-DDE by means of frequency-lifting.

⁴ This section is based on the published article [77], see also the List of Publications.

4.4.1 Linearisation of NTP-DDE into LTP-DDE formulation

The NTP-DDE state-space representation (4.38) is linearised around a periodic trajectory $\bar{\mathbf{p}}(t)$, which results in an LTP-DDE state-space formulation:

$$\dot{\tilde{\mathbf{x}}}(t) = \mathbf{A}(t)\tilde{\mathbf{x}}(t) + \mathbf{B}^{(1)}(t)\tilde{\mathbf{u}}(t) + \mathbf{B}^{(2)}(t)\tilde{\mathbf{w}}(t) \quad (4.42a)$$

$$\begin{cases} \tilde{\mathbf{y}}(t) = \mathbf{C}^{(1)}(t)\tilde{\mathbf{x}}(t) + \mathbf{D}^{(11)}(t)\tilde{\mathbf{u}}(t) + \mathbf{D}^{(12)}(t)\tilde{\mathbf{w}}(t) \\ \tilde{\mathbf{z}}(t) = \mathbf{C}^{(2)}(t)\tilde{\mathbf{x}}(t) + \mathbf{D}^{(21)}(t)\tilde{\mathbf{u}}(t) + \mathbf{D}^{(22)}(t)\tilde{\mathbf{w}}(t) \end{cases} \quad (4.42b)$$

$$\tilde{\mathbf{w}}(t) = \tilde{\mathbf{z}}(t, \mathbf{t}_d) \quad (4.42c)$$

$$\tilde{\mathbf{w}}(t) = \tilde{\mathbf{z}}(t, \mathbf{t}_d) \quad (4.42d)$$

with the periodic matrix coefficients given by:

$$\begin{bmatrix} \mathbf{A}(t) & \mathbf{B}^{(1)}(t) & \mathbf{B}^{(2)}(t) \\ \mathbf{C}^{(1)}(t) & \mathbf{D}^{(11)}(t) & \mathbf{D}^{(12)}(t) \\ \mathbf{C}^{(2)}(t) & \mathbf{D}^{(21)}(t) & \mathbf{D}^{(22)}(t) \end{bmatrix} = \frac{\partial(\mathbf{f}, \mathbf{g}, \mathbf{h})}{\partial(\mathbf{x}, \mathbf{u}, \mathbf{w})} \Big|_{(t, \bar{\mathbf{p}}(t))}. \quad (4.43)$$

Before applying frequency-lifting to (4.42), the description of the time delay of a signal by means of harmonic vectors is presented first. In the next paragraphs, the tilde notation is dropped to keep the notation simple.

4.4.2 Time delay of a signal in the frequency-lifted framework

The time delay of element $z^{(i)}(t)$ by t_{di} in (4.42d) can be written as its Fourier series:

$$z^{(i)}(t - t_{di}) = \sum_{k=-\infty}^{+\infty} z_k^{(i)}(t - t_{di}) e^{jk\omega_1(t - t_{di})} \quad (4.44a)$$

$$= \sum_{k=-\infty}^{+\infty} \left(e^{-jk\omega_1 t_{di}} z_k^{(i)}(t - t_{di}) \right) e^{jk\omega_1 t}, \quad (4.44b)$$

where it is recalled that deviation variables are not necessarily periodic, hence the fact that the Fourier coefficients may be time-dependent. Similarly, the delay of vector $\mathbf{z}(t)$ by the values in \mathbf{t}_d is given by:

$$\mathbf{z}(t, \mathbf{t}_d) = \sum_{k=-\infty}^{+\infty} \left(e^{-jk\omega_1 \mathbf{T}_d} \mathbf{z}_k(t, \mathbf{t}_d) \right) e^{jk\omega_1 t}, \quad (4.45)$$

where $\mathbf{T}_d \triangleq \text{diag}\{\mathbf{t}_d\}$. Consequently, the harmonic vector of $\mathbf{z}(t, \mathbf{t}_d)$ is obtained as:

$$\mathcal{K}\{\mathbf{z}(t, \mathbf{t}_d)\} = \underbrace{\begin{bmatrix} \ddots & & & \\ & e^{j\omega_1 \mathbf{T}_d} & & \\ & & e^0 & \\ & & & e^{-j\omega_1 \mathbf{T}_d} & \\ & & & & \ddots & \end{bmatrix}}_{\triangleq \mathcal{E}_{T_d}} \underbrace{\begin{bmatrix} \vdots \\ \mathbf{z}_{-1}(t, \mathbf{t}_d) \\ \mathbf{z}_0(t, \mathbf{t}_d) \\ \mathbf{z}_1(t, \mathbf{t}_d) \\ \vdots \end{bmatrix}}_{\triangleq \mathbf{z}(t, \mathbf{t}_d)}. \quad (4.46)$$

Eventually, the harmonic vector of $\mathbf{z}(t, \mathbf{t}_d)$ can be written as:

$$\mathcal{K}\{\mathbf{z}(t, \mathbf{t}_d)\} = \mathcal{E}_{T_d} \mathbf{z}(t, \mathbf{t}_d). \quad (4.47)$$

4.4.3 Transformation of LTP-DDE into DHSS formulation

Frequency-lifting is applied to (4.42a)-(4.42c) according to the ODE-based HSS method presented in Section 3.2. Vectors $\mathbf{x}(t)$, $\mathbf{u}(t)$, $\mathbf{y}(t)$, $\mathbf{w}(t)$ and $\mathbf{z}(t)$ are the harmonic vectors related to $\mathbf{x}(t)$, $\mathbf{u}(t)$, $\mathbf{y}(t)$, $\mathbf{w}(t)$ and $\mathbf{z}(t)$, respectively. Additionally, the block-Toeplitz matrices are defined based on the Fourier coefficients of the periodic matrices:

$$\begin{aligned} \mathcal{A} &= \mathcal{T}\{\mathbf{A}_k : k \in \mathbb{Z}\} & \mathcal{B}^{(i)} &= \mathcal{T}\{\mathbf{B}_k^{(i)} : k \in \mathbb{Z}\}, \quad i = 1, 2 \\ \mathcal{C}^{(i)} &= \mathcal{T}\{\mathbf{C}_k^{(i)} : k \in \mathbb{Z}\}, \quad i = 1, 2 & \mathcal{D}^{(i)} &= \mathcal{T}\{\mathbf{D}_k^{(i)} : k \in \mathbb{Z}\}, \quad i = 11, 12, 21, 22. \end{aligned} \quad (4.48)$$

Next, (4.42d) is transformed according to (4.47), and a frequency-lifted representation of (4.42) is eventually given by:

$$\begin{cases} \dot{\mathbf{x}}(t) = (\mathcal{A} - \mathcal{N})\mathbf{x}(t) + \mathcal{B}^{(1)}\mathbf{u}(t) + \mathcal{B}^{(2)}\mathbf{w}(t) \\ \mathbf{y}(t) = \mathcal{C}^{(1)}\mathbf{x}(t) + \mathcal{D}^{(11)}\mathbf{u}(t) + \mathcal{D}^{(12)}\mathbf{w}(t) \\ \mathbf{z}(t) = \mathcal{C}^{(2)}\mathbf{x}(t) + \mathcal{D}^{(21)}\mathbf{u}(t) + \mathcal{D}^{(22)}\mathbf{w}(t) \\ \mathbf{w}(t) = \mathcal{E}_{T_d} \mathbf{z}(t, \mathbf{t}_d), \end{cases} \quad (4.49)$$

which is the sought DHSS formulation.

4.4.4 Unforced DHSS for modal analysis

The stability assessment of the DHSS system (4.49) by means of modal analysis relies on the unforced formulation, which is obtained by setting $\boldsymbol{u}(t) = \mathbf{0}$:

$$\dot{\boldsymbol{x}}(t) = (\mathcal{A} - \mathcal{N})\boldsymbol{x}(t) + \mathcal{B}^{(2)}\boldsymbol{w}(t) \quad (4.50a)$$

$$\boldsymbol{z}(t) = \mathcal{C}^{(2)}\boldsymbol{x}(t) + \mathcal{D}^{(22)}\boldsymbol{w}(t) \quad (4.50b)$$

$$\boldsymbol{w}(t) = \boldsymbol{\mathcal{E}}_{T_d}\boldsymbol{z}(t, t_d). \quad (4.50c)$$

Next, intermediate variables $\boldsymbol{w}(t)$ and $\boldsymbol{z}(t)$ are eliminated. Beforehand, it is noted that, although the comma-based notation of delays in (4.40) is particularly convenient for practical implementations (such as the one considered in the Matlab toolbox developed as part of this thesis, see Appendix C.1), it is not compatible with the fundamentals of delayed systems presented in Section 4.3. Consequently, the following equality is introduced to bridge the gap between different delay notations:

$$\boldsymbol{z}(t, t_d) = \sum_{i=1}^d \boldsymbol{\Delta}_i \boldsymbol{z}(t - t_{di}, \mathbf{0}) \quad (4.51a)$$

$$= \sum_{i=1}^d \boldsymbol{\Delta}_i \boldsymbol{z}(t - t_{di}) \quad (4.51b)$$

where (4.41) was used and where $\boldsymbol{\Delta}_i$ is a diagonal matrix such that:

$$\boldsymbol{\Delta}_i \triangleq \begin{bmatrix} \ddots & & & \\ & \text{diag}(\boldsymbol{\delta}_i) & & \\ & & \text{diag}(\boldsymbol{\delta}_i) & \\ & & & \text{diag}(\boldsymbol{\delta}_i) \\ & & & & \ddots \end{bmatrix}, \quad (4.52)$$

with $\boldsymbol{\delta}_i$ a vector of length d containing 1 at the index i and 0 elsewhere. Hence, matrix $\boldsymbol{\Delta}_i$ selects all the elements of $\boldsymbol{z}(t, t_d)$ whose delay is equal to t_{di} .

Assumption 12. *Matrix $\mathcal{D}^{(22)}$ in (4.49) is equal to zero: $\mathcal{D}^{(22)} = \mathbf{0}$.*

Assumption 12 is valid for the models considered in this thesis, since none of the variables subject to a delay are functions of delayed variables. Under Assumption 12, (4.50c) becomes:

$$\boldsymbol{w}(t) = \boldsymbol{\mathcal{E}}_{T_d} \sum_{i=1}^d \boldsymbol{\Delta}_i \boldsymbol{z}(t - t_{di}) = \boldsymbol{\mathcal{E}}_{T_d} \sum_{i=1}^d \boldsymbol{\Delta}_i \mathcal{C}^{(2)} \boldsymbol{x}(t - t_{di}). \quad (4.53)$$

Eventually, (4.50a) becomes:

$$\dot{\boldsymbol{x}}(t) = (\mathcal{A} - \mathcal{N})\boldsymbol{x}(t) + \sum_{i=1}^d \mathcal{B}^{(2)} \mathcal{E}_{T_d} \Delta_i \mathcal{C}^{(2)} \boldsymbol{x}(t - t_{di}) \quad (4.54)$$

which has the anticipated form of the unforced LTI-DDE in (4.9), i.e.

$$\dot{\boldsymbol{x}}(t) = \mathcal{A}_{d0}\boldsymbol{x}(t) + \sum_{i=1}^d \mathcal{A}_{di}\boldsymbol{x}(t - t_{di}), \quad (4.55a)$$

with

$$\mathcal{A}_{d0} = \mathcal{A} - \mathcal{N}, \quad (4.55b)$$

$$\mathcal{A}_{di} = \mathcal{B}^{(2)} \mathcal{E}_{T_d} \Delta_i \mathcal{C}^{(2)}, \quad i = 1, \dots, d. \quad (4.55c)$$

In this thesis, characteristic roots of (4.55a) are obtained by means of the delay Arnoldi algorithm presented in [85], with the corresponding Matlab implementation available at [89]. This algorithm, which takes matrices \mathcal{A}_{di} and delays t_{di} as inputs, is specifically designed for the calculation of the characteristic roots of large delayed systems and is *a priori* suitable for frequency-lifted systems such as the DHSS representation. This point is further discussed in Section 4.6.

4.4.5 Transformation of DHSS into HTF formulation

For frequency-domain analyses, one can resort to the HTF approach described in Section 3.4. However, the same HTF can also be obtained by application of the Laplace transform to the DHSS formulation, which results in:

$$\left\{ \begin{array}{l} s\boldsymbol{x}(s) = (\mathcal{A} - \mathcal{N})\boldsymbol{x}(s) + \mathcal{B}^{(1)}\boldsymbol{u}(s) + \mathcal{B}^{(2)}\boldsymbol{w}(s) \end{array} \right. \quad (4.56a)$$

$$\left\{ \begin{array}{l} \boldsymbol{y}(s) = \mathcal{C}^{(1)}\boldsymbol{x}(s) + \mathcal{D}^{(11)}\boldsymbol{u}(s) + \mathcal{D}^{(12)}\boldsymbol{w}(s) \end{array} \right. \quad (4.56b)$$

$$\left\{ \begin{array}{l} \boldsymbol{z}(s) = \mathcal{C}^{(2)}\boldsymbol{x}(s) + \mathcal{D}^{(21)}\boldsymbol{u}(s) + \mathcal{D}^{(22)}\boldsymbol{w}(s) \end{array} \right. \quad (4.56c)$$

$$\left\{ \begin{array}{l} \boldsymbol{w}(s) = \mathcal{E}_{T_d} e^{-s\mathcal{T}_d} \boldsymbol{z}(s), \end{array} \right. \quad (4.56d)$$

with

$$\mathcal{T}_d \triangleq \text{blkdiag} \left\{ \left[\cdots \ T_d \ T_d \ T_d \ \cdots \right] \right\}. \quad (4.57)$$

Substituting (4.56c) into (4.56d) gives:

$$\left\{ \begin{array}{l} s\boldsymbol{x}(s) = (\mathcal{A} - \mathcal{N})\boldsymbol{x}(s) + \mathcal{B}^{(1)}\boldsymbol{u}(s) + \mathcal{B}^{(2)}\boldsymbol{w}(s) \end{array} \right. \quad (4.58a)$$

$$\left\{ \begin{array}{l} \boldsymbol{y}(s) = \mathcal{C}^{(1)}\boldsymbol{x}(s) + \mathcal{D}^{(11)}\boldsymbol{u}(s) + \mathcal{D}^{(12)}\boldsymbol{w}(s) \end{array} \right. \quad (4.58b)$$

$$\left\{ \begin{array}{l} \boldsymbol{w}(s) = (\mathcal{I} - \mathcal{E}_{T_d}e^{-s\mathcal{T}_d}\mathcal{D}^{(22)})^{-1}\mathcal{E}_{T_d}e^{-s\mathcal{T}_d}\mathcal{C}^{(2)}\boldsymbol{x}(s) \\ + (\mathcal{I} - \mathcal{E}_{T_d}e^{-s\mathcal{T}_d}\mathcal{D}^{(22)})^{-1}\mathcal{E}_{T_d}e^{-s\mathcal{T}_d}\mathcal{D}^{(21)}\boldsymbol{u}(s) \end{array} \right. \quad (4.58c)$$

with \mathcal{I} the identity matrix of infinite dimension. Lastly, eliminating $\boldsymbol{x}(s)$ and $\boldsymbol{w}(s)$ by substituting (4.58a) and (4.58c) into (4.58b) allows to solve for the input-output HTF matrix $\mathcal{H}(s)$ such that $\boldsymbol{y}(s) = \mathcal{H}(s)\boldsymbol{u}(s)$.

Frequency responses of lifted systems can be obtained by evaluating the HTF over a vector of frequencies of interest. Alternatively, when the frequency responses must be retrieved over a large number of frequencies, more-efficient approaches can be considered. For instance, the results in this thesis are obtained by calling Matlab's `freqresp` function directly on DHSS models: when called on a state-space system, this function relies on Hessenberg forms to accelerate⁵ the frequency response calculation [92].

4.5 Numerical application to an MMC-based system

This section illustrates the application of modal and transfer-function-based analyses to an elaborate converter-based offshore system, where periodic and delayed characteristics are addressed via the DHSS approach. The results obtained with the DHSS are compared with those obtained with the Nyquist criterion in the frequency domain as well as numerical integration in the time domain.

The system presented in Fig. 4.6 is considered for this illustrative numerical application. It consists of an MMC connected to an ideal direct voltage source at its DC side. An alternating voltage controller with a fixed frequency setpoint controls the converter as an alternating voltage source for a cable-based AC

⁵ According to [90, 91], it can be assumed that, for efficiency, `freqresp` calculates first the response of the non-delayed system from combined inputs $[\boldsymbol{u}(s); \boldsymbol{w}(s)]$ to combined outputs $[\boldsymbol{y}(s); \boldsymbol{z}(s)]$. This is where Hessenberg forms help accelerate the calculations. Next, the frequency response of the complex exponential is obtained by a direct numerical evaluation. Lastly, the complete frequency response is obtained as the feedback interconnection of the non-delayed system with the delays. More precisely, the feedback loop is established from the $\boldsymbol{z}(s)$ part of the outputs to the $\boldsymbol{w}(s)$ part of the inputs, which results in the complete input-output delayed system.

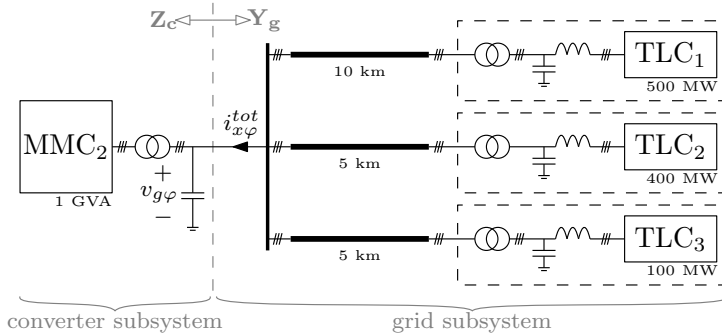


Figure 4.6: Offshore MMC-based system with location of split point for the application of frequency-domain analysis

offshore grid and its three aggregated offshore wind farms, which are represented by up-scaled TLCs whose models are established in Appendix B.3. For simplicity, the TLCs are also connected to ideal direct voltage sources on their DC sides, and are controlled to meet active and reactive power objectives. In Fig. 4.6, the equivalent capacitor located at the point of common coupling (PCC) of the MMC is not a physical device but a representation of the capacitive behaviour of the cables at that particular location.

All three TLCs are assumed to have a control delay of 1.5 times the sampling period, i.e. $150 \mu\text{s}$ for a typical sampling frequency of 10 kHz [20, 21]. The delay of the MMC is longer and, for the purpose of the example, is assumed to lie in the range of $450 \mu\text{s}$ to $550 \mu\text{s}$, in agreement with the values reported in [13]. Further details on modelling aspects of this offshore test system are provided in Appendix B.4.

4.5.1 Modal stability analysis

Keeping delays of the equivalent TLCs to a constant $150 \mu\text{s}$, the delay of the MMC is swept from $480 \mu\text{s}$ to $505 \mu\text{s}$ by increments of $5 \mu\text{s}$. In the assumed range of delay values, only these values are retained as they result in modes near the imaginary axis, as shown below. The periodic trajectories are determined⁶ for the given set of circuit and control parameters, thus one trajectory is obtained for each delay value. The computation of these trajectories accounts for harmonics up to the sixth rank. Two sets of differential equations are considered: the

⁶This calculation relies on the collocation method presented in Section 5.4.

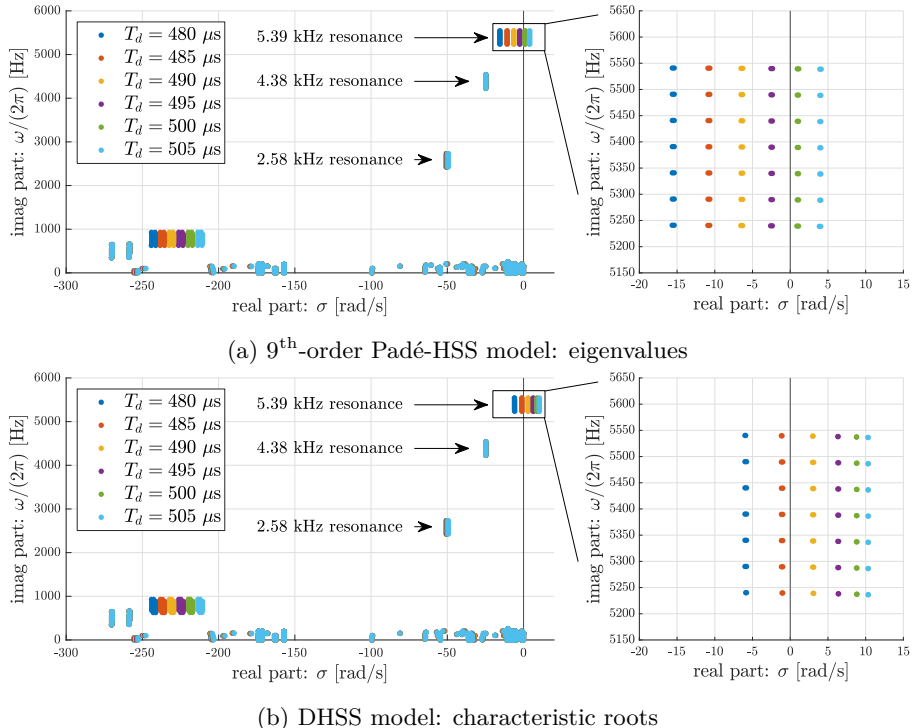


Figure 4.7: Modal analysis: MMC delay sweep from $480 \mu s$ to $505 \mu s$

original set of DDEs where delays are expressed as a pure time shift, and a set of ODEs where delays are replaced with a 9th-order Padé approximation.

The two sets of equations are linearised around the periodic trajectories and, in both cases, time-periodicity of the resulting state-space coefficients is tackled via frequency-lifting. The DDEs become a DHSS model and the ODEs become a "simple" HSS system, referred to as the Padé-HSS model. The lifted systems⁷ are truncated to rank $h_t = 3$. The eigenvalues of the state matrix of the Padé-HSS model are calculated and displayed in Fig. 4.7a. Likewise, characteristic roots of the DHSS model are obtained via the delay Arnoldi algorithm and are displayed in Fig. 4.7b. For clarity, modes with real part smaller than -300 rad/s are not

⁷ The non-lifted DDE system is of dimension 114 (33 states for the closed-loop MMC, 22 states for each of the three closed-loop TLCs, and 15 states for the grid). The lifted and truncated DHSS system ($h_t = 3$) is of dimension 798. The non-lifted 9th-order Padé-based ODE system is of dimension 222 since the approximation brings 54 more states for the MMC and 18 more states for each of the three TLCs. The lifted and truncated Padé-HSS system ($h_t = 3$) is of dimension 1554.

shown and, exploiting symmetry, only modes with a positive imaginary part are displayed.

The figures show three lightly-damped resonances located at 2.58 kHz, 4.38 kHz and 5.39 kHz according to the centremost eigenvalue of the corresponding eigensets. It is observed that the damping of the 5.39 kHz resonance is sensitive to the tested delay values. (Anticipating a later point of discussion, it is worth noting that, for every delay value, the eigensets related to the three natural resonances are in fact two nearly-overlapping eigensets.) On the one hand, the 9th-order Padé approximation indicates that the 5.39 kHz resonance is still stable for an MMC delay of 495 μ s but becomes unstable for a delay of 500 μ s. On the other hand, the characteristic roots of the DHSS model indicate that a delay of 490 μ s would already cause the trajectory to become unstable, while a delay of 485 μ s should preserve stability.

According to Fig. 4.2b, the identified phenomena in this example are outside the range of validity of the 9th-order Padé approximation, as it is located beyond the 5° error limit frequency. Otherwise stated, for delays near 500 μ s, the error made by a 9th-order Padé approximation is larger than 5° at frequencies above \sim 4.7 kHz. Consequently, the results from the DHSS model should be more accurate than those of the Padé-HSS model. This hypothesis is verified against two other approaches: first with the generalised Nyquist criterion (GNC), i.e. the generalisation of the Nyquist criterion to MIMO systems, and second with a direct numerical integration of the nonlinear differential equations.

Before proceeding to the comparison with the GNC and numerical integration, the centremost eigenvalue in one of the two nearly-overlapping eigensets related to the destabilised resonance is studied further. Its participation factors are obtained according to Section 1.3.2 and the results are provided in Table 4.1 up to a cumulative participation of 99.5%. It is observed that currents and voltages related to the AC cables of the offshore grid ($i_{x1\varphi}$ to $i_{x3\varphi}$, $v_{x2\varphi}$ and $v_{x3\varphi}$) are involved in the phenomenon and explain the resonant behaviour. Interestingly, the alternating voltage $v_{g2\phi}$ at the PCC is also involved to a significant extent (18.3%), and the fact that this voltage is controlled by the MMC explains the impact of the control delay on the observed risk of instability. Eventually, the transformer currents at TLC₂ ($i_{t2\varphi}$) and all other states of the system (not shown in the table) weigh for less than 1% in the unstable mode.

4.5.2 Transfer-function-based stability analysis

The results of the modal analysis are verified with the GNC in the frequency domain. The reader is referred to [44, Section 4.9] for a general statement of the

| states and their location | participation [%] | cumulative sum [%] |
|--|----------------------|-----------------------|
| $i_{x2\varphi}$ AC cable 2 | 24.6 | 24.6 |
| $i_{x3\varphi}$ AC cable 3 | 22.4 | 47.0 |
| $v_{g2\phi}$ MMC ₂ PCC | 18.3 | 65.3 |
| $v_{x2\varphi}$ TLC ₂ PCC | 16.8 | 82.1 |
| $v_{x3\varphi}$ TLC ₃ PCC | 14.6 | 96.7 |
| $i_{x1\varphi}$ AC cable 1 | 2.2 | 98.9 |
| $i_{t2\varphi}$ TLC ₂ transformer | 0.6 | 99.5 |

Table 4.1: Participation factors of the centremost 5.39 kHz resonant mode in the DHSS model

GNC and to [82, Section 2.4.2] for an in-depth discussion of the methodology and assumptions.

The system is split into two subsystems, as depicted in Fig. 4.6. The first subsystem is referred to as the *converter subsystem*, which comprises the MMC and the equivalent shunt capacitor at its PCC. The rest of the system is referred to as the *grid subsystem*, which encompasses the cables and the equivalent TLCs. Both subsystems are linearised around the calculated periodic trajectories and are transformed into DHSS models via frequency-lifting. Truncation is again applied at rank $h_t = 3$. Next, the full HTF is calculated from the DHSS model by means of Matlab's `freqresp` function. Lastly, only the *no-shift* frequency responses are retrieved from the larger set of *shift* frequency responses delivered by the HTF framework.

According to Fig. 4.6, the frequency responses have the following physical interpretation: the converter subsystem is represented by a three-phase impedance $\mathbf{Z}_c(s)$ with current deviations $\tilde{i}_{x,abc}^{tot}$ as inputs and voltage deviations $\tilde{v}_{g,abc}$ as outputs. The grid subsystem is presented by a three-phase admittance $\mathbf{Y}_g(s)$, with voltage deviations $\tilde{v}_{g,abc}$ as inputs and current deviations $-\tilde{i}_{x,abc}^{tot}$ as outputs, where the minus sign ensures that the admittance satisfies the load convention. The dynamics of the complete system are obtained by considering the two subsystems in closed loop, with the corresponding closed-loop transfer function $\mathbf{T}(s)$ proportional to:

$$\mathbf{T}(s) \sim (\mathbf{I} + \mathbf{L}(s))^{-1}, \quad \text{with } \mathbf{L}(s) = \mathbf{Y}_g(s)\mathbf{Z}_c(s), \quad (4.59)$$

where $\mathbf{L}(s)$ is here the return ratio of the closed-loop connection [82].

The application of the GNC consists in studying the encirclements made by the eigenvalues of $\mathbf{L}(s)$ around the $(-1, 0)$ point of the complex plane, as Laplace variable s evolves along the boundary of the right-hand complex plane. For

systems whose return ratio tends towards zero when s tends towards infinity, this is equivalent to simply increasing s from $-j\omega_m$ to $+j\omega_m$, with ω_m a sufficiently large value⁸.

Without providing a complete description of the GNC but relying on [44, 82], it can be stated that the number of clockwise encirclements N made by the eigenvalues of $\mathbf{L}(s)$ around $(-1, 0)$ is equal to the number N_T of unstable poles of $\mathbf{T}(s)$, minus the number N_L of unstable poles of $\mathbf{L}(s)$:

$$N = N_T - N_L. \quad (4.60)$$

Knowing both N and N_L allows determining N_T without the need for a direct calculation of the poles of $\mathbf{T}(s)$. A well-known challenge related to using the Nyquist criterion, already briefly mentioned at the beginning of this chapter, emerges: a preliminary stability assessment of the subsystems is needed to know N_L . Applying the Nyquist criterion to determine the number of unstable poles of each subsystem would be an option, however this merely shifts the need of detecting unstable poles to their own subsystems. In this thesis, the DHSS framework offers a solution to this problem. Specifically, the characteristic roots of the converter and grid subsystems are retrieved by means of the delay Arnoldi algorithm, which informs about the stability of their respective trajectories. As none of the subsystems have unstable poles, neither does $\mathbf{L}(s)$ and $N_L = 0$. Consequently, any strictly positive number of clockwise encirclements N will warn about the existence of unstable poles of $\mathbf{T}(s)$.

At this point, the value of N must still be obtained. As both $\mathbf{Y}_g(s)$ and $\mathbf{Z}_c(s)$ describe the relationship between three-phase quantities, they are 3-by-3 matrices and so is $\mathbf{L}(s)$. Consequently, for every value of s , $\mathbf{L}(s)$ has three eigenvalues. Their curves in the complex plane are noted Λ_1 , Λ_2 and Λ_3 , and are depicted in Figs. 4.8a and 4.8b for delays of 485 μs and 490 μs respectively. In both cases, Λ_1 , Λ_2 are nearly overlapping, while Λ_3 is equal to zero and is not visible. Fig. 4.8a shows no encirclement of the $(-1, 0)$ point, which indicates that the closed-loop system is stable. On the other hand, a visual inspection of Fig. 4.8b reveals a total of four complete clockwise encirclements, which confirms that the 490 μs trajectory is unstable, as was predicted by the characteristic roots of the DHSS.

As modal analysis and the application of the GNC are reflections of the same model, it is concluded that the four encirclements correspond to the two (nearly-overlapping) unstable eigensets at positive frequencies and their complex conjugates. One may wonder why the GNC does not reveal a total of 28 unstable modes, corresponding to two 7-mode eigensets at positive frequencies

⁸ For this particular example, a sufficiently large value is such that it covers the phenomenon of interest: a maximum frequency of e.g. 10 kHz largely satisfies this requirement.

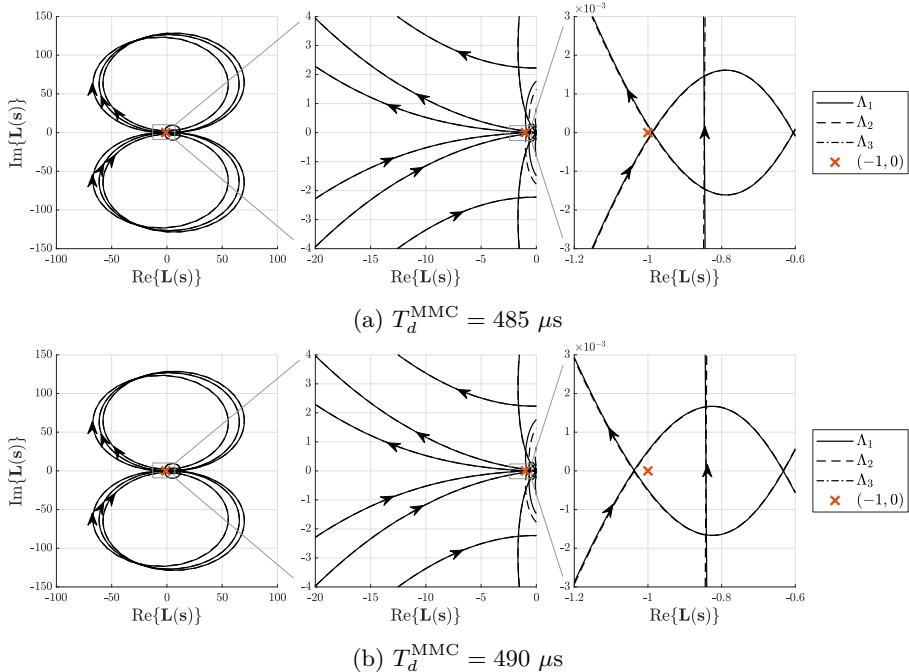


Figure 4.8: Nyquist plots

and their complex conjugates, with each eigenset being the result of a truncation at rank $h_t = 3$. This would have been the case if the GNC had been applied to the full HTF obtained with $h_t = 3$. However, the GNC is applied only to the no-shift frequency responses, which in themselves are not lifted models, hence the apparent truncation rank of $h_t = 0$ in the above paragraphs.

4.5.3 Validation against numerical integration

Numerical integration is used to verify the results obtained via modal analysis and the GNC. In this section, the simulations are carried out with the `ode15s` solver in Matlab, with the relative tolerance set to 10^{-8} . Even though the `ode15s` solver is normally dedicated to ODEs, DDEs can also be solved with ODE solvers by splitting the integration into sub-intervals: the principle consists in relying on the solution of sub-interval k to provide the delayed variables as

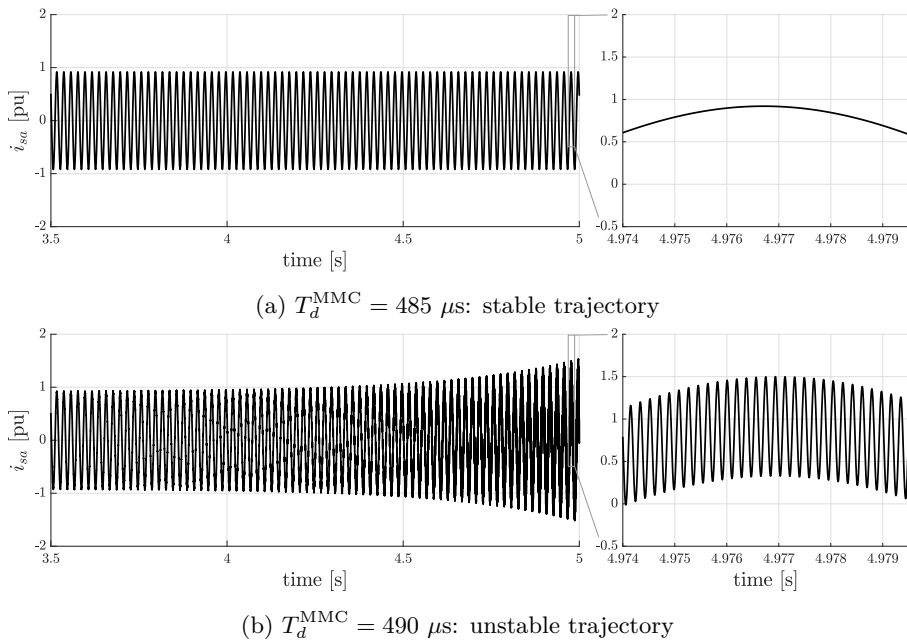


Figure 4.9: Numerical integration of the nonlinear DDEs: alternating current waveform (i_{sa})

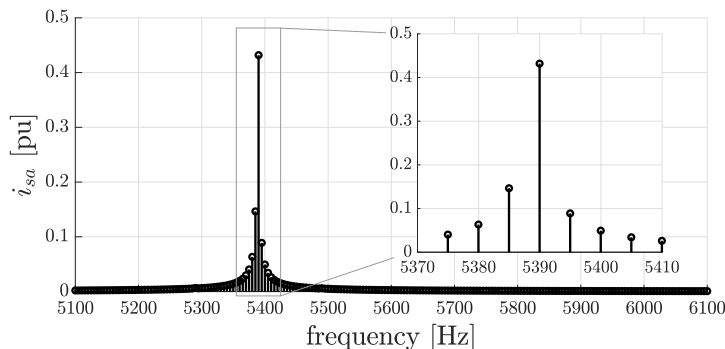


Figure 4.10: Frequency spectrum of MMC alternating currents over the last 0.2 s of simulation (unstable case)

inputs for the integration of sub-interval $k + 1$. This approach⁹ is described in more detail in Appendix C.2.

The complete nonlinear system is simulated with the initial state (i.e. the initial function segment) set on the studied periodic trajectory, and the results are provided in Fig. 4.9. Two periodic trajectories are considered: in Fig. 4.9a, the delay of the MMC is equal to $485 \mu\text{s}$, and the simulation remains stable despite a 20% disturbance on the power output of the largest TLC between $t = 5 \text{ ms}$ and $t = 10 \text{ ms}$ (not visible in the figure). In Fig. 4.9b the delay is increased to $490 \mu\text{s}$. In this case, the simulation slowly becomes unstable. In Fig. 4.10, a DFT applied to the last 10 fundamental periods of simulation (i.e. on the last 0.2 s) shows that the unstable oscillation is centred around 5.39 kHz , as predicted by the modal analysis.

These simulations give an additional confirmation that the stability limit has been correctly identified by the modal analysis of the DHSS model.

4.6 Discussion and chapter conclusion

This chapter was dedicated to addressing the small-signal stability analysis of periodic trajectories followed by nonlinear delayed systems. The chosen approach was to use frequency-lifting in the form of HSS to tackle periodicity in the coefficients of the delayed LTP systems that result from linearisation. It was shown how exact delays can be introduced in the HSS formulation of Section 3.2, thereby resulting in a delayed but time-invariant frequency-lifted model. Relying on a new generation of algorithms capable of determining characteristic roots of DDEs, modal analysis can be performed in a similar fashion as for non-delayed HSS models.

One advantage of the chosen approach is that the complete state-space model is made time-invariant in the transformation process, which allows applying the Laplace transform to the DHSS to retrieve an HTF model.

A numerical application showed the anticipated match between the results of modal analysis in the time domain with those of the GNC in the frequency domain, eventually confirmed against numerical integration of the

⁹ Considering another solver than `dde23` for the numerical integration of delayed systems is motivated by the fact that different solvers display different levels of numerical damping. Different solvers may thus lead to conflicting conclusions on whether the analysed periodic trajectory is stable or not, in particular when the system presents unstable modes at high frequencies (large imaginary part) but close to the imaginary axis (small real part). For the specific system considered in this section, the `ode15s` Matlab solver delivered more reliable results than the `dde23` solver.

nonlinear system. The flexibility of a frequency-lifting approach, combined with the increased accuracy that results from avoiding rational polynomial approximations of complex exponential transfer functions, makes that the DHSS is capable of largely reducing the number of simplifying assumptions that are otherwise necessary to carry out modal analyses of MMC-based systems.

A current challenge of the presented method is its calculation time. First, the delay Arnoldi algorithm dedicated to the calculation of the characteristic roots of DDEs is, for a given system order, more computationally-intensive than the algorithms dedicated to the calculation of eigenvalues of ODEs. Secondly, the fact that the proposed framework relies on frequency-lifting to tackle time-periodicity implies that the size of the eigenvalue problem to solve is also significantly larger than non-lifted counterparts, which contributes to noticeably longer calculation times.

A reduction of the calculation times can be foreseen if modal analysis is instead directly applied to the delayed LTP system, by obtaining the eigenvalues of a discretised monodromy operator ("Approach 1" in Section 4.2). Although not investigated in this thesis, this approach would allow reaching the objective of performing modal analysis of periodic delayed systems, however without relying on frequency-lifting. The drawback would be that frequency responses are not easily retrieved with this approach, in which case a separate modelling effort based on the HTF in Section 3.4 would be necessary.

At times, the Nyquist criterion has been advertised as the most viable way of assessing the small-signal stability of trajectories of delayed systems by circumventing the use of Padé approximations [93]. Yet, regardless of how the subsystems are chosen, the requirement of knowing the number of their unstable poles is synonymous of a recursive use of the Nyquist criterion on subsystems of subsystems, all of which may also contain delays. The state-space formalism provides a solution to this drawback of the Nyquist criterion by enabling a calculation of the characteristic roots of the subsystems, if not directly those of the complete system.

At this stage, it is recalled that the periodic trajectories of interest in Chapters 2, 3 and 4 have been assumed to be known *a priori*. Their calculation is addressed in the following chapter.

Chapter 5

Calculation of periodic trajectories

5.1 Introduction

Whenever a nonlinear dynamic system is supposed to follow a given trajectory in steady state, the calculation of this trajectory is of significant importance as it is a prerequisite to its small-signal stability assessment. This is clear from the fact that assessing whether a system will go back to its steady-state trajectory after a disturbance naturally depends on the system properties around that particular trajectory. Besides, such analysis also helps determining whether the system will be able to reach this trajectory in the first place.

Specifically, in this thesis, a steady-state trajectory determination refers to the calculation of the waveforms followed by the variables when the behaviour of the system is such that it repeats itself as long as it remains undisturbed, which is in agreement with Definition 1. Such calculation is valid for the given set of circuit and control parameters, as well as for the given external conditions defined by the inputs of the system. A change of parameters or external conditions may cause a transient, possibly leading to another trajectory which must then be (re)calculated.

For small-signal stability assessments of periodic trajectories, knowledge of the steady-state waveforms allows calculating the time-dependent coefficients of the LTP representation that results from linearising the initial system around the trajectory. From this point of view, the periodic trajectory determination is

essential to the application of frequency-lifting techniques such as the HSS/HTF framework.

For other approaches relying on a transformation of the periodic trajectory into a constant operating point, such as frame rotations and dynamic-phasor-based methods, the small-signal stability assessment relies on the calculation of the equilibrium of the transformed system. However, the calculation of the periodic trajectory of the original system remains relevant also in these cases: it enables determining which harmonic components should normally be taken into account in the transformation and, in three-phase systems, such calculation provides information on the sequence of these oscillatory components.

The knowledge of a periodic trajectory is also valuable in other studies than stability assessments. For instance, in the case of the MMC, a sum-capacitor voltage waveform determination, with its distinctive "ripple", is a helpful step in the adequate sizing of submodule capacitors and semiconductor devices [12, Ch.2]. Furthermore, steady-state trajectory calculations play a role in the initialisation of numerical integration methods: setting the initial conditions of the studied system at an equilibrium or on a periodic trajectory is a way of avoiding lengthy start-up transients and significantly reducing simulation times [94]. More generally, in electrical power systems, periodic trajectory calculations can be synonymous of harmonic power flows, harmonic propagation studies and harmonic distortion calculations. In such studies, the objective is generally to assess the impact of undesired oscillatory components on power quality [2, Ch.5-6], e.g. ensuring that harmonic distortion remains within tolerated levels, evaluating the risk of interference with communication, control and protection systems, or estimating the additional cost of harmonic-related power losses [95].

Mathematically, the identification of constant operating points $(\bar{\mathbf{x}}(t), \bar{\mathbf{u}}(t)) = (\mathbf{x}_0, \mathbf{u}_0)$, where subscript 0 refers to the Fourier coefficient of index $k = 0$, relies on the observation that the time derivatives of the states $\dot{\mathbf{x}}(t) = \mathbf{x}_0$ are equal to zero:

$$\dot{\mathbf{x}}_0 = \mathbf{0}. \quad (5.1)$$

For state-space representations such that $\dot{\mathbf{x}}(t) = \mathbf{f}(\mathbf{x}(t), \mathbf{u}(t))$ where $\mathbf{u}(t) = \mathbf{u}_0$ is known, the fact that time derivatives are equal to zero implies that \mathbf{x}_0 is not the solution of a differential equation anymore, but the solution of a set of algebraic equations:

$$\mathbf{f}(\mathbf{x}_0, \mathbf{u}_0) = \mathbf{0}. \quad (5.2)$$

The calculation of periodic trajectories is a more complicated matter since the time derivative of the states $\dot{\mathbf{x}}(t)$ is not equal to zero at all points of the fundamental period $[0, T_1]$, and a more general equation must be solved:

$$\dot{\mathbf{x}}(t) - \mathbf{f}(\bar{\mathbf{x}}(t), \bar{\mathbf{u}}(t)) = \mathbf{0}, \quad t \in [0, T_1] \quad (5.3)$$

where the solution is not a point but the continuum of points over the fundamental period.

In light of the above, this chapter¹ is dedicated to addressing the calculation of steady-state periodic trajectories of nonlinear delayed systems such as the stationary-frame arm-averaged model of the MMC in closed-loop with its controller. This chapter is structured as follows.

Section 5.2 provides a brief overview of methods dedicated to periodic trajectories calculations, which fulfils Objective 1a. A comparison of time-domain, frequency-domain and hybrid-domain methods based on their respective advantages and limitations allows identifying Fourier-based collocation methods [97, 98] as a way of addressing unsolved challenges touching upon the MMC specifically. It is the main original contribution of this chapter to develop such a method and to apply it to the MMC, which fulfils Objective 1b. Before diving into its derivation in Section 5.4, frequency-domain methods and hybrid-domain methods are described in more detail in Section 5.3 to introduce the necessary notation and establish clear points of reference for the mathematical developments on which the Fourier-based collocation method relies.

5.2 Overview of calculation methods

Periodic trajectory calculation techniques can be sorted according to their physical domain of application [95]: time-domain methods, frequency-domain methods, and hybrid-domain methods. This section provides a brief overview of each category of methods.

Time-domain methods

In time-domain methods, the unknown variables are functions of time. This directly leads to the main advantage of this class of methods, which resides in the fact that they can naturally account for nonlinearity within the differential equations. In this thesis, a distinction is made between two types of time-domain methods: numerical integration methods and collocation methods.

A first numerical integration method is referred here to as the *simple numerical integration* method [87, Ch.17]. It consists in solving the differential equations from a given initial condition until a (possibly periodic) steady state is reached. The main disadvantage of this method is its high computational burden, as slow transients mean lengthy simulation times before a steady state is

¹ This chapter is based on the submitted article [96], see also the List of Publications.

achieved. Another disadvantage is that it is unable to find unstable steady-state trajectories. Having ensured that the starting point was close enough to the targeted operating trajectory and eliminated the possibility that instability be caused by the integration method itself, the fact that a numerical integration does not converge to a steady state for a given set of inputs and parameters may hint towards the fact that the targeted operating trajectory is unstable. However, this observation does not provide insights into the reasons preventing the set of inputs and parameters from driving the system to the targeted steady state. This could be addressed by means of modal analysis, would the trajectory be known in the first place. Consequently, it is important that such unstable trajectories also be identified precisely.

Single shooting methods [87, Ch.18], also known as accelerated time-domain methods, are introduced as a way of accelerating the solution of the differential equations towards steady state. The principle consists in integrating the equations repeatedly over one fundamental period and recalculating the initial condition at the start of each new fundamental period [99]. The initial condition is updated at each iteration based on the error between the start and end points of the fundamental period, i.e. the distance separating the end point from a (possibly periodic) steady-state trajectory. This iterative process is run until the error between start and end points becomes smaller than a predefined tolerance.

Multiple shooting methods apply a similar principle in which the fundamental period is split into multiple sub-intervals [98, 99]. The initial point of each sub-interval is recalculated after each run based on the error between the first point of the sub-interval and the last point of the previous one. Single and multiple shooting methods remain rather slow methods as they still rely on integrating the differential equations. An advantage of shooting methods is that the monodromy matrix, and thus the Floquet multipliers, can be readily obtained as a by-product of the iterative process. However, a disadvantage of shooting methods is that their convergence properties decrease near unstable trajectories [99], for which they may not converge at all. For stable trajectories, it may happen that shooting methods display worse performance than a simple numerical integration, if the number of shooting iterations needed for convergence corresponds to a number of fundamental periods larger than the duration of the transient that would otherwise be observed from the selected initial conditions. A number of limitations of integration-based methods are tackled by collocation methods.

Following a similar approach to that presented in Section 4.3.4 for the discretisation of the infinitesimal generator of delayed systems, the principle of collocation methods consists in associating known interpolation functions to the unknown steady-state waveforms. Specifically, the interpolation functions are introduced into the differential equations in order to replace the unknown variables. The requirement that the differential equations should be satisfied

over a discrete grid of time points (called the *collocation points*) transforms the system of differential equations into a system of algebraic equations where the new unknowns are the values taken by the interpolation functions at the collocation points [97]. By avoiding the need to numerically integrate the differential equations, collocation methods are less computationally intensive and are capable of finding both stable and unstable operating trajectories. Collocation methods differ based on the type of interpolation functions, the distribution of collocation points, etc. Two main categories of interpolation functions are polynomials and Fourier series. In the latter case, it is emphasised that the unknowns are the values taken by the interpolation functions over the grid of collocation points, and not the Fourier coefficients, since this would make the formulation a frequency-domain method.

Frequency-domain methods

In frequency-domain methods [95], the unknown variables are functions of frequency. Specifically for systems with periodic solutions, it is assumed that the sought waveforms can be represented by truncated Fourier series which, just as in collocation methods, are substituted into the differential equations. Next, the Fourier coefficients of the sought variables are chosen as unknowns and are determined as the solution of the set of algebraic equations that results from the application of the harmonic balance principle (see Definition 2). Often, the system of equations is nonlinear with respect to the unknown Fourier coefficients and is solved by means of an iterative root finding algorithm (RFA). In that regard, frequency-domain methods are quite similar to collocation methods and benefit from some of their advantages: they offer a lower computational burden than integration-based methods and are capable of finding both stable and unstable trajectories. However, they do not benefit from the main strength of time-domain methods. Namely, nonlinearity within dynamic equations cannot generally be expressed in terms of Fourier coefficients and only products of variables can be described straightforwardly in the frequency domain by means of discrete convolution products. This limitation has motivated the development of hybrid-domain methods.

Hybrid-domain methods

Hybrid-domain methods combine advantages of both time and frequency domains [95, 100–102], and the unknown variables are expressed successively in one or the other domain, depending on the type of calculation being performed. Often, the core of hybrid-domain methods is set in the frequency domain, where the dynamic equations are again described by a system of algebraic equations

with Fourier coefficients as unknowns. However, they rely on partitioning the mathematical operations into two sets: the linear operations are treated directly in the frequency domain while nonlinear operations are treated in the time domain. At each iteration of the RFA, signals subject to nonlinear operations are transformed from the frequency domain to the time domain, and then back after application of the nonlinear operations. This requirement for explicit direct and inverse Fourier transformations to convert variables from one domain to the other is a drawback of hybrid-domain methods and increases their computational burden.

Choice of calculation method for periodic trajectories of the MMC

In the literature, the majority of approaches specifically dedicated to determining periodic trajectories of the MMC have relied on an analytical description of the unknown waveforms by means of either complex or real-valued truncated Fourier series [103–109], where for each variable, it is assumed prior to calculating the trajectory which harmonics should be zero and which might be non-zero. The analytical expressions are manually introduced into the differential equations which, after application of the harmonic balance principle, become algebraic equations with the Fourier coefficients as unknowns. This mainstream approach, despite being a frequency-domain technique and benefiting from a characteristically low computational burden, presents a number of disadvantages: (i) the proposed formulations are based on preliminary assumptions regarding the harmonic frequencies at which non-zero components are expected and, as a consequence, the algebraic equations must be re-derived when additional harmonic components are of interest; (ii) the analytical manipulations involved in the application of the harmonic balance principle quickly become cumbersome for complete MMC models, even when the control equations are disregarded; (iii) the approach is strongly case-dependent and must be revised for every new model, thereby preventing a straightforward generalisation to other types of converter topologies and other control strategies; (iv) the approach does not allow to account in a simple way for other nonlinear operations than the product of variables, which is a direct consequence of working within the frequency domain.

As a result of these limitations, most approaches proposed in the literature have neglected the control equations and relied on open-loop control [103–105, 107–109] or on a simplified feedback controller [106]. However, different control strategies and control parameters may lead to different steady-state trajectories with possibly different stability properties. In the context of small-signal stability analyses, this means that not only the electrical circuit but also the controller should be taken into account for trajectories calculations. Moreover, trajectories

of nonlinear systems must normally be recalculated each time a parameter is changed in order to adjust the coefficients of the linearised model accordingly. Eventually, in small-signal stability studies and sensitivity analyses, trajectories calculations may be responsible for a large share of the total computational burden, and methods dedicated to trajectories identification should thus be particularly efficient.

In addition to neglecting control dynamics, the vast majority of methods dedicated to the MMC trajectory calculation have primarily focused on balanced phases and balanced operating conditions, and in most cases it is not straightforward to generalise the proposed approaches to the unbalanced case. References [106, 107] have covered the case of unbalanced phases, however the analytical developments are cumbersome. This limitation was addressed in e.g. [109] by relying on an HSS model of the power stage of the MMC, thus restricted to an open-loop study of the converter. Lastly, none of the provided references have accounted for control time delays, while in this thesis, accounting for time delays in trajectories calculations is a prerequisite to the application of the HTF approach in Section 3.4 and of the DHSS approach in Section 4.4.

Integration-based methods and hybrid-domain methods tackle most of the above-described limitations as they are capable of accounting for both nonlinearity and time delays. Yet, they suffer from their higher computational burden and, in the case of shooting methods, from their decreased convergence properties near unstable trajectories.

Overall, collocation methods are the only methods that combine both the advantage of naturally accounting for nonlinearity while avoiding the need to numerically integrate the differential equations, which justifies selecting this class of methods for the periodic trajectory determination of the MMC. Although polynomial-based collocation methods have a number of advantages, a Fourier-based method is developed in Section 5.4. The simplicity of the proposed formulation is seen as a significant advantage, in particular when weighed against the range of systems it covers and the number of identified problems it allows to solve. Furthermore, Fourier-based methods are the most natural way of addressing the calculation of periodic solutions. Lastly, [97, Ch.1] explains that, in the vast majority of applications, the best choice of basis functions are Fourier series or Chebyshev series, the latter being obtained from the former with a change of variables. Fourier-based methods are thus regarded as an ideal starting point for a presentation of collocation methods.

In order to provide a clear point of reference for the Fourier-based collocation method, frequency-domain and hybrid-domain methods are first presented in more detail in the next section.

| Symbol | Definition | Typeset |
|--|-------------------------------------|--------------------|
| x | scalar quantity | light lowercase |
| x_k | k^{th} Fourier coefficient | with subscript |
| $x^{(i)}$ | i^{th} variable | with (superscript) |
| \boldsymbol{x} | vector quantity | boldface lowercase |
| \boldsymbol{X} | matrix quantity | boldface uppercase |
| $\boldsymbol{\alpha}$ | harmonic vector | round lowercase |
| $\underline{\boldsymbol{x}}$ | vector of harmonic vectors | underlined |
| $\boldsymbol{\mathcal{X}}$ | Toeplitz matrix | round uppercase |
| $\underline{\boldsymbol{\mathcal{X}}}$ | block-matrix of Toeplitz matrices | underlined |
| \mathbf{x} | sampled-time vector | roman lowercase |
| $\underline{\mathbf{x}}$ | vector of sampled-time vectors | underlined |

Table 5.1: Supplemented nomenclature

5.3 Frequency-domain and hybrid-domain methods

In this section, frequency-domain and hybrid-domain methods are reviewed to introduce the notation as well as a clear point of reference for the development of the Fourier-based collocation method in the next section. Table 5.1 provides an extended overview of the notation used in this chapter.

The derivation of a frequency-domain formulation is typically initiated by replacing all variables in the differential equations with their truncated Fourier series. Next, the harmonic balance principle is applied in such a way that one set of equations is obtained for every harmonic index between $-h$ and $+h$, with h the maximum harmonic index of the truncated Fourier series. Consequently, frequency-domain formulations are tightly related to frequency-lifting (see Definition 3). However, the calculations considered in this chapter can rely on the fact that the sought waveforms are periodic, which implies that their Fourier coefficients are constant: unlike in the frequency-lifting technique, no time-dependent Fourier coefficients are involved. In this context, the fundamental mathematical operations discussed in Sections 3.2 and 4.4 for harmonic vectors are briefly revisited.

5.3.1 Mathematical operations with harmonic vectors

For mathematical operations in the frequency domain, the steady-state harmonic content of a continuous time-domain periodic scalar signal $x(t)$ is conveniently

written as a vector \boldsymbol{x} of its constant complex-valued Fourier coefficients. As in Section 3.2, such vectors are referred to as *harmonic vectors*, with as main difference the fact that harmonic vectors are constant in this chapter. Considering harmonic components up to rank h , harmonic vector \boldsymbol{x} has a total of $n_h = 2h + 1$ components and is defined as:

$$\mathcal{R}\{x(t)\} \triangleq \boldsymbol{x} \triangleq \begin{bmatrix} x_{-h} \\ \vdots \\ x_h \end{bmatrix}, \quad (5.4)$$

where the operator \mathcal{R} indicates the action of describing a periodic signal in terms of a constant harmonic vector². The following fundamental operations are considered:

1. multiplication of a periodic signal by a constant scalar parameter;
2. addition of two periodic signals;
3. multiplication of periodic signals;
4. time derivation of a periodic signal;
5. time delay of a periodic signal;

Relying on the developments in Section 3.2, these operations can be described by means of constant harmonic vectors as follows:

$$\mathcal{R}\{\alpha x(t)\} = \alpha \boldsymbol{x} \quad (5.5a)$$

$$\mathcal{R}\{x(t) + y(t)\} = \boldsymbol{x} + \boldsymbol{y} \quad (5.5b)$$

$$\mathcal{R}\{x(t)y(t)\} = \boldsymbol{x}\boldsymbol{y} = \boldsymbol{y}\boldsymbol{x} \quad (5.5c)$$

$$\mathcal{R}\{\dot{x}(t)\} = \dot{\boldsymbol{x}} + \mathcal{N}\boldsymbol{x} = \mathcal{N}\boldsymbol{x} \quad (5.5d)$$

$$\mathcal{R}\{x(t - t_d)\} = \mathcal{E}(t_d)\boldsymbol{x}(t - t_d) = \mathcal{E}(t_d)\boldsymbol{x} \quad (5.5e)$$

where $x(t)$ and $y(t)$ are two arbitrary periodic scalar signals, α is a constant scalar parameter, and t_d is a constant delay value.

² A new operator \mathcal{R} is introduced here to distinguish it from the frequency-lifting operator \mathcal{K} , where the harmonic vector is not necessarily constant.

In (5.5c), matrix \mathcal{X} has a Toeplitz structure and is defined as:

$$\mathcal{X} \triangleq \mathcal{T}\{x_k : k = -h, \dots, h\} = \begin{bmatrix} x_0 & \cdots & x_{-h} & & & \\ \vdots & x_0 & \ddots & \ddots & & \\ x_h & \ddots & \ddots & \ddots & x_{-h} & \\ & \ddots & \ddots & x_0 & & \vdots \\ & & x_h & \cdots & x_0 & \end{bmatrix}, \quad (5.6)$$

and similarly for matrix \mathcal{Y} .

In (5.5d) and (5.5e), matrices \mathcal{N} and $\mathcal{E}(t_d)$ are defined as:

$$\mathcal{N} \triangleq \text{diag}\{[-jh\omega_1 \ \cdots \ -j\omega_1 \ 0 \ j\omega_1 \ \cdots \ jh\omega_1]\} \quad (5.7a)$$

$$\mathcal{E}(t_d) \triangleq e^{-t_d \mathcal{N}}. \quad (5.7b)$$

Lastly, in (5.5d) and (5.5e), the simplifications $\dot{\mathbf{x}} = \mathbf{0}$ and $\mathbf{x}(t - t_d) = \mathbf{x}$ are naturally related to the fact that the elements of \mathbf{x} are constant.

The above definitions only cover the case where the original signals are scalars. The extension of the notation to the vector case, which differs slightly from that used in the previous chapters, is presented in the following paragraph.

Vector extension of the harmonic notation

A time-periodic vector $\mathbf{x}(t) = \mathbf{x}(t + T_1) \in \mathbb{R}^n$, whose elements are n scalar signals, is considered:

$$\mathbf{x}(t) = \begin{bmatrix} x^{(1)}(t) \\ x^{(2)}(t) \\ \vdots \\ x^{(n)}(t) \end{bmatrix}. \quad (5.8)$$

In this chapter, the corresponding frequency-domain quantity is obtained by stacking the harmonic vectors $\mathbf{x}^{(i)}$ related to the original scalar elements $x^{(i)}(t)$. The result is a vector of harmonic vectors, noted with an underline:

$$\underline{\mathcal{R}\{\mathbf{x}(t)\}} \triangleq \underline{\mathbf{x}} \triangleq \begin{bmatrix} \mathcal{R}\{x^{(1)}(t)\} \\ \mathcal{R}\{x^{(2)}(t)\} \\ \vdots \\ \mathcal{R}\{x^{(n)}(t)\} \end{bmatrix} = \begin{bmatrix} \underline{\mathbf{x}}^{(1)} \\ \underline{\mathbf{x}}^{(2)} \\ \vdots \\ \underline{\mathbf{x}}^{(n)} \end{bmatrix}. \quad (5.9)$$

Relying on (5.9), the multiplication by a scalar and the sum of periodic signals are easily generalised to the vector case. Next, we consider the product of $\mathbf{x}(t)$ with a time-periodic matrix $\mathbf{A}(t) = \mathbf{A}(t + T_1) \in \mathbb{R}^{m,n}$, written as:

$$\mathbf{A}(t) = \begin{bmatrix} a^{(1,1)}(t) & \cdots & a^{(1,n)}(t) \\ \vdots & \ddots & \vdots \\ a^{(m,1)}(t) & \cdots & a^{(m,n)}(t) \end{bmatrix}. \quad (5.10)$$

The steady-state frequency-domain equivalent of $\mathbf{A}(t)\mathbf{x}(t)$ is given by:

$$\mathcal{R}\{\mathbf{A}(t)\mathbf{x}(t)\} = \underline{\mathbf{A}}\underline{\mathbf{x}} \quad (5.11)$$

with

$$\underline{\mathbf{A}} \triangleq \begin{bmatrix} \mathcal{A}^{(1,1)} & \cdots & \mathcal{A}^{(1,n)} \\ \vdots & \ddots & \vdots \\ \mathcal{A}^{(m,1)} & \cdots & \mathcal{A}^{(m,n)} \end{bmatrix} \quad (5.12)$$

where $\mathcal{A}^{(i,j)}$ are Toeplitz matrices:

$$\mathcal{A}^{(i,j)} = \mathcal{T}\{a_k^{(i,j)} : k = -h, \dots, h\}. \quad (5.13)$$

Lastly, steady-state frequency-domain equivalents of time derivatives and time delays of periodic vectors are given by:

$$\mathcal{R}\{\dot{\mathbf{x}}(t)\} = \mathcal{N}_n \underline{\mathbf{x}} \quad (5.14a)$$

$$\mathcal{R}\{\mathbf{x}(t, \mathbf{t}_d)\} = \mathcal{E}_d(\mathbf{t}_d) \underline{\mathbf{x}} \quad (5.14b)$$

where \mathcal{N}_n is a diagonal matrix with n times matrix \mathcal{N} on its diagonal:

$$\mathcal{N}_n \triangleq \text{blkdiag}\{[\mathcal{N} \ \mathcal{N} \ \cdots \ \mathcal{N}]\}, \quad (5.15)$$

and where $\mathcal{E}_d(\mathbf{t}_d)$ is a diagonal matrix with d matrices $\mathcal{E}(t_{di})$ on its diagonal, thus covering the d delay values of vector \mathbf{t}_d :

$$\mathcal{E}_d(\mathbf{t}_d) \triangleq \text{blkdiag}\{[\mathcal{E}(t_{d1}) \ \mathcal{E}(t_{d2}) \ \cdots \ \mathcal{E}(t_{dd})]\}. \quad (5.16)$$

As pointed out, the above vector extension, which is valid in this chapter, differs slightly from the one used in Chapters 3 and 4 for the description of frequency-lifting methods. In Chapter 3 specifically, harmonic vectors were defined as vectors of Fourier coefficients, regardless of whether the coefficients were scalars or vectors. On the contrary, in this chapter, a harmonic vector is necessarily related to only one scalar variable; the extension to the vector case is done by stacking these harmonic vectors. Moreover, in Chapter 3, the

frequency-lifted counterparts of periodic matrices were block-Toeplitz matrices, whose block-elements were matrix Fourier coefficients. On the contrary, in this chapter, matrix $\underline{\mathbf{A}}$ in (5.12) does not have a block-Toeplitz structure, however its block-elements $\underline{\mathbf{A}}^{(i,j)}$ do have a Toeplitz structure.

It is worth noting that it is possible to switch from one stacking approach to the other with simple permutations of elements within the vectors, and with simple permutations of rows and columns within the matrices (i.e. by means of similarity transformations). In fact, both frequency-lifting in Chapter 3 and the developments in this chapter can be described with either of the two stacking approaches, and both approaches are commonly encountered in the literature. The choice of switching to a different notation in this chapter aims at simplifying practical implementations of the methods. Precisely, the approach in this chapter lends itself better to element-wise operations at the level of the scalar equations within a dynamic model, an advantage that will become clearer in the following sections.

5.3.2 Frequency-domain methods for linear and quadratic systems

Having described the mathematical operations on constant harmonic vectors, frequency-domain methods are described in this section for two simple categories of systems, namely linear and quadratic systems.

Linear systems

The following LTP system is considered:

$$\dot{\underline{\mathbf{x}}}(t) = \underline{\mathbf{A}}(t)\underline{\mathbf{x}}(t) + \underline{\mathbf{B}}(t)\underline{\mathbf{u}}(t). \quad (5.17)$$

Relying on the presented notation, the steady-state frequency-domain counterpart of this system of LTP differential equations is given by the following system of LTI algebraic equations:

$$\mathcal{N}_n \underline{\mathbf{x}} = \underline{\mathbf{A}}\underline{\mathbf{x}} + \underline{\mathbf{B}}\underline{\mathbf{u}}. \quad (5.18)$$

If the harmonic content of $\underline{\mathbf{A}}(t)$, $\underline{\mathbf{B}}(t)$ and $\underline{\mathbf{u}}(t)$ is known, their frequency-domain counterparts $\underline{\mathbf{A}}$, $\underline{\mathbf{B}}$ and $\underline{\mathbf{u}}$ are also known and the system can be solved for the unknown $\underline{\mathbf{x}}$, provided that $\underline{\mathbf{A}} - \mathcal{N}_n$ is invertible:

$$\underline{\mathbf{x}} = -(\underline{\mathbf{A}} - \mathcal{N}_n)^{-1}\underline{\mathbf{B}}\underline{\mathbf{u}}. \quad (5.19)$$

In references such as [109], this formulation is used to determine the variables of the open-loop MMC in steady state. For instance, considering the power stage model in (1.10), it is observed that (5.19) can indeed be applied if the insertion indices are seen as known time-periodic parameters given in matrices $\mathbf{A}(t)$ and $\mathbf{B}(t)$, instead of input variables. However, this approach does not reflect the fact that the insertion indices are themselves functions of the states. For sufficiently simple control structures, the insertion indices can be linear functions of the states, in which case the closed-loop MMC can be written as a quadratic system. Such systems are considered next.

Quadratic systems

The quadratic case is represented by a particular but simple example:

$$\dot{\mathbf{x}}(t) = \alpha \mathbf{x}(t) \odot \mathbf{x}(t) \quad (5.20)$$

where \odot refers to the element-wise product. The steady-state frequency-domain equivalent is given by:

$$\mathcal{N}_n \underline{\mathbf{x}} = \alpha \underline{\mathbf{X}} \underline{\mathbf{x}}. \quad (5.21)$$

This time, the system of algebraic equations is nonlinear with respect to the elements of the unknown $\underline{\mathbf{x}}$, which are also present in $\underline{\mathbf{X}}$. Consequently, the unknown vector cannot be isolated as in (5.19), and an RFA is used to solve the system.

In spite of their simplicity, the main disadvantage of frequency-domain formulations such as (5.18) and (5.21) is that nonlinear operations other than the (time-domain) product of variables cannot be described in a straightforward manner in terms of Fourier coefficients³. As mentioned in the previous section, a workaround to this limitation consists in opting for a hybrid-domain formulation. Since hybrid-domain methods rely not only on calculations in the frequency domain but also in the time domain, mathematical operations with sampled-time vectors are presented next.

5.3.3 Mathematical operations with sampled-time vectors

We consider the discretisation depicted in Fig. 5.1, where n_h time values t_l are uniformly distributed over the fundamental period:

$$t_l \triangleq \frac{(l-1)T_1}{n_h}, \quad l = 1, \dots, n_h. \quad (5.22)$$

³ Two notable exceptions to this observation are the (integer) powers of variables, obtained by successive applications of (5.5c), and the division by a variable, which can rely on inverting matrices $\underline{\mathbf{X}}$ or $\underline{\mathbf{Y}}$ in (5.5c).

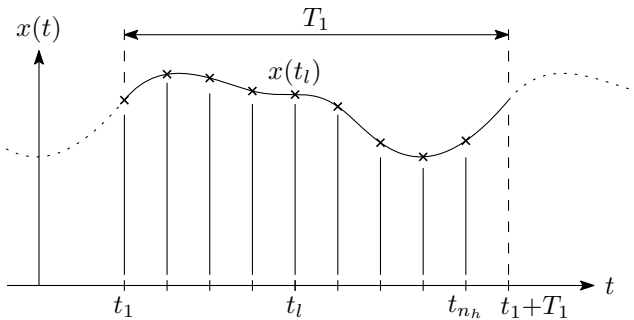


Figure 5.1: Time-domain sample points of a continuous periodic signal $x(t)$

The values of a signal $x(t)$ sampled at times t_l are noted $x_l = x(t_l)$. These sample points x_l are conveniently written as a vector referred to as a *sampled-time vector* and noted \mathbf{x} :

$$\mathcal{S}\{x(t)\} \triangleq \mathbf{x} \triangleq x(\mathbf{t}) = \begin{bmatrix} x(t_1) \\ x(t_2) \\ \vdots \\ x(t_{n_h}) \end{bmatrix}, \quad \text{with } \mathbf{t} \triangleq \begin{bmatrix} t_1 \\ t_2 \\ \vdots \\ t_{n_h} \end{bmatrix}, \quad (5.23)$$

where the operator \mathcal{S} indicates the action of writing $x(t)$ as a vector of its sample points.

Relationship between sample points and Fourier coefficients

Sample points x_l of a continuous periodic variable $x(t)$ are transformed into constant complex-valued Fourier coefficients x_k by means of the (direct) discrete Fourier transform (DFT). The inverse operation corresponds to the inverse discrete Fourier transform (IDFT). Possible formulations⁴ of the DFT and IDFT

⁴ In this thesis, the DFT and IDFT formulations are shuffled versions of those in [110, Ch.2]. Additionally, the normalisation by the number of elements n_h is done in the direct DFT instead of its inverse, in a way that the magnitude of the Fourier coefficients can be related to half the amplitude of the corresponding time-domain sinusoidal waveforms.

are respectively given by [110, Ch.2]:

$$x_k = \frac{1}{n_h} \sum_{l=1}^{n_h} x_l e^{-j2\pi k(l-1)/n_h}, \quad \forall k = -h, \dots, h \quad (5.24a)$$

$$x_l = \sum_{k=-h}^h x_k e^{j2\pi k(l-1)/n_h}, \quad \forall l = 1, \dots, n_h. \quad (5.24b)$$

Noting \mathcal{F} and \mathcal{F}^{-1} the DFT and IDFT, the relationship between sampled-time vectors and harmonic vectors is given by:

$$\boldsymbol{x} = \mathcal{F}\{\mathbf{x}\}, \quad \mathbf{x} = \mathcal{F}^{-1}\{\boldsymbol{x}\}. \quad (5.25)$$

Although DFTs are most efficiently carried out by means of Fast Fourier Transform algorithms [87, Ch.12], (5.24) can be written in matrix form:

$$\boldsymbol{x} = \mathcal{F}\{\mathbf{x}\} = \mathbf{M}\mathbf{x}, \quad \mathbf{x} = \mathcal{F}^{-1}\{\boldsymbol{x}\} = \mathbf{M}^{-1}\mathbf{x}, \quad (5.26)$$

with \mathbf{M} the DFT matrix (based on [110, Ch.2], however reshuffled and normalised to agree with (5.24)):

$$\mathbf{M} \triangleq \frac{1}{n_h} \begin{bmatrix} 1 & a^{-h} & \dots & a^{(n_h-2)(-h)} & a^{(n_h-1)(-h)} \\ 1 & a^{-h+1} & \dots & a^{(n_h-2)(-h+1)} & a^{(n_h-1)(-h+1)} \\ \vdots & \vdots & \ddots & \vdots & \vdots \\ 1 & a^{h-1} & \dots & a^{(n_h-2)(h-1)} & a^{(n_h-1)(h-1)} \\ 1 & a^h & \dots & a^{(n_h-2)(h)} & a^{(n_h-1)(h)} \end{bmatrix} \quad (5.27)$$

where $a = e^{-2\pi j/n_h}$.

It is noted that, according to the Nyquist–Shannon sampling theorem [87, Ch.12], $n_h = 2h + 1$ samples in the time domain are sufficient to preserve the frequency-content information up to harmonic rank h . Consequently, a sampled-time vector \mathbf{x} with a total of n_h sample points contains the same information regarding the harmonic content of periodic signal $x(t)$ as a harmonic vector \boldsymbol{x} with a total of n_h complex-valued Fourier coefficients (i.e. the average value, complex coefficients up to rank h and their complex conjugates).

Description of mathematical operations

In the time domain, the five types of operations previously introduced are applied to sampled-time vectors as follows:

$$\mathcal{S}\{\alpha x(t)\} = \alpha \mathbf{x} \quad (5.28a)$$

$$\mathcal{S}\{x(t) + y(t)\} = \mathbf{x} + \mathbf{y} \quad (5.28b)$$

$$\mathcal{S}\{x(t)y(t)\} = \mathbf{x} \odot \mathbf{y} \quad (5.28c)$$

$$\mathcal{S}\{\dot{x}(t)\} = \mathbf{N}\mathbf{x} \quad (5.28d)$$

$$\mathcal{S}\{x(t - t_d)\} = \mathbf{E}(t_d)\mathbf{x}, \quad (5.28e)$$

where $x(t)$ and $y(t)$ are once again periodic scalar signals, and \odot refers to the element-wise product.

In (5.28a), (5.28b) and (5.28c), the operations come down to an element-wise application on the elements of the sample-time vectors. More generally, any linear or nonlinear function f can be evaluated in an element-wise manner with respect to its arguments in the sampled-time framework:

$$\mathcal{S}\{f(x(t))\} = f(\mathbf{x}) = \begin{bmatrix} f(x(t_1)) \\ f(x(t_2)) \\ \vdots \\ f(x(t_{n_h})) \end{bmatrix}. \quad (5.29)$$

Some overloading of notation is involved since the dimension of the function is modified, however the same function notation is kept for simplicity.

In (5.28d) and (5.28e), matrices \mathbf{N} and $\mathbf{E}(t_d)$ are referred to as the Fourier differentiation and delay matrices, respectively. The reader is referred to [67, Ch.2] for more information on the Fourier differentiation matrix specifically. These matrices give the sampled-time vectors of the time derivative and time delay of $x(t)$. The following paragraphs are dedicated to providing an intuitive approach to the calculation of these matrices. Specifically, matrices \mathbf{N} and $\mathbf{E}(t_d)$ can be obtained by merging three steps into one:

- (i) First, the sampled-time vector \mathbf{x} is transformed into a harmonic vector \boldsymbol{x} , with the DFT matrix \mathbf{M} from (5.27):

$$\mathcal{R}\{x(t)\} = \mathbf{M}\mathcal{S}\{x(t)\} \iff \boldsymbol{x} = \mathbf{M}\mathbf{x}. \quad (5.30)$$

- (ii) Next, the harmonic vectors of the time derivatives and time delays are evaluated as in (5.5d) and (5.5e), repeated here for convenience:

$$\mathcal{R}\{\dot{x}(t)\} = \mathcal{N}\boldsymbol{x},$$

$$\mathcal{R}\{x(t - t_d)\} = \mathcal{E}(t_d)\boldsymbol{x}.$$

- (iii) Eventually, the results are transformed back into sampled-time vectors using the IDFT matrix \mathbf{M}^{-1} :

$$\mathcal{S}\{\dot{x}(t)\} = \mathbf{M}^{-1}\mathcal{R}\{\dot{x}(t)\}, \quad (5.32a)$$

$$\mathcal{S}\{x(t - t_d)\} = \mathbf{M}^{-1}\mathcal{R}\{x(t - t_d)\}. \quad (5.32b)$$

The three steps are combined to obtain the sampled-time vectors of time derivatives and time delays of $x(t)$:

$$\mathcal{S}\{\dot{x}(t)\} = \underbrace{\mathbf{M}^{-1}\mathcal{N}\mathbf{M}}_{\triangleq \mathcal{N}}\boldsymbol{x}, \quad (5.33a)$$

$$\mathcal{S}\{x(t - t_d)\} = \underbrace{\mathbf{M}^{-1}\mathcal{E}(t_d)\mathbf{M}}_{\triangleq \mathbf{E}(t_d)}\boldsymbol{x}. \quad (5.33b)$$

It is important to emphasise that the DFT and IDFT in steps (i) and (iii) are only made explicit in order to find expressions for matrices \mathcal{N} and $\mathbf{E}(t_d)$, but they become implicit within these matrices.

Just as for operations on harmonic vectors, it is convenient to introduce an extension of the sampled-time notation to the vector case, which is covered next.

Vector extension of the sampled-time notation

Considering once again $\boldsymbol{x}(t)$, a periodic vector of n scalar signals, the corresponding sampled-time object is obtained by stacking the sampled-time vectors $\mathbf{x}^{(i)}$ related to the scalar elements $x^{(i)}(t)$. The result is a vector of sampled-time vectors, noted with an underline:

$$\mathcal{S}\{\underline{\boldsymbol{x}}(t)\} \triangleq \underline{\mathbf{x}} \triangleq \begin{bmatrix} \mathcal{S}\{x^{(1)}(t)\} \\ \mathcal{S}\{x^{(2)}(t)\} \\ \vdots \\ \mathcal{S}\{x^{(n)}(t)\} \end{bmatrix} = \begin{bmatrix} \mathbf{x}^{(1)} \\ \mathbf{x}^{(2)} \\ \vdots \\ \mathbf{x}^{(n)} \end{bmatrix}. \quad (5.34)$$

Relying on (5.34), the multiplication by a scalar and the sum of periodic signals are easily generalised to the vector case. Next, the steady-state sampled-time equivalent of the product $\mathbf{A}(t)\mathbf{x}(t)$, with $\mathbf{A}(t)$ defined in (5.10), is given by:

$$\mathcal{S}\{\mathbf{A}(t)\mathbf{x}(t)\} = \underline{\mathbf{A}}\underline{\mathbf{x}} \quad (5.35)$$

with

$$\underline{\mathbf{A}} \triangleq \begin{bmatrix} \text{diag}\{\mathbf{a}^{(1,1)}\} & \cdots & \text{diag}\{\mathbf{a}^{(1,n)}\} \\ \vdots & \ddots & \vdots \\ \text{diag}\{\mathbf{a}^{(m,1)}\} & \cdots & \text{diag}\{\mathbf{a}^{(m,n)}\} \end{bmatrix} \quad (5.36)$$

where $\mathbf{a}^{(i,j)} = \mathcal{S}\{a^{(i,j)}(t)\}$, $i = 1, \dots, m$, $j = 1, \dots, n$. Furthermore, steady-state sampled-time equivalents of time derivatives and time delays of periodic vectors are given by:

$$\mathcal{S}\{\dot{\mathbf{x}}(t)\} = \mathbf{N}_n \underline{\mathbf{x}} \quad (5.37a)$$

$$\mathcal{S}\{\mathbf{x}(t, t_d)\} = \mathbf{E}_d(t_d) \underline{\mathbf{x}} \quad (5.37b)$$

where \mathbf{N}_n is a block-diagonal matrix with n times matrix \mathbf{N} on its diagonal:

$$\mathbf{N}_n \triangleq \text{blkdiag}\{[\mathbf{N} \quad \mathbf{N} \quad \cdots \quad \mathbf{N}]\}, \quad (5.38)$$

and where $\mathbf{E}_d(t_d)$ is a block-diagonal matrix with d matrices $\mathbf{E}(t_{di})$ on its diagonal, covering once again the d delay values of vector t_d :

$$\mathbf{E}_d(t_d) \triangleq \text{blkdiag}\{[\mathbf{E}(t_{d1}) \quad \mathbf{E}(t_{d2}) \quad \cdots \quad \mathbf{E}(t_{dd})]\}. \quad (5.39)$$

Lastly, the vector extension of relationship (5.26) between harmonic vectors and sampled-time vectors is given by:

$$\underline{\mathbf{x}} = \mathbf{M}_n \underline{\mathbf{x}}, \quad \underline{\mathbf{x}} = \mathbf{M}_n^{-1} \underline{\mathbf{x}}, \quad (5.40)$$

where \mathbf{M}_n is defined as a block matrix with n times the DFT matrix \mathbf{M} on its diagonal:

$$\mathbf{M}_n \triangleq \text{blkdiag}\{[\mathbf{M} \quad \mathbf{M} \quad \cdots \quad \mathbf{M}]\}. \quad (5.41)$$

Having described fundamental mathematical operations with sampled-time vectors, the hybrid-domain method is briefly described next.

5.3.4 Hybrid-domain method for nonlinear systems

The principle of hybrid-domain formulations consists in transforming the harmonic vectors into time-domain data to carry out the nonlinear operations,

and to transform the time-domain results back into the frequency domain, which is done by means of the DFT and IDFT.

For illustration purposes, the following system is considered:

$$\dot{\mathbf{x}}(t) = \mathbf{A}(t)\mathbf{x}(t) + \mathbf{B}(t)\mathbf{u}(t) + \mathbf{f}(\mathbf{x}(t), \mathbf{u}(t)) \quad (5.42)$$

where it is assumed that linear and nonlinear operations can be separated, i.e. \mathbf{f} temporarily contains only nonlinear operations.

In order to find the steady-state harmonic content of $\mathbf{x}(t)$, the time derivative and the linear part of the system are transformed into their steady-state frequency-domain counterparts as in (5.18). As far as the nonlinear part is concerned, the harmonic vectors \mathbf{x} and \mathbf{u} are first transformed into their sampled-time vectors $\underline{\mathbf{x}}$ and $\underline{\mathbf{u}}$ on which the nonlinear operations can be applied in an element-wise manner. The resulting sampled-time vector is transformed back into a harmonic vector. Equivalently, (5.42) becomes:

$$\mathcal{N}_n \underline{\mathbf{x}} = \underline{\mathbf{Ax}} + \underline{\mathbf{Bu}} + \mathcal{F}\{\mathbf{f}(\mathcal{F}^{-1}\{\underline{\mathbf{x}}\}, \mathcal{F}^{-1}\{\underline{\mathbf{u}}\})\} \quad (5.43a)$$

$$= \underline{\mathbf{Ax}} + \underline{\mathbf{Bu}} + \mathbf{M}_n \mathbf{f}(\mathbf{M}_n^{-1} \underline{\mathbf{x}}, \mathbf{M}_n^{-1} \underline{\mathbf{u}}). \quad (5.43b)$$

In the hybrid-domain formulation (5.43), the unknown $\underline{\mathbf{x}}$ cannot be isolated and the system must be solved iteratively with an RFA. The main disadvantage of hybrid-domain methods is the need for back-and-forth DFTs at every iteration step of the RFA. Consequently, the DFTs complicate practical implementations and increase their computational burden. A natural extension of the hybrid-domain method consists in bringing also the time derivatives and the linear operations into the time domain, thereby avoiding the need for DFTs altogether. This results in the Fourier-based collocation method, which is presented in the next section.

5.4 Fourier-based collocation method

This section is dedicated to presenting the Fourier-based collocation method for periodic trajectories calculations. Discussed for instance in [67, Ch.2] and [111] in the case of non-delayed systems, it is presented here for nonlinear delayed systems in state-space form:

$$\begin{cases} \dot{\mathbf{x}}(t) = \mathbf{f}(t, \mathbf{x}(t), \mathbf{u}(t), \mathbf{w}(t)) \\ \mathbf{z}(t) = \mathbf{g}(t, \mathbf{x}(t), \mathbf{u}(t), \mathbf{w}(t)) \\ \mathbf{w}(t) = \mathbf{z}(t, t_d). \end{cases} \quad (5.44)$$

Noting $\underline{\mathbf{x}} = \mathcal{S}\{\mathbf{x}(t)\}$, $\underline{\mathbf{u}} = \mathcal{S}\{\mathbf{u}(t)\}$, $\underline{\mathbf{z}} = \mathcal{S}\{\mathbf{z}(t)\}$ and $\underline{\mathbf{w}} = \mathcal{S}\{\mathbf{w}(t)\}$, the steady-state sampled-time equivalent of (5.44) is obtained by application of (5.28d), (5.28e) and (5.29):

$$\begin{cases} \mathbf{N}_n \underline{\mathbf{x}} = \mathbf{f}(\mathbf{t}, \underline{\mathbf{x}}, \underline{\mathbf{u}}, \underline{\mathbf{w}}) \\ \underline{\mathbf{z}} = \mathbf{g}(\mathbf{t}, \underline{\mathbf{x}}, \underline{\mathbf{u}}, \underline{\mathbf{w}}) \\ \underline{\mathbf{w}} = \mathbf{E}_d(\mathbf{t}_d) \underline{\mathbf{z}}, \end{cases} \quad (5.45)$$

with \mathbf{t} as defined in (5.23). In (5.45), matrices \mathbf{N}_n and $\mathbf{E}_d(\mathbf{t}_d)$ are especially useful as they enable the evaluation of time derivatives and time delays of periodic variables directly in the time domain, without explicitly involving harmonic vectors as in the frequency-domain and hybrid-domain formulations. Eliminating the intermediate variable $\underline{\mathbf{z}}$ gives⁵:

$$\begin{cases} \mathbf{N}_n \underline{\mathbf{x}} = \mathbf{f}(\underline{\mathbf{x}}, \underline{\mathbf{u}}, \underline{\mathbf{w}}) \\ \mathbf{E}_d(-\mathbf{t}_d) \underline{\mathbf{w}} = \mathbf{g}(\underline{\mathbf{x}}, \underline{\mathbf{u}}, \underline{\mathbf{w}}), \end{cases} \quad (5.46)$$

where we used the fact that $\mathbf{E}_d^{-1}(\mathbf{t}_d) = \mathbf{E}_d(-\mathbf{t}_d)$, and where the time-dependency of \mathbf{f} and \mathbf{g} has been dropped to keep the notation simple throughout the remainder of this chapter. However, the generalisation of the approach to NTP systems is straightforward as it simply consists in replacing all time-periodic parameters with their sampled-time vectors, as done for the time-periodic variables of the system.

To facilitate practical implementations and further simplify the notation, the unknown vectors $\mathbf{x}(t)$ and $\mathbf{w}(t)$ are stacked together in an extended unknown vector $\boldsymbol{\xi}(t)$ of size $n + d$ with corresponding sampled-time vector $\underline{\boldsymbol{\xi}} = \mathcal{S}\{\boldsymbol{\xi}(t)\}$:

$$\boldsymbol{\xi}(t) \triangleq \begin{bmatrix} \mathbf{x}(t) \\ \mathbf{w}(t) \end{bmatrix} \implies \underline{\boldsymbol{\xi}} = \begin{bmatrix} \underline{\mathbf{x}} \\ \underline{\mathbf{w}} \end{bmatrix}. \quad (5.47a)$$

Likewise, an extended function λ brings functions \mathbf{f} and \mathbf{g} together:

$$\lambda(\boldsymbol{\xi}(t), \mathbf{u}(t)) \triangleq \begin{bmatrix} \mathbf{f}(\mathbf{x}(t), \mathbf{u}(t), \mathbf{w}(t)) \\ \mathbf{g}(\mathbf{x}(t), \mathbf{u}(t), \mathbf{w}(t)) \end{bmatrix} \implies \lambda(\underline{\boldsymbol{\xi}}, \underline{\mathbf{u}}) = \begin{bmatrix} \mathbf{f}(\underline{\mathbf{x}}, \underline{\mathbf{u}}, \underline{\mathbf{w}}) \\ \mathbf{g}(\underline{\mathbf{x}}, \underline{\mathbf{u}}, \underline{\mathbf{w}}) \end{bmatrix}. \quad (5.48a)$$

Lastly, matrix \mathbf{P} is defined as:

$$\mathbf{P} \triangleq \begin{bmatrix} \mathbf{N}_n & \\ & \mathbf{E}_d(-\mathbf{t}_d) \end{bmatrix}. \quad (5.49)$$

⁵ The delayed variables $\underline{\mathbf{w}}$ are also intermediate variables and could be eliminated too. In this thesis, it is chosen to keep the system as presented in (5.46), as this allows for a more structured approach to the calculation of its Jacobian.

System (5.46) simply becomes:

$$\mathbf{P}\underline{\xi} = \lambda(\underline{\xi}, \underline{\mathbf{u}}). \quad (5.50)$$

This system consists of nonlinear algebraic equations and constitutes the proposed Fourier-based collocation formulation, which can be solved for the extended unknown sampled-time vector $\underline{\xi}$ by means of an RFA. To this end, a residual function $\Delta(\underline{\xi}, \underline{\mathbf{u}})$ is defined as the difference between left and right sides of (5.50):

$$\Delta(\underline{\xi}, \underline{\mathbf{u}}) \triangleq \lambda(\underline{\xi}, \underline{\mathbf{u}}) - \mathbf{P}\underline{\xi}. \quad (5.51)$$

The objective of the RFA is thus to find the roots of $\Delta(\underline{\xi}, \underline{\mathbf{u}})$, i.e. the unknowns $\underline{\xi}$ such that $\Delta(\underline{\xi}, \underline{\mathbf{u}}) = \mathbf{0}$. Noting $\underline{\xi}_{[k]}$ an approximation of the solution at the k^{th} iteration step, the next approximation according to, for instance, Newton's method [87, Ch.9], is obtained as:

$$\underline{\xi}_{[k+1]} = \underline{\xi}_{[k]} - \mathbf{J}^{-1}(\underline{\xi}_{[k]}, \underline{\mathbf{u}})\Delta(\underline{\xi}_{[k]}, \underline{\mathbf{u}}), \quad (5.52)$$

where \mathbf{J} is the Jacobian of Δ . Its calculation is detailed in the following paragraphs.

Jacobian calculation for Newton-based RFAs

For systems whose nonlinear functions are continuously differentiable, the Jacobian \mathbf{J} of Δ is given by:

$$\mathbf{J}(\underline{\xi}, \underline{\mathbf{u}}) = \frac{\partial \Delta}{\partial \underline{\xi}}(\underline{\xi}, \underline{\mathbf{u}}) = \frac{\partial \lambda}{\partial \underline{\xi}}(\underline{\xi}, \underline{\mathbf{u}}) - \mathbf{P}, \quad (5.53)$$

or *in extenso*,

$$\mathbf{J}(\underline{\mathbf{x}}, \underline{\mathbf{u}}, \underline{\mathbf{w}}) = \begin{bmatrix} \frac{\partial \mathbf{f}}{\partial \underline{\mathbf{x}}}(\underline{\mathbf{x}}, \underline{\mathbf{u}}, \underline{\mathbf{w}}) - \mathbf{N}_n & \frac{\partial \mathbf{f}}{\partial \underline{\mathbf{w}}}(\underline{\mathbf{x}}, \underline{\mathbf{u}}, \underline{\mathbf{w}}) \\ \frac{\partial \mathbf{g}}{\partial \underline{\mathbf{x}}}(\underline{\mathbf{x}}, \underline{\mathbf{u}}, \underline{\mathbf{w}}) & \frac{\partial \mathbf{g}}{\partial \underline{\mathbf{w}}}(\underline{\mathbf{x}}, \underline{\mathbf{u}}, \underline{\mathbf{w}}) - \mathbf{E}_d(-\mathbf{t}_d) \end{bmatrix}. \quad (5.54)$$

In (5.53), matrix \mathbf{P} does not depend on the value of $\underline{\xi}$ and can be defined numerically for an arbitrary maximum harmonic rank prior to solving the system. This is done relying on (5.38) and (5.39).

On the other hand, matrix $\frac{\partial \lambda}{\partial \underline{\xi}}(\underline{\xi}, \underline{u})$ is obtained by considering the following relationship:

$$\frac{\partial \lambda}{\partial \underline{\xi}}(\underline{\xi}, \underline{u}) \underline{\xi} = \mathcal{S} \left\{ \frac{\partial \lambda}{\partial \underline{\xi}}(\underline{\xi}(t), \underline{u}(t)) \underline{\xi}(t) \right\} \quad (5.55a)$$

\iff

$$\begin{bmatrix} \frac{\partial f}{\partial \underline{x}}(\underline{\xi}, \underline{u}) & \frac{\partial f}{\partial \underline{w}}(\underline{\xi}, \underline{u}) \\ \frac{\partial g}{\partial \underline{x}}(\underline{\xi}, \underline{u}) & \frac{\partial g}{\partial \underline{w}}(\underline{\xi}, \underline{u}) \end{bmatrix} \underline{\xi} = \mathcal{S} \left\{ \begin{bmatrix} \frac{\partial f}{\partial \underline{x}}(\underline{\xi}(t), \underline{u}(t)) & \frac{\partial f}{\partial \underline{w}}(\underline{\xi}(t), \underline{u}(t)) \\ \frac{\partial g}{\partial \underline{x}}(\underline{\xi}(t), \underline{u}(t)) & \frac{\partial g}{\partial \underline{w}}(\underline{\xi}(t), \underline{u}(t)) \end{bmatrix} \underline{\xi}(t) \right\}. \quad (5.55b)$$

By analogy with (5.35) and (5.36), we have:

$$\frac{\partial f}{\partial \underline{x}}(\underline{\xi}, \underline{u}) = \begin{bmatrix} \text{diag} \left\{ \mathcal{S} \left\{ \frac{\partial f^{(1)}}{\partial x^{(1)}}(\underline{\xi}(t), \underline{u}(t)) \right\} \right\} & \cdots & \text{diag} \left\{ \mathcal{S} \left\{ \frac{\partial f^{(1)}}{\partial x^{(n)}}(\underline{\xi}(t), \underline{u}(t)) \right\} \right\} \\ \vdots & \ddots & \vdots \\ \text{diag} \left\{ \mathcal{S} \left\{ \frac{\partial f^{(n)}}{\partial x^{(1)}}(\underline{\xi}(t), \underline{u}(t)) \right\} \right\} & \cdots & \text{diag} \left\{ \mathcal{S} \left\{ \frac{\partial f^{(n)}}{\partial x^{(n)}}(\underline{\xi}(t), \underline{u}(t)) \right\} \right\} \end{bmatrix}, \quad (5.56)$$

and likewise for the other partial derivatives. Further on, the transformation of each scalar partial derivative $\frac{\partial f^{(i)}}{\partial x^{(j)}}$ into its corresponding sampled-time vector comes down to an element-wise numerical evaluation of the derivative at point $(\underline{\xi}, \underline{u})$, in agreement with (5.29):

$$\mathcal{S} \left\{ \frac{\partial f^{(i)}}{\partial x^{(j)}}(\underline{\xi}(t), \underline{u}(t)) \right\} = \frac{\partial f^{(i)}}{\partial x^{(j)}}(\underline{\xi}, \underline{u}), \quad \forall i, j = 1, \dots, n. \quad (5.57)$$

To keep the computational burden low, all partial derivatives can be calculated analytically prior to solving the system numerically, for instance by means of symbolic calculations.

As an alternative to the numerical evaluation of an analytically-precalculated Jacobian, most readily available RFAs also implement numerical differentiation to obtain the Jacobian matrix based on e.g. forward or centred finite differences [87, Ch.5]. While the symbolic Jacobian calculation may be computationally expensive for large systems, its numerical evaluation is generally more accurate

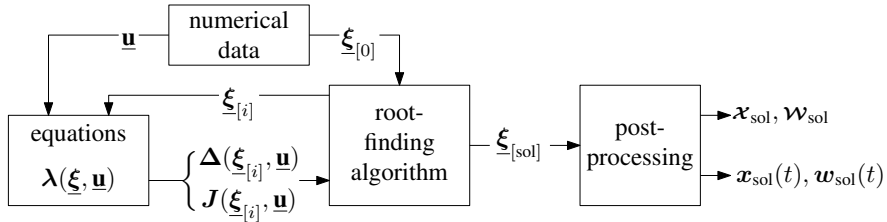


Figure 5.2: Structure of the algorithm

than the result of numerical differentiation, hence it is the preferred option when the system is available in analytical form, which is assumed to be the case in this chapter.

Algorithm

An algorithm dedicated to practical implementations of the Fourier-based collocation method is sketched in Fig. 5.2 and is decomposed into five steps:

1. Defining the equations

The first step consists in defining the differential equations in (5.44). Functions \mathbf{f} and \mathbf{g} are established, which gives the residual Δ in analytical form. The partial derivatives within Jacobian \mathbf{J} are precalculated analytically and matrices \mathbf{N}_n and $\mathbf{E}_d(-\mathbf{t}_d)$ are precalculated numerically for a chosen maximum harmonic rank h .

2. Initialising the inputs

The second step consists in defining the input values $\mathbf{u}^{(i)}$ within $\underline{\mathbf{u}}$:

$$\mathbf{u}^{(i)} = \mathbf{u}^{(i)}(\mathbf{t}) \quad \forall i = 1, \dots, m, \quad (5.58)$$

with \mathbf{t} defined in (5.23). Alternatively, $\mathbf{u}^{(i)}$ can be obtained from the harmonic content of $u^{(i)}(t)$, i.e. by applying the IDFT to its harmonic vector:

$$\mathbf{u}^{(i)} = \mathcal{F}^{-1}\{\mathbf{u}^{(i)}\}. \quad (5.59)$$

3. Initialising the unknowns

The third step consists in defining the initial values $\mathbf{x}_{[0]}^{(i)}$ and $\mathbf{w}_{[0]}^{(j)}$ within $\underline{\xi}_{[0]}$:

$$\mathbf{x}_{[0]}^{(i)} = \mathbf{x}_{\text{guess}}^{(i)}(\mathbf{t}), \quad \forall i = 1, \dots, n, \quad (5.60a)$$

$$\mathbf{w}_{[0]}^{(j)} = \mathbf{w}_{\text{guess}}^{(j)}(\mathbf{t}), \quad \forall j = 1, \dots, d, \quad (5.60b)$$

with $x_{\text{guess}}^{(i)}(t)$ and $w_{\text{guess}}^{(j)}(t)$ initial guesses. Alternatively, $\mathbf{x}^{(i)}$ and $\mathbf{w}^{(j)}$ can be obtained from the harmonic content of $x_{\text{guess}}^{(i)}(t)$ and $w_{\text{guess}}^{(j)}(t)$:

$$\mathbf{x}_{[0]}^{(i)} = \mathcal{F}^{-1}\{\boldsymbol{\chi}_{\text{guess}}^{(i)}\}, \quad (5.61\text{a})$$

$$\mathbf{w}_{[0]}^{(j)} = \mathcal{F}^{-1}\{\boldsymbol{\omega}_{\text{guess}}^{(j)}\}. \quad (5.61\text{b})$$

4. Solving for the unknowns

The fourth step consists in running the RFA to solve system (5.50). At each iteration step, the residual vector $\Delta(\underline{\xi}_{[k]}, \underline{\mathbf{u}})$ and the Jacobian matrix $\mathbf{J}(\underline{\xi}_{[k]}, \underline{\mathbf{u}})$ are evaluated and the next value $\underline{\xi}_{[k+1]}$ is calculated until convergence is reached, i.e. until the residual vector is sufficiently close to $\mathbf{0}$, or until a maximum number of iterations has been reached. If the solver has converged, the value of $\underline{\xi}_{[k+1]}$ at the last iteration is the solution of the problem and is noted $\underline{\xi}_{[\text{sol}]}$. This solution corresponds the sought periodic trajectory, of which it contains frequency content up to the chosen maximum harmonic rank h .

5. Post-processing

The last step consists in transforming the resulting sampled-time vectors $\mathbf{x}_{[\text{sol}]}^{(i)}$ and $\mathbf{w}_{[\text{sol}]}^{(j)}$ into harmonic vectors, thereby obtaining the harmonic content of each state and delayed variable:

$$\boldsymbol{\chi}_{\text{sol}}^{(i)} = \mathcal{F}\{\mathbf{x}_{[\text{sol}]}^{(i)}\}, \quad \forall i = 1, \dots, n, \quad (5.62\text{a})$$

$$\boldsymbol{\omega}_{\text{sol}}^{(j)} = \mathcal{F}\{\mathbf{w}_{[\text{sol}]}^{(j)}\}, \quad \forall j = 1, \dots, d. \quad (5.62\text{b})$$

For waveforms visualisation, time-domain vectors can be retrieved with a higher sampling frequency by evaluation of the Fourier series (3.4).

It is emphasised that the DFT and IDFT only appear in the initialisation steps 2 and 3, where they are optional, and in the post-processing step 5, but not at every iteration of the RFA in step 4.

Characteristics of the method

1. The presented approach is a collocation method in the sense that it consists in enforcing that the differential equations be satisfied over a discrete grid of time points. The underlying interpolation functions are truncated Fourier series, which allow defining expressions for the time derivatives and time delays. However, the interpolation functions do not appear

explicitly in the formulation, which gives the method its simplicity. In particular, the cumbersome analytical manipulations often proposed for the MMC in the literature are discarded, which simplifies the approach.

2. Being defined in the time domain, the element-wise application of mathematical operations to the sampled-time vectors allows for a straightforward account of other types of nonlinearities than the product of variables, such as divisions and trigonometric operations. Additionally, the proposed formulation treats both linear and nonlinear operations within function λ in the same way, thereby avoiding a partition of the equations into two different sets, as customarily done in hybrid-domain methods.
3. The formulation accounts for exact time delays, and no approximation of the DDEs by ODEs is needed.
4. The choice of relying on evenly-spaced time points in (5.22) is justified by the intention of using the method for the calculation of periodic solutions. Convergence properties of the Fourier-based collocation method are available in e.g. [97, Ch.4].
5. Aside from the chosen maximum harmonic rank h , no assumption is made on the unknown harmonic content *a priori*, and the maximum harmonic rank h can be set and changed arbitrarily in a practical implementation.
6. Aside from a sufficient smoothness of the nonlinear operations, no assumption is made on the physical nature of the initial differential equations in (5.44). In the case of the closed-loop MMC model, no distinction is thus needed nor made between circuit and control dynamics. Consequently, control equations are included in a seamless way, which allows assessing the impact that different control strategies may have on the actual steady-state behaviour of the converter. When opting for a new control strategy, functions f and g are modified as needed and Jacobian J is updated accordingly.
7. Just as for frequency-lifting, but unlike most methods that have been applied to the MMC in the literature, the absence of assumptions on the physical nature of the differential equations allows applying the method to various types of dynamic systems (balanced and unbalanced circuits, single-phase or multi-phase systems, AC or DC networks,...).
8. The method benefits from a low computational burden by avoiding the integration of the differential equations as well as back-and-forth DFTs at each iteration step of the RFA. Being integration-free, the method is capable of solving for both stable and unstable trajectories.

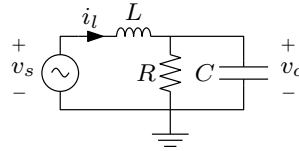


Figure 5.3: Simple RLC circuit diagram

9. Despite matrices \mathbf{M} , \mathbf{N} and $\mathcal{E}(t_d)$ being complex-valued, the resulting matrices \mathbf{N} and $\mathbf{E}(t_d)$ are real-valued. Consequently, the proposed method has the advantage of being naturally real-valued and its algebraic equations can be solved with commonly available RFAs.
10. Unlike the calculation of the characteristic roots of delayed systems in Section 4.4, which relied on the assumption that none of the delayed variables are functions of other delayed variables (Assumption 12), the proposed Fourier-based collocation method is also capable of solving for trajectories of systems whose delayed variables are themselves functions of delayed variables.
11. The Fourier-based collocation method is said to be *spectral*, in the sense that the basis functions are global [97, Ch.1] or, in other words, that the complex exponentials in the Fourier-series used as interpolation functions are non-zero over the complete interval under consideration (except at isolated points).

5.5 Validation and numerical applications

5.5.1 Application to a simple RLC circuit

While the developed approach has the capability to target elaborate nonlinear delayed systems, its working principle is first made clear by applying the steps of the procedure to a simple example. A basic RLC circuit is considered and displayed in Fig 5.3, with $L = 1$ H, $C = 10^{-3}$ F and $R = 0.8$ Ω.

1. Defining the equations

The set of differential equations is given by

$$\begin{cases} \frac{di_l}{dt} = -\frac{1}{L}v_c + \frac{1}{L}v_s \\ \frac{dv_c}{dt} = \frac{1}{C}i_l - \frac{1}{RC}v_c. \end{cases} \quad (5.63)$$

The states are the inductor current i_l and capacitor voltage v_c ($n = 2$), the input is the source voltage v_s ($m = 1$). We are interested in the steady-state solution of the system when the excitation contains both constant and fundamental-frequency components:

$$v_s(t) = v_0 + v_1 \sin(\omega_1 t). \quad (5.64)$$

We take the fundamental frequency equal to 1 Hz, so $\omega_1 = 2\pi$ rad/s. The system being linear and free of delays ($d = 0$), it is easily solved by application of the Laplace transform and the superposition principle. Yet, for the sake of illustration, it is now solved numerically by means of the collocation method.

Assuming that harmonic components up to rank $h = 1$ are of interest, the solution will comprise both constant and fundamental components. With $n_h = 2h + 1 = 3$, the matrices related to time derivation are

$$\mathcal{N} = \begin{bmatrix} -2\pi j & & \\ & 0 & \\ & & 2\pi j \end{bmatrix}, \quad (5.65a)$$

$$\mathbf{M} = \begin{bmatrix} 1 & e^{2\pi j/3} & e^{4\pi j/3} \\ 1 & 1 & 1 \\ 1 & e^{-2\pi j/3} & e^{-4\pi j/3} \end{bmatrix}, \quad (5.65b)$$

$$\mathbf{N} = \begin{bmatrix} 0 & 3.6275... & -3.6275... \\ -3.6275... & 0 & 3.6275... \\ 3.6275... & -3.6275... & 0 \end{bmatrix} \quad (5.65c)$$

where \mathbf{N} is obtained numerically. The matrices related to time delays are not needed in this example. The time points are:

$$\mathbf{t} = [0T_1/n_h \quad 1T_1/n_h \quad 2T_1/n_h]^T = [0 \quad 1/3 \quad 2/3]^T. \quad (5.66)$$

The input vector has size $m \cdot n_h = 3$:

$$\underline{\mathbf{u}} = \mathbf{v}_s = [v_s(t_1) \quad v_s(t_2) \quad v_s(t_3)]^T. \quad (5.67)$$

The unknown vector has size $(n + d) \cdot n_h = 6$:

$$\underline{\xi} = \underline{\mathbf{x}} = [\mathbf{i}_l^T \quad \mathbf{v}_c^T]^T \quad (5.68a)$$

$$= [i_l(t_1) \quad i_l(t_2) \quad i_l(t_3) \quad v_c(t_1) \quad v_c(t_2) \quad v_c(t_3)]^T. \quad (5.68b)$$

The function set λ , mismatch Δ and Jacobian J are given by:

$$\lambda(\underline{\xi}, \underline{u}) = \begin{bmatrix} -\frac{1}{L}\mathbf{v}_c + \frac{1}{L}\mathbf{v}_s \\ \frac{1}{C}\mathbf{i}_l - \frac{1}{RC}\mathbf{v}_c \end{bmatrix}, \quad (5.69)$$

$$\Delta(\underline{\xi}, \underline{u}) = \begin{bmatrix} -\frac{1}{L}\mathbf{v}_c + \frac{1}{L}\mathbf{v}_s - N\mathbf{i}_l \\ \frac{1}{C}\mathbf{i}_l - \frac{1}{RC}\mathbf{v}_c - N\mathbf{v}_c \end{bmatrix}, \quad (5.70)$$

$$J(\underline{\xi}, \underline{u}) = \begin{bmatrix} -N & -\frac{1}{L}\mathbf{I}_{n_h} \\ \frac{1}{C}\mathbf{I}_{n_h} & -\frac{1}{RC}\mathbf{I}_{n_h} - N \end{bmatrix} \quad (5.71)$$

where \mathbf{I}_{n_h} is the identity matrix of dimension n_h .

2. Initialising the inputs

Taking $v_0 = 1$ and $v_1 = 0.5$, the sampled-time input vector is given by:

$$v_s(t) = \begin{bmatrix} v_0 + v_1 \sin(0\pi/3) \\ v_0 + v_1 \sin(2\pi/3) \\ v_0 + v_1 \sin(4\pi/3) \end{bmatrix} \approx \begin{bmatrix} 1 \\ 1.4330 \\ 0.5670 \end{bmatrix} \quad (5.72)$$

with corresponding harmonic vector:

$$\mathbf{v}_s = \begin{bmatrix} v_{s,-1} \\ v_{s,0} \\ v_{s,1} \end{bmatrix} = \begin{bmatrix} 0.25j \\ 1 \\ -0.25j \end{bmatrix}. \quad (5.73)$$

3. Initialising the unknowns

Any vector of complex values would normally be suitable as initial guess, although initial vectors close to the expected solution will generally reduce the required number of iterations and thus the computation time. Here, we take $\underline{\xi}_{[0]} = \mathbf{0}$ for simplicity.

4. Solving for the unknowns

For this simple system, two iterations of Newton's method are enough for convergence to the resulting sampled-time vectors:

$$\mathbf{i}_{l,[\text{sol}]} = \begin{bmatrix} 1.1716 \\ 1.2978 \\ 1.2805 \end{bmatrix}, \quad \mathbf{v}_{c,[\text{sol}]} = \begin{bmatrix} 0.9373 \\ 1.0380 \\ 1.0247 \end{bmatrix}. \quad (5.74)$$

5. Post-processing

The IDFT delivers the harmonic vectors of the two states:

$$\boldsymbol{x}_{l,\text{sol}} = \begin{bmatrix} -0.0392 + 0.005j \\ 1.25 \\ -0.0392 - 0.005j \end{bmatrix}, \quad \boldsymbol{v}_{c,\text{sol}} = \begin{bmatrix} -0.0314 + 0.0038j \\ 1 \\ -0.0314 - 0.0038j \end{bmatrix}. \quad (5.75)$$

Analytically, the transfer functions of the RLC circuit are obtained as:

$$i_l(s) = H_1(s)v_s(s), \quad \text{with} \quad H_1(s) = \frac{sC + \frac{1}{R}}{s^2LC + s\frac{L}{R} + 1} \quad (5.76a)$$

$$v_c(s) = H_2(s)v_s(s), \quad \text{with} \quad H_2(s) = \frac{1}{s^2LC + s\frac{L}{R} + 1}. \quad (5.76b)$$

The following evaluations validate the results in (5.75):

$$i_{l,-1} = H_1(-2\pi j)v_{s,-1} = -0.0392 + 0.005j \quad (5.77a)$$

$$i_{l,0} = H_1(0)v_{s,0} = 1.25 \quad (5.77b)$$

$$i_{l,1} = H_1(2\pi j)v_{s,1} = -0.0392 - 0.005j \quad (5.77c)$$

$$v_{c,-1} = H_2(-2\pi j)v_{s,-1} = -0.0314 + 0.0038j \quad (5.77d)$$

$$v_{c,0} = H_2(0)v_{s,0} = 1 \quad (5.77e)$$

$$v_{c,1} = H_2(2\pi j)v_{s,1} = -0.0314 - 0.0038j. \quad (5.77f)$$

Having shown the applicability of the collocation method to a very simple circuit, the next section is dedicated to applying it to the MMC.

5.5.2 Application to the MMC

The collocation method is applied to the complete three-phase closed-loop MMC model presented in Section 1.2.

Validation against numerical integration

In this section, the capability of the collocation method to provide the steady-state periodic trajectories of the MMC is validated by comparing its results with those of an independent approach, specifically the numerical integration method, applied to the same sets of equations with the same numerical parameters.

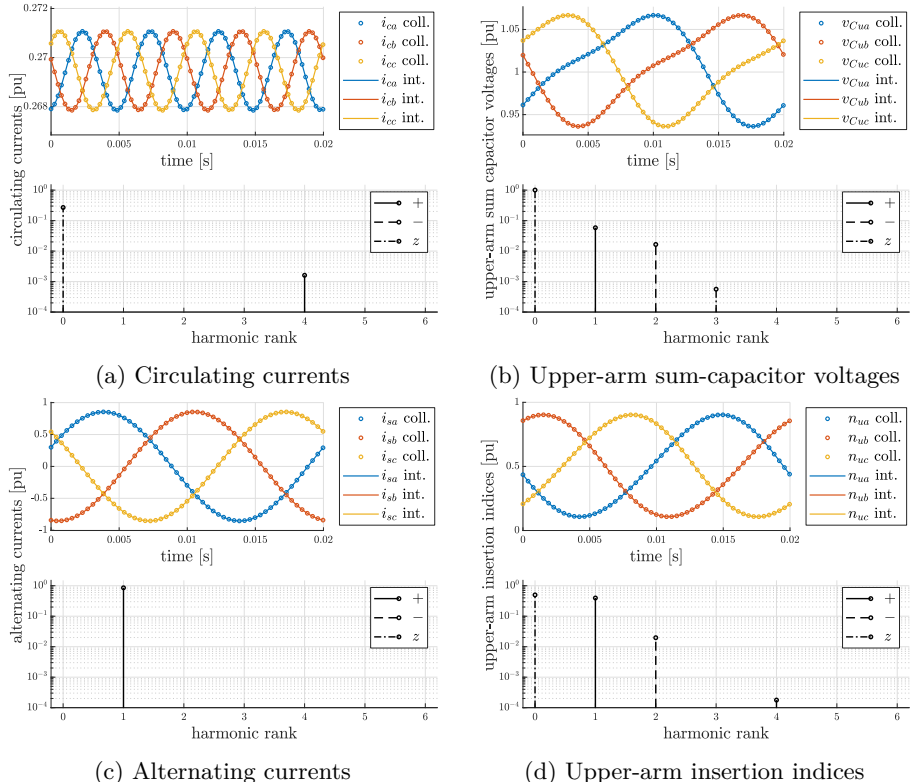


Figure 5.4: Comparison of collocation (coll.) and integration (int.) waveforms, along with the sequence-harmonic spectra of the collocation results

For the time-domain integration, the differential equations are solved with the `ode15s` and `dde23` solvers for the non-delayed and delayed cases, respectively, with both relative and absolute tolerances set to 10^{-9} . The integration lasts until a steady-state is reached.

For the collocation method, system (5.50) is solved with the Levenberg-Marquardt RFA [112] available in Matlab's Optimization Toolbox via the `fsolve` function, of which both function and step tolerances are set to 10^{-9} .

Fig. 5.4 presents a comparison between the waveforms obtained with the collocation method (run with maximum harmonic rank $h = 12$) and the integration method. Qualitatively, a visual inspection of the waveforms shows a nearly-perfect match between the two results.

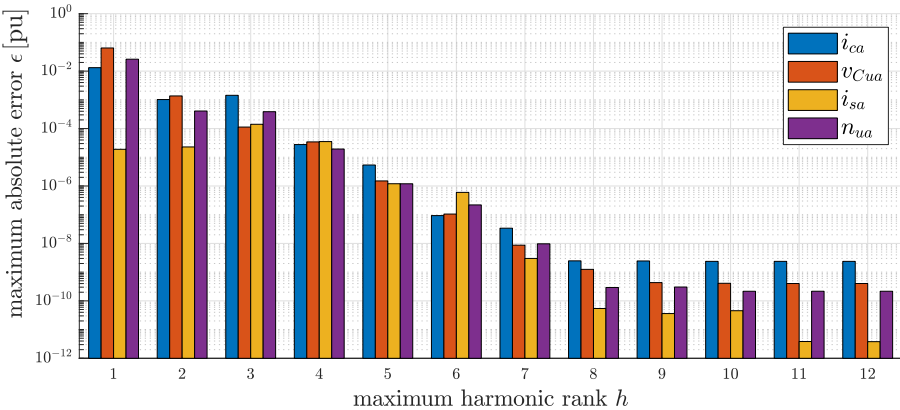


Figure 5.5: Comparison of collocation and numerical integration methods: Evolution of maximum absolute error with increasing maximum harmonic rank

The maximum element-wise absolute error ε is used to quantify the difference between the time-domain waveforms corresponding to the solutions of the integration method (\mathbf{x}_s) and the collocation method (\mathbf{x}_c), respectively:

$$\varepsilon \triangleq \max(|\mathbf{x}_c - \mathbf{x}_s|). \quad (5.78)$$

The results are given in Fig. 5.5 for the circulating currents, the upper-arm sum-capacitor voltages, the alternating currents and the upper-arm insertion indices in phase a . It is emphasised that the figure does not display the spectrum of the error for each harmonic rank, but the evolution of the time-domain error as the maximum harmonic rank h of the collocation method is increased.

Specifically, it is observed that increasing the maximum harmonic rank leads to a reduction of the error with respect to the results of the numerical integration used as reference. For the particular case under study, a maximum harmonic rank $h = 6$ leads to a maximum absolute error of about 10^{-6} pu among the considered variables. Beyond $h = 8$, the error falls below 10^{-8} pu for the tested variables and does not decrease significantly anymore in this specific case.

Comparison of calculation times

This subsection is dedicated to comparing the calculation times of the simple numerical integration method, the shooting method described in [51], and the presented Fourier-based collocation method. For a fair comparison, the non-delayed case ($t_d = 0$) is considered and all solvers start from the same initial guess.

| | trajectory | stable | unstable | unstable |
|--|------------|-------------|-------------|-------------|
| $\max_i(\text{Re}\{\lambda_i\})$ [rad/s] | | -5.83 | +4.51 | +1114.60 |
| integration method | | 70 – 80 s | ∞ | ∞ |
| shooting method | | 100 – 110 s | 110 – 120 s | ∞ |
| collocation method | | 0.1 – 0.3 s | 1.1 – 1.3 s | 1.1 – 1.3 s |

Table 5.2: Indicative calculation times of time-domain methods

Three trajectories are considered. Firstly, relying on the circuit and control parameters in Appendix B.2, a stable trajectory is determined. Secondly, the bandwidth of the alternating current control loop is reduced from 150 Hz to 10 Hz to obtain an unstable trajectory with slowly growing oscillations. Thirdly, an unstable periodic trajectory with quickly growing oscillations is obtained by purposely multiplying the PR parameters of the alternating current controller by -1. Even though unrealistic, this case aims to further compare the capabilities of the different methods. For the two unstable trajectories, the real parts of the most dominant eigenvalues are respectively equal to +4.51 rad/s and +1114.60 rad/s, as also indicated in Table 5.2.

All calculations are run on the same laptop with an Intel Core i7-8650U CPU (1.90 GHz, 4 cores), with Matlab R2021b. For the shooting method, a two-point scheme is used for the stable case and the first unstable case, and a 50-point scheme is used for the second unstable case.

The results are provided in Table 5.2 and show that the collocation method is significantly faster than the simple numerical integration method and the shooting method. The shooting method shows particularly poor performance for the studied system with the chosen initial guess and the requested accuracy, as it is slower than the numerical integration method in the stable case. The collocation method is capable of solving for both stable and unstable trajectories, while the shooting method is only able to find the stable and first unstable trajectories. Naturally, the simple integration method does not converge in any of the unstable cases. In terms of computation times, the collocation method has thus the upper hand with respect to the numerical integration method and the shooting method for the determination of periodic trajectories of the considered closed-loop MMC model.

5.5.3 The Floquet exponents from the collocation method

The numerical applications in this section have shown the capability of the Fourier-based collocation method to determine the periodic trajectories of the closed-loop MMC and, by extension, of the MMC-based systems considered

in the numerical applications of Chapters 3 and 4, where periodic trajectories calculations were a prerequisite to their small-signal stability assessment. Once a periodic trajectory is determined, nonlinear systems can be linearised around that trajectory and the Fourier coefficients of periodic matrices in the resulting LTP systems are calculated by means of a DFT. Eventually, frequency-lifting methods such as the HSS and DHSS approaches allow obtaining time-invariant systems whose characteristic roots describe the stability of the original periodic trajectory.

This paragraph relies on [111] to show that, for non-delayed systems, the same eigenvalues can be obtained directly from the Jacobian \mathbf{J} of Δ in the Fourier-based collocation method.

In the case of non-delayed systems, (5.44) simplifies into:

$$\dot{\mathbf{x}}(t) = \mathbf{f}(t, \mathbf{x}(t), \mathbf{u}(t)), \quad (5.79)$$

with unforced small-signal approximation:

$$\dot{\tilde{\mathbf{x}}}(t) = \mathbf{A}(t)\tilde{\mathbf{x}}(t). \quad (5.80)$$

Discarding the tilde notation, the corresponding frequency-lifted formulation is recalled from (3.28):

$$\dot{\mathbf{x}}(t) = (\mathbf{A} - \mathbf{N})\mathbf{x}(t). \quad (5.81)$$

The same relationship can also be written in this chapter's notation, i.e. as in (5.5d):

$$\dot{\underline{\mathbf{x}}}(t) = (\underline{\mathbf{A}} - \underline{\mathbf{N}}_n)\underline{\mathbf{x}}(t). \quad (5.82)$$

As mentioned in Section 5.3.1, matrices $\mathbf{A} - \mathbf{N}$ and $\underline{\mathbf{A}} - \underline{\mathbf{N}}_n$ can be transformed into one another by means of rows and columns permutations, i.e. by means of similarity transformations. Consequently, these matrices have the same eigenvalues.

Returning to the case of periodic signals for which $\dot{\underline{\mathbf{x}}} = \mathbf{0}$, and relying on the relationship between harmonic vectors and sampled-time vectors in (5.40), we have:

$$(\underline{\mathbf{A}} - \underline{\mathbf{N}}_n)\underline{\mathbf{x}} = \underline{\mathbf{A}}\underline{\mathbf{x}} - \underline{\mathbf{N}}_n\underline{\mathbf{x}} \quad (5.83a)$$

$$= \mathcal{R}\{\mathbf{A}(t)\mathbf{x}(t)\} - \mathcal{R}\{\dot{\mathbf{x}}(t)\} \quad (5.83b)$$

$$= \mathbf{M}_n\mathcal{S}\{\mathbf{A}(t)\mathbf{x}(t)\} - \mathbf{M}_n\mathcal{S}\{\dot{\mathbf{x}}(t)\}, \quad (5.83c)$$

with $n = \infty$ in the non-truncated case.

Relying on (5.35) and (5.37a), we further obtain:

$$(\underline{\mathbf{A}} - \mathbf{N}_n)\underline{\mathbf{x}} = \mathbf{M}_n \underline{\mathbf{A}} \underline{\mathbf{x}} - \mathbf{M}_n \mathbf{N}_n \underline{\mathbf{x}} \quad (5.84a)$$

$$= \mathbf{M}_n (\underline{\mathbf{A}} - \mathbf{N}_n) \underline{\mathbf{x}} \quad (5.84b)$$

$$= \mathbf{M}_n (\underline{\mathbf{A}} - \mathbf{N}_n) \mathbf{M}_n^{-1} \underline{\mathbf{x}}. \quad (5.84c)$$

The equality of matrices $\underline{\mathbf{A}} - \mathbf{N}_n$ and $\mathbf{M}_n (\underline{\mathbf{A}} - \mathbf{N}_n) \mathbf{M}_n^{-1}$ implies that $\underline{\mathbf{A}} - \mathbf{N}_n$ and $\underline{\mathbf{A}} - \mathbf{N}_n$ are similar matrices and thus have the same eigenvalues. Lastly, on the periodic trajectory described by $(\underline{\mathbf{x}}, \underline{\mathbf{u}})$, the Jacobian is such that

$$\mathbf{J}(\underline{\mathbf{x}}, \underline{\mathbf{u}}) = \frac{\partial \mathbf{f}}{\partial \underline{\mathbf{x}}}(\underline{\mathbf{x}}, \underline{\mathbf{u}}) - \mathbf{N}_n = \underline{\mathbf{A}} - \mathbf{N}_n. \quad (5.85)$$

Consequently, $\mathbf{J}(\underline{\mathbf{x}}, \underline{\mathbf{u}})$ and $\underline{\mathbf{A}} - \mathbf{N}_n$ are equal. It can be concluded that the eigenvalues of $\mathbf{J}(\underline{\mathbf{x}}, \underline{\mathbf{u}})$ are thus equal to those of $\underline{\mathbf{A}} - \mathbf{N}_n$ and, by similarity, to those of the state matrix $\underline{\mathbf{A}} - \mathbf{N}$ of the HSS model, at least in the infinite, non-truncated case. These eigenvalues are the duplicated-shifted Floquet exponents of the considered linear (or linearised) periodic system [111]. In other words, the Floquet exponents are obtained as a by-product of the collocation method. This observation implies that it is in fact sufficient to solve for the periodic trajectory by means of the collocation method in order to characterise the stability of this trajectory.

The above considerations are illustrated in the case of the MMC-based HVDC link presented in Appendix B.4, whose eigenvalues are calculated in the non-delayed case in two ways: first as the eigenvalues of the state matrix of the HSS system, and second as the eigenvalues of the Jacobian matrix. The two sets of eigenvalues are compared in Fig. 5.6. It is observed that, although the majority of eigenvalues within the eigensets are indeed the same, differences are observed among the spurious eigenvalues. This is the consequence of truncation, which causes the considered matrices to not be exactly similar as they would have been in a non-truncated case.

Remark concerning delayed systems

In the case of delayed systems, the eigenvalues of the Jacobian of the Fourier-based collocation formulation are not equal to the characteristic roots of the related DHSS representation. One reason is that the proposed Jacobian structure is that of an extended system where the vector of unknowns comprises both states and delayed variables, hence it does not correspond to a state matrix. For delayed systems, one can rely instead on the Fourier-based collocation method

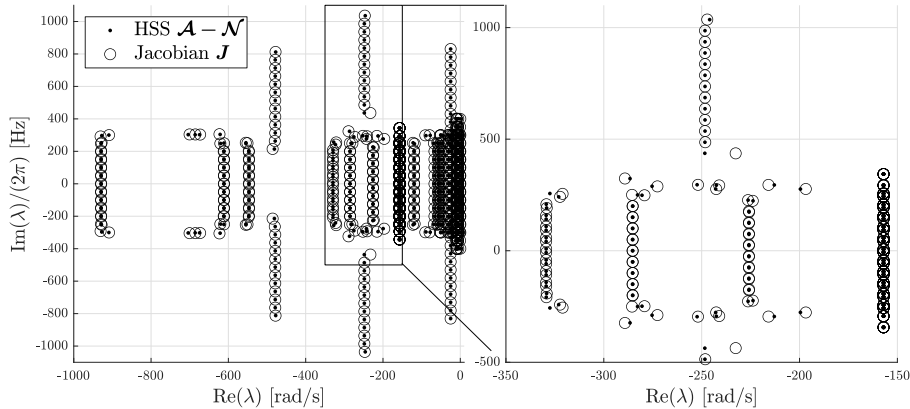


Figure 5.6: Comparison of the eigenvalues of the collocation Jacobian and the state matrix $\mathcal{A} - \mathcal{N}$ of the corresponding HSS model, with $h = h_t = 6$

in combination with the DHSS formulation and an appropriate algorithm such as the delay Arnoldi algorithm for the calculation of the characteristic roots (see Section 4.4), which was the selected approach for the numerical application in Section 4.5.

Alternatively, other types of collocation methods can be considered. For instance, polynomial-based collocation methods can be formulated in such a way that the monodromy operator and its Floquet multipliers are obtained as a by-product of solving for a periodic trajectory of a delayed system [83, Ch.6]. In fact, while Fourier-based collocation intrinsically assumes periodicity of the sought trajectory, determining Floquet multipliers requires a formulation capable of also representing growth/decay of the trajectory, which is possible when polynomials are chosen as interpolation functions.

5.5.4 Illustrative harmonic propagation study

The Fourier-based collocation method, as a calculation approach for steady-state waveforms being able to account for nonlinearity, is also suitable for harmonic analyses and harmonic propagation studies. In this section, the collocation method is applied to the complete model of the MMC-based HVDC link connecting an offshore grid (see Appendix B.4) to calculate the propagation of parasitic harmonic injections throughout the system. The diagram of the system is given in Fig. 5.7.

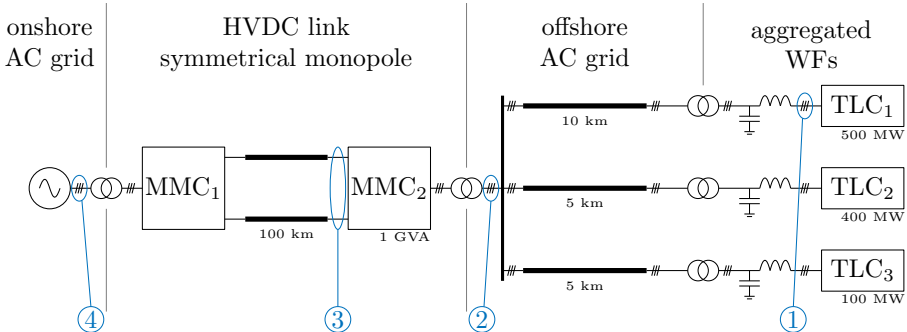


Figure 5.7: MMC-based HVDC and offshore grid test system, with in blue the location of harmonic measurements

For this example, a fifth-harmonic negative-sequence disturbance and a seventh-harmonic positive-sequence disturbance are introduced through the modulation indices of the TLCs. At these harmonic frequencies, it is realistic to expect amplitudes of about 2-3% in large offshore wind farms [113]. In this illustrative application, larger amplitudes of 10% are used to facilitate their visualisation. The collocation method, solved up to harmonic rank $h = 8$, shows the impact that these disturbances have on currents and voltages, as shown in Figs. 5.8 and 5.9. In these figures, the waveforms and sequence-harmonic spectra of disturbed voltages and currents are given at the locations numbered 1 to 4 in Fig. 5.7. The undisturbed reference case is also provided.

At the terminals of the TLCs (location 1), the initial disturbances cause harmonics from ranks 4 to 7 to appear with magnitudes of about 10% of rated values at $h = 5, 7$ and 0.1% at $h = 4, 6$. Components at the same ranks and with similar magnitudes are observed at the terminals of the offshore MMC (location 2). Through couplings within the converter, the disturbances are transmitted to the HVDC link (location 3), where oscillations at ranks $h = 5, 6$ have magnitudes between 0.1% and 1% of rated values. Eventually, the parasitic components have reduced to a great extent once reaching the AC-side of the onshore station (location 4), where their magnitudes drop below the 0.1% mark. At that location, these components are only visible in the alternating currents and not in the alternating voltages, since the onshore grid is represented by a three-phase alternating voltage source with pure fundamental frequency components.

It should be kept in mind that the results of such harmonic studies strongly depend on the modelling assumptions, such as the specific winding configuration of transformers, the tuning of passive filters as well as measurement filters.

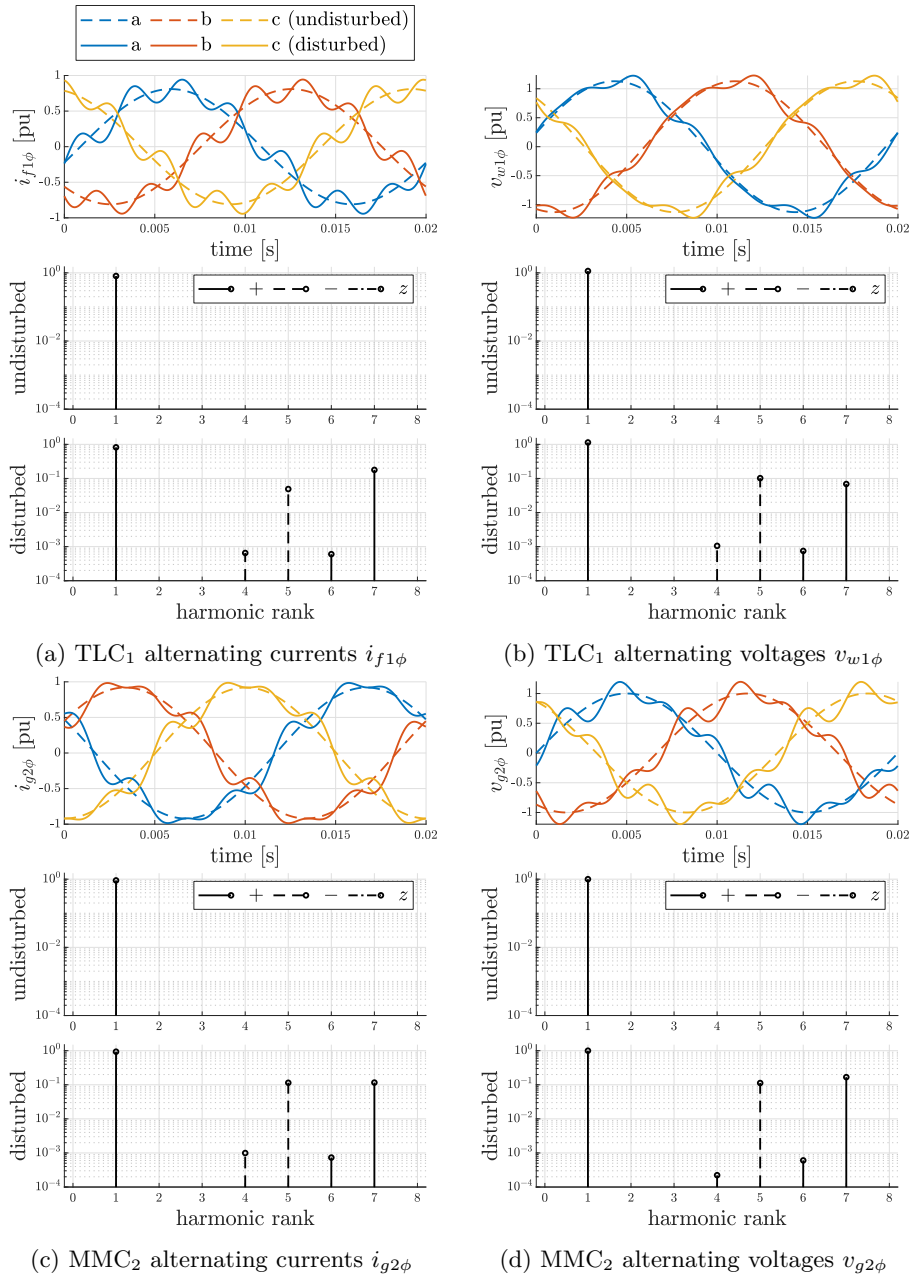


Figure 5.8: Harmonic propagation through the test system, part 1

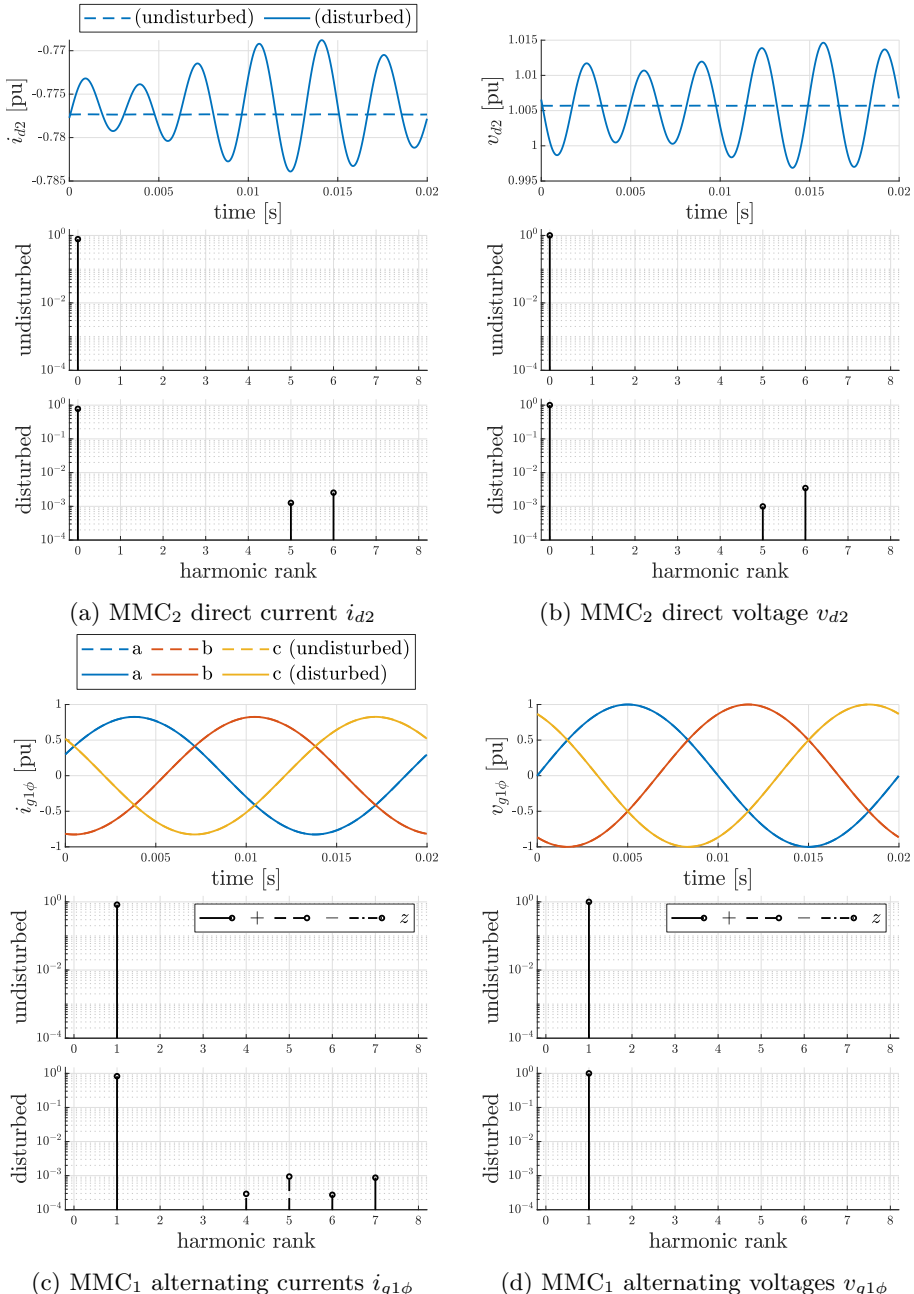


Figure 5.9: Harmonic propagation through the test system, part 2

5.6 Chapter conclusion

This chapter was dedicated to reviewing methods for the calculation of steady-state trajectories of nonlinear dynamic systems such as the closed-loop MMC and, by extension, of MMC-based systems. A review of time-domain, frequency-domain and hybrid-domain methods showed that collocation methods benefit from a compelling set of advantages with respect to alternative methods. By relying on known interpolation functions and enforcing that differential equations be satisfied over a discrete grid of time points, collocation methods are less computationally intensive than integration-based methods. Being defined in the time domain, collocation methods also account straightforwardly for nonlinearity within the differential equations.

Among collocation methods, the presented Fourier-based approach addresses precisely the prerequisites of applying frequency-lifting transformation methods such as the HSS, DHSS and HTF approaches, as it is capable of determining the harmonic content of the sought periodic trajectory up to an arbitrary harmonic rank. By relying on a generic formulation, the Fourier-based collocation method accounts for both circuit and control dynamics in a seamless way.

Lastly, in the context of small-signal stability analyses, the identification of steady-state trajectories with the collocation method has the significant advantage of being able to solve for both stable and unstable trajectories, where other integration-based methods, such as shooting methods, may fail to converge. Overall, Fourier-based collocation methods are a particularly efficient and flexible tool enabling harmonic and stability studies of the closed-loop MMC and MMC-based systems.

Conclusion and future work

The following concluding sections comprise a summary of the thesis, an overview of the main contributions as well as perspectives of future work.

Summary and conclusions

Over the last decades, the landscape of electrical power systems has witnessed rapid changes in energy sources and devices, reflecting the ongoing shift from fossil fuels to renewable energy sources as well as the continued electrification of the industry, transportation, residential and commercial sectors. The need to interconnect areas rich in resources with load centres has also promoted the development of HVDC networks carrying the potential of becoming a foundational layer of future electrical transmission systems. Overall, the share of power-electronic converters is increasing as these devices play a crucial role interconnecting renewable energy sources to the grid, and more generally to interface AC and DC systems. However, the dynamic behaviour of power-electronic converters differs from that of traditional synchronous generators, leading to power quality issues and new types of adverse interactions. This thesis has explored methods to address converter-related challenges and preserve power system stability.

In this context, **Chapter 1** was dedicated to describing the operation of the MMC, the prevalent VSC topology in HVDC applications. Despite its numerous advantages, the MMC has been involved in real-life problematic events which advocate for rigorous studies of MMC-based systems using appropriate mathematical models and analysis methods. Relying on common simplifying assumptions, a stationary-frame model of the MMC's power stage was established. The dynamic behaviour of converters being also largely influenced by the way they are operated, a controller was presented with its differential equations.

Three important characteristics of the closed-loop MMC model were identified: the equations feature nonlinear operations, their variables follow periodic trajectories in steady state, and the control structure is subject to time delays. To facilitate interaction studies of such systems via small-signal stability analyses, notions of linearisation were reviewed along with the fundamentals of LTI and LTP systems. The observation that linearising differential equations around periodic trajectories results in LTP systems raised the challenge of their stability assessment, in particular since traditional stability analysis methods from LTI systems theory are not directly applicable to LTP systems. The need to address this issue motivated the investigation of specific techniques in the subsequent chapters.

Chapter 2 covered calculation, transformation and approximation techniques not relying on the frequency-lifting technique. In this chapter, neglecting the oscillatory components in the coefficients of LTP systems was explored as a way of approximating LTP systems by LTI systems to enable conventional eigenvalues analysis. A criterion was established to assess whether stability of the initial system could be inferred from the resulting approximation. However, the criterion remained inconclusive for the tested models, which further motivated the examination of methods capable of addressing periodicity in dynamic systems.

The monodromy matrix, a characteristic matrix with constant eigenvalues, was presented as a fundamental tool in the stability analysis of periodic systems and trajectories. Although its calculation is possible with a direct numerical integration of the differential equations, the rather low efficiency of this approach justified considering alternative approaches. The Floquet transformation was also reviewed and was shown to rely on a time-periodic change of variables to convert LTP systems into other LTP systems with a constant state matrix, making conventional eigenvalues calculations once again possible. However, the lack of *a priori* knowledge of the periodic Floquet transformation matrix hindered its application to the MMC.

Frame rotations were examined next as an alternative transformation technique also relying on periodic changes of variables, but with known transformation matrices describing the rotation of vectors in orthogonal reference frames. The set of their underlying assumptions was highlighted to determine the types of systems and trajectories for which this approach is suitable. Specifically, sets of three-phase variables with more oscillatory components than either a positive or negative sequence at a single frequency, plus a zero sequence at a single frequency, cannot be transformed into constant operating points via frame rotations. Besides, the application of this technique is limited by the requirement for balanced phase parameters and simple types of nonlinearities. It was concluded that transformation methods with a broader range of applicability are required to

study MMC-based systems with nonlinearities other than products of variables, under harmonic disturbances and/or unbalanced conditions.

Chapter 3 delved into transformation techniques based on frequency-lifting, which reflects the idea of transforming LTP systems into LTI systems by expressing varying quantities as vectors of their Fourier coefficients. In the time domain, the most generic form of frequency-lifting results in the HSS representation. Observing that this LTI representation has infinite dimensions led to discussing truncation and its impact on stability assessments.

The HL approach was also presented and supported a discussion of frequency couplings within LTP systems. While its numerical application corresponds to the widely applied frequency scan method, its typical analytical application may quickly become cumbersome even for simple systems, which motivated a detailed presentation of the HTF approach. Multiple derivations of the HTF were revisited, specifically the derivation of the HTF from the HSS model, and its derivation from the impulse response of LTP systems. A third derivation, particularly suitable for systems with dynamics initially written in terms of transfer functions, was suggested as a streamlined and generalised version of the analytical HL procedure.

Relationships among frequency-lifting methods and between lifting and non-lifting methods were also clarified. It was concluded that frequency-lifting benefits from its capability of addressing periodicity in a very generic way, hence reducing the number of simplifying assumptions necessary for small-signal stability assessments.

Chapter 4 was dedicated to reviewing the fundamentals of delayed systems and to identify techniques from the literature able to retrieve characteristic roots without relying on Padé approximations, thereby opening the way towards more-accurate modal analyses of delayed systems. Having established the possibility of including exact delay representations in the HTF but lacking a state-space counterpart, the DHSS was introduced as an extension of the original HSS, which enables the transformation of delayed LTP systems into delayed LTI systems for characteristic root calculations, and where periodicity is tackled via frequency-lifting.

The capability of the DHSS to accurately capture stability properties of models outside the range of validity of Padé approximations was shown through a numerical application with an MMC-based offshore grid. The results matched both the outcome of the Nyquist criterion and of numerical integration. Not only does the DHSS further eliminate simplifying assumptions generally involved in the stability study of MMC-based systems, it also offers a pragmatic solution to determining unstable poles of delayed subsystems when applying the Nyquist

criterion.

Chapter 5 addressed an essential prerequisite to the methods presented in the previous chapters, namely the calculation of the periodic trajectories followed by nonlinear delayed systems in steady state. An overview of methods was provided, showing that collocation methods benefit from a large set of advantages in comparison with alternative methods, among others the ability to address nonlinearity in the time domain without the need to numerically integrate differential equations. A particular collocation method based on Fourier theory was developed and successfully applied to MMC-based systems, demonstrating the capability of the approach to correctly identify the harmonic contents predicted by numerical integration, as well as to calculate unstable periodic trajectories, a valuable feature in the context of small-signal stability assessments aiming to understand their cause and prevent their occurrence in real-life projects. The Fourier-based collocation method proved to be a particularly efficient and highly flexible method also applicable in harmonic propagation studies.

For non-delayed systems, the eigenvalues of the Jacobian of the collocation formulation provide the same stability information delivered by the eigenvalues of the state matrix of HSS models. Lacking a straightforward way of generalising this outcome to the case of delayed systems justifies relying on a calculation of the characteristic roots of the DHSS after linearisation around the periodic trajectory retrieved from the Fourier-based collocation method, but also encourages a continued exploration of alternative mathematical methods capable of studying the stability properties of periodic trajectories of the MMC and MMC-based systems.

Overview of contributions

Main contributions

- A sufficient stability criterion relying on an averaging technique. This criterion determines whether stability of a linear time-periodic system can be inferred from the linear time-invariant system obtained by neglecting oscillatory components in its periodic coefficients. (Section 2.3)
- A presentation of the harmonic transfer function as a generalised formulation of the harmonic linearisation technique. This new derivation, suitable for systems whose dynamics are described by means of transfer functions benefits from the generality of the frequency-lifting technique. (Section 3.4)

- A comparison of lifting and non-lifting transformation methods enabling small-signal stability analyses of nonlinear systems following periodic trajectories. This comparison helps choosing a suitable method according to the characteristics of the model under study. (Chapters 2 and 3)
- The calculation of characteristic roots of frequency-lifted delayed systems based on a generalisation of the harmonic state-space formulation. This new formulation is capable of addressing both time-periodic and time-delayed behaviours of the modular multilevel converter without relying on Padé approximations for the delays. (Section 4.4)
- A Fourier-based collocation method for periodic trajectories calculations of nonlinear delayed systems. This efficient and system-independent method provides the harmonic spectrum of all variables up to an arbitrary maximum harmonic rank. (Section 5.4)
- A computer toolbox for periodic trajectories calculations, frequency-lifting transformations and small-signal stability analyses of nonlinear delayed systems. This set of Matlab functions simplifies the calculation processes by harnessing the system-agnostic properties of the Fourier-based collocation method and of the delayed harmonic state-space framework. (Appendix C.1)

Other contributions

- An analogy to explain in a didactic manner the concepts of sequences, harmonics and frame rotations in three-phase systems. Developing an intuitive understanding of these notions is made possible by relying on the familiar concepts of orbits in a solar system. (Appendix A.1)

Contributions from a published article not covered in this thesis

- A comprehensive literature review of problematic real-life events directly or indirectly involving power-electronic converters. This review covers prominent types of electrical systems, including wind farms, photovoltaic systems, electrical railways and HVDC networks. (See [8] in the List of Publications)
- A classification of mechanisms behind converter-related issues in power systems based on the aforementioned overview of real-life events. Three main classes of identified mechanisms are converter or control limitations, power quality degradation and control interactions. (See [8] in the List of Publications)

Future work

The focus of this section is to provide suggestions for future research and highlight unresolved challenges that could be addressed as a natural extension of this thesis.

Developing criteria to assess whether harmonic components can be neglected

Although transformation methods such as frequency-lifting are capable of accounting for oscillatory components in the coefficients of LTP systems up to an arbitrary harmonic rank, the eigenvalue-based stability assessment of lifted systems lacks to some extent the simplicity offered by non-lifted approaches. Consequently, it remains of interest to determine if and when oscillatory components can be neglected in the context of small-signal stability analyses. The averaging technique and the stability criterion presented in Section 2.3 align with that perspective. However, considering that the developed criterion is rather conservative and remains inconclusive for the tested converter models, further research is necessary to determine which oscillatory components can indeed be neglected in stability assessments.

A possible approach could rely on further harnessing the potential of frequency-lifting methods, which can be used as a way of determining whether particular oscillatory components have an impact on the stability assessment, for instance by increasing the forced periodic rank until the results of the analysis do not change anymore. Yet, such tests could remain largely case-dependent.

More generally, an appropriate truncation criterion, possibly inspired by Proposition 1, would not only be able to tell whether oscillatory components can be neglected as a whole, but also which oscillatory components can be neglected individually depending on their amplitude and frequency. It is suggested that the averaging theories in e.g. [35, 37] could deliver the necessary insights required to obtain rigorous yet less conservative criteria.

Applying the developed stability criterion to rotating frame MMC models

As discussed in Section 2.4, frame rotations are capable of transforming three-phase sets of periodic variables into constant operating points when specific requirements related to frequency and sequence contents are met. This approach offers a tool to bring specific selections of oscillatory components of the MMC's state variables to constant values in steady state. For instance, only fundamental-frequency components could be transformed. Similarly, both fundamental-

frequency and second-harmonic components could be addressed. In all cases, harmonics of higher rank persist after transformation. It is suggested that the stability criterion presented in Section 2.3 could be applied to such models of the MMC as a way of determining whether, after linearisation, the remaining oscillatory components in the coefficients of the resulting LTP systems could be neglected according to Proposition 1.

Assessing the impact of shift transfer functions on stability

Frequency-domain models of LTP systems in the form of the HTF may comprise, in theory, an infinite number of transfer functions describing frequency-coupling dynamics. In the context of power-electronic converters such as the MMC, only the no-shift transfer function is generally retained for small-signal stability analyses relying for instance on the Nyquist criterion, which is in agreement with the classical application of the HL approach. Further research is recommended to determine if and when additional shift transfer functions could in fact have an impact on the stability assessment and should thus not be neglected when performing such studies.

Bridging the gap between different derivations of the harmonic transfer function

In Section 3.4, several approaches have been described for the derivation of the HTF of an LTP system. On the one hand, applying the Laplace transform to the HSS formulation gives the classical formula to obtain the HTF from state-space matrix coefficients. On the other hand, the approach based on the impulse response of LTP systems provides information on the particular structure of the HTF. Interestingly, the two approaches are such that the HTF seems to take the form of mappings between *a priori* different quantities. Building upon proofs of equivalence such as in [76], further research is suggested to establish a better understanding of the relationship between the two formulations, thereby fully bridging the gap between the different derivations of the HTF.

Calculating the Floquet exponents from the Fourier coefficients

Considering again the increased complexity of modal analysis of frequency-lifted systems, in particular due to the presence of spurious eigenvalues, further research is necessary to establish ways of simplifying the stability assessment of HSS models.

One option could rely on comparing the eigenvalues calculated with different truncation ranks, as a way of locating those that do not move significantly in the complex plane. Such eigenvalues have converged and are thus not spurious. However, this approach implies that the eigenvalues must be calculated at least twice.

An alternative method that avoids the truncation-related limitations of frequency-lifted systems is to retrieve the Floquet multipliers first by calculating the monodromy matrix of the LTP system, and then transform the Floquet multipliers into Floquet exponents. However, as discussed in Section 2.2.2, the disadvantage of this calculation is that the Floquet exponents are not uniquely defined, which prevents finding the true oscillatory frequency of the modes. Since these oscillatory frequencies are in fact provided by the centremost eigenvalues in the eigensets of frequency-lifted models, an improved eigenvalue calculation method could be developed, with the objective of delivering directly the converged centremost eigenvalues of the state matrix of HSS models, instead of the complete eigensets with their undesirable spurious eigenvalues.

Calculating the characteristic roots of delayed systems

While the DHSS framework presented in Chapter 4 is capable of addressing both time-periodic and time-delayed properties of the closed-loop MMC, the calculation of the characteristic roots via the delay Arnoldi algorithm is, for the systems considered in this thesis, a computationally-intensive task. The main reason for the longer calculation times is the particularly large size of the matrices involved, which is a consequence of using frequency-lifting as a way of obtaining time-invariant models. Developing improved algorithms capable of dealing with such high-dimensional delayed systems in a more efficient way is suggested as future work.

Also on the topic of characteristic roots of delayed systems, it is recalled that the calculations carried out in Chapter 4 rely on Assumption 12, which limits the use of (4.55a) to the modelling of systems such that none of their variables subject to a delay are functions of delayed variables. This assumption would be invalid when considering the more realistic case of cascaded delays, modelling for instance the distributed nature of e.g. communication, calculation and modulation delays throughout the control structure, instead of their aggregation. A more general formulation of (4.55a) would thus be necessary and could be obtained via further work, keeping in mind the particular feedback structure taken by (4.50b) and (4.50c) in that case.

Lastly, further research is necessary to also extend the proposed framework to account for non-constant and possibly stochastic delays in the control structure

of the MMC, thereby assessing their potential impact on the stability properties of its trajectories.

Investigating polynomial-based collocation methods

As described in Chapter 5, Fourier-based collocation methods are such that, for non-delayed systems, the eigenvalues of the Jacobian correspond to the duplicated-shifted Floquet exponents, i.e. the eigenvalues of the state matrix of the HSS model. However, such result is not applicable when exact delays are involved. Consequently, it is suggested to continue the investigation of alternative collocation methods, in particular polynomial-based collocation methods. Unlike formulations relying on Fourier theory, polynomial-based formulations do not intrinsically assume periodicity of the sought trajectory. This implies that polynomial-based approaches lend themselves better to obtaining a discretisation of the monodromy operator, and thus the Floquet multipliers as a by-product of calculating periodic trajectories of delayed systems, see for instance [53, 114–116]. Consequently, such methods based on polynomial collocation appear as an attractive alternative to frequency-lifting when it comes to the stability analysis of periodic trajectories and are thus a logical next step to consider as an extension of this thesis for both delayed and non-delayed systems. Nevertheless, specific limitations of approaches relying on the monodromy matrix or operator ought to be kept in mind, in particular the ambiguity on oscillatory mode frequencies (as discussed in Section 2.2.2), and the fact that such approaches do not easily support the calculation of frequency responses of periodic systems.

Improving high-frequency modelling fidelity

The use of dedicated algorithms to calculate DDE characteristic roots allows for a more accurate study of trajectory stability in delayed systems, especially in the frequency range where Padé approximations introduce non-negligible errors. In the context of MMC-based systems, which typically involve delays, this frequency range extends beyond a few kilohertz. The capability of the DHSS representation to support interaction studies in that frequency range should motivate improvements in modelling accuracy, for instance by accounting for frequency dependency and for parasitic capacitive components of the MMC itself and of transformers [22]. This challenge pertains to accurately representing reality in parallel to improving the methods dedicated to analysing the resulting models. This also raises the issue of reliably and efficiently identifying or measuring the relevant parameter values.

Improving numerical integration of unstable delayed systems

Even when both modal analysis and the application of Nyquist criterion agree and show that a given periodic trajectory is unstable, it may happen that the numerical integration of the nonlinear differential equations, starting from that particular periodic trajectory, remains stable when subjected to small perturbations. In the framework of this thesis, such behaviours were observed for systems with high-frequency unstable modes having rather small positive real parts, and for which the anticipated divergence from the starting trajectory appeared to be compensated by numerical damping. A better understanding of the numerical damping of solvers for nonlinear differential equations along such unstable trajectories would be necessary to predict and prevent such apparently incorrect depictions of the true system dynamics.

Appendix A

Supporting content on transformations

A.1 Sequence and harmonic components: intuitive description

This section gives a short didactic presentation of the concepts of harmonic and sequence components in three-phase systems, relying on an analogy.

Three-phase systems

Let us consider three cities in the northern hemisphere of planet Earth: Adashi (Japan), Brussels (Belgium) and Chicago (USA). For the analogy, these cities are considered to be roughly located at 120° with respect to each other along the longitude, and will be referred to as A for Adashi, B for Brussels and C for Chicago.

Sequence components

Instead of an heliocentric configuration, let us exceptionally consider the **geocentric** configuration depicted in Fig. A.1a, where the Earth is at rest at the centre of its stellar system. As seen from above the north pole, the sun rotates clockwise in the plane of the equator and shines first above A, next above B

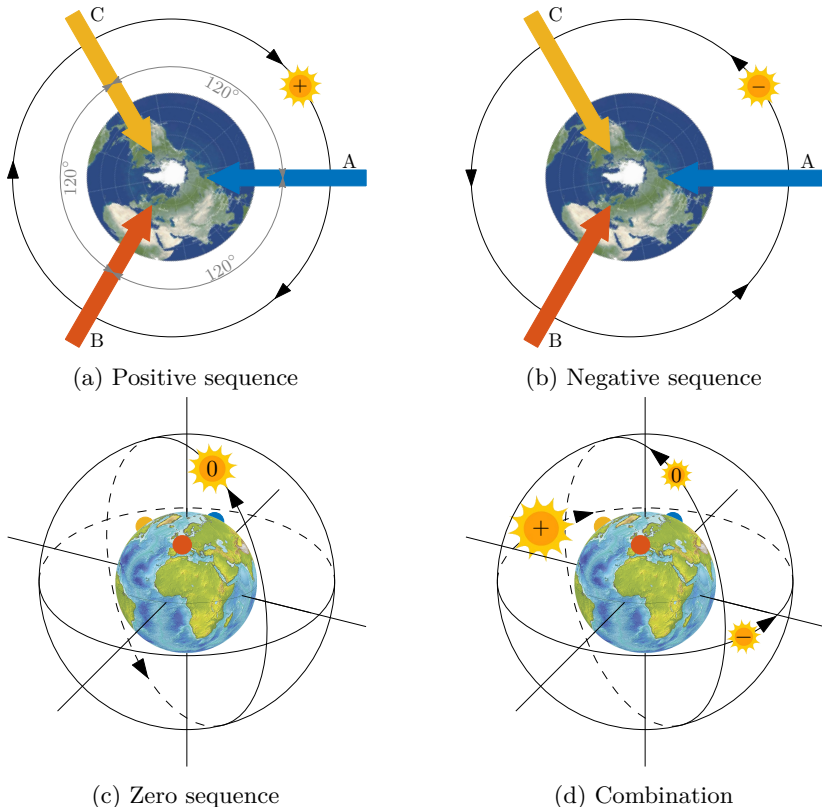


Figure A.1: Stellar analogy: positive, negative and zero sequence representations

and lastly above C before repeating the same cycle the next day. Brightness is measured in each of the three cities and the corresponding measurements are displayed in Fig. A.2a. Each city detects a sinusoidal variation of brightness from the sun, with the same amplitude and the same frequency. However, the variations are shifted by one third of a day between them. This sun is said to generate a *positive sequence* of brightness in the cities.

In Fig. A.1b, another sun is imagined to rotate around the Earth, also in the plane of the equator, however in the direction opposite to that of the first one. This second sun shines first above A, next above C and lastly above B. The variations of brightness in each city caused by this sun are once more sinusoidal, with same frequency and same amplitude, as displayed in Fig. A.2b. Here too, the variations are shifted by one third of a day. The difference with respect to

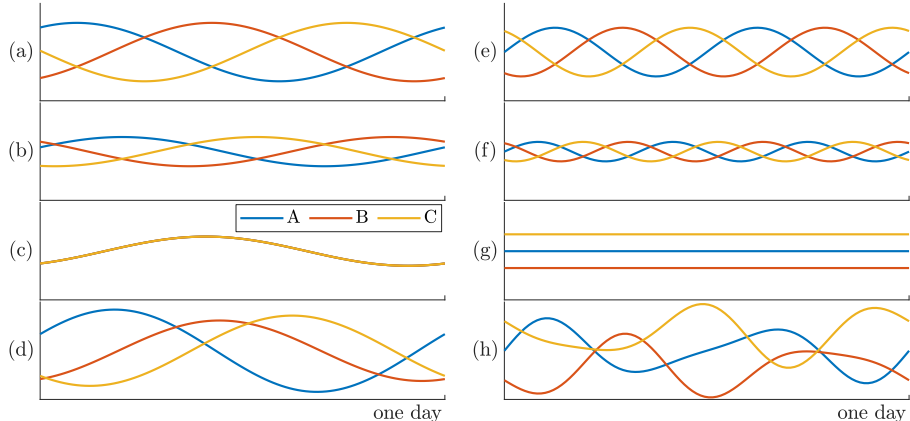


Figure A.2: Three-phase quantities with various sequence-harmonic contents

the positive sequence induced by the previous sun is thus the order in which the cities perceive the variations. The second sun is said to generate a *negative sequence* of brightness in the cities.

With the help of Fig. A.1c, the reader is encouraged to imagine a third sun rotating around the Earth. However, this sun does not revolve within the plane of the equator, but in a plane perpendicular to it. Considering that the three cities are located at rather high latitudes in the northern hemisphere, this third sun contributes to variations of brightness that are perceived in a roughly simultaneous way¹ in A, B and C: there is no phase shift between the induced variations of brightness (Fig. A.2c). This sun is said to contribute to a *zero (or homopolar) sequence* of brightness in the cities.

Relying on Fig. A.1d, the three types of suns can be imagined to revolve together around the planet². The suns may shine with different intensities: a brighter star sheds more light onto the Earth and its contribution to brightness is larger. Regardless, all three suns contribute to the brightness levels measured in the cities, and the measurements corresponding to the positive, negative and zero sequences are summed and displayed in Fig. A.2d. The three resulting measurements are said to be *unbalanced*, unless both negative and zero sequences are zero, in which case the three quantities are said to be *balanced*.

¹ For the sake of the analogy, let us assume that the variations induced by the third sun are *precisely* simultaneous in all three cities.

² For the sake of the analogy, no collisions are possible in this imaginary system.

Harmonic components

So far, the suns have been considered to rotate at the frequency of one complete cycle every day. An additional triplet of suns is brought into the picture: a positive-sequence sun, a negative-sequence sun and a zero-sequence sun which rotate faster around the Earth and achieve two complete revolutions every day. Similarly, triplets of suns with three, four, five daily cycles can be considered, and the resulting variations of brightness in A, B and C are referred to as *harmonic components*. Such harmonics are illustrated in Fig. A.2e and Fig. A.2f, with a second harmonic positive sequence and a third harmonic negative sequence, respectively.

The analogy is further enhanced by considering a last triplet of suns in a geostationary orbit: these suns are immobile with respect to the Earth and contribute to a constant offset of brightness (Fig. A.2g). Naturally, this constant offset might not be the same in every city. The zero-sequence sun defines their mean value, while the suns in the equatorial plane describe the offset with respect to that mean value.

Lastly, Fig. A.2h corresponds to the sums of signals in Figs A.2e to A.2g. This analogy may help the reader considering the electrical signals in the three phases of an electrical circuit as sums of constant and sinusoidal contributions at harmonic frequencies, in the same way Fourier series describe periodic quantities. At each harmonic frequency, the signals observed in the three phases can be decomposed into a sum of positive, negative and zero sequences.

Orthogonal frames of reference

Instead of three northern cities located 120° apart, brightness variations could also be observed from two cities near the equator, located 90° apart such as Libreville (Gabon) and Singapore, plus an extra measurement station at the geographic north pole. The north pole station would detect variations due to zero-sequence suns but would be insensitive to positive and negative sequences. On the other hand, Libreville and Singapore would detect combinations of positive sequences and negative sequences from the suns with orbits in the equatorial plane. Lastly, for the sake of the analogy, it is considered that these cities would not be sensitive to zero sequences. In these equatorial cities, variations of brightness from positive- or negative-sequence suns would have the same amplitude and same frequency, but would be shifted by a quarter of a day between the two cities. Positive-sequence suns would shine first above Singapore and a quarter of cycle later above Libreville, and the opposite is true for negative-sequence suns. This new orthogonal configuration relates

to the original A, B, C cities in the same way $\alpha\beta z$ variables obtained via Clarke transformation (see Appendix A.2) relate to abc variables of an electrical three-phase system.

Frame rotations

The proposed analogy can help understand how frame rotations (see Section 2.4) impact the way in which different sequences at different frequencies are perceived. So far, the Earth was assumed to be stationary. It is now given a clockwise rotation around its polar axis at the fundamental daily frequency. The suns in the equatorial plane that were initially geostationary now generate a negative sequence in Libreville and Singapore, while the original fundamental-frequency positive-sequence sun is now in a geostationary orbit. This is unlike the original fundamental-frequency negative-sequence sun, which now contributes to brightness variations at twice the fundamental frequency, still in a negative sequence.

Giving the Earth a counterclockwise rotation at twice the fundamental frequency sets an original second-harmonic negative-sequence sun on a geostationary orbit. Under this rotation, an original fundamental-frequency negative-sequence sun becomes a positive-sequence sun while keeping the same frequency. Clearly, the rotation of the Earth around its polar axis has no impact on the zero-sequence measurements at the north pole station, which explains why transforming zero sequences into constant quantities must be done independently from the positive- and negative sequences (a transformation that cannot be easily described with this analogy). Eventually, realising that the Earth can only be assigned a unique rotation speed in a unique direction (either clockwise or counterclockwise) explains why frame rotations can only successfully address systems of variables with either a positive or a negative sequence at a single frequency, with possibly also a zero sequence at a single frequency, to be transformed separately.

A.2 Basic frame transformations

Clarke transformation, frame rotations, Park transformation [117], and Fortescue transformation [118] are briefly reviewed in this section.

A.2.1 Clarke transformation

The direct and inverse peak-preserving Clarke transformations \mathbf{T} and \mathbf{T}^{-1} express the relationship between three-phase abc variables and orthogonal $\alpha\beta z$ variables, when the amplitude of transformed variables is preserved. These transformations are expressed in matrix form as:

$$\begin{bmatrix} x_\alpha \\ x_\beta \\ x_z \end{bmatrix} = \underbrace{\begin{bmatrix} \frac{2}{3} & -\frac{1}{3} & -\frac{1}{3} \\ 0 & \frac{1}{\sqrt{3}} & -\frac{1}{\sqrt{3}} \\ \frac{1}{3} & \frac{1}{3} & \frac{1}{3} \end{bmatrix}}_{\triangleq \mathbf{T}} \begin{bmatrix} x_a \\ x_b \\ x_c \end{bmatrix}, \quad \begin{bmatrix} x_a \\ x_b \\ x_c \end{bmatrix} = \underbrace{\begin{bmatrix} 1 & 0 & 1 \\ -\frac{1}{2} & \frac{\sqrt{3}}{2} & 1 \\ -\frac{1}{2} & -\frac{\sqrt{3}}{2} & 1 \end{bmatrix}}_{\triangleq \mathbf{T}^{-1}} \begin{bmatrix} x_\alpha \\ x_\beta \\ x_z \end{bmatrix} \quad (\text{A.1})$$

where x refers to quantities such as voltages and currents. Starting from a set of three-phase abc variables with positive, negative and zero sequences, the corresponding x_α and x_β variables contain only positive and negative sequences, while x_z corresponds to the zero-sequence component. When the latter is known to be zero, the original set of three abc variables can be reduced to two $\alpha\beta$ variables without any loss of information.

A.2.2 Frame rotations

The direct and inverse frame rotations $\mathbf{R}_\omega(t)$ and $\mathbf{R}_\omega^{-1}(t)$ express the relationship between $\alpha\beta$ variables in a stationary orthogonal frame and direct-quadrature (dq) variables in a rotating frame with angular frequency ω . The zero-sequence component z remains unchanged through this transformation. These rotations are expressed in matrix form as:

$$\begin{bmatrix} x_d \\ x_q \\ x_z \end{bmatrix} = \underbrace{\begin{bmatrix} \cos(\theta) & \sin(\theta) & 0 \\ -\sin(\theta) & \cos(\theta) & 0 \\ 0 & 0 & 1 \end{bmatrix}}_{\triangleq \mathbf{R}_\omega(t)} \begin{bmatrix} x_\alpha \\ x_\beta \\ x_z \end{bmatrix}, \quad \begin{bmatrix} x_\alpha \\ x_\beta \\ x_z \end{bmatrix} = \underbrace{\begin{bmatrix} \cos(\theta) & -\sin(\theta) & 0 \\ \sin(\theta) & \cos(\theta) & 0 \\ 0 & 0 & 1 \end{bmatrix}}_{\triangleq \mathbf{R}_\omega^{-1}(t)} \begin{bmatrix} x_d \\ x_q \\ x_z \end{bmatrix} \quad (\text{A.2})$$

where $\theta = \omega t$. It is noted that the direct rotation is characterised by an initial alignment of d and α axes and a leading q -axis in the direction of the rotation.

A.2.3 Park transformation

The direct and inverse Park transformations $\mathbf{P}_\omega(t)$ and $\mathbf{P}_\omega^{-1}(t)$ refer to the relationship between abc and dqz variables, which can be obtained from the combination of Clarke transformation and a frame rotation. Peak-preserving Park transformations with an initial alignment of d and α axes and a leading q -axis in the direction of rotation are expressed in matrix form as:

$$\begin{bmatrix} x_d \\ x_q \\ x_z \end{bmatrix} = \underbrace{\frac{2}{3} \begin{bmatrix} \cos(\theta) & \cos(\theta - \frac{2\pi}{3}) & \cos(\theta + \frac{2\pi}{3}) \\ -\sin(\theta) & -\sin(\theta - \frac{2\pi}{3}) & -\sin(\theta + \frac{2\pi}{3}) \\ \frac{1}{2} & \frac{1}{2} & \frac{1}{2} \end{bmatrix}}_{\triangleq \mathbf{P}_\omega(t)} \begin{bmatrix} x_a \\ x_b \\ x_c \end{bmatrix}, \quad (\text{A.3a})$$

$$\begin{bmatrix} x_a \\ x_b \\ x_c \end{bmatrix} = \underbrace{\begin{bmatrix} \cos(\theta) & -\sin(\theta) & 1 \\ \cos(\theta - \frac{2\pi}{3}) & -\sin(\theta - \frac{2\pi}{3}) & 1 \\ \cos(\theta + \frac{2\pi}{3}) & -\sin(\theta + \frac{2\pi}{3}) & 1 \end{bmatrix}}_{\triangleq \mathbf{P}_\omega^{-1}(t)} \begin{bmatrix} x_d \\ x_q \\ x_z \end{bmatrix} \quad (\text{A.3b})$$

where $\theta = \omega t$.

A.2.4 Fortescue transformation

The direct and inverse Fortescue transformations \mathbf{F} and \mathbf{F}^{-1} refer to the relationship between three-phase abc and zero-, positive-, and negative-sequence zpn variables. For complex-valued Fourier coefficients (or phasors) of three-phase quantities at harmonic rank $k \in \mathbb{N}$, i.e. corresponding to positive frequencies, the Fortescue transformations can be expressed as:

$$\begin{bmatrix} x_{zk} \\ x_{pk} \\ x_{nk} \end{bmatrix} = \underbrace{\frac{1}{3} \begin{bmatrix} 1 & 1 & 1 \\ 1 & a & a^2 \\ 1 & a^2 & a \end{bmatrix}}_{\triangleq \mathbf{F}} \begin{bmatrix} x_{ak} \\ x_{bk} \\ x_{ck} \end{bmatrix}, \quad \begin{bmatrix} x_{ak} \\ x_{bk} \\ x_{ck} \end{bmatrix} = \underbrace{\begin{bmatrix} 1 & 1 & 1 \\ 1 & a^2 & a \\ 1 & a & a^2 \end{bmatrix}}_{\triangleq \mathbf{F}^{-1}} \begin{bmatrix} x_{zk} \\ x_{pk} \\ x_{nk} \end{bmatrix} \quad (\text{A.4})$$

with $a = e^{j2\pi/3}$.

Appendix B

Supporting content on modelling

B.1 Additional MMC control loops

This section completes the description of the MMC controller started in Section 1.2. It provides the differential equations describing the direct voltage (DV) controller, the alternating voltage (AV) controller and the circulating current (CC) controller.

B.1.1 Direct voltage control

The objective of the DV controller is to control the CM (or pole-to-pole) direct voltage to its reference by acting on the d -axis alternating current reference (i_{sd}^*). In this thesis, the direct voltage controller takes the form of a DC-bus energy controller, with the DC-bus energy w_d and its reference w_d^* given by:

$$w_d = \frac{C_{d,eq}}{2} v_d^2, \quad w_d^* = \frac{C_{d,eq}}{2} (v_d^*)^2, \quad (\text{B.1})$$

with $C_{d,eq}$ the equivalent DC-bus capacitor and v_d^* the pole-to-pole direct voltage reference. The control is achieved by means of a PI controller with proportional and integral coefficients K_p^{DV} and K_i^{DV} . The corresponding transfer function is:

$$p_g^* = - \left(K_p^{\text{DV}} + \frac{K_i^{\text{DV}}}{s} \right) (w_d^* - w_d). \quad (\text{B.2})$$

The i_{sd}^* current reference is then obtained via an appropriate scaling of the active power reference:

$$i_{sd}^* = \frac{2kp_g^*}{3\hat{v}_g}, \quad (\text{B.3})$$

with \hat{v}_g/k the amplitude of the alternating voltage brought to the converter side of the transformer and, considering the balanced case for simplicity,

$$\hat{v}_g = \sqrt{v_{g\alpha}^2 + v_{g\beta}^2}. \quad (\text{B.4})$$

An equivalent state-space representation is given by:

$$\begin{cases} \frac{d\eta_{\text{DV}}}{dt} = -K_i^{\text{DV}}(w_d^* - w_d) \\ i_{sd}^* = \frac{2k}{3\hat{v}_g}(\eta_{\text{DV}} - K_p^{\text{DV}}(w_d^* - w_d)). \end{cases} \quad (\text{B.5})$$

In this mode, the q component reference is provided by the reactive power controller.

Calculation of equivalent DC-bus capacitor

According to [12, Ch.3], both the HVDC cables and the MMC total arm capacitance contribute to the equivalent DC-bus capacitor $C_{d,eq}$. For a three-phase MMC, $C_{d,eq} = 6C_a + C_{d,p2p}$, with $C_{d,p2p}$ the pole-to-pole capacitance as contributed by the cables. Considering that the HVDC cables have a total capacitance C_d , then the pole-to-neutral capacitance at one end of the cable can be approximated by $C_d/2$ in a π -section representation. Eventually, the pole-to-pole capacitance is obtained as the series connection of twice the pole-to-neutral capacitance, i.e. $C_{d,p2p} = C_d/4$.

B.1.2 Alternating voltage control

The objective of the AV controller is to control the three-phase alternating voltages $v_{g\varphi}$ to their references by acting on the alternating current references. The controlled voltages are located on the grid-side of the MMC transformer, as depicted in Fig. B.1. The control loops are implemented in the $\alpha\beta$ frame by means of a PR controller with a resonance at the fundamental frequency ω_1 , and with proportional and resonant coefficients K_p^{AV} and K_r^{AV} . A feedforward term

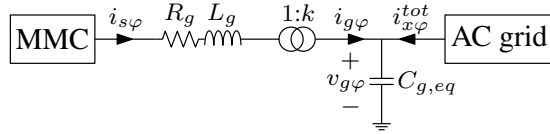


Figure B.1: Scheme of the AC-grid connection

consisting of the current $i_{g\varphi}$ aims at compensating for AC-grid disturbances¹. For simplicity, this current is not filtered in this model. The transfer function is:

$$i_{g\varphi}^* = i_{g\varphi} + \left(K_p^{\text{AV}} + \frac{K_r^{\text{AV}} s}{s^2 + \omega_1^2} \right) (v_{g\varphi}^* - v_{g\varphi}). \quad (\text{B.6})$$

The current reference is then brought to the converter-side of the transformer by:

$$i_{s\varphi}^* = k i_{g\varphi}^*. \quad (\text{B.7})$$

An equivalent state-space representation is given by:

$$\begin{cases} \frac{d\eta_{\text{AV}1\varphi}}{dt} = -\omega_1 \eta_{\text{AV}2\varphi} \\ \frac{d\eta_{\text{AV}2\varphi}}{dt} = \omega_1 \eta_{\text{AV}1\varphi} + K_r^{\text{AV}} (v_{g\varphi}^* - v_{g\varphi}) \\ i_{s\varphi}^* = k(i_{g\varphi} + \eta_{\text{AV}2\varphi} + K_p^{\text{AV}} (v_{g\varphi}^* - v_{g\varphi})). \end{cases} \quad (\text{B.8})$$

B.1.3 Circulating current control in uncompensated modulation

This section covers the CC control in uncompensated modulation. The compensated modulation is not provided as not specifically used in the numerical examples of this thesis, but its description is available in [12, Ch.3].

Circulating current references: equal phase distribution

In the uncompensated modulation, no specific arm-energy controller is used and the circulating current references are defined to be the same in all three

¹ In a practical system, there is no actual shunt capacitor bank at the AC-grid side of the transformer. The equivalent capacitor $C_{g,eq}$ displayed in Fig. B.1 is a modelling representation of the capacitive behaviour of the AC grid as seen from the transformer. This justifies selecting $i_{g\varphi}$ instead of $-i_{x\varphi}^{tot}$ as feedforward term in (B.6).

phases, i.e. to be equal to one third of the direct current. However, defining the circulating current reference as a function of the circulating currents themselves² is avoided by expressing the direct current as the ratio of DC-side active power and direct voltage, and by approximating the DC-side active power by the converter mid-point active power p_a :

$$i_c^* = \frac{i_d}{3} = \frac{p_d}{3v_d} \approx \frac{p_a}{3v_d}. \quad (\text{B.9})$$

Mathematically, however, it is difficult to calculate p_a directly from the alternating current $i_{s\phi}$ and mid-point voltage $v_{a\phi}$ since the latter is neither an input nor a state variable. This issue is purely a modelling limitation and, in practical applications, $v_{a\phi}$ could be measured directly. In this thesis, p_a is obtained as:

$$p_a = p_g + p_{loss} \quad (\text{B.10})$$

where p_{loss} corresponds to the power losses within the transformer:

$$p_{loss} = R_g(i_{sa}^2 + i_{sb}^2 + i_{sc}^2). \quad (\text{B.11})$$

Circulating current control: second harmonic suppression control

In the uncompensated modulation, the circulating current controller is implemented by means of a PR controller, with proportional and resonant coefficients K_p^{CC} and K_r^{CC} . The resonance is located at the second harmonic, i.e. at $2\omega_1$. This forces to zero the undesired second-harmonic components that otherwise naturally arise in the circulating currents. A feedforward term³ compensates for the disturbances related to the direct voltage v_d . The transfer function is:

$$v_{c\phi}^* = \frac{v_d}{2} - \left(K_p^{\text{CC}} + \frac{K_r^{\text{CC}} s}{s^2 + (2\omega_1)^2} \right) (i_c^* - i_{c\phi}). \quad (\text{B.12})$$

An equivalent state-space representation of the CC controller is given by:

$$\begin{cases} \frac{d\eta_{\text{CC}1\phi}}{dt} = -2\omega_1\eta_{\text{CC}2\phi} \\ \frac{d\eta_{\text{CC}2\phi}}{dt} = 2\omega_1\eta_{\text{CC}1\phi} - K_r^{\text{CC}}(i_c^* - i_{c\phi}) \\ v_{c\phi}^* = \frac{v_d}{2} + \eta_{\text{CC}2\phi} - K_p^{\text{CC}}(i_c^* - i_{c\phi}). \end{cases} \quad (\text{B.13})$$

² As expressed by (1.9), the direct current is the sum of the circulating currents.

³ In [12, Ch.3], there is also an additional feed-forward term aiming at compensating for the voltage drop across the equivalent arm resistance. Although this term improves performance, it is not fundamentally necessary for the proper operation of the controller and, for the sake of simplicity, it is not included in this thesis.

B.2 MMC control tuning

This section presents the approach used for the tuning of the control loops. It is noted that the goal is not to obtain an optimised performance for each control loop, but to develop a working controller which, together with the power stage equations of the converter, can be studied by means of the calculation and transformation methods presented in this thesis.

B.2.1 Phase-locked loop

Following the notation introduced in Section 1.2.3, it is recalled that the PLL rotation angle is decomposed in (1.23) as:

$$\theta_{\text{PLL}} = \theta_1 + \theta_\epsilon \quad (\text{B.14})$$

with $\theta_1 = \frac{1}{s}\omega_1$ an angle of known value. Likewise, the true angle θ_{true} tracked by the PLL can be decomposed as:

$$\theta_{\text{true}} = \theta_1 + \theta_\epsilon^*. \quad (\text{B.15})$$

Consequently, θ_{PLL} is equal to θ_{true} if θ_ϵ is equal to θ_ϵ^* . The objective of the PLL can thus be rethought into controlling angle θ_ϵ to the unknown reference θ_ϵ^* , which is done by acting on the frequency deviation $\delta\omega_{\text{PLL}}$. The control error corresponds to the deviation angle:

$$\delta\theta_{\text{PLL}} = \theta_\epsilon^* - \theta_\epsilon. \quad (\text{B.16})$$

From (1.21b) and (1.23), we have

$$\theta_\epsilon = \theta_{\text{PLL}} - \frac{1}{s}\omega_1 = \frac{1}{s}\delta\omega_{\text{PLL}}. \quad (\text{B.17})$$

From (1.21a) and the reasoning above, we have:

$$\delta\omega_{\text{PLL}} = \left(K_p^{\text{PLL}} + \frac{K_i^{\text{PLL}}}{s} \right) (\theta_\epsilon^* - \theta_\epsilon). \quad (\text{B.18})$$

Combining the transfer functions gives:

$$\theta_\epsilon = \frac{1}{s} \left(K_p^{\text{PLL}} + \frac{K_i^{\text{PLL}}}{s} \right) (\theta_\epsilon^* - \theta_\epsilon), \quad (\text{B.19})$$

which is shown as a block diagram in Fig. B.2. The closed-loop transfer function

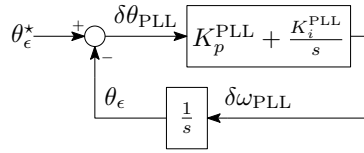


Figure B.2: Block-diagram of linearised PLL dynamics

from θ_ϵ^* to θ_ϵ is:

$$\theta_\epsilon = \frac{sK_p^{\text{PLL}} + K_i^{\text{PLL}}}{s^2 + sK_p^{\text{PLL}} + K_i^{\text{PLL}}} \theta_\epsilon^*. \quad (\text{B.20})$$

A simple tuning of the proportional and integral parameters comes down to choosing the poles of the closed-loop transfer function to obtain a stable system with acceptable performance. The closed-loop transfer function (B.20) is compared with the following second-order transfer function:

$$\frac{2\zeta\omega_n s + \omega_n^2}{s^2 + 2\zeta\omega_n s + \omega_n^2} \quad (\text{B.21})$$

with ω_n the natural frequency. It is noted that the zero at the numerator of this transfer function results in a different dynamic behaviour than that of a simple second-order harmonic oscillator. In particular, setting parameter $\zeta = \sqrt{2}$ gives a step-response overshoot equal to 8.3%. In this case, the bandwidth, i.e. the frequency beyond which the gain of the transfer function drops below -3 dB, is approximately given by $\omega_{bw} \approx 3\omega_n$. Relying on a direct comparison of (B.20) with (B.21), the PI parameters are obtained as:

$$K_p^{\text{PLL}} = 2\sqrt{2}\omega_n = \frac{2\sqrt{2}}{3}\omega_{bw}^{\text{PLL}} \quad (\text{B.22a})$$

$$K_i^{\text{PLL}} = \omega_n^2 = \left(\frac{1}{3}\omega_{bw}^{\text{PLL}}\right)^2 \quad (\text{B.22b})$$

with ω_{bw}^{PLL} the desired bandwidth of the PLL.

B.2.2 Power control loops

In the absence of zero-sequence alternating currents, the instantaneous AC-side active and reactive powers (p_g, q_g) are expressed in terms of abc components

as:

$$p_g = v_{ga}i_{sa} + v_{gb}i_{sb} + v_{gc}i_{sc} \quad (\text{B.23a})$$

$$q_g = \frac{1}{\sqrt{3}}(v_{ga}(i_{sc} - i_{sb}) + v_{gb}(i_{sa} - i_{sc}) + v_{gc}(i_{sb} - i_{sa})), \quad (\text{B.23b})$$

and in terms of dq (peak-invariant) components as [12, Ch.3]:

$$p_g = \frac{3}{2}(v_{gd}i_{sd} + v_{gq}i_{sq}), \quad q_g = \frac{3}{2}(v_{gq}i_{sd} - v_{gd}i_{sq}). \quad (\text{B.24})$$

Relying on the fact that the alternating-voltage filter does not introduce any phase shift at the fundamental frequency and assuming that the PLL perfectly tracks the d -axis component of the alternating voltage in steady state, the q -axis component is equal to zero in steady state ($v_{gq} = 0$). Consequently,

$$p_g = \frac{3}{2}v_{gd}i_{sd}, \quad q_g = -\frac{3}{2}v_{gd}i_{sq}. \quad (\text{B.25})$$

Besides, for the purpose of control tuning, the d -axis component is considered to be equal to the rated voltage magnitude \hat{V}_g :

$$p_g = \frac{3}{2}\hat{V}_g i_{sd} = \xi i_{sd}, \quad q_g = -\frac{3}{2}\hat{V}_g i_{sq} = -\xi i_{sq}, \quad (\text{B.26})$$

with $\xi \triangleq \frac{3}{2}\hat{V}_g$. Relying on the principle of time-scale separation, it is assumed that the alternating current control loops are much faster than the power control loops, implying that $i_{s,dq} \approx i_{s,dq}^*$. Based on this assumption, combining (B.26) with (1.29) gives a relationship between the active and reactive powers and their control errors:

$$p_g = \xi \left(K_p^{\text{PQ}} + \frac{K_i^{\text{PQ}}}{s} \right) (p_g^* - p_g), \quad (\text{B.27a})$$

$$q_g = \xi \left(K_p^{\text{PQ}} + \frac{K_i^{\text{PQ}}}{s} \right) (q_g^* - q_g). \quad (\text{B.27b})$$

The -1 factor in the reactive power formula (B.26) is compensated by that of the reactive power controller in (1.29). The tuning becomes the same for both control loops and only the active power controller is considered further. The closed-loop transfer function from p_g^* to p_g is:

$$p_g = \frac{\xi K_p^{\text{PQ}} s + \xi K_i^{\text{PQ}}}{(\xi K_p^{\text{PQ}} + 1)s + \xi K_i^{\text{PQ}}} p_g^*. \quad (\text{B.28})$$

The PI parameters can be tuned in such a way that the closed-loop transfer function is sufficiently well approximated by a first order system of bandwidth ω_{bw}^{PQ} :

$$p_g \approx \frac{\omega_{bw}^{PQ}}{s + \omega_{bw}^{PQ}} p_g^*. \quad (\text{B.29})$$

This is made possible by taking $\xi K_p^{PQ} \ll 1$ and $\xi K_i^{PQ} = \omega_{bw}^{PQ}$, or equivalently, $K_p^{PQ} \ll \frac{2}{3\hat{V}_f}$ and $K_i^{PQ} = \frac{2}{3\hat{V}_f} \omega_{bw}^{PQ}$. The desired bandwidth ω_{bw}^{PQ} is also constrained by the time-scale separation: $\omega_{bw}^{PQ} \ll \omega_{bw}^{AC}$.

B.2.3 Direct voltage control loop

According to [12, Ch.3], the dynamics of the DC-bus energy w_d are given by:

$$w_d = \frac{1}{s}(p_d - p_g), \quad (\text{B.30})$$

with p_d and p_g the DC-side and AC-side active powers, respectively. In (B.3), the alternating current reference was associated with the active power reference p_g^* . If the AC controller is sufficiently faster than the DV controller, then p_g in (B.30) can be replaced by the expression of p_g^* in (B.2), which gives the open-loop transfer function:

$$w_d = \frac{1}{s} \left(p_d + \left(K_p^{DV} + \frac{K_i^{DV}}{s} \right) (w_d^* - w_d) \right). \quad (\text{B.31})$$

The closed-loop transfer functions from w_d^* and p_g to w_d are:

$$w_d = \frac{sK_p^{DV} + K_i^{DV}}{s^2 + sK_p^{DV} + K_i^{DV}} w_d^* + \frac{s}{s^2 + sK_p^{DV} + K_i^{DV}} p_d. \quad (\text{B.32})$$

It is noticed that the static gain from p_d to w_d is equal to zero for any non-zero value of K_i^{DV} , thereby ensuring disturbance rejection at 0 Hz. The tuning of the PI parameters relies on the same procedure as for the PLL. The PI parameters are obtained as:

$$K_p^{DV} = \frac{2\sqrt{2}}{3} \omega_{bw}^{DV} \quad (\text{B.33a})$$

$$K_i^{DV} = \left(\frac{1}{3} \omega_{bw}^{DV} \right)^2 \quad (\text{B.33b})$$

with ω_{bw}^{DV} the desired bandwidth of the DV controller.

B.2.4 Alternating voltage control loop

Applying Kirchhoff's current law to the MMC PCC in Fig. B.1 gives the dynamic behaviour of the controlled alternating voltage $v_{g\varphi}$ as:

$$C_{g,eq} \frac{dv_{g\varphi}}{dt} = i_{g\varphi} + i_{x\varphi}^{tot}, \quad (\text{B.34})$$

with $C_{g,eq}$ the equivalent capacitor. The corresponding transfer function is:

$$v_{g\varphi} = \frac{1}{sC_{g,eq}} (i_{g\varphi} + i_{x\varphi}^{tot}). \quad (\text{B.35})$$

If the AC controller is sufficiently faster than the AV controller, then $i_{g\varphi}$ can be considered equal to its reference and thus be replaced with the expression of $i_{g\varphi}^*$ from (B.6). Further assuming that the feedforward current in (B.6) approximately cancels $i_{x\varphi}^{tot}$, the following transfer function is obtained:

$$v_{g\varphi} = \frac{1}{sC_{g,eq}} \left(K_p^{\text{AV}} + \frac{K_r^{\text{AV}} s}{s^2 + \omega_1^2} \right) (v_{g\varphi}^* - v_{g\varphi}). \quad (\text{B.36})$$

The transfer function from $v_{g\varphi}^*$ to $v_{g\varphi}$ is obtained as:

$$v_{g\varphi} = \frac{s^2 K_p^{\text{AV}} + s K_r^{\text{AV}} + \omega_1^2 K_p^{\text{AV}}}{s^3 C_{g,eq} + s^2 K_p^{\text{AV}} + s(K_r^{\text{AV}} + \omega_1^2 C_{g,eq}) + \omega_1^2 K_p^{\text{AV}}} v_{g\varphi}^*. \quad (\text{B.37})$$

The chosen control design relies on selecting proportional and resonant coefficients in such a way that the third-order transfer function (B.37) is close to a first order transfer function of desired bandwidth ω_{bw}^{AV} . Practically, (B.37) is compared with:

$$\frac{as^2 + bs + c}{(ds + 1)(as^2 + bs + c)}. \quad (\text{B.38})$$

By developing the denominator and identifying all coefficients one by one, the following conditions are obtained:

$$\begin{aligned} a &= K_p^{\text{AV}} & ad &= C_{g,eq} \\ b &= K_r^{\text{AV}} & a + bd &= K_p^{\text{AV}} \\ c &= \omega_1^2 K_p^{\text{AV}} & b + cd &= \omega_1^2 C_{g,eq} + K_r^{\text{AV}} \\ & & c &= \omega_1^2 K_p^{\text{AV}} \end{aligned} \quad (\text{B.39})$$

with $d = 1/\omega_{bw}^{\text{AV}}$. The set of relationships can be reduced to the following conditions:

$$\begin{cases} K_p^{\text{AV}} = \omega_{bw}^{\text{AV}} C_{g,eq} \\ K_r^{\text{AV}} = 0. \end{cases} \quad (\text{B.40})$$

Although the tuning approach suggests that K_r^{AV} should be zero, in this thesis it is simply set to a small value.

B.2.5 Alternating current control loop

The dynamic behaviour of the controlled alternating current $i_{s\varphi}$ is given by:

$$L_e \frac{di_{s\varphi}}{dt} = -R_e i_{s\varphi} + v_{s\varphi} - \frac{1}{k} v_{g\varphi} \quad (\text{B.41})$$

with k the transformation ratio. The corresponding transfer function is:

$$i_{s\varphi} = \frac{1}{sL_e + R_e} (v_{s\varphi} - \frac{1}{k} v_{g\varphi}). \quad (\text{B.42})$$

Assuming that $v_{s\varphi}$ is equal to its reference, it can be replaced with the expression of $v_{s\varphi}^*$ from (1.31a). Observing that the feedforward voltage in (1.31a) approximately cancels $-\frac{1}{k} v_{g\varphi}$, the following transfer function is obtained:

$$i_{s\varphi} = \frac{1}{sL_e + R_e} \left(K_p^{\text{AC}} + \frac{K_r^{\text{AC}} s}{s^2 + \omega_1^2} \right) (i_{s\varphi}^* - i_{s\varphi}). \quad (\text{B.43})$$

The transfer function from $i_{s\varphi}^*$ to $i_{s\varphi}$ is obtained as:

$$i_{s\varphi} = \frac{s^2 K_p^{\text{AC}} + s K_r^{\text{AC}} + \omega_1^2 K_p^{\text{AC}}}{s^3 L_e + s^2 (K_p^{\text{AC}} + R_e) + s (K_r^{\text{AC}} + \omega_1^2 L_e) + \omega_1^2 (K_p^{\text{AC}} + R_e)} i_{s\varphi}^*. \quad (\text{B.44})$$

The chosen control design relies on selecting proportional and resonant coefficients in such a way that the third-order transfer function (B.44) is close to a first order transfer function of desired bandwidth ω_{bw}^{AC} . Practically, (B.44) is compared with:

$$\frac{as^2 + bs + c}{(ds + 1)(as^2 + bs + c)}. \quad (\text{B.45})$$

By developing the denominator and identifying all coefficients one by one, the following conditions are obtained:

$$\begin{aligned} a &= K_p^{\text{AC}} & ad &= L_e \\ b &= K_r^{\text{AC}} & a + bd &= K_p^{\text{AC}} + R_e \\ c &= \omega_1^2 K_p^{\text{AC}} & b + cd &= \omega_1^2 L_e + K_r^{\text{AC}} \\ & & c &= \omega_1^2 (K_p^{\text{AC}} + R_e) \end{aligned} \quad (\text{B.46})$$

with $d = 1/\omega_{bw}^{\text{AC}}$. The set of relationships can be reduced to the following conditions:

$$\begin{cases} K_p^{\text{AC}} = \omega_{bw}^{\text{AC}} L_e \quad \text{and} \quad K_p^{\text{AC}} \gg R_e \\ K_r^{\text{AC}} = \omega_{bw}^{\text{AC}} R_e. \end{cases} \quad (\text{B.47})$$

B.2.6 Circulating current control loop

The dynamic behaviour of the controlled circulating current $i_{c\phi}$ is given by:

$$L_a \frac{di_{c\phi}}{dt} = -R_a i_{c\phi} + \frac{v_d}{2} - v_{c\phi}. \quad (\text{B.48})$$

The corresponding transfer function is:

$$i_{c\phi} = \frac{1}{sL_a + R_a} \left(\frac{v_d}{2} - v_{c\phi} \right). \quad (\text{B.49})$$

Assuming that $v_{c\phi}$ is equal to its reference, it can be replaced with the expression of $v_{c\phi}^*$ from (B.12). Observing that the feedforward voltage in (B.12) cancels $\frac{v_d}{2}$, the following transfer function is obtained:

$$i_{c\phi} = \frac{1}{sL_a + R_a} \left(K_p^{\text{CC}} + \frac{sK_r^{\text{CC}}}{s^2 + (2\omega_1)^2} \right) (i_c^* - i_{c\phi}). \quad (\text{B.50})$$

The transfer function from i_c^* to i_c is obtained as:

$$i_{c\phi} = \frac{s^2 K_p^{\text{CC}} + s K_r^{\text{CC}} + 4\omega_1^2 K_p^{\text{CC}}}{s^3 L_a + s^2 (K_p^{\text{CC}} + R_a) + s(4\omega_1^2 L_a + K_r^{\text{CC}}) + 4\omega_1^2 (K_p^{\text{CC}} + R_a)} i_c^*. \quad (\text{B.51})$$

As for the AC and AV controllers, the design relies on selecting proportional and resonant coefficients in such a way that the third-order transfer function (B.44) is close to a first order transfer function of desired bandwidth ω_{bw}^{CC} .

The procedure results in the following conditions:

$$\begin{cases} K_p^{\text{CC}} = \omega_{bw}^{\text{CC}} L_a \quad \text{and} \quad K_p^{\text{CC}} \gg R_a \\ K_r^{\text{CC}} = \omega_{bw}^{\text{CC}} R_a. \end{cases} \quad (\text{B.52})$$

B.2.7 Summary of parameters

The following relationships are used to define base quantities and to convert values from pu to SI:

$$\begin{aligned} V_a^{\text{base}} &= \sqrt{2/3} U_{a,\text{rmsLL}} & R_a &= R_a^{\text{pu}} Z_a^{\text{base}} \\ I_a^{\text{base}} &= \frac{2}{3} \frac{S_a^{\text{base}}}{V_a^{\text{base}}} & R_g &= R_g^{\text{pu}} Z_a^{\text{base}} \\ Z_a^{\text{base}} &= \frac{V_a^{\text{base}}}{I_a^{\text{base}}} & X_g &= X_g^{\text{pu}} Z_a^{\text{base}} \\ & & L_g &= \frac{X_g}{\omega_1}. \end{aligned} \quad (\text{B.53})$$

Here, LL indicates line-to-line (or phase-to-phase) voltages. The nominal amplitude of line-to-line voltages is also written U while the letter V denotes the nominal amplitude of line-to-ground (or phase-to-ground) voltages.

Table B.1: Parameters: MMC circuit [119]

| Symbol | Description | Value [SI] | Value [pu] |
|------------------|----------------------------------|--------------------|------------|
| S_{nom} | nominal apparent power | 1 GVA | |
| U_a | line-to-line alternating voltage | 320 kVrms LL | |
| V_d | pole-to-pole direct voltage | 640 kV | |
| C_a | equivalent arm capacitance | 32.5 μF | |
| R_a | equivalent arm resistance | 1.024 Ω | 0.01 |
| L_a | arm inductance | 48 mH | |
| X_g | transformer reactance | 18.43 Ω | 0.18 |
| L_g | transformer inductance | 58.7 mH | |
| R_g | transformer resistance | 0.512 Ω | 0.005 |
| C_s | submodule capacitance | 13 mF | |
| N_s | number of submodules per arm | 400 | |
| f_1 | fundamental grid frequency | 50 Hz | |

Table B.2: Parameters: MMC controller

| Symbol | Description | Value/Relation | Units |
|----------------------------|------------------------------|---------------------------------------|-------------------|
| K_p^{AV} | AV control proportional gain | $\omega_{bw}^{\text{AV}} C_{g,eq}$ | Ω |
| K_r^{AV} | AV control resonant gain | 0.01 | Ω/s |
| ω_{bw}^{AV} | AV control bandwidth | $2\pi 200$ | rad/s |
| K_p^{AC} | AC control proportional gain | $\omega_{bw}^{\text{AC}} L_e$ | Ω |
| K_r^{AC} | AC control resonant gain | $\omega_{bw}^{\text{AC}} R_e$ | Ω/s |
| ω_{bw}^{AC} | AC control bandwidth* | $2\pi 150$ | rad/s |
| ω_{bw}^{AC} | AC control bandwidth** | $2\pi 300$ | rad/s |
| K_p^{CC} | CC control proportional gain | $\omega_{bw}^{\text{CC}} L_a$ | Ω |
| K_r^{CC} | CC control resonant gain | $\omega_{bw}^{\text{CC}} R_a$ | Ω/s |
| ω_{bw}^{CC} | CC control bandwidth | $2\pi 150$ | rad/s |
| K_p^{PQ} | PQ control proportional gain | $2/(3V_g)0.05$ | $1/\text{V}$ |
| K_i^{PQ} | PQ control integral gain | $2/(3V_g)\omega_{bw}^{\text{PQ}}$ | $1/(\text{Vs})$ |
| ω_{bw}^{PQ} | PQ control bandwidth | $2\pi 5$ | rad/s |
| K_p^{PLL} | PLL proportional gain | $2\sqrt{2}/3\omega_{bw}^{\text{PLL}}$ | $1/\text{s}$ |
| K_i^{PLL} | PLL integral gain | $(1/3\omega_{bw}^{\text{PLL}})^2$ | $1/\text{s}^2$ |
| ω_{bw}^{PLL} | PLL bandwidth | $2\pi 10$ | rad/s |
| K_p^{DV} | DV control proportional gain | $2\sqrt{2}/3\omega_{bw}^{\text{DV}}$ | $1/\text{s}$ |
| K_i^{DV} | DV control integral gain | $(1/3\omega_{bw}^{\text{DV}})^2$ | $1/\text{s}^2$ |
| ω_{bw}^{DV} | DV control bandwidth | $2\pi 5$ | rad/s |
| t_d | control time delay | See Section 4.5 | μs |

*in AC-grid-following mode **in AC-grid-forming mode

B.3 TLC modelling and control

This section presents two models of the two-level converter (TLC): a stationary-frame model with a complete controller, used to represent aggregated wind farms in the offshore grid described in Appendix B.4, and a rotating-frame model with a simplified controller, used in Section 2.3 to illustrate the application of the developed stability criterion.

B.3.1 Stationary-frame TLC model

Circuit differential equations

In this thesis, the model of the three-phase TLC relies on Assumptions 1 and 2, which simplify the transformer modelling and allow neglecting the zero-sequence

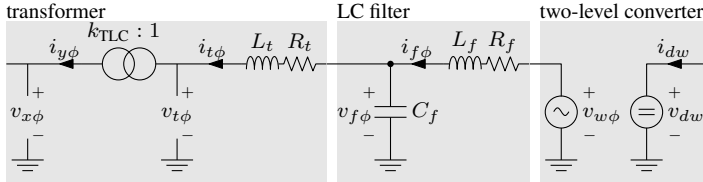


Figure B.3: Two-level converter: circuit diagram

dynamics, thereby describing the system in terms of $\alpha\beta$ variables instead of abc variables. Additionally, the following assumption is introduced:

Assumption 13. *The two-level converter operates with an ideal modulation; switching dynamics and switching harmonics are negligible.*

Under Assumption 13, an averaged model is used and the TLC is represented by controlled voltage sources. The voltage at the AC terminals of the converter is thus given by:

$$v_{w\varphi} = \frac{1}{2}v_{dw}m_{w\varphi}, \quad (\text{B.54})$$

with $\varphi \in \{\alpha, \beta\}$, v_{dw} the direct voltage and $m_{w\varphi}$ the phase modulation indices, which take continuous values over $[-1; 1]$. All subscripts w refer to the TLC specifically and stand for *wind* in the context of the offshore wind farm system in Appendix B.4.

As depicted in Fig. B.3, the TLC is connected to the AC grid via an inductance-capacitance (LC) filter and a transformer. The LC filter is represented by its series components R_f and L_f , and shunt capacitance C_f . Under Assumption 1, the transformer is represented by its series components R_t and L_t , as well as by a real-valued transformation ratio k_{TLC} . Under Assumption 2, no zero-sequence current flows on the converter side of the transformer. This assumption is extended to the LC filter. Eventually, the circuit equations are obtained from the application of Kirchhoff's Laws:

$$\begin{cases} L_f \frac{di_{f\varphi}}{dt} = -R_f i_{f\varphi} + v_{w\varphi} - v_{f\varphi} \\ C_f \frac{dv_{f\varphi}}{dt} = i_{f\varphi} - i_{t\varphi} \\ L_t \frac{di_{t\varphi}}{dt} = -R_t i_{t\varphi} + v_{f\varphi} - v_{t\varphi}. \end{cases} \quad (\text{B.55})$$

The voltage and currents on the grid side of the transformer are obtained as $v_{x\varphi} = k_{\text{TLC}}v_{t\varphi}$ and $i_{y\varphi} = \frac{1}{k_{\text{TLC}}}i_{t\varphi}$.

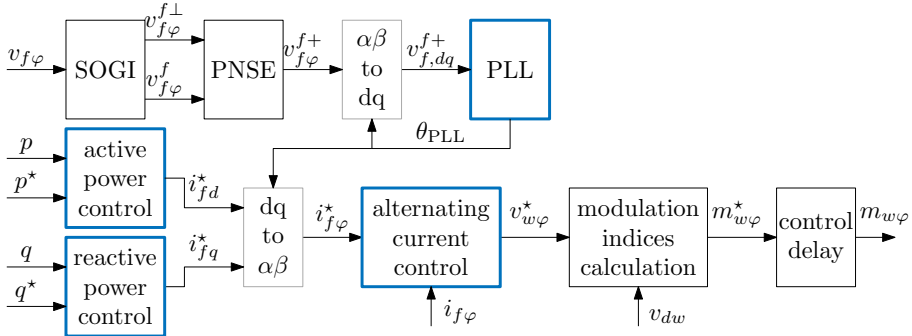


Figure B.4: Overview of TLC control structure, with control blocks in blue, frame rotations in grey, filters and other calculations in black.

Overview of TLC control

The TLC control structure used in this thesis is displayed in Fig B.4: the alternating voltage reference $v_{w\varphi}^*$ is obtained from a PR alternating current controller implemented in the $\alpha\beta$ frame. The alternating current references $i_{f\varphi}^*$ are provided by the active and reactive power controller and a frame rotation is used to transform the dq current references into $\alpha\beta$ references. The rotation angle is obtained from a PLL relying on the filtered positive-sequence voltage $v_{f\varphi}^{f+}$ across the capacitor of the LC filter. The alternating voltage is filtered and the positive-sequence components are separated from potential negative-sequence components by means of a SOGI and a PNSE. All dynamic equations of the alternating current controller, power controller, PLL and SOGI-PNSE are equivalent to those presented in Section 1.2 and are not repeated here.

At the modulation stage, the modulation index references $m_{w,\varphi}^*$ are obtained from the alternating voltage references and a control time delay is represented by an aggregated constant time-shift of the modulation index references:

$$m_{w,\varphi}^* = 2 \frac{v_{w,\varphi}^*}{v_{dw}}, \quad (\text{B.56a})$$

$$m_{w\varphi}(t) = m_{w\varphi}^* (t - t_d^{\text{TLC}}). \quad (\text{B.56b})$$

Parameters: TLC circuit and controller

The control parameters are obtained based on the same tuning rules presented in Section B.2 for the MMC, which are thus not repeated here. All circuit and

control parameters are provided in Table B.3. It is noted that the offshore grid in Appendix B.4 comprises three TLCs with different power ratings noted S_{wi}^{base} , $i = \{1, 2, 3\}$. The base values and the circuit parameters of converter i are obtained by means of the following formulas:

$$\begin{aligned} V_w^{\text{base}} &= \sqrt{2/3} U_{w,\text{rmsLL}} & X_{L,fi} &= X_{L,f}^{\text{pu}} Z_{wi}^{\text{base}} & R_{fi} &= R_f^{\text{pu}} Z_{wi}^{\text{base}} \\ I_{wi}^{\text{base}} &= \frac{2}{3} \frac{S_{wi}^{\text{base}}}{V_w^{\text{base}}} & L_{fi} &= \frac{X_{L,fi}}{\omega_1} & X_{L,yi} &= X_y^{\text{pu}} Z_{wi}^{\text{base}} \\ Z_{wi}^{\text{base}} &= \frac{V_w^{\text{base}}}{I_{wi}^{\text{base}}} & X_{C,fi} &= X_{C,f}^{\text{pu}} Z_{wi}^{\text{base}} & L_{yi} &= \frac{X_{L,yi}}{\omega_1} \\ & & C_{fi} &= \frac{1}{X_{C,fi}\omega_1} & R_{yi} &= R_y^{\text{pu}} Z_{wi}^{\text{base}} \end{aligned} \quad (\text{B.57a})$$

Table B.3: Parameters: TLC circuit and controller [120]

| Symbol | Description | Value/Relation | Units |
|----------------------------|--------------------------------|---|-----------------------|
| R_f^{pu} | LC filter resistance | 0.01 | pu |
| $X_{L,f}^{\text{pu}}$ | LC filter inductive reactance | 0.2 | pu |
| $X_{C,f}^{\text{pu}}$ | LC filter capacitive reactance | 6.67 | pu |
| X_y^{pu} | transformer series reactance | 0.1 | pu |
| R_y^{pu} | transformer series resistance | 0.04 | pu |
| K_p^{AC} | AC control* | $\omega_{bw}^{\text{AC}} L_f$ | Ω |
| K_r^{AC} | AC control* | $\omega_{bw}^{\text{AC}} R_f$ | Ω/s |
| K_p^{AC} | AC control** | $\frac{2}{3}\sqrt{2}\omega_{bw}^{\text{PLL}} L_f$ | Ω |
| K_i^{AC} | AC control** | $(\frac{1}{3}\omega_{bw}^{\text{PLL}})^2 L_f$ | Ω/s |
| ω_{bw}^{AC} | AC control | $2\pi 150$ | rad/s |
| K_p^{PQ} | PQ control | $2/(3V_w)0.05$ | $1/\text{V}$ |
| K_i^{PQ} | PQ control | $2/(3V_w)\omega_{bw}^{\text{PQ}}$ | $1/(\text{Vs})$ |
| ω_{bw}^{PQ} | PQ control | $2\pi 5$ | rad/s |
| K_p^{PLL} | PLL | $\frac{2}{3}\sqrt{2}\omega_{bw}^{\text{PLL}}$ | $1/\text{s}$ |
| K_i^{PLL} | PLL | $(\frac{1}{3}\omega_{bw}^{\text{PLL}})^2$ | $1/\text{s}^2$ |
| ω_{bw}^{PLL} | PLL | $2\pi 10$ | rad/s |
| t_d^{TLC} | control time delay | 150 | μs |

*stationary-frame model **rotating-frame model

B.3.2 Simplified rotating-frame TLC model

A simplified rotating-frame model of the TLC is used in Section 2.3 to illustrate the application of the developed stability criterion. The model consists of the circuit equations (B.55) brought to a synchronously-rotating dq frame. The controller is simplified: the $\alpha\beta$ -frame current controller is replaced with a typical decoupled dq -frame current controller [6, 120]. Filters, PLL dynamics and time delays are discarded. The complete set of differential equations is thus given by:

$$\left. \begin{aligned} \frac{di_{td}}{dt} &= \omega_1 i_{tq} + \frac{1}{L_t} (-R_t i_{td} + v_{fd} - v_{td}) \end{aligned} \right\} \quad (\text{B.58a})$$

$$\frac{di_{tq}}{dt} = -\omega_1 i_{td} + \frac{1}{L_t} (-R_t i_{tq} + v_{fq} - v_{tq}) \quad (\text{B.58b})$$

$$\frac{dv_{fd}}{dt} = \omega_1 v_{fq} + \frac{1}{C_f} (i_{fd} - i_{td}) \quad (\text{B.58c})$$

$$\frac{dv_{fq}}{dt} = -\omega_1 v_{fd} + \frac{1}{C_f} (i_{fq} - i_{tq}) \quad (\text{B.58d})$$

$$\frac{di_{fd}}{dt} = \omega_1 i_{fq} + \frac{1}{L_f} (-R_f i_{fd} + v_{wd} - v_{fd}) \quad (\text{B.58e})$$

$$\frac{di_{fq}}{dt} = -\omega_1 i_{fd} + \frac{1}{L_f} (-R_f i_{fq} + v_{wq} - v_{fq}) \quad (\text{B.58f})$$

$$\frac{d\eta_{ACd}}{dt} = K_i^{AC} (i_{fd}^* - i_{fd}) \quad (\text{B.58g})$$

$$\frac{d\eta_{ACq}}{dt} = K_i^{AC} (i_{fq}^* - i_{fq}) \quad (\text{B.58h})$$

$$\frac{d\eta_{PQd}}{dt} = K_i^{PQ} (p_f^* - p_f) \quad (\text{B.58i})$$

$$\left. \begin{aligned} \frac{d\eta_{PQq}}{dt} &= -K_i^{PQ} (q_f^* - q_f), \end{aligned} \right\} \quad (\text{B.58j})$$

with

$$\left. \begin{aligned} p_f &= \frac{3}{2}(i_{fd}v_{fd} + i_{fq}v_{fq}) \\ q_f &= \frac{3}{2}(i_{fd}v_{fq} - i_{fq}v_{fd}) \end{aligned} \right\} \quad (\text{B.59a})$$

$$q_f = \frac{3}{2}(i_{fd}v_{fq} - i_{fq}v_{fd}) \quad (\text{B.59b})$$

$$i_{fd}^* = \eta_{PQd} + K_p^{PQ}(p_f^* - p_f) \quad (\text{B.59c})$$

$$i_{fq}^* = \eta_{PQq} - K_p^{PQ}(q_f^* - q_f) \quad (\text{B.59d})$$

$$v_{wd}^* = \eta_{ACd} + v_{fd} - \omega_1 L_f i_{fq} + K_p^{AC}(i_{fd}^* - i_{fd}) \quad (\text{B.59e})$$

$$v_{wq}^* = \eta_{ACq} + v_{fq} + \omega_1 L_f i_{fd} + K_p^{AC}(i_{fq}^* - i_{fq}) \quad (\text{B.59f})$$

$$v_{wd} = v_{wd}^* \quad (\text{B.59g})$$

$$v_{wq} = v_{wq}^*. \quad (\text{B.59h})$$

In this model, v_{wd} corresponds to the d -axis component of alternating voltage $v_{w\varphi}$, while v_{dw} corresponds to the DC-bus voltage of the TLC.

B.4 MMC-based test systems

This section presents a complete MMC-based system, which consists of a point-to-point MMC-based HVDC link connecting an offshore grid. Considered as a whole for an illustrative harmonic propagation study in Section 5.5, its sub-parts taken separately are also used as illustrative examples. For instance, the HVDC link is considered independently from the offshore grid in Section 3.2. The offshore grid is considered independently from the HVDC link in Section 4.5.

The system layout is presented first and the HVDC and AC cables models are described next. The layout and the values of parameters are based on [120], with a few adaptations, and to the exception of the HVDC link voltages, which are based on [119]. All parameters are given in Table B.4.

B.4.1 System layout

Fig. B.5 presents the layout and the voltage ratings of the test system. The HVDC link is in the symmetrical monopole configuration, and the offshore grid acts as collection system for a set of three aggregated wind farms. The onshore AC grid is represented by a three-phase alternating voltage source. The first MMC (MMC_1) corresponds to the onshore converter and is operated

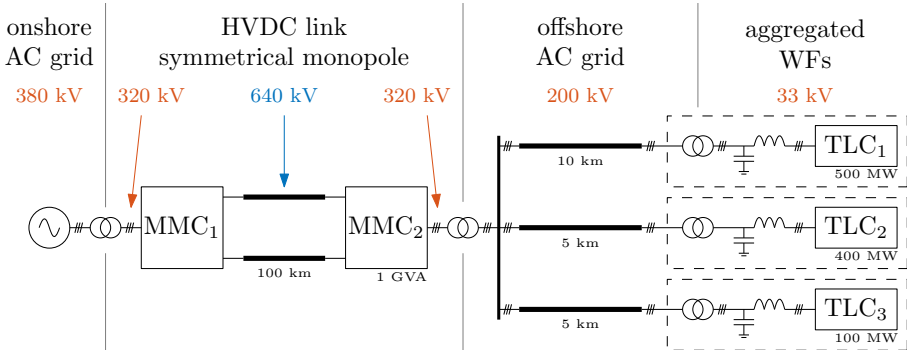


Figure B.5: Offshore HVDC system: circuit diagram

Table B.4: Parameters: MMC-based test system (nominal values) [119, 120]

| Symbol | Definition | Value | Units |
|-----------|--------------------------------|-------|----------|
| f_1 | fundamental frequency | 50 | Hz |
| S_{MMC} | apparent power of $MMC_{1,2}$ | 1 | GVA |
| S_{w1} | apparent power of TLC_1 | 500 | MVA |
| S_{w2} | apparent power of TLC_2 | 400 | MVA |
| S_{w3} | apparent power of TLC_3 | 100 | MVA |
| U_t | onshore AC-grid voltage | 380 | kVrms LL |
| U_g | offshore AC-grid voltage | 200 | kVrms LL |
| U_a | MMC terminal voltage | 320 | kVrms LL |
| U_w | TLC terminal voltage | 33 | kVrms LL |
| V_d | pole-to-pole HVDC link voltage | 640 | kV |
| V_{dw} | TLC DC-bus voltage | 65 | kV |

in AC-grid following mode. It controls the pole-to-pole direct voltage on the HVDC link as well as the reactive power exchanged with the onshore grid. The second MMC (MMC_2) corresponds to the offshore converter and is operated in AC-grid forming mode. It acts as a three-phase alternating voltage source for the offshore AC grid and collects the power generated by the aggregated wind farms. The wind farms are represented with TLCs in agreement with the following assumption:

Assumption 14. *A wind farm can be represented in an aggregated way by means of a single equivalent voltage-source TLC with adequately scaled power and voltage ratings. The internal wind-farm dynamics are neglected: the DC-side of the TLC is represented by a fixed direct voltage source and the converter is operated in active and reactive power control mode.*

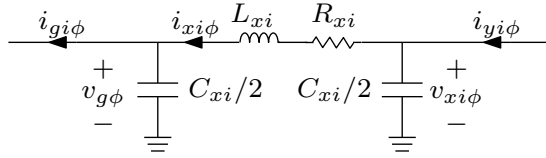


Figure B.6: i^{th} AC cable π -equivalent model (only one phase shown)

B.4.2 Cable models

The test system comprises two types of cables, namely AC cables and HVDC cables, whose models are described in the following paragraphs. All parameters are provided in Table B.5.

AC cable model

Each of the three-phase cables that constitute the offshore AC grid are represented by three uncoupled single-phase cables. These cables being rather short (with a maximum length of 10 km), they are described with π -equivalent models displayed in Fig. B.6. A π -equivalent model comprises the total inductance and total resistance as series elements, and the total capacitance is split equally between the beginning and the end of the cable. The differential equations related to voltage $v_{xi\phi}$ and currents $i_{xi\phi}$ of cable $i \in \{1, 2, 3\}$ are given by:

$$\left\{ \begin{array}{l} \frac{C_{xi}}{2} \frac{dv_{xi\phi}}{dt} = i_{yi\phi} - i_{xi\phi} \\ L_{xi} \frac{di_{xi\phi}}{dt} = -R_{xi} i_{xi\phi} + v_{xi\phi} - v_{g\phi}, \end{array} \right. \quad (\text{B.60a})$$

$$\left\{ \begin{array}{l} \frac{C_{xi}}{2} \frac{dv_{xi\phi}}{dt} = i_{yi\phi} - i_{xi\phi} \\ L_{xi} \frac{di_{xi\phi}}{dt} = -R_{xi} i_{xi\phi} + v_{xi\phi} - v_{g\phi}, \end{array} \right. \quad (\text{B.60b})$$

with $\phi \in \{a, b, c\}$. Since the three cables are connected together at the PCC of the offshore MMC, the dynamics of voltage $v_{g\phi}$ are described by:

$$C_{g,eq} \frac{dv_{g\phi}}{dt} = (i_{x\phi}^{tot} + i_{g\phi}) \quad (\text{B.61})$$

with

$$C_{g,eq} = \frac{1}{2}(C_{x1} + C_{x2} + C_{x3}) \quad (\text{B.62})$$

and

$$i_{x\phi}^{tot} = i_{x1\phi} + i_{x2\phi} + i_{x3\phi}. \quad (\text{B.63})$$

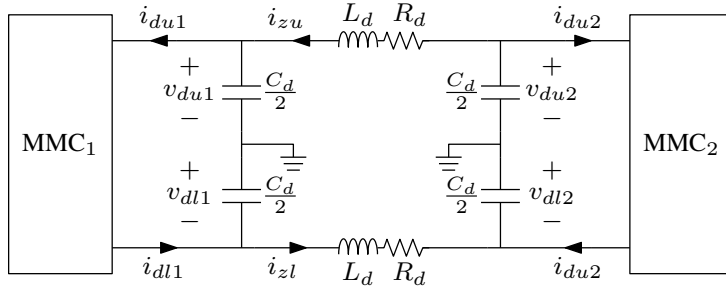


Figure B.7: HVDC cable π -equivalent model in a symmetrical monopole configuration

HVDC cable model

In a symmetrical monopole configuration, an HVDC link is composed of one cable for the positive pole and one cable for the negative pole. Although models of long lines and cables should ideally account for the frequency-dependent characteristics of parameter values, a relative modelling simplicity is once more preserved in this thesis by relying on the π -equivalent model depicted in Fig. B.7. The corresponding set of differential equations is:

$$\left\{ \begin{array}{l} \frac{C_d}{2} \frac{dv_{du1}}{dt} = i_{zu} - i_{du1} \\ \frac{C_d}{2} \frac{dv_{dl1}}{dt} = i_{zl} - i_{dl1} \\ L_d \frac{di_{zu}}{dt} = -R_d i_{zu} + v_{du2} - v_{du1} \\ L_d \frac{di_{zl}}{dt} = -R_d i_{zl} + v_{dl2} - v_{dl1} \\ \frac{C_d}{2} \frac{dv_{du2}}{dt} = -i_{zu} - i_{du2} \\ \frac{C_d}{2} \frac{dv_{dl2}}{dt} = -i_{zl} - i_{dl2}. \end{array} \right. \quad (\text{B.64})$$

Table B.5: Parameters: AC and HVDC cables [120]

| Symbol | Value/Relation | Definition | Units |
|------------|--|--------------------------------|-------|
| l_0 | length of HVDC cable | 100 | km |
| l_1 | length of AC cable connecting TLC ₁ | 10 | km |
| l_2 | length of AC cable connecting TLC ₂ | 5 | km |
| l_3 | length of AC cable connecting TLC ₃ | 5 | km |
| R_d | HVDC cable (one pole) resistance | 15 | mΩ/km |
| L_d | HVDC cable (one pole) inductance | 0.3 | mH/km |
| C_d | HVDC cable (one pole) capacitance | 0.12 | μF/km |
| R_{x1} | AC cable 1 resistance | 15 | mΩ/km |
| R_{x2} | AC cable 2 resistance | 16.5 | mΩ/km |
| R_{x3} | AC cable 3 resistance | 16.5 | mΩ/km |
| L_{x1} | AC cable 1 inductance | 0.3 | mH/km |
| L_{x2} | AC cable 2 inductance | 0.33 | mH/km |
| L_{x3} | AC cable 3 inductance | 0.33 | mH/km |
| C_{x1} | AC cable 1 capacitance | 0.12 | μF/km |
| C_{x2} | AC cable 2 capacitance | 0.11 | μF/km |
| C_{x3} | AC cable 3 capacitance | 0.11 | μF/km |
| $C_{g,eq}$ | MMC ₂ : equivalent AC-bus capacitor | $(C_{x1} + C_{x2} + C_{x3})/2$ | |
| $C_{d,eq}$ | MMC ₁ : equivalent DC-bus capacitor | $6C_a + C_d/4$ | |

B.5 Simplified MMC: Analytical expressions of partial derivatives

The time-periodic state matrix $\mathbf{A}(t)$ of the simplified closed-loop MMC model described in Section 1.2.5 is given by:

$$\mathbf{A}(t) = \left(\begin{array}{ccccccccc} \frac{\partial f_1}{\partial i_s} \Big|_{\bar{\mathbf{p}}} & \frac{\partial f_1}{\partial i_c} \Big|_{\bar{\mathbf{p}}} & \frac{\partial f_1}{\partial v_{Cu}} \Big|_{\bar{\mathbf{p}}} & \frac{\partial f_1}{\partial v_{Cl}} \Big|_{\bar{\mathbf{p}}} & \frac{\partial f_1}{\partial i_d^f} \Big|_{\bar{\mathbf{p}}} & 0 & \frac{\partial f_1}{\partial \eta_{AC2}} \Big|_{\bar{\mathbf{p}}} & 0 & \frac{\partial f_1}{\partial \eta_{CC2}} \Big|_{\bar{\mathbf{p}}} \\ \frac{\partial f_2}{\partial i_s} \Big|_{\bar{\mathbf{p}}} & \frac{\partial f_2}{\partial i_c} \Big|_{\bar{\mathbf{p}}} & \frac{\partial f_2}{\partial v_{Cu}} \Big|_{\bar{\mathbf{p}}} & \frac{\partial f_2}{\partial v_{Cl}} \Big|_{\bar{\mathbf{p}}} & \frac{\partial f_2}{\partial i_d^f} \Big|_{\bar{\mathbf{p}}} & 0 & \frac{\partial f_2}{\partial \eta_{AC2}} \Big|_{\bar{\mathbf{p}}} & 0 & \frac{\partial f_2}{\partial \eta_{CC2}} \Big|_{\bar{\mathbf{p}}} \\ \frac{\partial f_3}{\partial i_s} \Big|_{\bar{\mathbf{p}}} & \frac{\partial f_3}{\partial i_c} \Big|_{\bar{\mathbf{p}}} & 0 & 0 & \frac{\partial f_3}{\partial i_d^f} \Big|_{\bar{\mathbf{p}}} & 0 & \frac{\partial f_3}{\partial \eta_{AC2}} \Big|_{\bar{\mathbf{p}}} & 0 & \frac{\partial f_3}{\partial \eta_{CC2}} \Big|_{\bar{\mathbf{p}}} \\ \frac{\partial f_4}{\partial i_s} \Big|_{\bar{\mathbf{p}}} & \frac{\partial f_4}{\partial i_c} \Big|_{\bar{\mathbf{p}}} & 0 & 0 & \frac{\partial f_4}{\partial i_d^f} \Big|_{\bar{\mathbf{p}}} & 0 & \frac{\partial f_4}{\partial \eta_{AC2}} \Big|_{\bar{\mathbf{p}}} & 0 & \frac{\partial f_4}{\partial \eta_{CC2}} \Big|_{\bar{\mathbf{p}}} \\ 0 & \omega_1/5 & 0 & 0 & -\omega_1/5 & 0 & 0 & 0 & 0 \\ 0 & 0 & 0 & 0 & 0 & 0 & -\omega_1 & 0 & 0 \\ -K_r^{AC} & 0 & 0 & 0 & 0 & \omega_1 & 0 & 0 & 0 \\ 0 & 0 & 0 & 0 & 0 & 0 & 0 & 0 & -2\omega_1 \\ 0 & K_r^{CC} & 0 & 0 & -K_r^{CC} & 0 & 0 & 2\omega_1 & 0 \end{array} \right) \quad (\text{B.65})$$

with analytical expressions of the partial derivatives given by:

$$\frac{\partial f_1}{\partial i_s} \Big|_{\bar{\mathbf{p}}} = -\frac{1}{2L_e \bar{v}_d} (K_p^{AC}(\bar{v}_{Cl} + \bar{v}_{Cu}) + 2R_e \bar{v}_d)$$

$$\frac{\partial f_1}{\partial i_c} \Big|_{\bar{\mathbf{p}}} = \frac{K_p^{CC}}{2L_e \bar{v}_d} (\bar{v}_{Cl} - \bar{v}_{Cu})$$

$$\frac{\partial f_1}{\partial v_{Cu}} \Big|_{\bar{\mathbf{p}}} = -\frac{1}{2L_e \bar{v}_d} \left(\bar{\eta}_{CC2} - \bar{\eta}_{AC2} + \frac{\bar{v}_d}{2} - \bar{v}_g + K_p^{AC}(\bar{i}_s - \bar{i}_s^\star) + K_p^{CC}(\bar{i}_c - \bar{i}_d^f) \right)$$

$$\frac{\partial f_1}{\partial v_{Cl}} \Big|_{\bar{\mathbf{p}}} = \frac{1}{2L_e \bar{v}_d} \left(\bar{\eta}_{AC2} + \bar{\eta}_{CC2} + \frac{\bar{v}_d}{2} + \bar{v}_g - K_p^{AC}(\bar{i}_s - \bar{i}_s^\star) + K_p^{CC}(\bar{i}_c - \bar{i}_d^f) \right)$$

$$\frac{\partial f_1}{\partial i_d^f} \Big|_{\bar{\mathbf{p}}} = -\frac{K_p^{CC}}{2L_e \bar{v}_d} (\bar{v}_{Cl} - \bar{v}_{Cu})$$

$$\frac{\partial f_1}{\partial \eta_{AC2}} \Big|_{\bar{\mathbf{p}}} = \frac{\bar{v}_{Cl} + \bar{v}_{Cu}}{2L_e \bar{v}_d}$$

$$\begin{aligned}
\frac{\partial f_1}{\partial \eta_{CC2}} \Big|_{\bar{\boldsymbol{p}}} &= \frac{\bar{v}_{Cl} - \bar{v}_{Cu}}{2L_e \bar{v}_d} \\
\frac{\partial f_2}{\partial i_s} \Big|_{\bar{\boldsymbol{p}}} &= \frac{K_p^{AC}}{2L_a \bar{v}_d} (\bar{v}_{Cl} - \bar{v}_{Cu}) \\
\frac{\partial f_2}{\partial i_c} \Big|_{\bar{\boldsymbol{p}}} &= -\frac{1}{2L_a \bar{v}_d} (K_p^{CC}(\bar{v}_{Cl} + \bar{v}_{Cu}) + 2R_a \bar{v}_d) \\
\frac{\partial f_2}{\partial v_{Cu}} \Big|_{\bar{\boldsymbol{p}}} &= -\frac{1}{2L_a \bar{v}_d} \left(\bar{\eta}_{CC2} - \bar{\eta}_{AC2} + \frac{\bar{v}_d}{2} - \bar{v}_g + K_p^{AC}(\bar{i}_s - \bar{i}_s^*) + K_p^{CC}(\bar{i}_c - \bar{i}_d^f) \right) \\
\frac{\partial f_2}{\partial v_{Cl}} \Big|_{\bar{\boldsymbol{p}}} &= -\frac{1}{2L_a \bar{v}_d} \left(\bar{\eta}_{AC2} + \bar{\eta}_{CC2} + \frac{\bar{v}_d}{2} + \bar{v}_g - K_p^{AC}(\bar{i}_s - \bar{i}_s^*) + K_p^{CC}(\bar{i}_c - \bar{i}_d^f) \right) \\
\frac{\partial f_2}{\partial i_d^f} \Big|_{\bar{\boldsymbol{p}}} &= \frac{K_p^{CC}}{2L_a \bar{v}_d} (\bar{v}_{Cl} + \bar{v}_{Cu}) \\
\frac{\partial f_2}{\partial \eta_{AC2}} \Big|_{\bar{\boldsymbol{p}}} &= -\frac{\bar{v}_{Cl} - \bar{v}_{Cu}}{2L_a \bar{v}_d} \\
\frac{\partial f_2}{\partial \eta_{CC2}} \Big|_{\bar{\boldsymbol{p}}} &= -\frac{\bar{v}_{Cl} + \bar{v}_{Cu}}{2L_a \bar{v}_d} \\
\frac{\partial f_3}{\partial i_s} \Big|_{\bar{\boldsymbol{p}}} &= \frac{1}{2C_a \bar{v}_d} \left(\bar{\eta}_{CC2} - \bar{\eta}_{AC2} + \frac{\bar{v}_d}{2} - \bar{v}_g + K_p^{AC}(\bar{i}_s - \bar{i}_s^*) + K_p^{CC}(\bar{i}_c - \bar{i}_d^f) \right. \\
&\quad \left. + K_p^{AC} (2\bar{i}_c + \bar{i}_s) \right) \\
\frac{\partial f_3}{\partial i_c} \Big|_{\bar{\boldsymbol{p}}} &= \frac{1}{C_a \bar{v}_d} \left(\bar{\eta}_{CC2} - \bar{\eta}_{AC2} + \frac{\bar{v}_d}{2} - \bar{v}_g + K_p^{AC}(\bar{i}_s - \bar{i}_s^*) + K_p^{CC}(\bar{i}_c - \bar{i}_d^f) \right. \\
&\quad \left. + K_p^{CC} \left(\bar{i}_c + \frac{\bar{i}_s}{2} \right) \right) \\
\frac{\partial f_3}{\partial i_d^f} \Big|_{\bar{\boldsymbol{p}}} &= -\frac{K_p^{CC}}{C_a \bar{v}_d} \left(\bar{i}_c + \frac{\bar{i}_s}{2} \right) \\
\frac{\partial f_3}{\partial \eta_{AC2}} \Big|_{\bar{\boldsymbol{p}}} &= -\frac{1}{C_a \bar{v}_d} \left(\bar{i}_c + \frac{\bar{i}_s}{2} \right)
\end{aligned}$$

$$\begin{aligned}
\frac{\partial f_3}{\partial \eta_{CC2}} \Big|_{\bar{\boldsymbol{p}}} &= \frac{1}{C_a \bar{v}_d} \left(\bar{i}_c + \frac{\bar{i}_s}{2} \right) \\
\frac{\partial f_4}{\partial i_s} \Big|_{\bar{\boldsymbol{p}}} &= -\frac{1}{2C_a \bar{v}_d} \left(\bar{\eta}_{AC2} + \bar{\eta}_{CC2} + \frac{\bar{v}_d}{2} + \bar{v}_g - K_p^{AC}(\bar{i}_s - \bar{i}_s^*) + K_p^{CC}(\bar{i}_c - \bar{i}_d^f) \right. \\
&\quad \left. - K_p^{AC}(2\bar{i}_c - \bar{i}_s) \right) \\
\frac{\partial f_4}{\partial i_c} \Big|_{\bar{\boldsymbol{p}}} &= \frac{1}{C_a \bar{v}_d} \left(\bar{\eta}_{AC2} + \bar{\eta}_{CC2} + \frac{\bar{v}_d}{2} + \bar{v}_g - K_p^{AC}(\bar{i}_s - \bar{i}_s^*) + K_p^{CC}(\bar{i}_c - \bar{i}_d^f) \right. \\
&\quad \left. + K_p^{CC} \left(\bar{i}_c - \frac{\bar{i}_s}{2} \right) \right) \\
\frac{\partial f_4}{\partial i_d^f} \Big|_{\bar{\boldsymbol{p}}} &= -\frac{K_p^{CC}}{C_a \bar{v}_d} \left(\bar{i}_c - \frac{\bar{i}_s}{2} \right) \\
\frac{\partial f_4}{\partial \eta_{AC2}} \Big|_{\bar{\boldsymbol{p}}} &= \frac{\partial f_4}{\partial \eta_{CC2}} \Big|_{\bar{\boldsymbol{p}}} = \frac{1}{C_a \bar{v}_d} \left(\bar{i}_c - \frac{\bar{i}_s}{2} \right).
\end{aligned}$$

Appendix C

Supporting content on implementation

C.1 Matlab toolbox

A dedicated Matlab toolbox¹ has been developed to facilitate the analysis of continuous-time nonlinear delayed systems that follow periodic trajectories. The focus is set on the calculation of such trajectories, on the linearisation of the system around periodic trajectories and on their stability assessment.

This section gives an overview of the toolbox functions. It is important to note that this section should not be considered a user manual: a separate document provided with the toolbox gives a detailed description of the code and parameters, as well as instructions on how to utilise the toolbox effectively.

Fig. C.1 provides an overview of the toolbox capabilities, which are briefly elaborated below. The numerical examples in Chapters 1 to 5 rely on a direct use of the toolbox.

System definition

Dynamic systems are defined by means of their analytical differential equations and output equations in state-space form, together with the numerical value

¹ The toolbox can be accessed via electa's HVDC research portal at:
www.esat.kuleuven.be/electa/hvdcresearch/dsanalysis

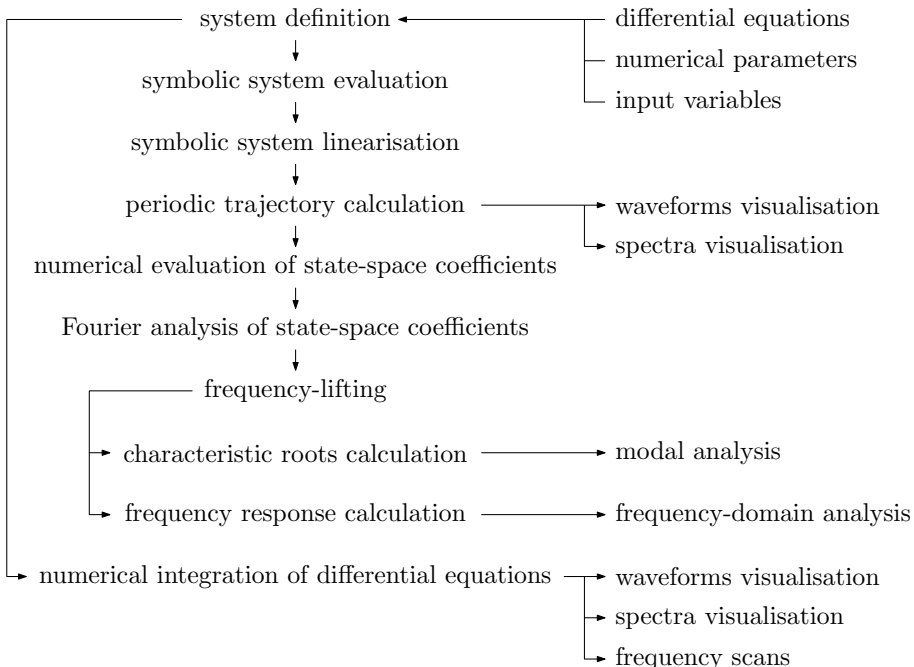


Figure C.1: Overview of the Matlab toolbox capabilities

of the parameters. For the calculation of periodic trajectories, the inputs are specified as harmonic spectra. For the numerical integration of the differential equations, the inputs are specified as functions of time.

Symbolic system evaluation and linearisation

A symbolic evaluation of the analytical differential equations and output equations allows for an automated and efficient determination of the partial derivatives of the said equations. These partial derivatives serve two key purposes: firstly, they are used in the calculation of periodic trajectories to establish the Jacobian of the Fourier-based collocation formulation. Secondly, they are employed to define the state-space matrix coefficients of the linearised time-periodic system.

Periodic trajectory calculation

Periodic trajectories calculations are carried out by solving the Fourier-based collocation formulation for the unknown states and delayed variables. Relying on the flexibility of the formulation, the trajectories can be solved for an arbitrary maximum harmonic rank. The capability of setting a previous solution of the collocation method as initial guess enables an efficient calculation of new trajectories for varying numerical parameters. Resampling the sampled-time vectors at a higher frequency than that of the collocation method allows visualising the waveforms of all system variables. Additionally, the DFT provides the corresponding harmonic spectra and the Fortescue transformation their sequence components.

Numerical evaluation and Fourier analysis of the state-space coefficients

The analytical partial derivatives obtained from the symbolic system are evaluated numerically for a particular set of input variables, numerical parameters and periodic trajectories of state variables and of variables subject to a delay, if any. This evaluation results in waveforms for the coefficients of the linearised state-space model, and the DFT provides the corresponding harmonic spectra. Equivalently, the harmonic content of the state-space periodic matrix coefficients can be represented as their Fourier coefficients. The maximum singular value of each Fourier coefficient is calculated as a way of quantifying of the *weight* of oscillatory components in the behaviour of linearised time-periodic systems. Furthermore, the periodic rank h_m can be determined such that the periodic state-space coefficients are described accurately by truncated Fourier series up to a chosen error.

Frequency-lifting

The linearised time-periodic system is transformed into a linear time-invariant system by means of frequency-lifting. This transformation is rather direct since the Fourier coefficients of the state-space matrix coefficients are already available. In this context, frequency-lifting comes down to building the Toeplitz matrices of the HSS or DHSS representations from the Fourier coefficients of the periodic state-space matrices. The Toeplitz matrices are defined for a chosen truncation rank and, if applicable, a chosen forced periodic rank.

Characteristic roots calculations

Once the HSS system defined, the eigenvalues and eigenvectors of its state matrix can be calculated. Likewise, for DHSS systems, the characteristic roots can be retrieved via a dedicated algorithm such as the delay Arnoldi algorithm². In both cases, the roots are displayed in the complex plane. The modes can be related to the system states through their participation factors, thereby providing insights into the small-signal stability of the periodic trajectory under consideration.

Frequency response calculations

Frequency responses of the lifted system from a selection of inputs to a selection of outputs enables frequency-domain studies. In particular, admittances and impedances provide further information about resonance, damping and passivity of the linearised system at the frequencies of interest. Generally, the resulting frequency-domain lifted representation, i.e. the HTF, is simplified according to the HL procedure, and the no-shift frequency response is extracted from the broader set of available shift frequency responses. Further on, the calculation of frequency responses of subsystems from their point of connection enables applying the Nyquist criterion to also assess stability of the periodic trajectory under consideration.

Numerical integration of differential equations

The numerical integration of the differential equations relies on the available Matlab solvers such as `ode45`, `ode15s`, `dde23`, etc. In this context, the toolbox facilitates the initialisation of the simulation, for instance by setting the initial point (or initial function segment) on a precalculated periodic trajectory. Besides, the toolbox provides an automatic processing of the integrated waveforms, for instance to obtain the harmonic spectrum of the variables over chosen time windows. The way in which the system definition is interfaced with the Matlab solvers for delayed and non-delayed systems is described in more detail in Appendix C.2.

² For this calculation, the developed Matlab toolbox is interfaced with the implementation of the delay Arnoldi algorithm relying on [85] and available at [89].

Main toolbox parameters

Aside from the dynamic equations in analytical form, the input variables specified as harmonic spectra and the numerical values of circuit and control parameters, the toolbox calculations rely on a number of user-defined parameters. For instance, the user indicates the maximum harmonic rank to be included in the calculation of steady-state trajectories based on the collocation method. The user also specifies the type of RFA to be used, a desired numerical accuracy for the solution as well as whether an analytical or a numerical Jacobian calculation is preferred.

Linearisation of the analytical equations around the calculated steady-state trajectory does not require specific inputs from the user.

For the application of frequency lifting, the user indicates the truncation rank and, optionally, the forced periodic rank. When the latter is not specified, it is automatically set equal to the maximum harmonic rank considered for the collocation method. An informed selection of appropriate truncation and periodic ranks may be based on the spectral norm of the Fourier coefficients of the state-space matrices.

No input is requested from the user for the calculation of eigenvalues of non-delayed systems. For the calculation of characteristic roots of delayed systems, the user specifies both the total number of roots to be retrieved and a desired accuracy on which the root convergence test is based.

Lastly, the calculation of frequency responses is carried out based on a user-defined vector of frequencies and on the set of input and output variables between which the responses are to be determined.

C.2 Numerical integration of differential equations

This section provides a high-level user-oriented description of the numerical integration of differential equations in Matlab. The theoretical principles of numerical integration methods are not discussed but are available in textbooks such as [87, 121].

C.2.1 Integrating ordinary differential equations

The considered ordinary differential equations (ODEs) are of the form:

$$\begin{cases} \dot{\mathbf{x}}(t) = \mathbf{f}(t, \mathbf{x}(t), \mathbf{u}(t)) \\ \mathbf{y}(t) = \mathbf{g}(t, \mathbf{x}(t), \mathbf{u}(t)). \end{cases} \quad (\text{C.1})$$

Initialisation

The initial condition can be an arbitrary point in the state-space, or be located on a periodic trajectory. In the latter case, the harmonic spectrum of every state variable is known, for instance as the solution of a periodic trajectory calculation. In other words, Fourier coefficients \mathbf{x}_k are known and describe the periodic trajectory. A point on the trajectory is obtained by evaluating the Fourier series at any initial time $t = t_0$:

$$\mathbf{x}(t_0) = \sum_{k=-h_m}^{h_m} \mathbf{x}_k e^{jk\omega_1 t_0}. \quad (\text{C.2})$$

Evaluation of the time derivatives

The numerical integration of ODEs is carried out via the dedicated Matlab solvers such as `ode45`, `ode15s`, etc. To integrate ODEs, the solver retrieves the derivatives $\dot{\mathbf{x}}(t)$ at times t within the integration range $[t_0, t_{\text{end}}]$. To do so, the solver provides the time value t as well as the vector $\mathbf{x}(t)$ at that time. The user-defined input variables $\mathbf{u}(t)$ are evaluated first. Next, the user-defined function $\mathbf{f}(t, \mathbf{x}(t), \mathbf{u}(t))$ is evaluated and returned to the solver.

C.2.2 Integrating delay differential equations

The considered delay differential equations (DDEs) are of the form:

$$\begin{cases} \dot{\mathbf{x}}(t) = \mathbf{f}(t, \mathbf{x}(t), \mathbf{u}(t), \mathbf{z}(t - t_{d1}), \dots, \mathbf{z}(t - t_{dd})) \\ \mathbf{y}(t) = \mathbf{g}(t, \mathbf{x}(t), \mathbf{u}(t), \mathbf{w}(t)) \\ \mathbf{z}(t) = \mathbf{h}(t, \mathbf{x}(t), \mathbf{u}(t)), \end{cases} \quad (\text{C.3})$$

where the notation of delayed variables is slightly adapted with respect to Chapters 4 and 5 to simplify the presentation of the procedure. Additionally,

for simplicity, the case of delayed variables being functions of themselves or of other delayed variables is not covered.

Initialisation

It is assumed that the delayed system is initially in steady state. If starting at a constant operating point, the initial function segment is simply obtained as:

$$\mathbf{x}(t) = \mathbf{x}(t_0), \quad t \in [t_0 - t_{dd}, t_0] \quad (\text{C.4})$$

where t_{dd} is the largest delay. If starting on a periodic trajectory, the initial function segment is described by the Fourier series:

$$\mathbf{x}(t) = \sum_{k=-h_m}^{h_m} \mathbf{x}_k e^{jk\omega_1 t}, \quad t \in [t_0 - t_{dd}, t_0]. \quad (\text{C.5})$$

Integrating DDEs with dde23

A first option for the numerical integration of DDEs in Matlab relies on the `dde23` solver. To integrate DDEs, the `dde23` solver retrieves the derivatives $\dot{\mathbf{x}}(t)$ at times t within the integration range $[t_0, t_{\text{end}}]$. Naturally, the evaluation of $\mathbf{f}(t, \mathbf{x}(t), \mathbf{u}(t), \mathbf{z}(t - t_{d1}), \dots, \mathbf{z}(t - t_{dd}))$ requires the values of delayed variables $\mathbf{z}(t - t_{d1})$, $\mathbf{z}(t - t_{d2})$, etc. To obtain these values, the solver provides the time value t as well as vector $\mathbf{x}(t)$ at that time, but also vectors $\mathbf{x}(t - t_{di})$, $\forall i = 1, \dots, d$. These past values of $\mathbf{x}(t)$ are automatically calculated by the solver, either by evaluation of the initial function segment (if $t - t_{dd} \leq t - t_{di} \leq t_0$) or by interpolation of the already-available solution (if $t_0 < t - t_{di} < t$).

The user-defined inputs $\mathbf{u}(t)$ are evaluated at times $t - t_{di}$. Next, delayed variables $\mathbf{z}(t - t_{di})$ are obtained by evaluating function $\mathbf{h}(t, \mathbf{x}(t), \mathbf{u}(t))$ at times $t - t_{di}$. All required variables are now available for the evaluation of $\mathbf{f}(t, \mathbf{x}(t), \mathbf{u}(t), \mathbf{z}(t - t_{d1}), \dots, \mathbf{z}(t - t_{dd}))$.

An advantage of this approach is the automatic interpolation of the already-available solution by `dde23`. A disadvantage is that `dde23` is the only Matlab solver dedicated to DDEs with constant delays. Since different solvers display different characteristics, such as different degrees of numerical damping, it is relevant to enable the solution of DDEs by means of other solvers than `dde23`, e.g. by means of Matlab solvers dedicated to ODEs. This approach is described next.

Integrating DDEs with ODE solvers

The challenge of integrating DDEs with ODE solvers is summarised in the observation that such solvers only provide the values of $\mathbf{x}(t)$ at time t , but not past values like `dde23` does. Consequently, vectors $\mathbf{x}(t - t_{di})$ are obtained by *manually* interpolating over the solved values of $\mathbf{x}(t)$. As solved values of the states are only available at the end of the integration interval, retrieving solved values is done by periodically interrupting the solver, retrieving the solved values, and starting again from the last available point. Practically, this is done by simply splitting the total time interval into subintervals of length equal to the smallest delay. Although the interpolation function could technically be called on all solved subintervals to retrieve past values of $\mathbf{x}(t)$, the computational efficiency of the approach is improved by only calling the interpolation function on a minimum number of buffered subintervals. The principle is illustrated in Fig. C.2, each step of which is detailed as follows:

1. Before starting the integration, the initial function segment is defined. Its length is such that it provides past values of $\mathbf{x}(t)$ at least as far back as the maximum time delay t_{dd} .
2. The integration starts over a first subinterval of length equal to the smallest delay t_{d1} . In this subinterval, all past values of $\mathbf{x}(t)$ are within the initial function segment.
3. At the end of the first subinterval, the first time delay ($t - t_{d1}$) is equal to the initial time t_0 , which marks the end of the initial function segment.
4. Solving the second subinterval requires using the first subinterval as *buffer* to provide the interpolation function with the past values of $\mathbf{x}(t)$ that are not covered by the initial function segment anymore.
5. For the example in Fig. C.2, where the largest delay is equal to 2.5 times the smallest delay, the largest delay becomes equal to the initial time t_0 while integrating the third subinterval. For all future times, past values of $\mathbf{x}(t)$ will be obtained by interpolation over buffered subintervals only.
6. Integrating the fourth subinterval still relies on buffered values from the first subinterval. Practically, the required number of buffered subintervals is given by `ceil(tdd/td1)` which, for the illustrated example, is equal to 3.
7. Accordingly, the integration of the fifth subinterval relies on buffered values from the three previous subintervals. The first subinterval is not part of the buffer anymore.

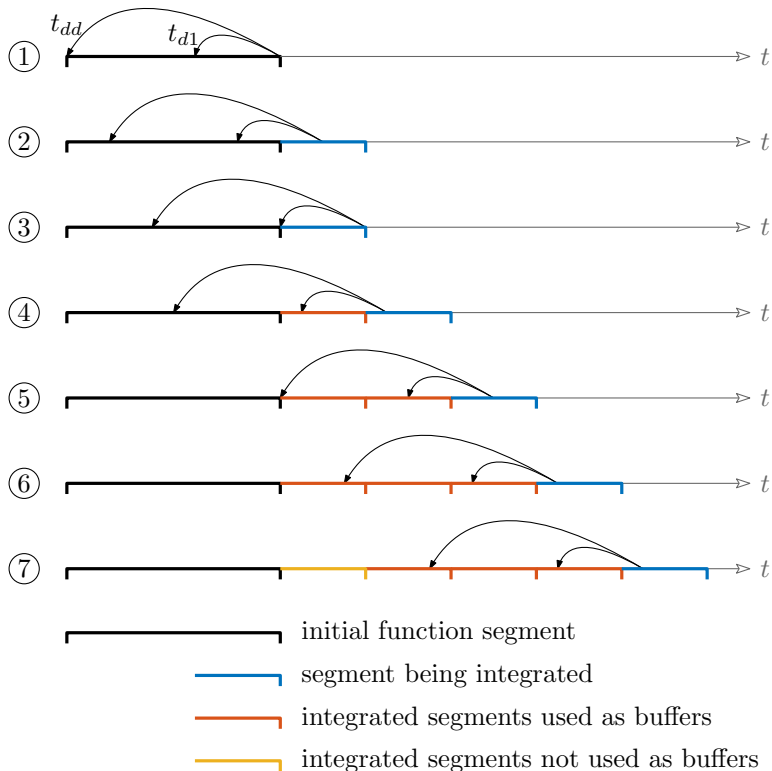


Figure C.2: Illustration of the use of buffers for the numerical integration of DDEs by means of ODE solvers ($t_{dd} = 2.5t_{d1}$)

Bibliography

- [1] “World Energy Outlook 2022,” tech. rep., International Energy Agency, 2022.
- [2] R. C. Dugan, M. F. McGranaghan, S. Santoso, and H. W. Beaty, *Electrical Power Systems Quality*. McGraw-Hill, second ed., 2004.
- [3] “World Energy Perspective – Variable Renewable Integration in Electricity Systems: How to get it right,” tech. rep., World Energy Council, 2016.
- [4] N. R. Watson and J. D. Watson, “An Overview of HVDC Technology,” *Energies*, vol. 13, no. 17, 2020.
- [5] M. Wang, T. An, H. Ergun, Y. Lan, B. Andersen, M. Szechtman, W. Leterme, J. Beerten, and D. Van Hertem, “Review and outlook of HVDC grids as backbone of transmission system,” *CSEE Journal of Power and Energy Systems*, vol. 7, no. 4, pp. 797–810, 2021.
- [6] R. Teodorescu, M. Liserre, and P. Rodriguez, *Grid Current Control*. John Wiley and Sons, Ltd, 2011.
- [7] IEEE PES Power System Dynamic Performance Committee, “Stability definitions and characterization of dynamic behavior in systems with high penetration of power electronic interfaced Technologies,” tech. rep., IEEE, April 2020.
- [8] P. De Rua, T. Roose, Özgür Can Sakinci, N. de Moraes Dias Campos, and J. Beerten, “Identification of mechanisms behind converter-related issues in power systems based on an overview of real-life events,” *Renewable and Sustainable Energy Reviews*, vol. 183, p. 113431, 2023.
- [9] CIGRE WG B4.67, “AC side harmonics and appropriate harmonic limits for VSC HVDC,” tech. rep., CIGRE, 2019.

- [10] L. Xiong, X. Liu, Y. Liu, and F. Zhuo, "Modeling and stability issues of voltage-source converter-dominated power systems: A review," *CSEE Journal of Power and Energy Systems*, vol. 8, no. 6, pp. 1530–1549, 2022.
- [11] A. Lesnicar and R. Marquardt, "An innovative modular multilevel converter topology suitable for a wide power range," in *2003 IEEE Bologna Power Tech Conference Proceedings*, vol. 3, pp. 6 pp. Vol.3–, 2003.
- [12] K. Sharifabadi, L. Harnefors, H. Nee, S. Norrga, and R. Teodorescu, *Design, Control, and Application of Modular Multilevel Converters for HVDC Transmission Systems*. IEEE, 2016.
- [13] C. Zou, H. Rao, S. Xu, Y. Li, W. Li, J. Chen, X. Zhao, Y. Yang, and B. Lei, "Analysis of Resonance Between a VSC-HVDC Converter and the AC Grid," *IEEE Trans. Power Electron.*, vol. 33, no. 12, pp. 10157–10168, 2018.
- [14] H. Saad, Y. Vernay, S. Dennetière, P. Rault, and B. Clerc, "System Dynamic Studies of Power Electronics Devices with Real-Time Simulation - A TSO operational experience," in *CIGRE Conf., Paris, France*, Aug. 2018.
- [15] C. Yin, X. Xie, S. Xu, and C. Zou, "Review of oscillations in VSC-HVDC systems caused by control interactions," *The Journal of Engineering*, vol. 2019, no. 16, pp. 1204–1207, 2019.
- [16] X. Yue, X. Wang, and F. Blaabjerg, "Review of Small-Signal Modeling Methods Including Frequency-Coupling Dynamics of Power Converters," *IEEE Transactions on Power Electronics*, vol. 34, no. 4, pp. 3313–3328, 2019.
- [17] J. Sun and H. Liu, "Impedance modeling and analysis of modular multilevel converters," in *2016 IEEE 17th Workshop on Control and Modeling for Power Electronics (COMPEL)*, pp. 1–9, 2016.
- [18] N. M. Wereley, *Analysis and control of linear periodically time varying systems*. Ph.d. thesis, Department of Aeronautics and Astronautics, Massachusetts Institute of Technology (MIT), 1991.
- [19] C. Wang, L. Xiao, H. Jiang, and T. Cai, "Analysis and Compensation of the System Time Delay in an MMC System," *IEEE Trans. Power Electron.*, vol. 33, no. 11, pp. 9923–9936, 2018.
- [20] L. Harnefors, A. G. Yepes, A. Vidal, and J. Doval-Gandoy, "Passivity-Based Stabilization of Resonant Current Controllers With Consideration of Time Delay," *IEEE Transactions on Power Electronics*, vol. 29, no. 12, pp. 6260–6263, 2014.

- [21] A. Neufeld, M. J. Alkemper, N. Schäkel, and L. Hofmann, "On the Influence of Time Delay Modelling in Grid-Connected Converters for Harmonic Studies," in *2020 IEEE 11th International Symposium on Power Electronics for Distributed Generation Systems (PEDG)*, pp. 46–50, 2020.
- [22] A. Bayo-Salas, *Control interactions in power systems with multiple VSC HVDC converters*. Ph.d. thesis, KU Leuven, Aug. 2018.
- [23] C. Dong, S. Yang, H. Jia, and P. Wang, "Padé-Based Stability Analysis for a Modular Multilevel Converter Considering the Time Delay in the Digital Control System," *IEEE Trans. Ind. Electron.*, vol. 66, no. 7, pp. 5242–5253, 2019.
- [24] Ørsted, "Ørsted Technical Report for National Grid ESO on the events of 9 August 2019 (Appendix of Ofgem Technical Report)," tech. rep., Ørsted, 2019.
- [25] C. Buchhagen, M. Greve, A. Menze, and J. Jung, "Harmonic Stability – Practical Experience of a TSO," in *Proceedings of the 15th Wind Integration Workshop, Vienna, Austria*, Nov. 2016.
- [26] C. Buchhagen, C. Rauscher, A. Menze, and J. Jung, "BorWin1 - First experiences with harmonic interactions in converter dominated grids," in *Proceedings of the 2015 International ETG Congress*, (Bonn, Germany), pp. 27–33, Nov. 2015.
- [27] A. Abdalrahman and E. Isabegovic, "DolWin1 - Challenges of connecting offshore wind farms," in *2016 IEEE International Energy Conference (ENERGYCON)*, pp. 1–10, 2016.
- [28] I. Erlich, B. Paz, M. K. Zadeh, S. Vogt, C. Buchhagen, C. Rauscher, A. Menze, and J. Jung, "Overvoltage phenomena in offshore wind farms following blocking of the HVDC converter," in *2016 IEEE Power and Energy Society General Meeting (PESGM)*, pp. 1–5, 2016.
- [29] M. Koochack Zadeh, T. Rendell, C. Rathke, and A. Menze, "Operating experiences of HVDC links - Behaviour during faults and switching events," in *Proceedings of the CIGRE B4 Colloquium*, (Winnipeg, Canada), Oct. 2017.
- [30] Y. Zhang, C. Hong, L. Tu, T. Zhou, and J. Yang, "Research on High-frequency Resonance Mechanism and Active Harmonic Suppression Strategy of Power Systems with Power Electronics," in *2018 International Conference on Power System Technology (POWERCON)*, pp. 2350–2356, 2018.

- [31] Y. Congqi, X. Xiaorong, L. Hui, W. Xiao, W. Zhibing, and C. Yongning, “Analysis and control of the oscillation phenomenon in VSC-HVDC transmission system,” *Power System Technology*, vol. 44, no. 4, pp. 1117–1123, 2018.
- [32] X. Guo, Z. Liu, Y. Li, and Y. Lu, “Characteristic analysis of high-frequency resonance of flexible high voltage direct current and research on its damping control strategy,” *Proceedings of the Chinese Society of Electrical and Electronics Engineers*, vol. 40, pp. 19–40, Jan 2020.
- [33] H. Ding, Y. Wu, Y. Zhang, Y. Ma, and R. Kuffel, “System stability analysis of Xiamen bipolar MMC-HVDC project,” in *12th IET International Conference on AC and DC Power Transmission (ACDC 2016)*, pp. 1–6, 2016.
- [34] S. Zhu, L. Qin, K. Liu, K. Ji, Y. Li, Q. Huai, X. Liao, and S. Yang, “Impedance Modeling of Modular Multilevel Converter in D-Q and Modified Sequence Domains,” *IEEE Journal of Emerging and Selected Topics in Power Electronics*, vol. 10, no. 4, pp. 4361–4382, 2022.
- [35] H. K. Khalil, *Nonlinear systems*. Upper Saddle River, NJ: Prentice-Hall, third ed., 2002.
- [36] M. Vidyasagar, *Nonlinear Systems Analysis*. Society for Industrial and Applied Mathematics, second ed., 2002.
- [37] S. Sastry, *Nonlinear Systems: Analysis, Stability, and Control*. Springer New York, 1999.
- [38] R. Cisneros, R. Ortega, M. Pirro, G. Ippoliti, G. Bergna, and M. M. Cabrera, “Global tracking passivity-based PI control for power converters: An application to the boost and modular multilevel converters,” in *2014 IEEE 23rd International Symposium on Industrial Electronics (ISIE)*, pp. 1359–1365, 2014.
- [39] W. S. Levine, *Fundamentals of Dynamical Systems*, pp. 3–20. Boston, MA: Birkhäuser Boston, 2005.
- [40] G. H. Golub and C. F. Van Loan, *Matrix Computations*. The Johns Hopkins University Press, third ed., 1996.
- [41] K. Kuttler, *Linear Algebra, Theory And Applications*. Saylor Foundation, 2012.
- [42] P. Kundur, *Power System Stability and Control*. New York: McGraw-Hill, 1994.

- [43] S. Lang, *Linear Algebra (Undergraduate Texts in Mathematics)*. Springer, third ed., 1987.
- [44] S. Skogestad and I. Postlethwaite, *Multivariable Feedback Control: Analysis and Design*. Wiley, second ed., 2005.
- [45] J. D. Aplevich, *The Essentials of Linear State-Space Systems, Supplementary chapters*. John Wiley and Sons, 2000.
- [46] S. Bittanti and P. Colaneri, *Periodic Systems: Filtering and Control*. Springer-Verlag London, 2009.
- [47] G. Bergna-Diaz, J. Freytes, X. Guillaud, S. D'Arco, and J. A. Suul, "Generalized Voltage-Based State-Space Modeling of Modular Multilevel Converters With Constant Equilibrium in Steady State," *IEEE Trans. Emerg. Sel. Topics Power Electron.*, vol. 6, no. 2, pp. 707–725, 2018.
- [48] E. Möllerstedt, *Dynamic Analysis of Harmonics in Electrical Systems*. Ph.d. thesis, Department of Automatic Control, Lund Institute of Technology (LTH), 2000.
- [49] H. E. Taha, M. R. Hajj, and A. H. Nayfeh, "Flight dynamics and control of flapping-wing MAVs: a review," *Nonlinear Dynamics*, vol. 70, no. 2, pp. 907–939, 2012.
- [50] P. Montagnier, R. J. Spiteri, and J. Angeles, "The control of linear time-periodic systems using Floquet–Lyapunov theory," *International Journal of Control*, vol. 77, no. 5, pp. 472–490, 2004.
- [51] G. Ducci, V. Colognesi, G. Vitucci, P. Chatelain, and R. Ronsse, "Stability and Sensitivity Analysis of Bird Flapping Flight," *Journal of Nonlinear Science*, vol. 31, no. 2, 2021.
- [52] N. Mallon, *Collocation: a method for computing periodic solutions of ordinary differential equations*. DCT rapporten, Technische Universiteit Eindhoven, 2002. DCT 2002.035.
- [53] E. Bueler, "Chebyshev collocation for linear, periodic ordinary and delay differential equations: a posteriori estimates," 2004.
- [54] R. A. Horn and C. R. Johnson, *Matrix Analysis*. USA: Cambridge University Press, second ed., 2013.
- [55] X. Mao, *Stochastic Differential Equations and Applications*. Woodhead Publishing Limited, second ed., 2008.
- [56] H. Akagi, "Active Harmonic Filters," *Proceedings of the IEEE*, vol. 93, no. 12, pp. 2128–2141, 2005.

- [57] Q. Hao, Z. Li, C. Yue, F. Gao, and S. Wang, "Small-Signal Model and Dynamics of MMC-HVDC Grid Under Unbalanced Grid Conditions," *IEEE Transactions on Power Delivery*, vol. 36, no. 5, pp. 3172–3184, 2021.
- [58] J. Zhu, J. Hu, Y. Li, S. Ma, and T. Wang, "Small-Signal Stability of MMC Grid-Tied System Under Two Typical Unbalanced Grid Conditions," *IEEE Transactions on Industry Applications*, vol. 58, no. 4, pp. 5005–5014, 2022.
- [59] G. Bergna-Diaz, J. A. Suul, and S. D'Arco, "Energy-based state-space representation of modular multilevel converters with a constant equilibrium point in steady-state operation," *IEEE Transactions on Power Electronics*, vol. 33, no. 6, pp. 4832–4851, 2018.
- [60] N. Blin, P. Riedinger, J. Daafouz, L. Grimaud, and P. Feyel, "A comparison of harmonic modeling methods with application to the interconnection and the control of switched systems," *European Journal of Control*, vol. 58, pp. 245–257, 2021.
- [61] S. Sanders, J. Noworolski, X. Liu, and G. Verghese, "Generalized averaging method for power conversion circuits," *IEEE Transactions on Power Electronics*, vol. 6, no. 2, pp. 251–259, 1991.
- [62] J. Rico, M. Madrigal, and E. Acha, "Dynamic harmonic evolution using the extended harmonic domain," *IEEE Transactions on Power Delivery*, vol. 18, no. 2, pp. 587–594, 2003.
- [63] J. Sun, "Small-Signal Methods for AC Distributed Power Systems—A Review," *IEEE Transactions on Power Electronics*, vol. 24, no. 11, pp. 2545–2554, 2009.
- [64] O. C. Sakinci, *Modeling of the Modular Multilevel Converter using Dynamic Phasors: Reduced-Order Models for Small-Signal Stability Analysis*. Ph.d. thesis, KU Leuven, Jan. 2022.
- [65] J. Dugundji and J. H. Wendell, "Some analysis methods for rotating systems with periodic coefficients," *AIAA Journal*, vol. 21, no. 6, pp. 890–897, 1983.
- [66] P. P. Khargonekar, K. Poolla, and A. Tannenbaum, "Robust control of linear time-invariant plants using periodic control," *IEEE Transactions on Automatic Control*, pp. 1088–1096, 1985.
- [67] J. Shen, T. Tang, and L. Wang, *Spectral Methods Algorithms, Analysis and Applications*. Springer, 2011.

- [68] T. M. Apostol, *Mathematical Analysis*. Addison Wesley, second ed., 1981.
- [69] R. M. Gray, “Toeplitz and Circulant Matrices: A Review,” *Foundations and Trends in Communications and Information Theory*, vol. 2, no. 3, pp. 155–239, 2006.
- [70] V. Salis, *Stability analysis of AC power system in the linear time periodic framework*. PhD thesis, University of Nottingham, November 2018.
- [71] P. De Rua, Özgür Can Sakinci, and J. Beerten, “Comparative Study of Dynamic Phasor and Harmonic State-Space Modeling for Small-Signal Stability Analysis,” *Electric Power Systems Research*, vol. 189, p. 106626, 2020.
- [72] T. Yang, S. Bozhko, J.-M. Le-Peuvredic, G. Asher, and C. I. Hill, “Dynamic Phasor Modeling of Multi-Generator Variable Frequency Electrical Power Systems,” *IEEE Transactions on Power Systems*, vol. 31, no. 1, pp. 563–571, 2016.
- [73] J. Sun and H. Liu, “Sequence Impedance Modeling of Modular Multilevel Converters,” *IEEE Trans. Emerg. Sel. Topics Power Electron.*, vol. 5, no. 4, pp. 1427–1443, 2017.
- [74] M. Nahalparvari, M. Asoodar, L. Bessegato, S. Norrga, and H.-P. Nee, “Modeling and Shaping of the DC-Side Admittance of a Modular Multilevel Converter under Closed-Loop Voltage Control,” *IEEE Trans. Power Electron.*, pp. 1–1, 2020.
- [75] J. Lyu, X. Zhang, X. Cai, and M. Molinas, “Harmonic State-Space Based Small-Signal Impedance Modeling of a Modular Multilevel Converter With Consideration of Internal Harmonic Dynamics,” *IEEE Transactions on Power Electronics*, vol. 34, no. 3, pp. 2134–2148, 2019.
- [76] H. Sandberg, E. Mollerstedt, and Bernhardsson, “Frequency-domain analysis of linear time-periodic systems,” *IEEE Transactions on Automatic Control*, vol. 50, no. 12, pp. 1971–1983, 2005.
- [77] P. De Rua and J. Beerten, “Generalization of Harmonic State-Space Framework to Delayed Periodic Systems for Stability Analysis of the Modular Multilevel Converter,” *IEEE Transactions on Power Delivery*, vol. 37, no. 4, pp. 2661–2672, 2022.
- [78] W. Michiels and S.-I. Niculescu, *Stability, Control, and Computation for Time-Delay Systems, An Eigenvalue-Based Approach*. Philadelphia, PA: Society for Industrial and Applied Mathematics, second ed., 2014.

- [79] The MathWorks Inc., “State-Space Realizations.” <https://nl.mathworks.com/help/ident/ug/canonical-state-space-realizations.html>, 2023. Accessed: April 07, 2023. [Online].
- [80] The MathWorks Inc., “Padé approximation of models with time delay.” <https://nl.mathworks.com/help/control/ref/dynamicsystem.pade.html>, 2023. Accessed: April 07, 2023. [Online].
- [81] Y. Li, T. An, D. Zhang, X. Pei, K. Ji, and G. Tang, “Analysis and Suppression Control of High Frequency Resonance for MMC-HVDC System,” *IEEE Transactions on Power Delivery*, vol. 36, no. 6, pp. 3867–3881, 2021.
- [82] T. Roose, *Small-Signal Modeling and Stability Analysis of Multi-Terminal DC Systems For Low- and High-Voltage Applications*. Ph.d. thesis, KU Leuven, Jan. 2023.
- [83] W. Michiels and S.-I. Niculescu, *Stability and Stabilization of Time-Delay Systems, An Eigenvalue-Based Approach*. Philadelphia, PA: Society for Industrial and Applied Mathematics, first ed., 2007.
- [84] O. A. Bobrenkov, E. A. Butcher, and B. P. Mann, “Application of the Liapunov–Floquet transformation to differential equations with time delay and periodic coefficients,” *Journal of Vibration and Control*, vol. 19, no. 4, pp. 521–537, 2013.
- [85] E. Jarlebring, K. Meerbergen, and W. Michiels, “A Krylov Method for the Delay Eigenvalue Problem,” *SIAM J. Sci. Comput.*, vol. 32, pp. 3278–3300, 2010.
- [86] Z. Wu and W. Michiels, “Reliably computing all characteristic roots of delay differential equations in a given right half plane using a spectral method,” *Journal of Computational and Applied Mathematics*, vol. 236, no. 9, pp. 2499–2514, 2012.
- [87] W. H. Press, S. A. Teukolsky, W. T. Vetterling, and B. P. Flannery, *Numerical Recipes: The Art of Scientific Computing*. USA: Cambridge University Press, third ed., 2007.
- [88] P. Gahinet and L. F. Shampine, “Software for modeling and analysis of linear systems with delays,” in *Proceedings of the 2004 American Control Conference*, vol. 6, pp. 5600–5605 vol.6, 2004.
- [89] K. L. Scientific Computing Research Group, Computer Science Department, “Compute eigenvalues of delay system with the delay Arnoldi scheme.” https://twr.cs.kuleuven.be/research/software/delay-control/tds_arnoldi.m. Accessed: May 11, 2021. [Online].

- [90] The MathWorks Inc., “setDelayModel: Construct state-space model with internal delays.” <https://nl.mathworks.com/help/control/ref/dynamicsystem.setdelaymodel.html>, 2023. Accessed: April 07, 2023. [Online].
- [91] The MathWorks Inc., “How does freqresp work with systems with internal delays?.” <https://nl.mathworks.com/matlabcentral/answers/1882417-how-does-freqresp-work-with-systems-with-internal-delays>, 2023. Accessed: April 07, 2023. [Online].
- [92] The MathWorks Inc., “freqresp: Evaluate system response over a grid of frequencies.” nl.mathworks.com/help/control/ref/dynamicsystem.freqresp.html, 2023. Accessed: April 07, 2023. [Online].
- [93] G. F. Franklin, J. D. Powell, and A. Emami-Naeini, *Feedback Control of Dynamic Systems*. USA: Pearson, sixth ed., 2010.
- [94] A. Stepanov, H. Saad, U. Karaagac, and J. Mahseredjian, “Initialization of Modular Multilevel Converter Models for the Simulation of Electromagnetic Transients,” *IEEE Trans. Power Deliv.*, vol. 34, no. 1, pp. 290–300, 2019.
- [95] A. Medina, J. Segundo-Ramirez, P. Ribeiro, W. Xu, K. L. Lian, G. W. Chang, V. Dinavahi, and N. R. Watson, “Harmonic Analysis in Frequency and Time Domain,” *IEEE Trans. Power Deliv.*, vol. 28, no. 3, pp. 1813–1821, 2013.
- [96] P. De Rua and J. Beerten, “Modular Multilevel Converter Periodic Trajectory Determination — A Generic Fourier-Based Collocation Method.” submitted to the International Journal of Electrical Power & Energy Systems, 2023.
- [97] J. P. Boyd, *Chebyshev and Fourier Spectral Methods*. DOVER Publications, Inc., 2 ed., 2000.
- [98] A. V. Rao, “A Survey of Numerical Methods for Optimal Control,” *Advances in the Astronautical Sciences*, vol. 135, 2010.
- [99] K. Lust, “Improved Numerical Floquet Multipliers,” *International Journal of Bifurcation and Chaos*, vol. 11, no. 09, pp. 2389–2410, 2001.
- [100] A. Semlyen and A. Medina, “Computation of the periodic steady state in systems with nonlinear components using a hybrid time and frequency domain methodology,” *IEEE Trans. Power Syst.*, vol. 10, no. 3, pp. 1498–1504, 1995.
- [101] S. Maas, *Nonlinear Microwave and RF Circuits*. Artech, 2 ed., 2003.

- [102] C. Zhang, M. Molinas, S. Føyen, J. A. Suul, and T. Isobe, “An Integrated Method for Generating VSCs’ Periodical Steady-State Conditions and HSS-Based Impedance Model,” *IEEE Trans. Power Deliv.*, vol. 35, no. 5, pp. 2544–2547, 2020.
- [103] S. Norrga, L. Ängquist, K. Ilves, L. Harnefors, and H.-P. Nee, “Decoupled steady-state model of the modular multilevel converter with half-bridge cells,” in *6th IET International Conference on Power Electronics, Machines and Drives (PEMD 2012)*, pp. 1–6, 2012.
- [104] Q. Song, W. Liu, X. Li, H. Rao, S. Xu, and L. Li, “A Steady-State Analysis Method for a Modular Multilevel Converter,” *IEEE Trans. Power Electron.*, vol. 28, no. 8, pp. 3702–3713, 2013.
- [105] A. Marzoughi, R. Burgos, D. Boroyevich, and Y. Xue, “Steady-state analysis of voltages and currents in modular multilevel converter based on average model,” in *2015 IEEE Energy Conversion Congress and Exposition (ECCE)*, pp. 3522–3528, 2015.
- [106] X. Shi, Z. Wang, B. Liu, Y. Li, L. M. Tolbert, and F. Wang, “Steady-State Modeling of Modular Multilevel Converter Under Unbalanced Grid Conditions,” *IEEE Trans. Power Electron.*, vol. 32, no. 9, pp. 7306–7324, 2017.
- [107] F. Zhao, G. Xiao, and T. Zhao, “Accurate Steady-State Mathematical Models of Arm and Line Harmonic Characteristics for Modular Multilevel Converter,” *IEEE Trans. Power Deliv.*, vol. 33, no. 3, pp. 1308–1318, 2018.
- [108] Z. Liu, K.-J. Li, J. Wang, W. Liu, Z. Javid, and Z.-D. Wang, “General Model of Modular Multilevel Converter for Analyzing the Steady-State Performance Optimization,” *IEEE Trans. Ind. Electron.*, vol. 68, no. 2, pp. 925–937, 2021.
- [109] X. Chen, J. Liu, Z. Deng, and S. Song, “A Generic Steady-State Analysis Model for Three-Phase Three-Wire Modular Multilevel Converter,” *CPSS Transactions on Power Electronics and Applications*, vol. 8, no. 2, pp. 199–209, 2023.
- [110] K. R. Rao and P. Yip, *The Transform and Data Compression Handbook*. CRC Press, Inc., 2000.
- [111] D. Laad, P. Elango, and R. Mohan, “Fourier Pseudospectral Method for Trajectory Optimization with Stability Requirements,” *Journal of Guidance, Control, and Dynamics*, vol. 43, no. 11, pp. 2073–2090, 2020.

- [112] J. J. Moré, “The Levenberg-Marquardt algorithm: Implementation and theory,” in *Numerical Analysis* (G. A. Watson, ed.), (Berlin, Heidelberg), pp. 105–116, Springer Berlin Heidelberg, 1978.
- [113] L. Kocewiak, *Harmonics in large offshore wind farms*. Ph.d. thesis, Aalborg University, March 2012.
- [114] K. Verheyden and K. Lust, “A Newton-Picard Collocation Method for Periodic Solutions of Delay Differential Equations,” *BIT Numerical Mathematics*, vol. 45, no. 3, pp. 605–625, 2005.
- [115] D. Breda, S. Maset, and R. Vermiglio, “Numerical computation of characteristic multipliers for linear time periodic coefficients delay differential equations,” *IFAC Proceedings Volumes*, vol. 39, no. 10, pp. 163–168, 2006. 6th IFAC Workshop on Time Delay Systems.
- [116] F. Borgioli, D. Hajdu, T. Insperger, G. Stepan, and W. Michiels, “Pseudospectral method for assessing stability robustness for linear time-periodic delayed dynamical systems,” *International Journal for Numerical Methods in Engineering*, vol. 121, no. 16, pp. 3505–3528, 2020.
- [117] C. J. O’Rourke, M. M. Qasim, M. R. Overlin, and J. L. Kirtley, “A Geometric Interpretation of Reference Frames and Transformations: dq0, Clarke, and Park,” *IEEE Transactions on Energy Conversion*, vol. 34, no. 4, pp. 2070–2083, 2019.
- [118] C. L. Fortescue, “Method of Symmetrical Co-ordinates Applied to the Solution of Polyphase Networks,” *Transactions of the American Institute of Electrical Engineers*, vol. XXXVII, no. 2, pp. 1027–1140, 1918.
- [119] J. Freytes, *Small-signal stability analysis of Modular Multilevel Converters and application to MMC-based Multi-Terminal DC grids*. Ph.d. thesis, Centrale Lille, Dec. 2017.
- [120] Y. Jing, *Control and operation of MMC-HVDC system for connecting offshore wind farm*. Ph.d. thesis, University of Strathclyde, Aug. 2019.
- [121] U. M. Ascher and L. R. Petzold, *Computer Methods for Ordinary Differential Equations and Differential-Algebraic Equations*. Society for Industrial and Applied Mathematics, 1998.

List of Figures

| | | |
|------|---|-----|
| 1 | Thesis structure | 15 |
| 1.1 | MMC circuit diagram | 20 |
| 1.2 | Overview of MMC control structure | 25 |
| 1.3 | Block-diagram of the phase-locked loop | 29 |
| 1.4 | Illustrative examples of transient behaviours | 33 |
| 1.5 | Typical MMC time-domain waveforms and harmonic spectra | 34 |
| 1.6 | Overview of system types through the linearisation process | 42 |
| 1.7 | Overview of system types and transformations | 58 |
| 2.1 | Stability criterion: analysis of Condition (2.54a) | 76 |
| 2.2 | Stability criterion: analysis of Condition (2.54b) | 77 |
| 2.3 | Stability criterion: application to the TLC | 78 |
| 2.4 | Stability criterion: application to the simplified MMC | 79 |
| 3.1 | Simple RLC circuit diagram | 108 |
| 3.2 | Simple RLC circuit: impact of truncation on HSS eigenvalues | 109 |
| 3.3 | Simplified MMC: relative norm of Fourier coefficients | 110 |
| 3.4 | Simplified MMC: impact of truncation on HSS eigenvalues | 111 |
| 3.5 | Truncated HSS state matrix of an LTP system | 112 |
| 3.6 | MMC-HVDC link: relative norm of Fourier coefficients | 113 |
| 3.7 | MMC-HVDC link: HSS eigenvalues | 113 |
| 3.8 | MMC-HVDC link: impact of harmonics on HSS eigenvalues | 114 |
| 3.9 | Frequency coupling mechanism in harmonic linearisation | 125 |
| 3.10 | Nonlinear-TF model: block diagram | 139 |
| 3.11 | LTP-TF model: block diagram | 140 |
| 3.12 | Frequency-lifted HTF representation | 141 |
| 3.13 | Complete MMC model: HTF-based admittances | 144 |
| 3.14 | Validation of HTF frequency response against integration | 146 |
| 3.15 | No-shift frequency response: impact of forced periodic rank | 147 |

| | |
|--|-----|
| 3.16 No-shift frequency response: relative error | 149 |
| 4.1 Padé approximation errors for different approximation orders | 157 |
| 4.2 Limit frequencies for different approximation orders | 157 |
| 4.3 DDEs: number of roots in the complex plane | 160 |
| 4.4 DDE states and abstract Cauchy problem: intuitive illustrations | 161 |
| 4.5 Initial value (ODE) and initial function segment (DDE) | 162 |
| 4.6 Offshore MMC-based system | 174 |
| 4.7 Modal analysis: MMC delay sweep | 175 |
| 4.8 Nyquist plots | 179 |
| 4.9 Numerical integration of the DDEs: alternating current | 180 |
| 4.10 Frequency spectrum of alternating currents (unstable case) | 180 |
| 5.1 Time-domain sample points of a continuous periodic signal $x(t)$ | 196 |
| 5.2 Structure of the algorithm | 205 |
| 5.3 Simple RLC circuit diagram | 208 |
| 5.4 Comparison of collocation and integration waveforms | 212 |
| 5.5 Comparison of collocation and numerical integration methods | 213 |
| 5.6 Eigenvalues of collocation Jacobian and HSS model | 217 |
| 5.7 Harmonic propagation: HVDC and offshore grid test system | 218 |
| 5.8 Harmonic propagation through the test system, part 1 | 219 |
| 5.9 Harmonic propagation through the test system, part 2 | 220 |
| A.1 Positive, negative and zero sequence representations | 234 |
| A.2 Three-phase quantities with various sequence-harmonic contents | 235 |
| B.1 Scheme of the AC-grid connection | 242 |
| B.2 Block-diagram of linearised PLL dynamics | 245 |
| B.3 TLC: circuit diagram | 253 |
| B.4 Overview of TLC control structure | 254 |
| B.5 Offshore HVDC system: circuit diagram | 258 |
| B.6 AC cable π -equivalent model | 259 |
| B.7 HVDC cable π -equivalent model | 260 |
| C.1 Overview of the Matlab toolbox capabilities | 266 |
| C.2 Numerical integration of DDEs by means of ODE solvers | 273 |

List of Tables

| | | |
|-----|--|-----|
| 1.1 | Illustrative classification of dynamic systems | 40 |
| 1.2 | Similarities between LTI and LTP systems | 53 |
| 2.1 | Relevant TLC and MMC circuit and control parameters | 80 |
| 2.2 | Frequency and sequence content of <i>abc</i> variables | 89 |
| 3.1 | Overview of transformation methods | 150 |
| 4.1 | Participation factors of a resonant mode in the DHSS model . . | 177 |
| 5.1 | Supplemented nomenclature | 190 |
| 5.2 | Indicative calculation times of time-domain methods | 214 |
| B.1 | Parameters: MMC circuit | 251 |
| B.2 | Parameters: MMC controller | 252 |
| B.3 | Parameters: TLC circuit and controller | 255 |
| B.4 | Parameters: MMC-based test system | 258 |
| B.5 | Parameters: AC and HVDC cables | 261 |

List of Publications

Journal articles

Published

- **Philippe De Rua**, Özgür Can Sakinci, and Jef Beerten, “Comparative Study of Dynamic Phasor and Harmonic State-Space Modeling for Small-Signal Stability Analysis,” *Electric Power Systems Research*, vol. 189, p. 106626, 2020, doi: 10.1016/j.epsr.2020.106626.
- **Philippe De Rua** and Jef Beerten, "Generalization of Harmonic State-Space Framework to Delayed Periodic Systems for Stability Analysis of the Modular Multilevel Converter," *IEEE Transactions on Power Delivery*, vol. 37, no. 4, pp. 2661-2672, 2022, doi: 10.1109/tpwrd.2021.3113702.
- **Philippe De Rua**, Thomas Roose, Özgür Can Sakinci, Nathalia de Morais Dias Campos, and Jef Beerten, “Identification of mechanisms behind converter-related issues in power systems based on an overview of real-life events,” *Renewable and Sustainable Energy Reviews*, vol. 183, p. 113431, 2023, doi: 10.1016/j.rser.2023.113431.

Submitted

- **Philippe De Rua** and Jef Beerten, "Modular Multilevel Converter Periodic Trajectory Determination — A Generic Fourier-Based Collocation Method," submitted to *International Journal of Electrical Power & Energy Systems*.

International conferences

Presented

- **Philippe De Rua**, Özgür Can Sakinci, and Jef Beerten, "Comparative Study of Dynamic Phasor and Harmonic State-Space Modeling for Small-Signal Stability Analysis", *Power Systems Computation Conference 2020*, Porto, Portugal, 2020 (Online).

Accepted

- Dennis Debree, **Philippe De Rua**, Geraint Chaffey, Jef Beerten, "Real-time Testing and Analysis of an MMC Controller in a Hardware Implementation", IECON 2023 — 49th Annual Conference of the IEEE Industrial Electronics Society, Singapore, 2023.

Curriculum Vitae

Philippe De Rua

Born on October 25th, 1993, in Namur, Belgium.

2018-2023 Ph.D. in Engineering Science: Electrical Engineering
Department of Electrical Engineering (ESAT)
KU Leuven
Leuven, Belgium

2017-2018 Consultant at Engie Laborelec
Wind and Hydro Department
Linkebeek, Belgium

2015-2017 M.Sc. in Engineering Science: Electromechanical Engineering
Specialisation: Energy
UCLouvain
Louvain-la-Neuve, Belgium
Graduated Magna Cum Laude

2012-2015 B.Sc. in Engineering Science
UCLouvain
Louvain-la-Neuve, Belgium
Graduated Summa Cum Laude

FACULTY OF ENGINEERING SCIENCE
DEPARTMENT OF ELECTRICAL ENGINEERING
ELECTA
Kasteelpark Arenberg 10 box 2445
B-3001 Leuven

